A University of Sussex PhD thesis

Available online via Sussex Research Online:

http://sro.sussex.ac.uk/

This thesis is protected by copyright which belongs to the author.

This thesis cannot be reproduced or quoted extensively from without first obtaining permission in writing from the Author

The content must not be changed in any way or sold commercially in any format or medium without the formal permission of the Author

When referring to this work, full bibliographic details including the author, title, awarding institution and date of the thesis must be given

Please visit Sussex Research Online for more information and further details

Characterisation of selected post-translational modifications mediating the response to stress in mammalian cells

Robert Baldock

A thesis submitted to the University of Sussex for the degree of Doctor of Philosophy

January 2016

Declaration

I hereby declare that this thesis has not been, and will not be, submitted in whole or in part to another university for the award of any degree. The work described herein is my own work except where otherwise stated.

Robert Baldock

January 2016

Acknowledgements

I would like to thank Dr Felicity Watts for giving me the opportunity to complete my doctoral research project in her laboratory and for the invaluable support she has provided over the last 3 and a half years.

I would like to acknowledge and thank Dr Ross Cloney for his significant contribution to these projects. Through his instruction and guidance, I gained a number of invaluable skills, without which I would not have been able to complete these projects.

I would like to thank the previous members of the Watts laboratory, Dr Jirapas (Mai) Jongjitwimol, Dr Oliver Wilkinson and Dr Lauren Small.

I would like to thank Dr Matthew Day, Dr Anthony Oliver, Prof Laurence Pearl and Prof Penelope Jeggo for their collaboration and helpful discussions on these exciting projects.

Lastly, I would like to express my gratitude to everyone in the Genome damage and stability centre for making it such a great place to work.

Abstract

Eukaryotic initiation factors (eIFs) govern assembly of ribosomes on nascent mRNAs to be translated. Many eIFs have been identified in proteomic screens which aim to identify proteins that are subject to post-translational modification by SUMO. Despite this, many remain to be biochemically validated or functionally characterised. In this project, the DEAD-box helicases eIF4A1 and eIF4A2 were found to be SUMOylated on conserved lysine residues K216 and K226 respectively using an *in vitro* SUMOylation assay and mass spectrometry. Additionally, the SUMOylation of eIF4A2 was found to increase in response to arsenite-treatment (a treatment known to induce stress granule formation in mammalian cells). Furthermore, mutation of K226 in eIF4A2 affects the formation of stress granules. Further work will be required to determine the potential effect of SUMOylation of eIF4A2 on global translation.

Double-strand breaks (DSBs) form some of the most deleterious and damaging lesions to DNA. The DNA damage mediator, 53BP1, governs the choice of repair method promoting error prone non-homologous end joining over homologous recombination. In this project, two novel phosphorylation sites within the N-terminus of 53BP1 were identified. Phosphorylation of these residues is critical for the localisation of TopBP1 to sites of damage. Pulse-labelling cells with traceable nucleotide analogues reveals that failure to phosphorylate these residues also results in a failure to sustain a G1/S-phase checkpoint when DSBs are present. These results indicate that 53BP1 integrates two elements of the stress response- choice of DSB repair pathway and cell-cycle regulation. Further work will elucidate the exact mechanism requiring both 53BP1 and TopBP1 to maintain the G1/S-phase checkpoint.

53BP1 is a reader of the histone code, recognising both methylation and ubiquitination of histones through distinct domains. In this project, the $BRCT_2$ domains at the C-terminus of 53BP1 were shown to recognise a third post-translational mark, phosphorylation. By analysing the dependence on phosphorylation of the localisation of the $BRCT_2$ domains in isolation to laser-induced DNA damage alongside structural and biochemical data, it was shown that the $BRCT_2$ domains interact directly with YH2AX *in vitro* and *in vivo*. Although not essential for localisation to DNA damage, abolition of this interaction results in a persistence of YH2AX foci at 'late' time points representing the heterochromatic fraction of breaks. Furthermore, it was shown that this defect is propagated by a failure to localise the activated checkpoint kinase, ATM. Further investigation will be required to determine the mechanism underlying the repair defect observed.

Abbreviations

4E-BP1	eIF4E- binding protein 1
4E-H	eIF4E-homolog
53BP1	Tumour suppressor p53-binding protein 1
8-oxoG	8-oxo-7,8-dihydro-guanine
9-1-1 complex	Rad9-Rad1-Hus1
A-site	Aminoacyl site
AAD	ATR activation domain
Ago	Argonaute proteins
alt-NHEJ	Alternative NHEJ (a.k.a MMEJ)
APE1	Apurinic/apyrimidinic endonuclease 1
APLF	Aprataxin and PNK-like factor
APS	Ammonium persulfate
ARE	Adenine and uracil-rich elements
ARE-BPs	ARE-binding proteins
ATM	Ataxia telangiectasia mutated
ATP	Adenosine triphosphate
ATR	Ataxia telangiectasia mutated and Rad3 related
ATRIP	ATR-interacting protein
BER	Base excision repair
BLAST	Basic local alignment search tool
BLM	Bloom syndrome helicase
BRCA	Breast cancer susceptibility protein

BRCT	BRCA1 C-terminal
BrdU	Bromodeoxyuridine
BSA	Bovine serum albumin
BTR	BLM, TopoIIIα, RM1 and RM2
$CaCl_2$	Calcium chloride
CAF1	Chromatin assembly factor 1
CAK	CDK-activating kinase
CCR4	Chemokine (C-C motif) receptor 4
cdc	cell division cycle
CDK	Cyclin-dependent kinase
cDNA	complementary DNA
CENPF	Centromere protein F
CENT2	Centrin 2
CHD3	Chromodomain-helicase-DNA-binding protein 3
Chk2	Checkpoint kinase 2
CPD	Cyclobutane-pyrimidine dimer
CPE	Cytoplasmic polyadenylation element
CPEB	CPE-binding proteins
CPK	Creatine phosphokinase
CRISPR	Clustered regulatory interspaced short palindromic repeats
CrPV	Cricket paralysis virus
CS	Cockayne syndrome
CSR	Class-switch recombination

CtBP	C-terminal binding protein
CtIP	CtBP-interacting protein
$CuSO_4$	Copper Sulfate
Cy5	Cyanine 5
DAPI	4',6-diamidino-2-phenylindole
Dcp	Decapping protein
DDR	DNA damage response
DEAD	Glutamate-aspartate-alanine-glutamate
DHJ	Double Holliday Junction
DIS3	chromosome disjunction
DMEM	Dulbecco's modified eagles medium
DNA	Deoxyribonucleic acid
DNA-PK	DNA-dependent protein kinase
dNTPs	deoxynucleotide
DSB	Double strand break
dsDNA	Double-stranded DNA
DTT	Dithioreitol
E2F-1	E2F transcription factor 1
EDC4	Enhancer of decapping 4
EDTA	Ethylenediaminetetraacetic acid
EdU	5-ethynyl-2'-deoxyuridine
EGTA	Ethylene glycol tetraacetic acid
eIF	eukaryotic initiation factor

eIF4E-T	eIF4E-transporter
EJC	Exon junction complex
EME1	Essential meiotic structure-specific endonuclease 1
EmGFP	Emerald green fluorescent protein
eRF	eukaryotic release factor
Exo1	Exonuclease 1
EXPAND1	Multiple myeloma 1 (a.k.a MUM1)
FACS	Fluorescence activated cell sorting
FAN1	Fanconi anaemia-associated nuclease 1
FANC	Fanconi anaemia associated
FAT	FRAP, ATM, TRRAP
FATC	C-terminal FAT domain
FCS	Fetal calf serum
FEN1	Flap endonuclease 1
FHA	Forkhead-associated
FITC	Fluoroscein
FoxM1	Forkhead box protein M1
G3BP1	GTPase-activating protein (SH3-domain) binding protein 1
G418	G418 disulfate
GAP	GTPase-activating protein
GAR	Glycine-arginine rich
GCN	General control nonderepressible
GDP	Guanosine diphosphate

GEF	Guanine nucleotide exchange factor
GEN1	Flap endonuclease GEN1 homolog 1
GFP	Green fluorescent protein
GG-NER	Global genome NER
gRNA	guideRNA
GST	Glutathione S-transferase
GTP	Guanosine triphosphate
H2A	Histone H2A
H2AX	Histone H2A variant X
H4K20me	methylation of histone H4 on lysine-20
H4K20me2	dimethylation of histone H4 on lysine-20
HA	Haemagglutinin
HAT	Histone acetyl transferase
HCV	Hepatitus C virus
HDR	Homology-directed repair
HEAT	Huntingtin, elongation factor 3, a subunit of protein phosphatase 2 and TOR1
HEPES	4-(2-hyroxyethyl)-1-piperaxineethanesulfonic acid
His	Histidine
HP1	Heterochromatin protein 1
HR	Homologous recombination
HRP	Horseradish peroxidase
TERT	Telomerase reverse transcriptase

TTP	Tristetraprolin
HU	Urea elution buffer
ICL	Interstrand crosslink
IPTG	Isopropyl β -D-1-thiogalactopyranoside
IR	Ionising radiation
IRES	Internal ribosome entry site
IRIF	Ionising radiation-induced foci
ISRIB	Integrated stress response inhibitor
ITAFs	IRES-trans-activating factors
JMJD2A	Lysine-specific demethylase 4A (aka KDM4A)
KAP-1	Kruppel-associated box (KRAB)-associated protein 1
KCl	Potassium chloride
KOAc	Potassium Acetate
Ku	Heterodimeric complex that binds broken DNA end
L3MBTL1	L(3)Mbt-like 1
LB	Lysogeny Broth
LC-MS/MS	Liquid chromatography tandem mass spectrometry
Lys-C	Endoproteinase Lys-C
m/z	Mass to charge ratio
MAPK	Mitogen-activated protein kinase
MCM	Minichromosome maintenance protein complex
MDC1	Mediator of DNA damage checkpoint 1
MeCN	Acetonitrile

MEF	Mouse embryonic fibroblast
MGMT	O^6-methylguanine-DNA methyltransferase
$MgSO_4$	Magnesium sulfate
miRNA	Micro-RNA
MLH1	MutL homolog 1
MMEJ	microhomology mediated end joining (aka alt-NHEJ)
MMR	Mismatch repair
MMSET	Multiple myeloma SET domain
$MnCl_2$	Manganese chloride
MNK-1	MAPK-interacting kinase
MOPS	3-(N-morpholino)propanesulfonic acid
Mre	Meiotic recombination
MRN	Mre11-Rad50-Nbs1
mRNA	messenger RNA
mRNAseq	mRNA sequencing
MSH	MutS homolog
mTOR	mammalian Target of Rapamycin
mTORC1	mTOR complex 1
MUS81	MUS81 structure-specific endonuclease subunit
Na_2HPO_4	Disodium phosphate
NaAc	Sodium acetate
NaCl	Sodium chloride
NaF	Sodium fluoride

NaOH	Sodium hydroxide
NER	Nucleotide excision repair
NETN	NaCl/EDTA/Tris-HCl/NP-40
NH_4HCO_3	Ammonium bicarbonate
NHEJ	Non homologous end joining
NMD	Non-sense mediated decay
NOT	Component of the CCR4-NOT deadenylation complex
NPM1	Nucleophosmin 1
OD	Oligomerisation domain
OGG1	8-oxoG DNA glycosylase 1
ORF	Open reading frame
P-bodies	Processing bodies
P-site	Peptidyl site
p53	Tumour protein
PABP	Poly (A)-binding protein
PAIP1	PABP-interacting protein 1
PAIP2	PABP-interacting protein 2
PAM	Protospacer adjacent motif
PAR	Poly ADP-ribose
PARN	Poly (A) ribonuclease
PARP	Poly ADP-ribose polymerase
PBS	Phosphate buffered saline
PCNA	Proliferating cell nuclear antigen

PDCD4	Programmed cell death protein 4
PI3K	Phosphatidylinositol 3-kinase
PIAS	Protein inhibitor of activated STAT
PIKK	Phosphatidylinositol kinase-like kinases
PIP	PCNA-interacting protein
PML	Promeylocytic leukaemia protein
PML-NB	PML-Nuclear bodies
PMS2	Postmeiotic segregation increased 2
PNK	Polynucleotide kinase
POH1	Proteasome 26S subunit, non ATPase 14
pol	Polymerase
PPI	Pyrophosphate
PRD	PIKK-regulatory domain
PRMT1	Protein arginine methyltransferase 1
PTB	Polypyrimidine-tract binding protein
PTC	Premature termination codon
PTIP	Pax transactivation domain-interacting protein
PTM	Post-translational modification
RAD	Radiation sensitive
Rb	Retinoblastoma protein
RbCl	Rubidium chloride
RECQ5	RECQ5 DNA helicase
RFC	Replication factor C

RHINO	Rad9-Rad1-Hus1 interacting nuclear orphan
RIF1	Replication timing regulatory factor 1
RNA	Ribonucleic acid
RNAi	RNA interference
RNF	Ring finger protein
RNP	Ribonucleoproteins
ROS	Reactive oxygen species
RPA	Replication protein A
S	Svedberg units (Ribosomal subunits)
SDS	Sodium dodecyl sulphate
SDS-PAGE	SDS-polyacrylamide gel electrophoresis
SDSA	Synthesis dependent strand annealing
SENP	Sentrin-specific protease
SETDB	Histone-lysine N-methyltransferase
SG	Stress granules
SIM	SUMO-interacting motif
siRNA	small interfering RNA
SIRT1	Silent mating type information regulation 2 homolog 1
Siz2	SAP and mIZ-finger domain
sld	DNA replication regulator
SLX	Synthetic lethal of unknown (X) function
SMG1	Suppressor with morphological defects on genitalia family member

Srs2	Suppressor of Rad6
SSBR	Single-strand break repair
ssDNA	Single-stranded DNA
ssODN	Single-stranded oligonucleotide
SUMO	Small ubiquitin-like modifier
SUV39	Histone H3 lysine-9 methyltransferase
TBE	Tris/Borate/EDTA buffer
TC	Ternary complex
TCR	Transcription-coupled repair
TdT	deoxyribonucleotidyl transferase
TE	Tris EDTA solution
TEMED	Tetramethylethylenediamine
TFA	Trifluoroacetic acid
TFIIH	Transcription initiation factor IIH
TIA-1	T-cell internal antigen 1
TLS	Translesion synthesis
TMZ	Temozolomide
TopBP1	Topoisomerase IIβ-binding protein 1
TRITC	Tetramethylrhodamine
tRNA	Transfer RNA
TRRAP	Transformation/transcription domain-associated family member
UBA	Ubiquitin activating enzyme

Ubc	Ubiquitin conjugating enzyme
UBM	Ubiquitin recognition motif
UBZ	Ubiquitin-binding zinc finger
UDR	Ubiquitin-dependent domain
uORF	Upstream ORFs
Upf	Regulator of non-sense transcripts
USP7	Ubiquitin-specific processing protease 7
UTR	Untranslated region
UV	Ultra violet
UV-DBB	UV-radiation-DNA damage-binding protein
UVA	Ultraviolet A
UVSSA	UV-stimulated scaffold protein A
V(D)J	Variable, diversity and joining
VEGF	Vascular endothelial growth factor
XBP1	X-box binding protein 1
XIAP	X-linked inhibitor of apoptosis
XLF	a.k.a Non homologous end joining factor 1 (NHEJ 1), Cernunnos
XP	Xeroderma pigmentosum
XRCC4	X-ray repair cross-complementing protein 4
XRN1	exoribonuclease 1
YFP	Yellow fluorescent protein

Contents

List of Figures

List of Tables

1. Introduction

In mammalian cells post-translational modifications govern many aspects of protein form and function. Crucially, these modifications are rapid and have the potential to quickly reprogram the physiology of the cell when needed. Alongside maintaining cellular homeostasis, post-translational modifications regulate the response to cellular stress. The causes of cellular stress take many forms, from oxidative stress to ultraviolet light, from ionising radiation to amino acid starvation. In all cases, the ability of the cell to tolerate these stresses is propagated by cascades of post-translational modifications that occur as a result. These serve as the chemical messages and intra-cellular switches that can alter gene expression, translation, genomic integrity and cell-cycle control.

1.1 Post-translational modification

Post-translational modifications (PTMs) allow cells to respond to changes in both the intracellular and extracellular environment. They mediate the chemical messages between protein sensors and effectors, often referred to as cascades, to maintain homeostasis under advantageous conditions and to reprogram the cell for survival under disadvantageous conditions. Most importantly, PTMs are rapid and reversible allowing the cell to respond to the ever-changing cellular environment [11].

PTMs function by altering the properties of proteins within the cell. For example, they can directly alter the enzymatic activity of a target protein, potentially via the induction of a conformational change in a protein's structure. Alternatively, PTMs can enhance or suppress protein-protein interactions, alter subcellular localisation or affect cellular abundance of proteins by targeting them for proteasomal degradation [12-14].

Given that over 200 types of PTM have been identified and that individual proteins may be modified by more than one type of modifications on several amino acids, this creates a difficult challenge to identify and characterise these networks [11]. Additionally, as many of these modifications have yet to be functionally characterised it becomes necessary to isolate and determine which individual PTMs are critical for facilitating particular functions. Mass spectrometry has accelerated the identification of PTMs, yet many remain to be validated biochemically and their function determined [15]. Table 1.1 summarises examples of regulation by phosphorylation, ubiquitination and SUMOylation. These examples are explained in more detail throughout this section.

Table 1.1 Examples of regulation by phosphorylation, ubiquitination and SUMOylation.

Protein	Cellular response	PTM	References
4E-BP	Suppression of global translation	phosphorylation	[13]
Rb	G1-S phase cell-cycle progression	phosphorylation	[16]
-	Targeting proteins for proteasomal degradation	ubiquitination	[17]
NPM1	Suppression of centrosome expansion	SUMOylation	[18]
PML	PML nuclear bodies	SUMOylation	[19]
SUMO-PML	Degradation of PML nuclear bodies	ubiquitination	[20]
XBP1 **FoxM1**	Regulation of transcription factors	SUMOylation	[21, 22]

1.1.1 Phosphorylation

Phosphorylation is a common PTM that plays important roles in regulating the cell-cycle as well as responses to metabolic and genotoxic stresses. Enzymes that phosphorylate proteins are referred to as kinases. Many kinases exist within cells and although one kinase may dictate the phosphorylation of overlapping protein networks, in mammalian cells the three most commonly phosphorylated residues are serine, threonine and tyrosine [23].

The phosphatidylinositol 3-kinase-related protein kinases (PIKKs) are a family of kinases which modulate cellular metabolism and checkpoint signalling in response to DNA damage. PIKKs phosphorylate serine or threonine residues followed by a glutamine residue (SQ/TQ motifs) [24]. The six PIKKs present in mammalian cells are mammalian target of rapamycin (mTOR), Transformation/transcription domain-associated protein (TRRAP), Suppressor with morphological defects on genitalia family member (SMG1), Ataxia telangiectasia-mutated (ATM), Ataxia telangiectasia-mutated and Rad3-related (ATR) and DNA-dependent protein kinase catalytic subunit (DNA-PKcs). This family of protein kinases all have comparable domain architecture include N-terminal Huntingtin, elongation factor 3, a subunit of protein phosphatase 2 and TOR1 (HEAT) repeats. Adjacent to the HEAT repeats is a FRAP, ATM, TRRAP (FAT) domain followed by the kinase domain, a PIKK- regulatory domain (PRD) and a C-terminal FAT domain (FATC) [25].

Predominantly, mTOR governs global translation. By hyperphosphorylating 4E-BP1, which would otherwise inhibit eIF4E availability in the cell, mTOR promotes cap-dependent translation [13]. TRRAP is a core component of Histone acetyl transferase (HAT) complexes and regulates PTM of chromatin via histone tails [26]. SMG1 is recruited to mRNAs during Non-sense mediated decay (NMD) and is incorporated into Stress granules (SGs) [27, 28]. The DNA

damage response kinases ATM, ATR and DNA-PKcs propagate signalling at double-strand breaks (DSBs), regions of single-stranded DNA (ssDNA) and during DSB repair, respectively [29-31].

Cyclin-dependent kinases (CDKs) regulate progression through the cell-cycle by phosphorylating protein targets on serine/threonine residues adjacent to a proline residue (S/TP motif) [32]. CDK activity is regulated throughout the cell-cycle by the availability and binding of cyclins to stimulate kinase activity. For example, in G1-phase mammalian cells cyclin D levels increase promoting kinase activity of CDKs 4 and 6, whereas towards S-phase levels of cyclin E increase, stimulating the activity of CDK2 [33, 34]. CDK2 proceeds to phosphorylate retinoblastoma (Rb), which releases the transcription factors E2F-1 to promote the G1-S phase transition [16]. The downstream effect of activation of this kinase relies not only on the phosphorylation of the protein targets but also the ability for the domains of other proteins to recognise and bind to the phosphorylated serine/threonine residues. This requires the phospho-binding capacity by distinct molecular motifs such as Forkhead-associated domains and BRCA1 C-terminal (BRCT) domains to name but a few [35].

1.1.2 Ubiquitination

Compared to phosphorylation, ubiquitination is a large PTM comprising the addition of an ~8.5kDa to a lysine residue by covalent linkage [15, 36]. Ubiquitination is required for many functions within the cell, including the DNA damage response and targeting proteins for degradation by the proteasome.

Unlike phosphorylation, four proteins are required to catalyse the ubiquitination of target proteins, including a deubiquitinating enzyme required for the generation of the mature ubiquitin protein from its protein precursor [37]. Initially, ubiquitin is attached to an E1 ubiquitin-activating enzyme in an ATP-dependent manner via the formation of a thioester bond. In mammalian cells, two ubiquitin-activating enzymes have been identified UBA1 and UBA6, with UBA1 being required for 53BP1 IRIF formation in response to DNA damage [38]. Ubiquitin is then transferred to an E2 ubiquitin-conjugating enzyme. Although there are many E2 ubiquitin-conjugating enzymes in mammalian cells, Ubc13 has been identified as an important mediator in the propagation of the DNA damage response [39]. Lastly, the ubiquitin complex is directed to and transferred to the target protein by an E3 ubiquitin ligase, which bridges interactions between the E2-ubiquitin complex and the target protein. As a result, it is the E3 ubiquitin ligases that provide target specificity for the ubiquitination machinery [40].

As with phosphorylation, the generation and abolition of protein-protein interactions by PTM requires both the modified protein and a specialised recognition motif. Many motifs have been identified including Ubiquitin-recognition motifs (UBMs) and Ubiquitin-binding zinc finger (UBZ) domains, both of which feature in the Y-family DNA polymerases utilised in translesion synthesis (TLS) [41, 42].

1.1.3 SUMOylation

Small Ubiquitin-like Modifier (SUMO) is a post-translational modification that is essential for a number of cellular processes from regulating transcription, DNA-damage repair and controlling the cellular response to stress.

There are four isoforms of SUMO in mammalian cells, SUMO1, SUMO2, SUMO3 and SUMO4. SUMO2 and 3 share approximately 97% homology, whereas SUMO1 shares only about 47% homology with SUMO2/3 [43]. All SUMOs are synthesised as inactive precursor proteins and have to be cleaved by specific cysteine isopeptidases, referred to as sentrin-specific proteases (SENPs), in order to yield the active protein that can then be conjugated to a target onto a lysine residue [44]. SUMO4 however, lacks the residue required for cleavage to produce the active protein and as a result cannot be conjugated to target proteins [45]. Similar to ubiquitin, SUMO2/3 are capable of forming SUMO chains on target proteins due to an available lysine residue (K11) present on both mammalian SUMO2 and 3 [46]. However, as SUMO1 lacks this lysine residue, only one SUMO1 molecule can modify a target protein, alternatively SUMO1 can act as a chain terminator of a polySUMOylated target [43].

1.1.3.1 Mechanism of SUMOylation and deSUMOylation

The mechanism by which SUMOylation occurs is comparable to that of ubiquitination of substrates. Following activation of the SUMO molecule by SENPs to reveal a C-terminal diglycine residue, SUMO-GG forms a thioester bond with an E1 SUMO activating enzyme (SAE) formed of a heterodimeric complex SAE1 and SAE2. SUMO is then transferred to an E2 SUMO conjugating enzyme, Ubc9. From there, SUMO can either be directly conjugated to a target protein containing SUMO consensus motif marked by a ψKxE motif, where ψ marks a hydrophobic residue [43]. Alternatively, an E3 SUMO ligase may be utilised to conjugate SUMO to non-consensus lysine residues (figure 1.1). Although only one E2 SUMO conjugating enzyme has been identified in mammalian cells, many E3 ligases continue to be identified. Recently TRIM28/KAP1, was found to catalyse SUMOylation of a DNA G-quadruplex binding protein specifically, nucleophosmin (NPM1) resulting in re-localisation to the centrosome required for the maintenance of genomic integrity [18]. Conversely, the SUMO E3 ligase, PIAS1 has been

demonstrated to bind to and mediate the SUMOylation of many targets that regulate transcription [47]. The SUMO E3 ligases provide specificity to the SUMOylation machinery directing the post-translational modification to specific subsets of targets within the cell.

SUMOylation is a highly dynamic way of regulating protein function with waves of SUMOylation occurring in response to cellular stress. Regulating deSUMOylation of protein targets is just as important and requires the same group of enzymes that cleave the SUMO precursor to yield the conjugation-competent isoform. Six SENPs exist in mammalian cells; SENP1, 2 and 5 are required for the maturation of SUMO, SENP1 is also predominantly involved in deSUMOylation. SENP6 and SENP7 facilitate deSUMOylation of polySUMOylated target proteins [43, 44].

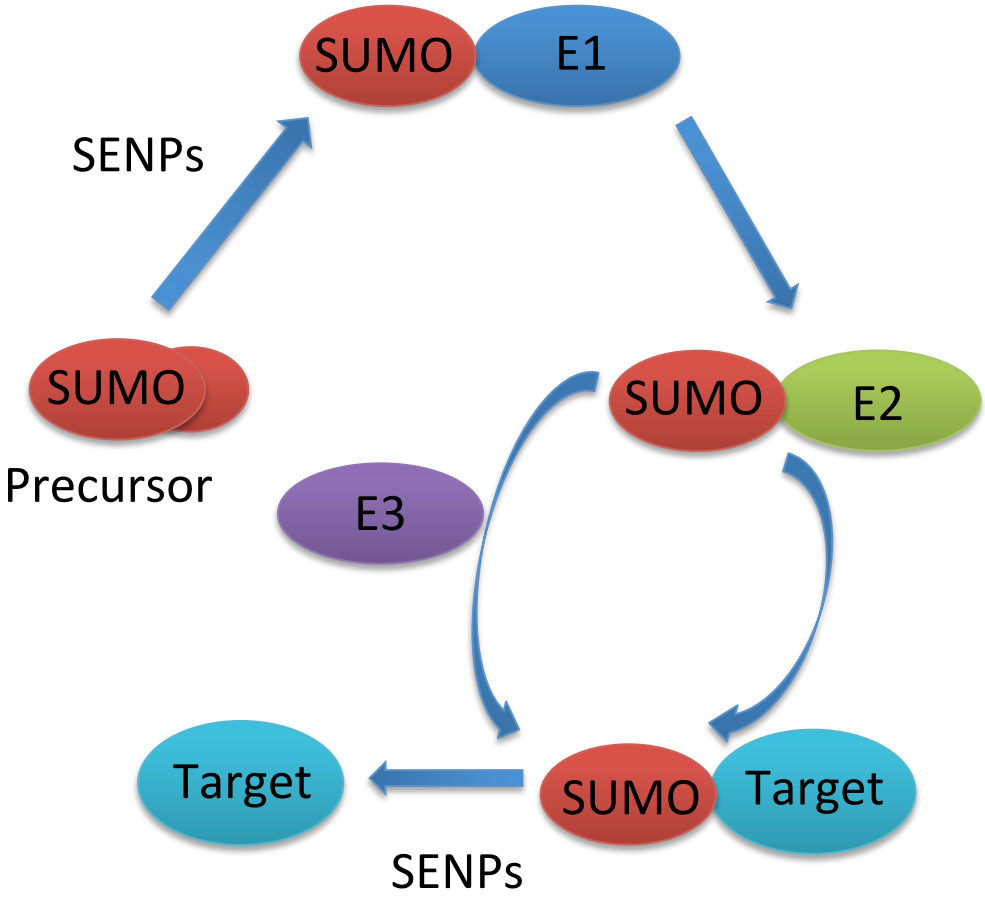

Figure 1.1 Mechanism of SUMOylation. SUMO is processed to the mature form by SENP proteases. SUMO is attached to an E1 SUMO activating enzyme, then passed to an E2 SUMO conjugating enzyme. SUMO is conjugated to the target protein either directly or via an E3 SUMO ligase. SENP proteases also mediate the deconjugation of SUMO from target proteins.

1.1.3.2 Diverse functions of SUMO

SUMO can act through a range of mechanisms, either by altering subcellular localisation, altering protein-protein interactions or promoting protein degradation. The role of SUMO varies depending upon the specific process involved, for example *S. cerevisiae* PCNA is SUMOylated during DNA replication. SUMOylated PCNA is then able to recruit Srs2 through a SUMO-interacting motif (SIM), which supresses Rad51 filament formation and homologous recombination (HR) [48].

SUMO can also alter numerous protein-protein interactions of large complexes by way of group modification. Group modification by SUMO was proposed following analysis of the ability of cells to repair DNA damage by HR. Following resection of the DNA ends, Siz2, an E3 SUMO ligase, catalyses the SUMOylation of a cluster of proteins involved in the repair pathway. The researchers noted that, typically, deletion of one or two of the SUMOylation sites in this pathway yielded only very mild HR defects and proposed that SUMOylation of other proteins, along with SUMO-interacting partners containing SIMs was sufficient to continue to repair the DNA breaks. Furthermore, only deletion of the E3 SUMO ligase directly prevented SUMOylation and SUMOylation-dependent repair [49].

Another well-studied example of protein group SUMOylation is in Promyelocytic nuclear bodies (PML-NBs). PML-NBs are nuclear aggregates that form in response to cellular stress [19]. PML protein has been shown to be SUMOylated on several residues and contains a SIM. Despite this, mutation of the acceptor-lysine residues or of the SIM does not prevent PML-NB formation [50]. PML has intrinsic E3 SUMO ligase activity and comparable to the loss of Siz2 in the DNA damage response, loss of PML results in a failure to form PML-NBs indicating its central role in catalysing SUMOylation of partner proteins [19, 20]. Partner proteins can also be recruited to PML-NBs through SIMs allowing group modification to hold these large nuclear structures together. Furthermore, PML-NBs have been demonstrated to facilitate the isolation and degradation of misfolded proteins, firstly by SUMOylating and re-localising the proteins to PML-NBs. Following incorporation into PML-NBs, the proteins are targeted for proteasomal degradation by RNF4-dependent ubiquitination [20].

The ubiquitination of SUMOylated-substrates is catalysed by a special subset of ubiquitin ligases that contain SIMs known as SUMO-targeted ubiquitin ligases (STUbLs). A well-studied example is RNF4, which targets SUMOylated PML and associated proteins for degradation in PML-nuclear bodies [20, 51]. RNF4 binds to SUMO-chains utilising two SIMs located with the N-terminus and functions as a dimer [52, 53].

SUMOylation is also capable of modulating the cellular response to stress by regulating transcription. It is commonly, reported that several transcription factors are negatively regulated by SUMOylation [54]. However, deSUMOylation can also be utilised to positively regulate transcription factors, for example endoplasmic reticulum (ER) stress or the unfolded-protein response results in deSUMOylation of the transcription factor XBP1 [21]. Recently, the SUMO protease SENP6 was demonstrated to activate the transcription factor, FoxM1, via the removal of SUMO to promote cell growth [21].

Post-translational modification by SUMO governs the ability of cells to tolerate different forms of stress, facilitating HR in response to DNA damage and reprogramming transcription to highlight a few examples [48, 55]. Regulation by SUMO is highly complex, involving different isoforms of SUMO capable of forming several intermediates alongside cross-talk with other post-translational modifications such as ubiquitin [56]. Finally, SUMO is capable of orchestrating, maintaining and disassembling large protein complexes by facilitating group protein-protein interactions [49]. As a result, it is quite likely that the ramifications of SUMO extend beyond the current understanding to other critical cellular processes in which the role of SUMO has yet to be elucidated.

1.1.3.3 Identification of the SUMO proteome

A number of approaches exist to study the SUMO proteome (reviewed in [43]). Primarily, these rely on the isolation of SUMO and its SUMOylated targets using several different approaches, followed by identification of the target proteins and modified residues using liquid chromatography-tandem mass spectrometry (LC-MS/MS). Classically, SUMOylated proteins have been isolated by exogenously introducing a variant of SUMO with either an affinity-tag that can be used to directly purify SUMOylated substrates or by using an antibody-specific epitope such as Flag [57, 58]. Using these approaches, SUMOylated proteins are then purified under denaturing conditions. This ensures that only proteins covalently modified on lysine residues co-purify/immunoprecipitate with SUMO and exclude protein-protein interactions that rely on natively folded structures such as SIMs.

Additionally, following lysis of cells and prior to denaturation of proteins, SENP-specific inhibitors are also added to prevent deSUMOylation of proteins during the purification process. The processing of samples for analysis by mass spectrometry requires digestion of the polypeptide chains by peptidases such as trypsin [58]. This generates small peptide-chains that can be easily ionised and detected by the mass spectrometer. However, digestion with trypsin generates a short peptide from the target protein with a long peptide side-chain if SUMO is

present, making it difficult to detect. As a result, the introduction of an arginine or lysine residue close to the C-terminus of SUMO generates a shorter peptide branch conjugated to a lysine residue if the substrate is SUMOylated [22]. These modifications are much easier for the mass spectrometer to detect by searching for a characteristic shift in the mass to charge ratio (m/z) produced by the additional diglycine residue. SUMOylated residues can be identified without the introduction of a lysine residue prior to the diglycine motif, either by searching for a larger side-group covalently attached to lysine or by using a different combination of peptidases, such as Trypsin and Lys-C [3].

SUMOylated substrates can also be purified without the introduction of an exogenously expressed SUMO. This is advantageous as overexpression of SUMO could affect the homeostatic mechanisms regulating SUMOylation and deSUMOylation in the cell making it difficult to study SUMOylation patterns in response to stress for example. To overcome this, SUMO and its substrates can be immunoprecipitated directly from cell lysates using specific antibodies or alternatively, SIM-traps can be used [2, 4]. SIM-traps utilise recognition motifs contained in some proteins to precipitate polySUMOylated targets by exploiting native protein-protein interactions. However, this method of purification is likely to generate false positive candidates given the networks of interactions facilitated by group modification by SUMO.

1.2 Initiating translation in Eukaryotic cells

1.2.1 Cap-dependent Translation initiation

Translation is the process by which nascent mRNAs transcripts are read by ribosomes to synthesise proteins. Translation is composed of three distinct stages, initiation, elongation and termination. Firstly, translation initiation involves the loading of ribosomal subunits on to the mRNA to be translated [1]. Secondly, the elongation step comprises the extension of the polypeptide chain by decoding the codon sequence. Finally, termination of the polypeptide chain requires the recognition of a stop codon by the translation machinery, releasing the ribosomes from the mRNA and yielding a newly synthesised polypeptide [59]. Following on from its generation, the polypeptide chain may require additional processing such as folding, cleavage or post-translational modification to form the active protein required to perform a specific function within the cell [60]. The initiation stage of translation is commonly thought of as the major regulatory stage of cap-dependent translation and is essentially rate limiting for global protein synthesis.

The basic mechanism of translation initiation can be thought of as the generation of two distinct complexes firstly, the preparation of the ribosomal subunit and secondly, the activation of the mRNA to be translated (figure 1.2). Preparation of the ribosomal subunit requires the isolation of the 40S subunit from the 60S subunit. Even in the absence of mRNA these ribosomal subunits are cycling in a dynamic equilibrium between the 80S complex (i.e. both subunits assembled) and the dissociated 40S and 60S subunits [1]. In order for translation to progress, the dissociated 40S subunit must be stabilised in the dissociated form to allow association with the mRNA to be translated.

The 40S subunit is maintained in the dissociated state by association with several other factors. As these factors are involved in the initiation of eukaryotic translation they are referred to as eukaryotic initiation factors (eIFs). The binding of eIF1, eIF1A and eIF3 stabilise the dissociated 40S ribosomal subunit. Both eIF1 and eIF1A are required to induce an 'open-latch' conformation in the structure of the 40S subunit to allow access to the mRNA binding channel [61]. The cryo-EM structure of eukaryotic initiation factor eIF3 reveals a large multicomponent complex formed of both core components and accessory factors. There are 13 subunits in total that make up eIF3 referred to as eIF3a-m. The core subunits comprise eIF3a, -c, -e, -k, -l, -m, -f and -h. The proteins eIF3b, -d, -g, -i and -j make up the accessory factors [62].

The maintenance of the 40S ribosomal subunit permits the association of the ternary complex (TC) along with eIF5. The TC is composed of eIF2 bound to the initiator $tRNA^{Met}$ (charged with an initiator methionine residue). The TC complex associates with the assembled smaller ribosomal subunit to form the 43S pre-initiation complex [1].

The second component required for the initiation of translation is the activation of the mRNA to be translated. This requires the formation of the eIF4F complex associated with the mRNA. The eIF4F complex is composed of three proteins, eIF4G- a large molecular scaffold protein, eIF4E- a protein that binds the 7-methylguanosine cap of the mRNA directly and eIF4A- an ATP-dependent RNA helicase. Along with the eIF4F complex, poly(A)-binding protein (PABP) binds to the polyadenylated tail of the mRNA transcript [1, 63].

The molecular scaffold protein eIF4G contains binding domains for eIF4E, eIF4A, eIF3 and PABP. Interactions between PABP and eIF4E are bridged by eIF4G. As a result, the mRNA is circularised with both vulnerable RNA ends sequestered by ribonucleoproteins. This protects the mRNA from degradation by exoribonucleases, requiring either deadenylation and de-

capping prior to degradation [64]. Following the activation of the mRNA and the preparation of the 43S complex, the two associate together to load the mRNA into the RNA binding channel of the ribosomal subunit to form the 48S ribosomal subunit. This recruitment requires interaction between eIF4G and three subunits of eIF3, -c, -d and -e [65].

The assembled complex then proceeds to scan the 5' end of the mRNA for the start codon. The scanning of the 5' untranslated region (UTR) of the mRNA requires factors, eIF1 and eIF1A. These factors, eIF1 and eIF1A, antagonise the hydrolysis of the GTP-bound eIF2 when the correct start codon does not occupy the peptidyl-site (P-site) of the 40S ribosomal subunit [66]. Once the start codon occupies the P-site, eIF1A stabilises the complementation of the codon by the tRNA. This causes a conformational change resulting in eIF1 dissociation, which permits the hydrolysis of eIF2-GTP to GDP stimulated by eIF5 [67, 68]. This changes the conformation of the 40S ribosomal subunit, closing the molecular 'latch' and locking the ribosome onto the mRNA. This results in the dissociation of the eukaryotic initiation factors allowing the association of the 60S subunit to form the complete 80S ribosome. Further GTP hydrolysis by eIF5B is required for its dissociation from the primed 80S ribosome [69, 70]. Elongation then proceeds with the delivery of amino acids charged to tRNAs that complement the codons in the mRNA to the aminoacyl-site (A-site) of the ribosome. From this point the polypeptide chain is extended to form the primary structure of the protein.

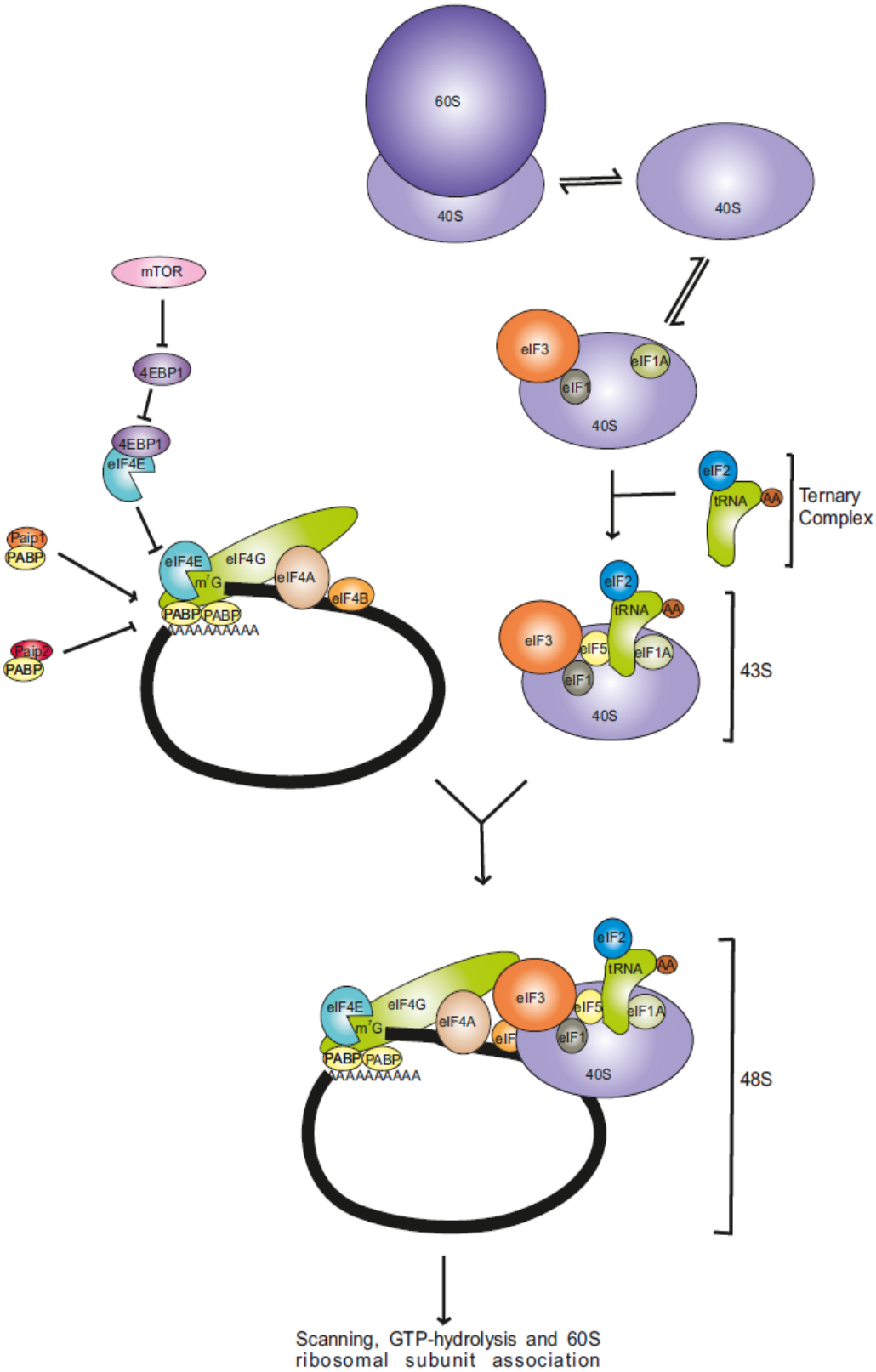

Figure 1.2 Overview of translation initiation and regulation of the eIF4F complex. (Adapted from [118]) The black line represents capped and polyadenylated mRNA. 60S and 40S represent large and small ribosomal subunits respectively.

1.2.2 Response to stress via post-translational modifications

Post-translational modifications (PTMs) regulate many of the components required for the initiation of translation. Table 1.2 details examples of several PTMs that govern rates of global translation and are described in more detail throughout this section.

Table 1.2 Examples of post-translational modifications governing metabolic responses to stress.

Protein	Cellular response	PTM	References
eIF2α	Suppression of global translation	phosphorylation	[12]
4E-BP1	Increased global translation	phosphorylation	[13]
eIF4E	Suppression of global translation	phosphorylation	[71]
PDCD4	Suppression of eIF4A-dependent translation	phosphorylation	[72]
PAIP1	Increased 48S complex formation	phosphorylation	[73]
PAIP2	Increased PABP-binding by PAIP2 degradation	ubiquitination	[63]
G3BP1	Suppression of SG formation	phosphorylation	[74]
eIF4E	Stabilisation of the eIF4F complex	SUMOylation	[75]
eIF4G	Response to stresses that induce SGs	SUMOylation	[76]

Global cap-dependent translation is regulated via the formation of the 43S pre-initiation complex and the activation of the mRNA. The formation of both complexes is regulated by post-translational modifications. In the case of the 43S pre-initiation complex, the ability of eIF2 to bind the initiator $tRNA^{Met}$ is modulated by a GTP/GDP molecular switch. The initiation factor eIF2 only binds the $tRNA^{Met}$ when guanosine triphosphate (GTP) is bound [1]. The exchange of GDP to GTP is catalysed by the guanine exchange factor, eIF2B. However, when eIF2 is phosphorylated on Ser51 within the α subunit, phosphorylated eIF2 bound to GDP becomes a potent inhibitor of eIF2B [12]. Inhibition of eIF2B prevents re-priming of eIF2 with GTP and prevents the formation of the TC. Ultimately, phosphorylation of eIF2 is a very rapid way of shutting down cap-dependent translation reducing the availability of eIF2-GTP and preventing the formation of the TC and the formation of the 43S pre-initiation complex. Importantly, eIF2 is targeted by a number of kinases that are activated by particular stresses such as GCN2, which in turn is activated in response to amino acid starvation [77].

Alternatively, global translation can be regulated at the level of mRNA activation by affecting the formation of the eIF4F complex. A small group of proteins compete with eIF4G for binding with the 7-methylguanosine cap binding protein, eIF4E. These proteins are called eIF4E-binding proteins (4E-BPs). A well-characterised example of regulation by 4E-BPs in response to

stress is through 4E-BP1, which preferentially binds to eIF4E when 4E-BP1 is hypo-phosphorylated state preventing eIF4E binding to eIF4G and assembling the eIF4F complex. Under normal conditions, 4E-BP1 is hyper-phosphorylated by mTORC1 (mammalian target of rapamycin complex 1) kinase, thereby preventing binding to eIF4E and allowing initiation of translation to proceed unhindered. However, under stress conditions, mTORC1 kinase activity is supressed leading to global sequestration of eIF4E and suppression of global translation [78].

The mRNA cap binding protein, eIF4E, is another example of a protein that can be phosphorylated. It is phosphorylated directly by MAPK-interacting kinase (MNK-1), which is recruited through the C-terminal region of eIF4G [71], a region recently shown to be subject to another post-translational modification, SUMOylation [76]. Phosphorylation of eIF4E serves to inhibit the translation of capped mRNAs containing an RNA loop structure within the 5' UTR [71]. Additional regulation at the level of eIF4E is introduced by eIF4E2/4E-H, a homolog of eIF4E capable of weak association with the capped mRNA but not able to interact with eIF4G. Recently, 4E-H was demonstrated to interact with eIF4E-binding protein (4E-T), a component of the mRNA degradation machinery [79, 80] linking both translational repression and mRNA degradation.

The third component of the eIF4F complex, eIF4A, is also subject to regulation. The DEAD-box helicase, eIF4A1, is required for the 43S pre-initiation complex to scan through secondary and tertiary RNA structures located within the 5' UTR of mRNAs. The unwinding of RNA structures by eIF4A1 requires hydrolysis of ATP, which is stimulated when eIF4A binds to eIF4G and a co-factor such as eIF4B or eIF4H [81]. Modulating the activity of eIF4A has the ability to re-program the cell by altering the selectivity regarding which mRNA will be translated. Programmed cell death protein 4 (PDCD4) binds to eIF4A and inhibits its incorporation into the eIF4F complex. PDCD4 is phosphorylated by p70S6 Kinase, which is activated downstream of mTORC1. When PDCD4 is phosphorylated it binds to eIF4A sequestering it from associating with the eIF4F complex [72]. Interestingly, ribosome footprinting of cells treated with silvestrol, an inhibitor of eIF4A, reveals a requirement for eIF4A to translate mRNA transcripts containing G-quadruplex RNA structures contained within the 5' UTR. Furthermore, analysis of mRNAs containing sequences predicted to form G-quadruplexes indicates their prevalence in oncogenic mRNAs, such as those encoding transcription factors [82]. Ultimately, translation of eIF4A-dependent mRNAs may be critical for promoting cell survival under cellular stress.

Furthermore, there are three isoforms of eIF4A, eIF4A1, -2 and -3. eIF4A1 and 2 both have RNA helicase activity. eIF4A3 forms part of the exon junction complex and is involved in non-sense

mediated decay, a quality control mechanism required for the degradation of mRNAs containing a premature stop codon [83]. Downregulation of eIF4A1 results in increased transcription of eIF4A2. Despite this apparent compensatory response, eIF4A2 cannot rescue the translational defect caused by downregulation of eIF4A1 [84]. Indicating that eIF4A1 and eIF4A2 serve different functions within the cell. This is the case, as eIF4A2 has been demonstrated to be required for miRNA-mediated gene silencing [85].

Eukaryotic translation initiation can also be regulated by the availability of poly (A) binding protein (PABP). Two co-factors, PABP-interacting proteins, PAIP1 and PAIP2, have opposing effects on translation initiation despite binding the same cellular target. PAIP1 promotes translation by binding to both PABP and eIF3g to promote formation of the 48S complex. Furthermore, the PAIP1-eIF3g interaction is thought to be phosphorylation dependent, requiring active mTORC1 and S6 kinases for interaction [73]. Conversely, PAIP2-binding of PABP blocks the conformational change, revealed by single-molecule fluorescence resonance energy transfer (smFRET), required for PABP to associate with the poly (A) tail [63]. Additionally, PAIP2 is itself is targeted for proteosomal degradation by another PTM, ubiquitination catalysed by EDD, an E3 ubiquitin ligase [86].

Although, many of the modifications identified in response to stress suppress global translation, suppression of cap-dependent translation promotes an alternative set of translation mechanisms to take over, which facilitate the translation of a specialised subset of mRNAs that help the cell tolerate stress and promote survival.

1.2.3 Mechanisms of Cap-independent translation

Following the induction of cellular stress and the suppression of global cap-dependent protein synthesis a number of physiological changes occur within the cell. Post-translational modifications facilitate the switching between cap-dependent to cap-independent mechanisms of translation. Despite the suppression of the majority of mRNA translation, there are some mRNAs that remain either unaffected or which are even up-regulated in response to cellular stress, such as *VEGF* (vascular endothelial growth factor) [1]. There are currently two methods of maintaining translation under conditions where either eIF2 is phosphorylated or the components of the eIF4F complex are scarce. Some mRNAs, such as *GCN4*, contain up-stream open reading frames (uORFs). uORFs are elements contained within the 5' UTR of the mRNA that, under normal physiological conditions, suppress the synthesis of the active protein. Under these conditions, the scanning ribosome initiates translation at one of the decoy ORFs. Following translation of the uORFs the majority of ribosomes would then

dissociate from the mRNA before reaching the start codon for the *GCN4* ORF. Under stress conditions for example, where the availability of the TC are low, the ribosome scans through the uORFs without initiating translation and only initiates translation further downstream, at the *GCN4* ORF [87]. As a result, protein synthesis of the transcriptional activator, GCN4 is increased when eIF2 is phosphorylated.

Alongside the use of uORFs to initiate translation when global cap-dependent translation is supressed, translation can be initiated via an internal ribosome entry site (IRES). These are formed by extensive secondary structures located within the 5' UTR of a subset of cellular and viral mRNAs that bypass the requirement for some or all initiation factors. IRESs guide the 40S ribosomal subunit with the initiator $tRNA^{Met}$ directly to the start codon. IRES-dependent translation was firstly identified in the Picornavirus, which has an RNA genome lacking a 5' cap. Despite the absence of eIF4E the Picornavirus RNA is still translated, thereby bypassing the eIF4E-dependent regulation of translation [88]. Since their initial identification, several other viral IRESs have been identified alongside some cellular mRNAs such as *XIAP* (X-linked inhibitor of apoptosis) and *VEGF*, mentioned earlier [89]. Each IRES demonstrates a different requirement for eukaryotic initiation factors. For example, Hepatitis C virus (HCV) bypasses the requirement for the eIF4F complex, only requiring eIF2 and eIF3 to initiate translation in an eIF5B-dependent manor [90-92]. The Cricket paralysis virus (CrPV) does not require any initiation factors or even the initiator $tRNA^{Met}$ to translate viral protein. The Cryo-EM structure of the elongating ribosome on the CrPV reveals that translation initiation is bypassed altogether [92].

Additionally, a number of co-factors facilitate cap-dependent translation via IRES called IRES-transactivating factors (ITAFs). Polypyrimidine-tract binding protein (PTB) is an ITAF, which has divergent functions within the cytoplasm and the nucleus. In the nucleus, PTB functions in pre-mRNA splicing whereas in the cytoplasm, PTB facilitates IRES-mediated translation by binding to and stabilising secondary RNA structures [93].

RNA G-quadruplexes are proposed to be inhibitory to cap-dependent translation, requiring an RNA helicase for efficient removal of these structures to promote translation. Furthermore, an RNA G-quadruplex was shown to be required for IRES-mediated translation of *VEGF* mRNA suggesting that these structures also may form part of the IRES [82, 94]. Additional complexity is revealed by the stabilisation of the RNA G-quadruplex by extending the guanine ribonucleotide stretches had an inhibitory effect on IRES-mediated translation [95]. Overall, this suggests a spectrum of translation initiation efficiencies governed by the complexity of

RNA structures within the 5' UTR of each mRNA. Additionally, indicating that each mRNA can be translationally activated or repressed depending on the availability of eIFs in the cellular environment.

1.3 mRNA stability, P-bodies and stress granules

Having reviewed how global mRNA translation is regulated by post-translational modifications in response to stress, it is also critical to consider what happens to the mRNA when it is not being translated. Ultimately, the cell faces a choice as to whether to store the mRNA or to degrade it.

1.3.1 mRNA stability and degradation

Degradation of mRNA occurs primarily through the deadenylation of the 3' end of the mRNA. Poly (A) binding-specific ribonucleases, CAF1/CCR4/NOT complex and poly (A) ribonuclease (PARN) all act to remove the poly (A) tail from mRNA resulting in the de-circularisation of the mRNA making it susceptible to decapping and degradation by ribonucleases [96]. Removal of the 7-methylguanosine cap is catalysed by the decapping complex Dcp1/Dcp2, the molecular scaffold EDC4 (enhancer of decapping 4) and XRN1 [97]. Following the removal of both the 3' poly (A) tail and the 5' cap, the mRNA can be degraded in either the 5' to 3' direction by XRN1 or in the 3' to 5' direction by hDIS3 associated with the exosome [98]. Additionally, some mRNAs can be targeted by directly endoribonucleases, which bypass the requirement for both deadenylation and decapping to allow 5' to 3' and 3' to 5' mRNA degradation [99] (figure 1.3).

As a result, targeting of deadenylases to the mRNA is a critical step in regulating mRNA turnover. Recruiting the deadenylation complex to mRNAs can occur through several mechanisms. Adenine and uracil-rich elements (AREs) located within the 3' UTR of the mRNA are capable of recruiting a range of ARE-binding proteins (ARE-BPs), such as TTP which recruits the CCR4/NOT deadenylation complex [100]. Alternatively, deadenylases can be recruited through miRNA-mediated mechanisms whereby, following translational repression the miRISC complex then recruits the CAF1/CCR4/NOT1 complex [101]. Recent investigation of the stability of *TP53* mRNA reveals functional interplay between miRNA-dependent and ARE-dependent recruitment of PARN for mRNA decay [102]. Deadenylases can also be recruited through a specialised mRNA quality control mechanism, nonsense-mediated decay (NMD). When pre-mRNAs are spliced an exon-junction complex (EJC) is deposited just upstream of the exon-exon junction. If the mRNA contains a premature termination codon (PTC) with an EJC downstream, the eukaryotic release factors (eRFs) recruit UPF1, UPF2, UPF3 and UPF3B, which

interact with the downstream EJC. This facilitates the recruitment of the mRNA degradation machinery [103, 104].

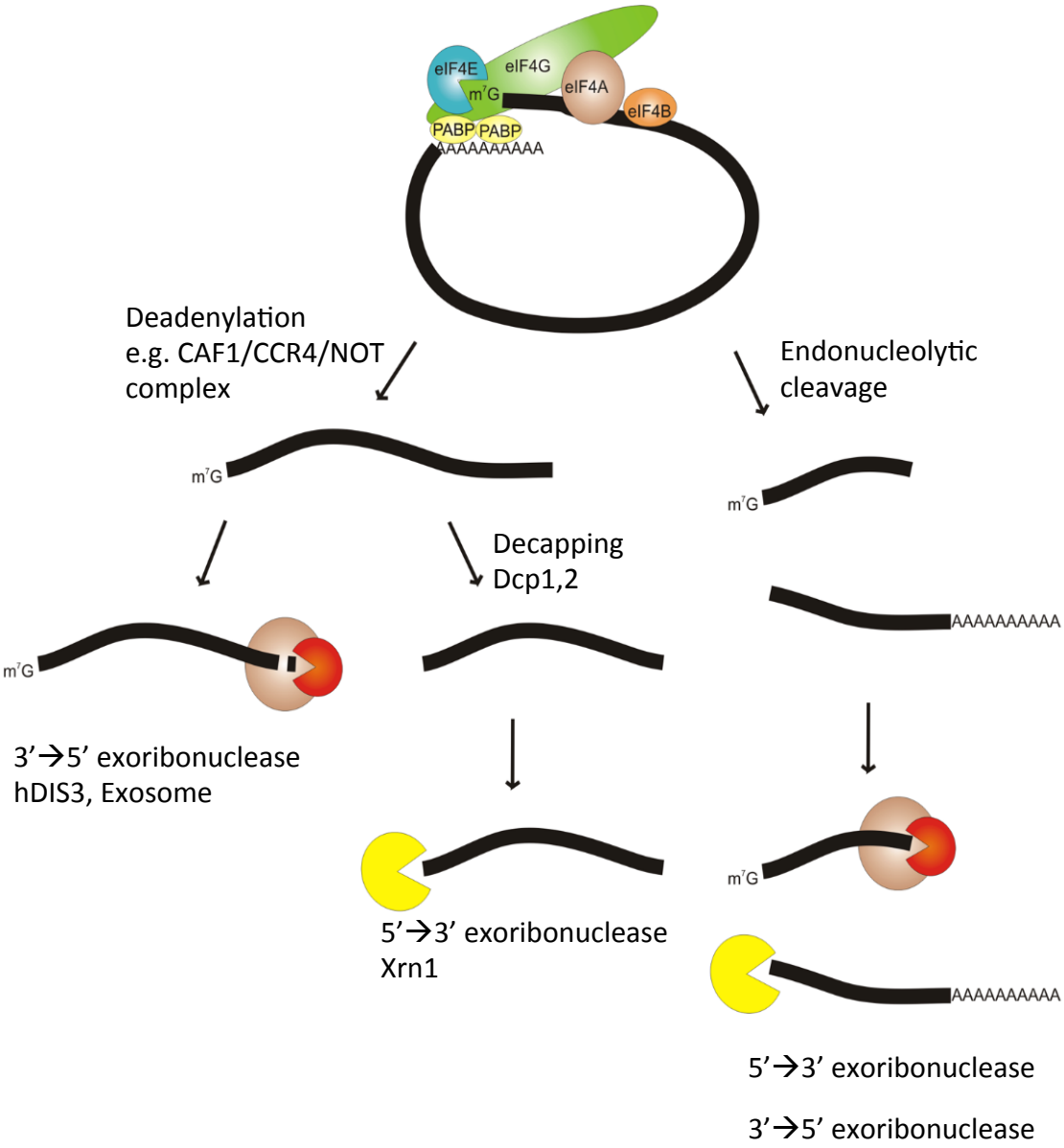

Figure 1.3 Overview of mRNA degradation pathways. The black line represents capped and polyadenylated mRNA. Brown circle represents the exosome and Dis3 is marked in red as the catalytic subunit.

1.3.2 mRNA regulation Processing bodies

Following translational repression mRNAs can enter processing bodies (P-bodies). P-bodies are cytoplasmic aggregates that serve as processing centres for mRNA. They can facilitate remodelling, storage, recycling and degradation of mRNA. P-bodies contain an array of proteins required for the translational repression such as eIF4E-T and CPEBs that supress translation through interactions with elements in the 3' UTR of mRNAs [96]. P-bodies also contain components required for both miRNA-mediated suppression including GW182 and Argonaute protein 2 (Ago2) and nonsense-mediated decay along with the deadenylation and decapping machinery [105, 106].

1.3.3 Stress granules

Alternatively, following exposure to cellular stress, mRNAs can be incorporated into stress granules (SGs). SGs are large cytoplasmic aggregates that form in response to stresses such as oxidative stress and commonly act via eIF2 phosphorylation-dependent inhibition of global cap-dependent translation [107]. The composition of SGs is distinguished from P-bodies by the presence eIFs and the 40S ribosomal subunit. As a result, it is thought that if translation initiation stalls, the mRNA will be targeted to SGs [108]. The formation of SGs requires the activity of two accessory proteins, T-cell internal antigen 1 (TIA-1) and GTPase-activating protein (SH3-domain) binding protein 1 (G3BP1) (figure 1.4). Interestingly, phosphorylation of G3BP1 prevents the formation of stress granules by preventing oligomerisation indicating further control of translational suppression by post-translational modifications [74].

Formation of stress granules occurs as a result of downregulating global translation of mRNAs commonly as a result of eIF2 phosphorylation. However, a number of stresses induce SG can formation the absence of eIF2 phosphorylation [109, 110]. Factors that affect the ability of the eIF4F complex to form, such as small-molecular inhibitors or direct depletion of eIF4A or accessory factors eIF4B and eIF4H result in the formation of stress granules [111, 112]. Disruption of factors acting downstream of eIF4F complex assembly i.e. eIF5B and 60S subunit association do not induce SG formation suggesting that the targeting of mRNA to SGs occurs early the during initiation step [112]. Interestingly, the type of stress introduced appears to affect the composition of the SGs. For example, a recent small-molecular inhibitor, ISRIB was identified that inhibited SG formation of sodium arsenite- and thapsigargin-induced SGs, but not those induced by pateamine A, suggesting that multiple mechanisms exist to promote stress granule formation following inhibition of translation [107].

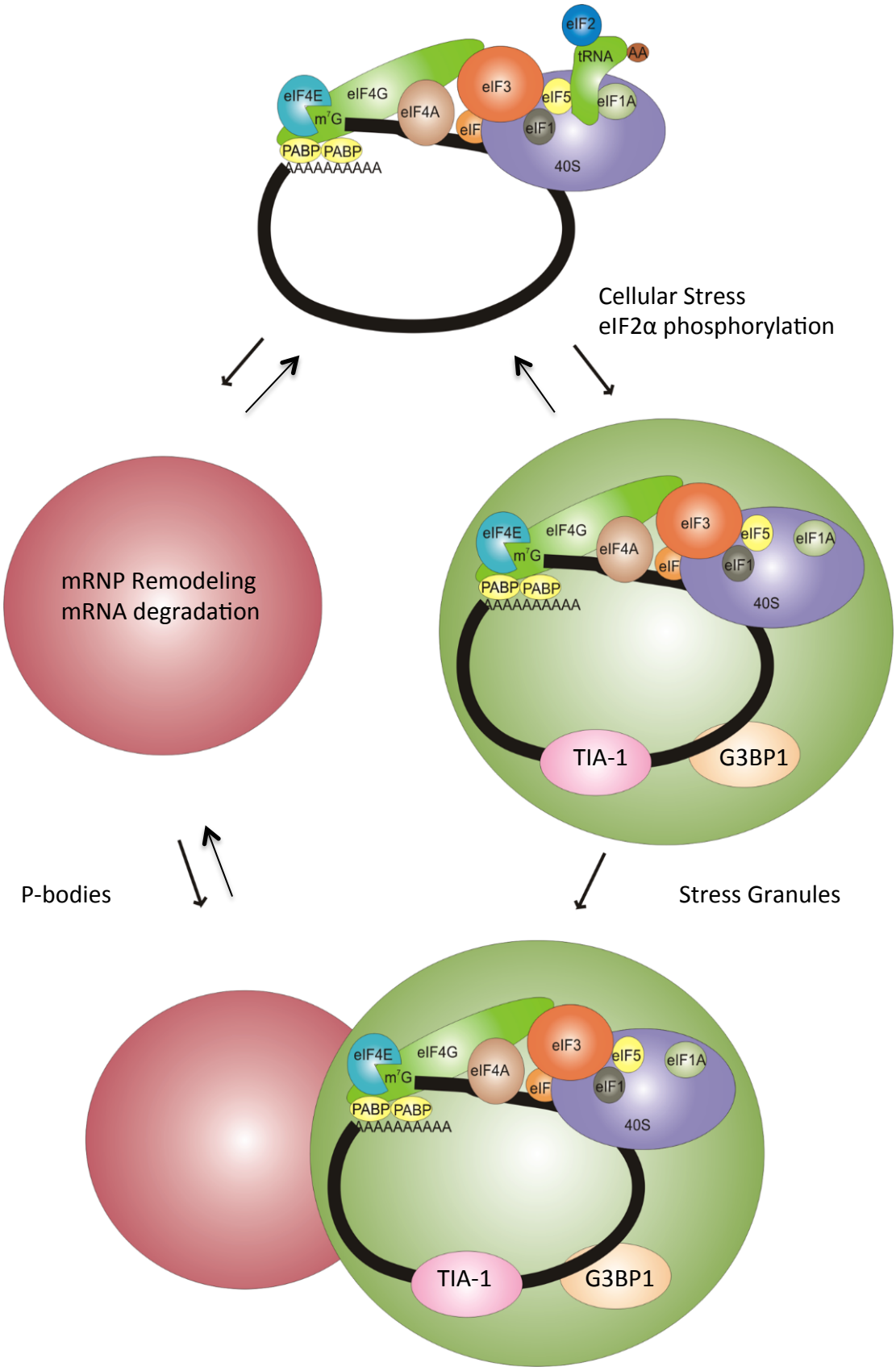

Figure 1.4 Overview of Stress Granules and P-bodies. P-bodies are shown in red. Stress granules are shown in green.

Following the removal of the stressor, the cell can choose to reinitiate translation, to continue to store the mRNA or degrade it [96]. Additional processing of the mRNA requires mRNP remodelling that requires components found in both SGs and P-bodies. Under certain conditions, SGs and P-bodies have been demonstrated to fuse together in the cell. It is thought that this allows an exchange of mRNAs and mRNPs to permit additional processing of mRNAs [113, 114].

Ultimately, the formation of SGs directly involves factors involved in translation initiation. Although canonical stress granules form in response to eIF2 phosphorylation, a number of eIF2 phosphorylation-independent mechanisms exist to form non-canonical SGs in response to different stresses. Non-canonical SG formation is propagated by inhibition of eIF4F complex formation either by depleting individual components or by using specific inhibitors. Further work is required to establish how components of the eIF4F complex are regulated in response to different stresses and determine whether or not these affect the ability to form SGs.

1.4 SUMOylation and the initiation of translation

The identification of SUMOylated substrates has been of keen interest for many years. Studies looking at the global SUMO proteome have primarily illustrated the wide range of cellular targets within the cell that govern different processes and in particular the response to cellular stress [4, 6]. Furthermore, validation and characterisation of the role of SUMO in regulating many of these newly identified protein targets remains to be established.

1.4.1 eIF SUMOylation

Intriguingly, numerous eukaryotic initiation factors have been identified, including all of the components of the eIF4F complex, in proteomic screens both in mammalian cells and in other organisms including *D. melanogaster* (see table 1.3). Despite their identification, few SUMOylated eIFs have been validated and investigated further to determine the role, if any, that SUMO has on their function. The mRNA cap-binding protein eIF4E has been shown to be SUMOylated on 5 lysine residues and the introduction of an unSUMOylatable mutant into cells impairs eIF4F assembly but not cap-binding suggesting that SUMO stabilises the eIF4E-eIF4G interaction [75]. Furthermore, the unSUMOylatable eIF4E mutant impairs translation of stress response mRNAs [75]. More recently, the molecular scaffold protein, eIF4G was shown to be SUMOylated on two residues within the C-terminus, with one site located within the eIF4A binding domain and the other in the MNK-1-binding domain [76]. Additionally, SUMOylation of eIF4G in *S. pombe* was increased following treatment with KCl which induces stress granule formation [76].

Table 1.3 eIFs identified in proteomic screens for SUMOylated substrates.

Protein	SUMO	Type of Screen/purification method	References
EIF1α	Rat SUMO-3	Immunoprecipitation of HA-SUMO3	[6]
EIF2A Subunit 1	Hs SUMO-1	Purification by crosslinking cysteine to beads	[3]
EIF2α	Drosophila SUMO	Dual purification of His-Flag-SUMO	[115]
EIF2B Subunit β	Hs SUMO-1/2	Purification of His-SUMO	[58]
EIF2B	Plant SUMO	Purification of His-SUMO1	[116]
EIF2 Subunit γ	Drosophila SUMO	Dual purification of His-Flag-SUMO	[115]
EIF3A	Hs SUMO-1	Purification by crosslinking cysteine to beads	[3]
EIF3B	Hs SUMO-1	Purification by crosslinking cysteine to beads	[3]
EIF3C	Hs SUMO-1/2	Purification of His-SUMO	[58]
EIF3D	Rat SUMO-3	Immunoprecipitation of HA-SUMO3	[6]
EIF3E	Hs SUMO-1/2	Purification of His-SUMO	[58]
EIF3I	Sp Smt3	Immunoprecipitation of ProtA-Smt3	[57]
eIF3M	Hs SUMO-1	Immunoprecipitation of endogenous SUMO1	[2]
EIF3X	Hs SUMO-2	Purification by crosslinking cysteine to beads	[3]
EIF4AI	Drosophila SUMO	Dual purification of His-Flag-SUMO	[115]
	Rat SUMO-3	Immunoprecipitation of HA-SUMO3	[6]
	Hs SUMO-2	Purification by polySUMO by SIM-trap	[4]
EIF4AII	Hs SUMO-1	Immunoprecipitation of endogenous SUMO1	[5]
EIF4E	Hs SUMO-1	Purification of His-SUMO1	[75]
EIF4GI	Hs SUMO-1/2	Purification by polySUMO SIM-trap immunoprecipitation of endogenous SUMO1	[4, 5]
eIF5A	Hs SUMO-1/2	Immunoprecipitation of endogenous SUMO1	[2]
PABP1	Hs SUMO-1 Sc SUMO	Purification by crosslinking cysteine to beads	[3, 117]
PABP4	Hs SUMO-1	Purification by crosslinking cysteine to beads	[3]

(Adapted from [118]: Table shows SUMOylated eukaryotic translation initiation factors identified in proteomic screens, Hs=Human, Sp=*Schizosaccharomyces pombe*, Sc=*Saccharomyces cerevisiae*, Plant=*Arabidopsis thaliana*).

Taken together these data suggest a potential role for SUMOylation of eIFs in regulating translation potentially linking the response to cellular stress with the formation of cytoplasmic stress granules. As SUMOylated eIF4E and eIF4G have been identified, it remains to be elucidated as to whether the third component of the eIF4F complex, the ATP-dependent helicase, eIF4A, can be SUMOylated and if so, what role this serves within mammalian cells.

1.5 Genotoxic stress and the response to DNA damage

Many types of DNA lesions arise as a consequence of genotoxic stress. The persistence of DNA lesions is highly detrimental, driving genomic instability, facilitating loss of genetic material and promoting incorporation of mutations, which may lead to genetic disorders including cancer [119]. Genotoxic stress can originate from either endogenous mechanisms, such as reactive oxygen species (ROS) or exposure to exogenous factors such as alkylating agents, ultraviolet (UV) light and ionising radiation (IR). Both types of cellular stress are capable of generating characteristic DNA lesions that require specialised mechanisms for their repair, collectively termed the DNA damage response (DDR). An extensive network of post-translational modifications orchestrates the DDR, and these modifications serve to enable DNA repair, dictate DNA repair pathway choice and activate cell-cycle controls. The following sections will briefly describe the mechanisms of repair including examples of PTMs (summarised in Table 1.4) that regulate the repair process, followed by more a more detailed overview of the Double-strand break (DSB) repair pathway.

Table 1.4 Examples of post-translational modifications governing repair pathways associated with genotoxic stress.

Protein	Cellular Response	PTM	References
PCNA	Recruitment of translesion synthesis polymerases	ubiquitination	[120]
PCNA	Suppression of Rad51 filament formation	SUMOylation	[48]
MutSα	Nuclear localisation of MMR repair factor	phosphorylation	[121]
OGG1	Increased base excision activity	phosphorylation	[122]
APE1	Increased DNA-binding capability	acetylation	[123]
XPC	Increased DNA-lesion recognition	ubiquitination	[124]
FANCI/D2	Controlled collapse of stalled replication forks	ubiquitination	[125]

1.5.1 Mismatch Repair (MMR)

An example of endogenously generated changes is during DNA replication, whereby replicative polymerases can facilitate the incorporation of an incorrect DNA base causing a mismatch. These events are rare and even when a mistake is made the replicative polymerases pol δ and pol ε are capable of proofreading the newly synthesised DNA sequence via 3' nuclease activity of these polymerases [126]. Mutations that affect the exonuclease activity of these polymerases cause an increase in misincorporation rates and result in an increased predisposition to cancer [127]. If DNA mismatches are not corrected by the polymerases, the cell can employ a specialised mechanism to identify and repair mismatches, termed mismatch repair (MMR). DNA mismatches are recognised by an MSH2-MSH6 heterodimer, which recruits PMS2 and MLH1. PCNA stimulates PMS2 and MLH1 to produce a nick in the DNA. The strand containing the mismatch is either removed by the exonuclease, Exo1 or displaced by the progressing polymerase, which resynthesizes the oligonucleotide to traverse the gap. Finally, the ends of the DNA fragments are ligated together to complete the repair process [128]. If DNA mismatches are not corrected before the next round of replication, a mutation will be incorporated.

The DNA mismatch recognition machinery, MSH2-MSH6 also referred to as the MutSα complex, is subject to post-translational modification by phosphorylation. Failure to phosphorylate MutSα impairs MMR by affecting its nuclear localisation [121].

1.5.2 Base Excision Repair (BER)

Reactive oxygen species (ROS), generated through cellular respiration, are capable of generating many different DNA lesions including 8-oxo-7,8-dihydro-guanine (8-oxoG). ROS-induced 8-oxoG is one of the best-characterised DNA lesions. 8-oxoG can base pair with an adenine nucleotide during replication, and if it remains unrepaired it can lead to a G:C to A:T transversion. As a result, it is important that these types of lesions are effectively repaired. The cell employs a repair mechanism to recognise, remove and correct the damaged base called base-excision repair (BER). BER of 8-oxoG requires the human 8-oxo-guanine DNA glycosylase 1 (hOGG1) protein that specifically recognises the lesion, flips out the base and catalyses its removal. Removal of guanine generates an apurinic base within the DNA strand. Additional processing by Apurinic/apyrimidinic endonuclease 1 (APE1) is required. APE1 cuts the DNA backbone to generate a 3' hydroxyl group in the sugar-phosphate backbone, thereby allowing the incorporation of a guanine nucleotide by polβ, which can then be ligated into the DNA backbone [129, 130]. Interestingly, OGG1 is post-translationally regulated, whereby phosphorylation by the serine/threonine kinase Cdk4 increases its activity [122].

DNA lesions can also be endogenously generated by deamination of 5-methycytosine to uracil by cytidine deaminases or by spontaneous depurination of adenine and guanine bases to generate an apurinic site [131, 132]. The removal of uracil from DNA requires BER via the use of uracil DNA glycosylase to generate an apyrimidinic nucleotide. However, repair of apurinic sites generated by depurination of bases can proceed directly to AP endonuclease-dependent processing of the break before replacement of the nucleotide by polβ [133]. APE1 is regulated by several post-translational modifications. Acetylation of APE1 enhances its ability to bind to DNA, conversely phosphorylation and subsequent ubiquitination of APE1 target it for proteasomal degradation [123, 134].

1.5.3 Nucleotide Excision Repair (NER)

Nucleotide excision repair facilitates the repair of a number of DNA lesions that distort the DNA helix structure, including ultraviolet (UV) light-induced photoproducts. The most common DNA lesions generated by exposure to UV light are cyclobutane-pyrimidine dimers (CPDs). There are two ways in which the NER machinery can recognise DNA lesions. Global genome NER (GG-NER) scans the genome for lesions, which distort the DNA helix. Following recognition of a lesion by XPC, RAD32, RAD32B, CETN2 and UV-radiation-DNA damage-binding protein (UV-DBB) [135], the transcription initiation factor IIH (TFIIH) complex is recruited to the site containing the lesion. Recently, it was demonstrated that binding of the CDK-activating kinase (CAK) module to TFIIH inhibits its intrinsic DNA binding capability, allowing XPC to direct recruitment of TFIIH to NER specific substrates. Once recruited, the CAK module then dissociates from TFIIH [136, 137]. Once TFIIH is recruited it opens up the DNA structure for further processing. XPF and XRCC1 commit to repair by NER by making an incision into the 5' side of the lesion. XPG generates an incision on the 3' side of the lesion allowing the lesion-containing DNA strand to be excised [135]. The region of single-stranded DNA (ssDNA) generated is protected by replication protein A (RPA). DNA polymerase fills the gap generated before DNA ligases seals the sugar-phosphate backbone to complete the repair process [138]. Furthermore, the association of XPC with the DNA lesion is enhanced by polyubiquitination, which is catalysed by the E3 ubiquitin ligase activity of its binding partner, UV-DBB [124].

A second mechanism exists for the recognition of DNA lesions requiring NER in highly transcribed genes. Transcription-coupled repair (TCR) allows the recruitment of the NER machinery directly to the stalled RNA polymerase (RNA polII): this requires CSA, CSB, UVSSA and USP7 [139]. Following recognition of the lesion, NER continues as before with the excision of the lesion-containing DNA strand before gap filling and ligation [135].

Some rare genetic disorders are associated with mutations in genes encoding NER and TCR proteins. Xeroderma Pigmentosum (XP) results from mutations in XP proteins required for NER and results in hypersensitivity to UV light in patients. Likewise, mutations in CSB or CSA result in Cockayne syndrome (CS), which is characterised by hypersensitivity to UV light and neurodegeneration [135]. Interestingly, CSB also has a ubiquitin-binding domain, which if deleted, produces a CS-like phenotype despite still being recruited to damage sites, indicating a role for post-translational modification in TCR [140].

1.5.4 Direct reversal of DNA damage

The formation of O^6-methylguanine by alkylating agents such as temozolomide (TMZ) can result in incorrect base pairing during replication. A specialised methyltransferase termed O^6-methylguanine-DNA methyltransferase (MGMT) removes the methyl group from guanine and in doing so the protein becomes non-functional i.e. each MGMT molecule can only remove one methyl group from a damaged base. As a result, epigenetic control of MGMT expression governs sensitivity of cancerous cells to alkylating agents such as TMZ [141]. Furthermore, targeting of MGMT using O^6-benzylguanine, an MGMT inhibitor, sensitises cells to DNA alkylating agents [142].

1.5.5 Translesion Synthesis

DNA lesions that are present during replication can cause replication to slow, stall, or if unresolved, even cause the replication fork to collapse. As a result, it is critical that the cell repairs or resolves these lesions prior to the following round of DNA replication. An additional mechanism enables the replicative polymerase to continue through DNA lesions at the expense of likely incorporating mutations into the newly synthesised DNA strand. A unique subset of polymerases can be utilised by the cell to bypass the DNA lesion during replication. The normal replicative polymerases display high fidelity and high processivity and are specialised for replicating large regions of DNA accurately whereas the Y-family polymerases possess a larger active site allowing the incorporation of nucleotides opposite DNA lesions. These polymerases are recruited to the replication fork through interactions with mono-ubiquitinated Proliferating Cell Nuclear Antigen (PCNA) via PCNA-interacting protein (PIP) boxes and ubiquitin-binding motifs [42, 120]. PCNA can be SUMOylated and ubiquitinated. When SUMOylated, PCNA recruits Srs2 through a SIM to suppress Rad51 filament formation, further highlighting the diverse role of functions directed by post-translational modification of proteins [48].

Some DNA lesions require more than one repair pathway to correct certain types of damage. Interstrand crosslinks (ICLs) occur between the two anti-parallel strands of DNA. Chemotherapeutic agents commonly generate ICLs, which are highly toxic to cells if unrepaired. The repair of ICLs occurs during S-phase and is triggered by the stalling of the replication fork. When the replication fork stalls, endonucleases are required to 'unhook' one of the strands containing the ICL, thereby resulting in the controlled collapse of the replication fork and the generation of a DSB. A TLS polymerase is required to read through the lesion containing the ICL. The DSB can then be resolved by homologous recombination (HR) before restarting the replication fork. Resolution of ICLs requires FANC proteins, associated with Fanconi anaemia (FA). It is currently thought that the monoubiquitinated FANCI-FANCD2 complex directly binds to the DNA structure produced by replication forks colliding with an ICL and that this complex recruits the specific endonucleases such as Fanconi-associated nuclease 1 (FAN1) [125].

1.5.6 Single-strand break repair (SSBR)

Different repair processes exist for the resolution of single- and double-stranded DNA breaks. Single-strand breaks (SSBs) can be generated by ROS as mentioned earlier, or as intermediates in BER. SSBs are recognised by direct binding and activation of PARP-1, which proceeds to PARylate proteins in the regions of the lesion including itself [143]. Following, PARylation PARP dissociates from the region of the break allowing the association of end processing factors. Due to the variation in the DNA ends produced (which is dependent upon the source of damage), the cell has to process the DNA ends to produce a 3' hydroxyl group and a 5' phosphate. This process can require a number of proteins including APE1 endonuclease, utilised in BER. After the preparation of the DNA ends, gap-filling by a polymerase can occur. Additional complexity is introduced by the ability of the polymerase to displace the 5' nucleotides to create a 5' DNA flap, known as 'long-patch' repair. The 5' DNA flap has to be removed by FEN1 endonuclease. Finally, the incorporated base or bases are ligated into DNA strand by DNA ligase IIIα [144].

1.6 DSB recognition

Double-strand breaks (DSBs) in DNA form some of the most deleterious lesions to the genome, potentially resulting in gross chromosomal loss or translocations [7]. DSBs are generated by ionising radiation, the collapse of replication forks or as part of cell-type specific functions such as V(D)J recombination in lymphocytes [145]. The recognition of the DSB site requires PTM of a number of targets to enable the recruitment of additional DSB repair mediators. Table 1.5

summarises examples of PTMs that occur at DSB sites. These examples are explained in more detail in this section.

Table 1.5 Examples of PTMs that occur at DSB sites.

Protein	Cellular response	PTM	References
H2AX	Recruitment of MDC1	phosphorylation	[146]
ATM	Activation of ATM kinase activity	phosphorylation	[147]
H2A	Recruitment of 53BP1	ubiquitination	[9]
Mre11	Regulation of nucleolytic activity	phosphorylation	[148]

The initial step in repairing DNA DSBs is the recognition and marking of the break site. DSBs are primarily recognised by the heterotrimeric complex MRN. MRN is composed of three subunits, MRE11, RAD50 and NBS1. DNA binding by the MRN complex is facilitated by the 'closed' conformation induced by Rad50 bound to ATP. Mre11 is a 3' to 5' endo-exonuclease that mediates the interaction of the MRN complex with the broken DNA ends. The 'closed' MRN conformation suppresses the nuclease activity of Mre11 to prevent unwarranted resection of broken DNA ends [149].

Recruitment of the MRN complex to the DNA ends serves as a recruitment platform for the DNA damage sensing PI3-kinase, Ataxia telangiectasia mutated (ATM). ATM is recruited through interactions with the C-terminal tail of Nbs1 [147]. In its inactive form ATM is a homodimer, but activation of the kinase stimulates autophosphorylation of serine-1981 and the kinase becomes a monomeric. Once recruited to DSBs, ATM proceeds to phosphorylate the histone variant H2AX on serine-139, to produce a form termed γH2AX [146]. γH2AX is widely accepted as a marker of DSBs within cells and is used to recruit DDR proteins to the site of DNA damage [150].

Mediator of DNA damage checkpoint protein 1 (MDC1) interacts directly with γH2AX through its BRCA1 C-terminal (BRCT) domains [151]. MDC1 recruits another MRN complex through phosphorylation-dependent interactions between NBS1 and the Forkhead-associated (FHA) domain of MDC1 [152]. The additional recruitment of MRN localises and activates more ATM resulting in the spreading of the γH2AX signal along the chromatin flanking the break site [153] (figure 1.5).

Following the marking of the break site by the generation of γH2AX along the chromatin, both histone H2A and H2AX are subject to further post-translational modification by ubiquitin. Ring finger protein 8 (RNF8), an ubiquitin E3 ligase, is rapidly localised to sites of DNA damage and

proceeds to polyubiquitinate histone H2A and H2AX via an E2 ubiquitin conjugating enzyme UBC13. The generation of K63-linked ubiquitin chains facilitates the recruitment of a second E3 ubiquitin ligase, RNF168 [154]. RNF168 proceeds to monoubiquitinate H2A and H2AX on K15, which along with histone 4 K20-dimethylation (H3K9me2), is recognised the DNA damage mediator 53BP1 [155] (figure 1.6).

Recently, Mre11 has been demonstrated to direct repair pathway choice by initiating the end resection of broken DNA ends. Once recruited to sites of double strand breaks, Mre11 can make an incision adjacent to the DSB and then resect DNA back towards the break site in the 3’ to 5’ direction. The endonucleolytic incision is viewed as a licencing step for progression towards homology directed repair (HDR). Subsequent activity by Mre11, Exo1 and CtIP are required for 5’ to 3’ resection away from the break in order to promote homology directed repair (HDR). Furthermore, inhibition of either the exonuclease or endonuclease activity of Mre11 confers a HDR defect and forces cells to repair DSBs by NHEJ [156]. Recently, two phosphorylation sites in Mre11, S676 and S678, were identified as ATM phosphorylation targets. Failure to phosphorylate these residues also results in defective HDR. Furthermore, un-phosphorylatable Mre11 results in aberrant control of end resection by Exo1, resulting in excessive resection, as measured by an increase RPA focus intensity [148].

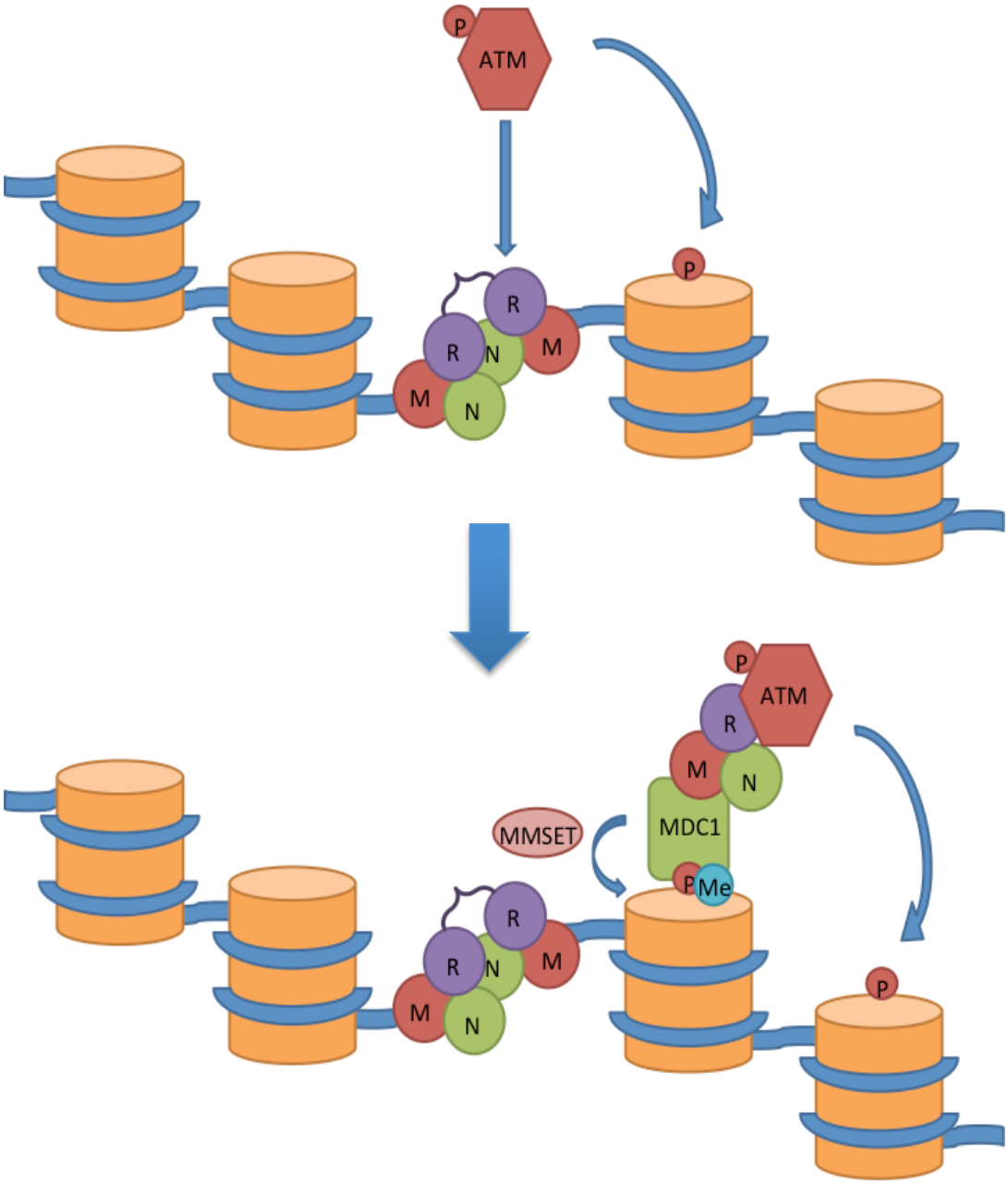

Figure 1.5 Mechanism of DSB recognition (γH2AX signal spreading along chromatin). dsDNA (blue) is wrapped around nucleosomes (organge). MRN complex (red, green and purple circles labelled 'M', 'R' and 'N') recognises broken DNA ends. MMSET methyltransferase (pink) methylates histone H4 (blue circle labeled 'Me'). Phosphorylation of histone H2AX (red circle labeled 'P').'

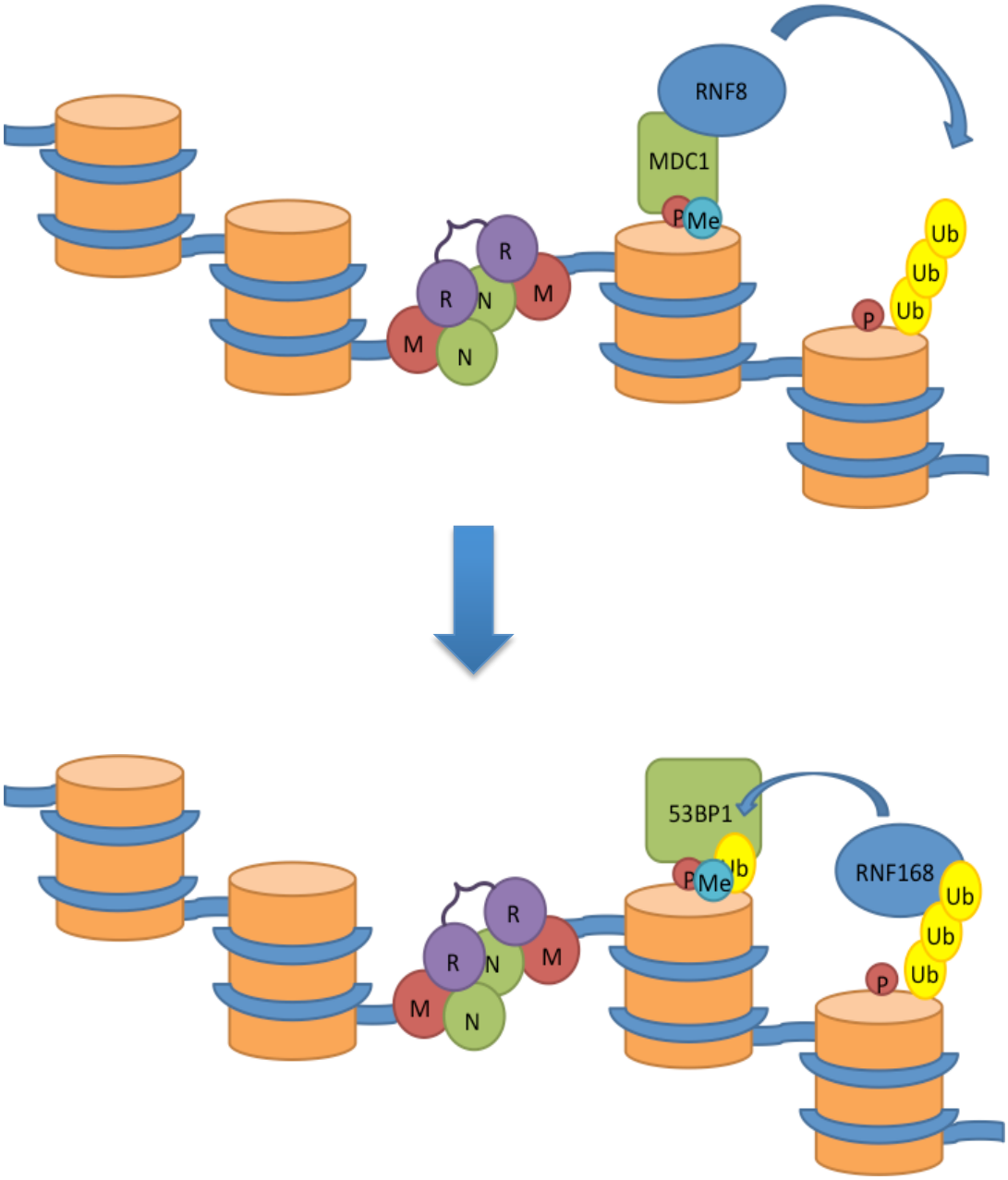

Figure 1.6 Mechanism of DSB recognition (recruitment of 53BP1). Ubiquitin E3 ligases RNF8 and RNF168 ubiquitinate histone H2A (yellow circle labelled 'Ub' histone).

1.7 DSB repair pathways

Following on from the recognition and marking of the DSB site by various post-translational modifications and the subsequent recruitment of mediator proteins, the DNA ends can be processed to allow repair of the break. Predominantly, four repair mechanisms exist within cells to repair these types of lesions, three of which require resection and the generation of ssDNA overhangs as a prerequisite for repair.

1.7.1 Non-homologous end joining (NHEJ)

NHEJ is one of the most prevalent repair pathways utilised by cells to repair DSBs. NHEJ can be employed throughout the cell-cycle as it does not rely on the availability of a sister chromatid for use as a template for repair. Essentially, NHEJ involves re-ligation of the broken DNA ends. However, if the broken ends are resected by nucleases prior to re-ligation, a loss of genetic material is incurred. As a result NHEJ is viewed as a highly error-prone mechanism of DNA repair.

DSB repair by NHEJ requires the recognition of the broken DNA ends by the heterodimeric Ku70/Ku80 complex [157]. The Ku complex serves as a binding platform for other factors. DNA protein kinase catalytic subunit (DNA-PKcs) is then recruited and together with Ku bound to DNA, collectively forms the active PI3-kinase, DNA-PK [158]. DNA-PK is capable of forming a synapse between the two broken ends, holding them within proximity to one another. Synapsis also protects the DNA ends from nucleases, which could cause deletion of bases prior to repair [31]. Recruitment of XRCC4, DNA ligase IV is promoted by APLF and together with XLF the complex re-ligates the broken DNA ends back together to complete the repair process [159] (figure 1.7).

Genotoxic stresses that induce DSBs can produce DNA breaks with single strand overhangs. Under these circumstances the cell is forced to employ specific nucleases, such as Artemis, to remove the overhang from these breaks prior to ligation [160]. Artemis is recruited following phosphorylation DNA-PK by ATM [161]. X-family polymerases can fill gaps generated by DNA end processing without the need for a template. In NHEJ, terminal deoxyribonucleotidyl transferase (TdT), pol μ or pol λ are required for gap filling [162].

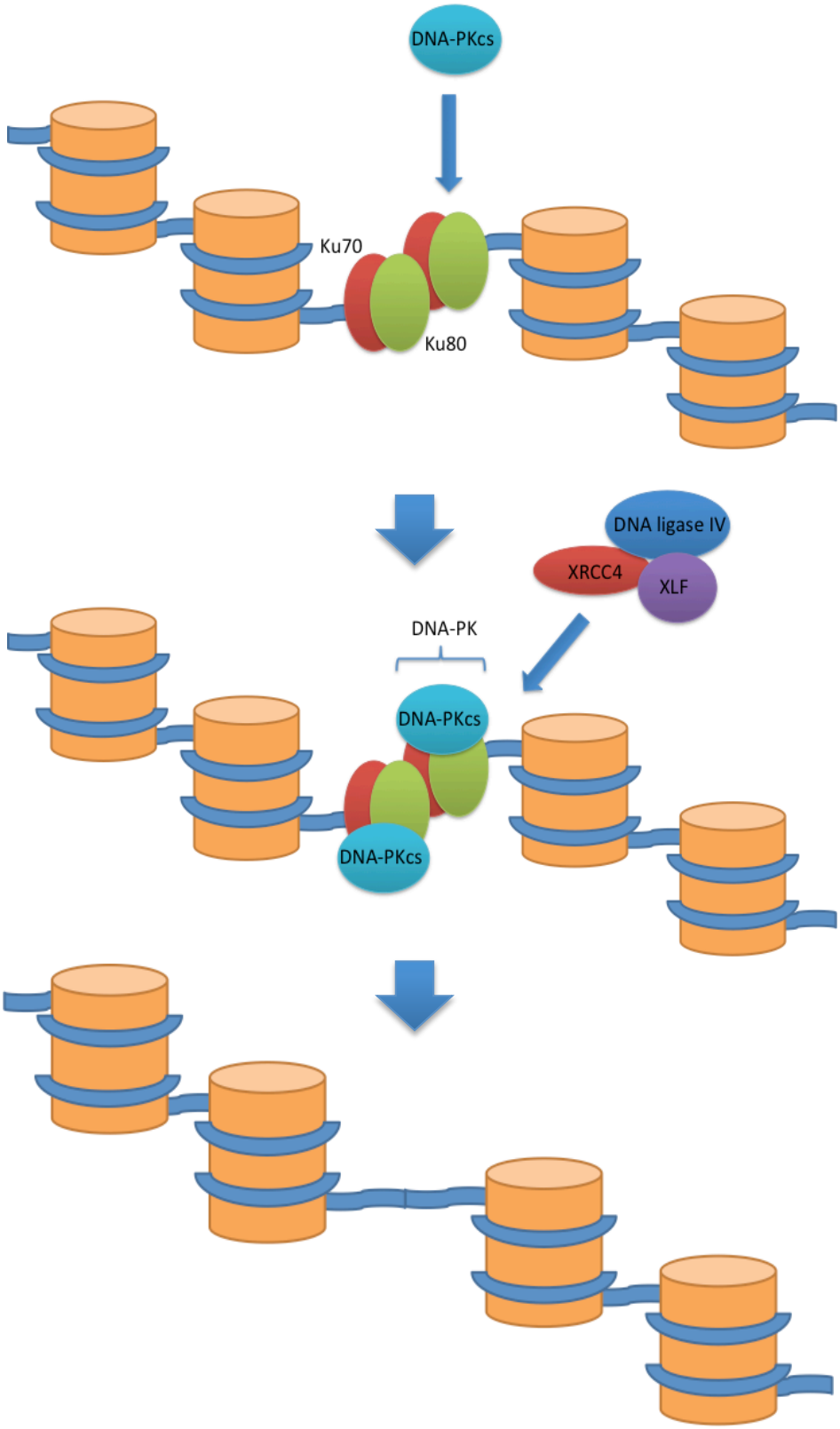

Figure 1.7 Repair of DSBs by NHEJ. Broken DNA ends are recognised by the Ku70/Ku80 heterodimer (red and green ovals).

1.7.2 Microhomology-mediated end joining (MMEJ)

MMEJ, also known as alternative-NHEJ (alt-NHEJ), requires recognition of the broken DNA ends by PARP-1 instead of the Ku heterodimer (used in classical-NHEJ) [163]. Following this, the broken DNA ends are resected by Mre11 and CtIP, to generate two single-stranded 3' overhangs. The overhangs generated in this process are used as substrates for either HR or MMEJ [164]. Unlike HR, Pol θ binds to 3' overhangs and is thought to use a unique helicase-like domain to promote microhomology binding between the two sets of overhangs [165]. Following binding, Pol θ extends each of the DNA strands using the other overhang as a template. Following extension the DNA ends can be ligated together. Due to the use of resection to facilitate microhomology search MMEJ will generate errors and only accounts for the repair of a small subset of DNA breaks [166] (figure 1.8).

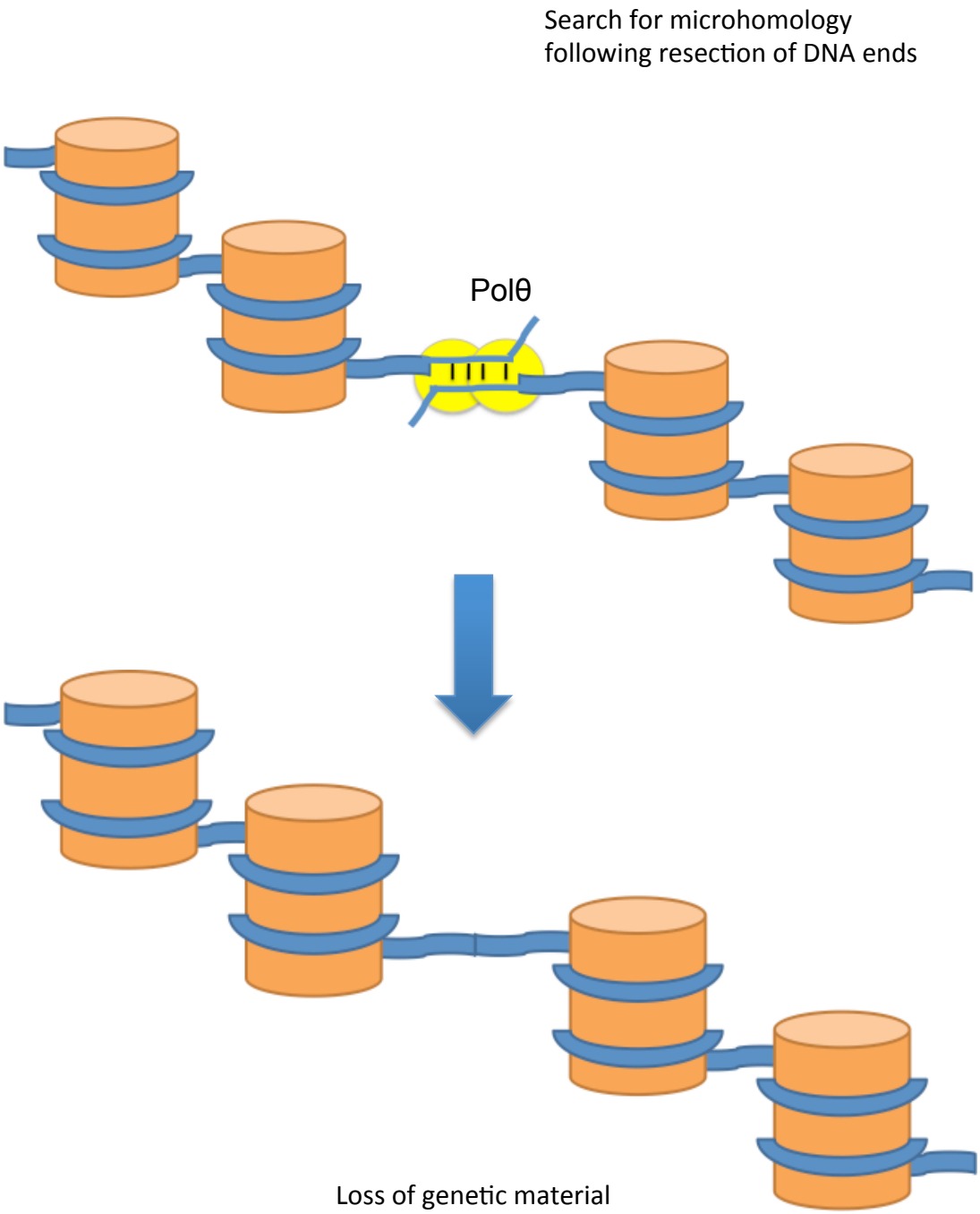

Figure 1.8 Repair of DSBs by MMEJ. Thin blue strand represents resected DNA ends. Black vertical dashes indicate regions of microhomology between resected DNA strands.

1.7.3 Homologous recombination (HR)

HR is a specialised repair pathway limited to S- and G2-phase cells due to the requirement of the sister chromatid for use as a template for repair. Due to the use of an exact copy as a template, this type of repair is error-free [167].

Repair by HR requires extensive end resection of the broken DNA ends initiated by Mre11 and extended by the 5' to 3' exonucleases, Exo1 and CtIP [156, 168]. The single stranded 3' overhangs generated are prevented from forming unwanted secondary structures by the association of RPA [169]. RPA is then removed from the ssDNA and replaced by Rad51. Rad51 forms a filament on the ssDNA, which is mediated by the Shu complex in yeast, which comprises several Rad51 paralogues and BRCA2 [170].

Following Rad51 filament formation the cell initiates the search for the homologous region. Two features of Rad51 nucleofilaments permit efficient searching for homology: firstly the nucleofilament has the ability to slide a short-range (approximately 16 bases) along the sister strand [171]. Secondly, nucleofilaments can bridge interactions with several non-contigous sequences on the sister strand, allowing homology search over a large distance simultaneously [172]. Upon identification, Rad51 mediates base pairing between the 3' overhang and the sister chromatid. Base pairing, facilitated by Rad54, results in the displacement of the complementing DNA strand of the sister, generating a D-loop structure [173]. Polymerases extend the crossed strands and fill in the gaps to form a secondary intermediate known as a double-Holliday junction (DHJ) [174] (figure 1.9).

Resolution of DHJs can give rise to either crossover or non-crossover events depending upon the orientation of incisions made at the junction. Three endonuclease complexes mediate these incisions, GEN1, MUS81-EME1 and SLX1-SLX4. Interestingly, MUS81-EME1 and SLX1-SLX4 have been demonstrated to work together with the former complex generating a nick in the DNA, which can then be efficiently processed by SLX1-SLX4 [175, 176]. Importantly, suppression of potential crossover events requires the BTR complex (BLM, TopoIIIα, RM1 and RM2), which suppresses both crossover and non-crossover events by promoting dissolution of the DHJ [177]. Furthermore, MUS81-EME1 and SLX1-SLX4 association requires CDK1 activity, indicating a role for post-translational modification in promoting potential crossover events [178].

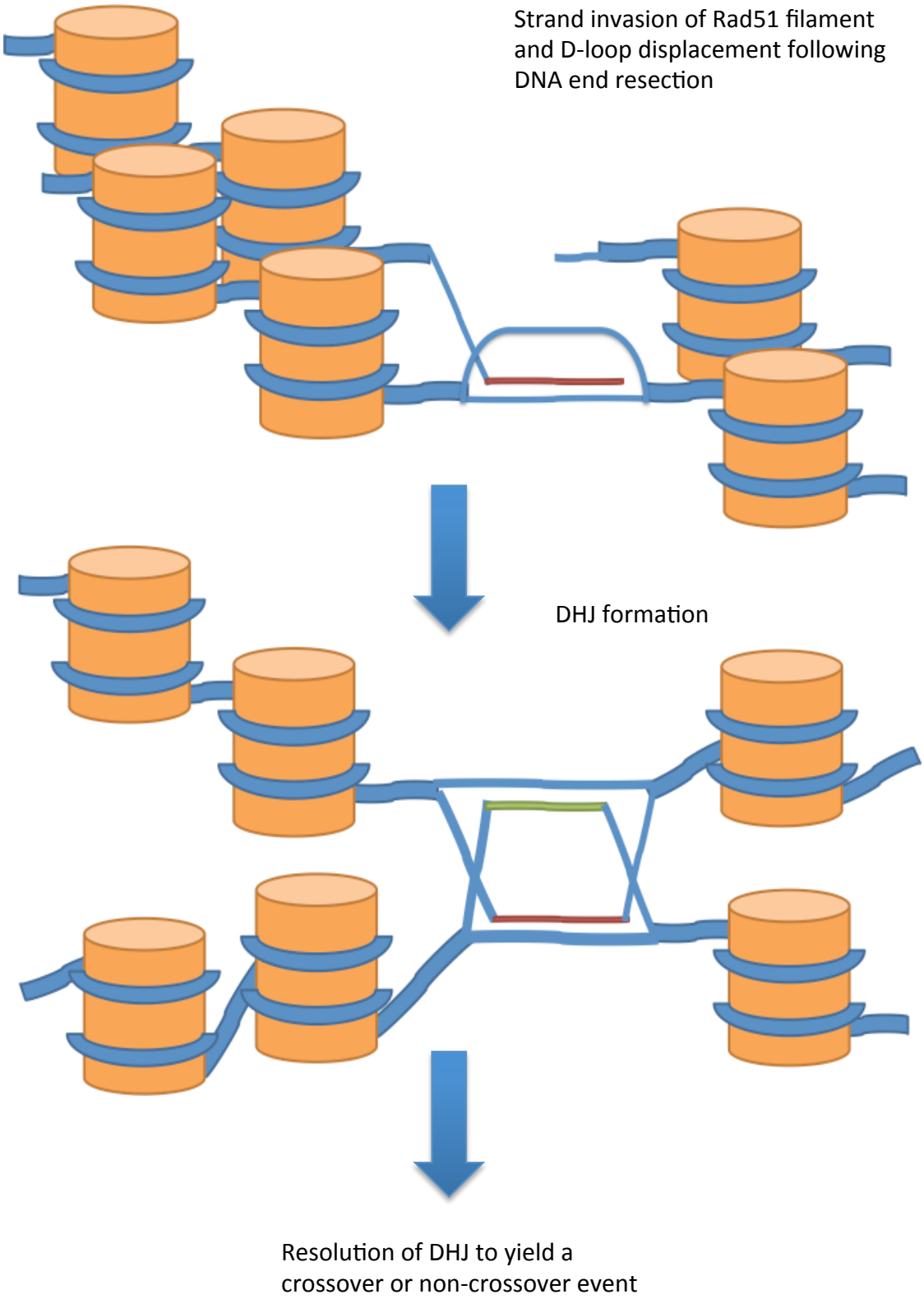

Figure 1.9 Repair of DSBs by HR. The invading ssDNA strand (red) displaces the 5'-3' strand of the sister chromatid. Red and green lines indicate extension of of the invading strand using the opposite strand as a repair template.

1.7.4 Synthesis dependent strand annealing (SDSA)

SDSA permits the resolution of DSBs using the sister chromatid as a template without the risk of generating a crossover event. As with HR, SDSA requires the resection of DNA ends, Rad51 filament formation, D-loop displacement and the extension of the invading nucleofilament. Instead of utilising endonucleases or the BTR complex to resolve the structure, RECQ5 helicase displaces Rad51 from the nucleofilament [179]. The newly synthesised DNA segment is re-annealed to the original strand to complete the sequence. DNA polymerases are then required to fill the gap generated as a result. Finally, the DNA ends are ligated together to complete the repair process [175] (figure 1.10).

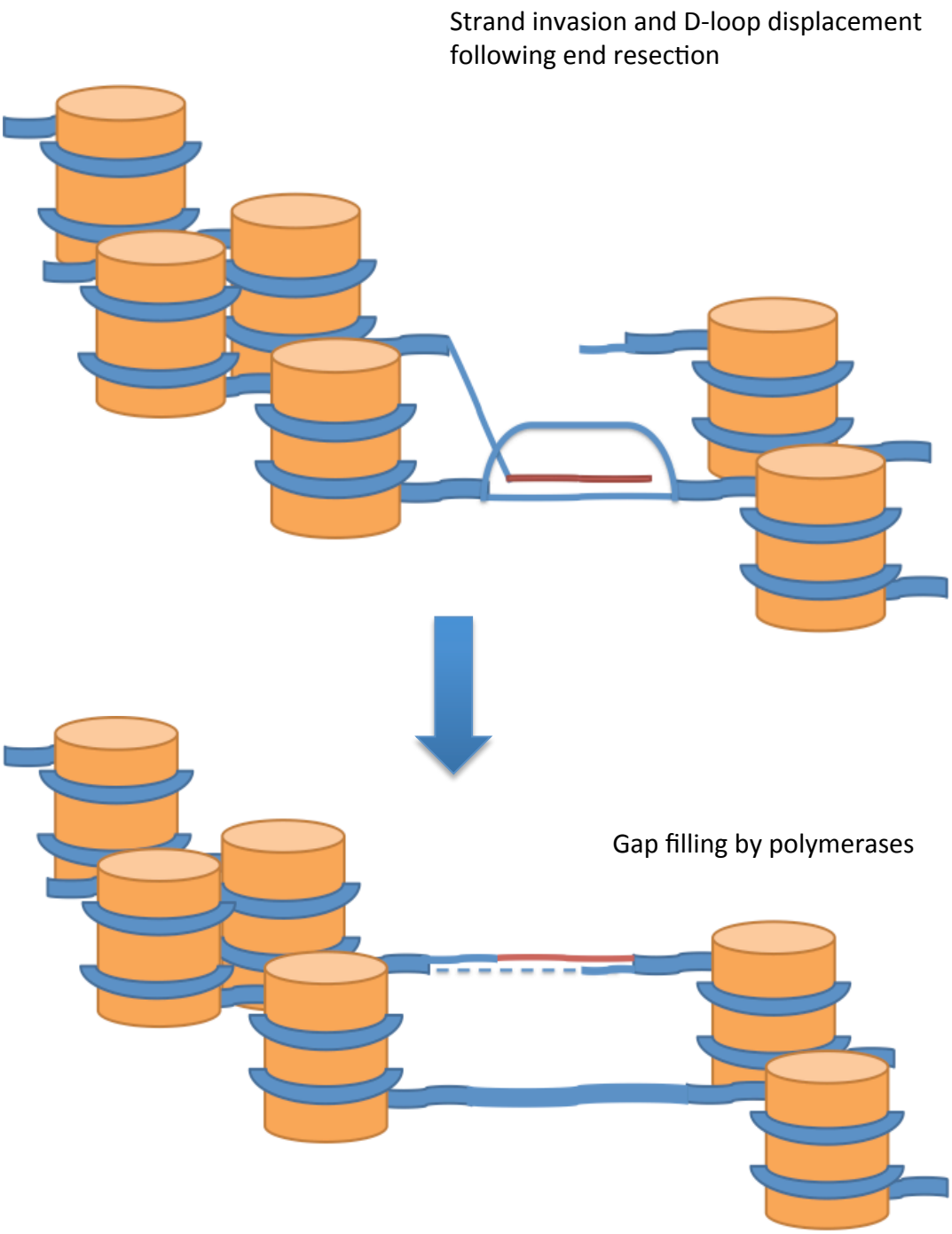

Figure 1.10 Repair of DSBs by SDSA. The red line indicates the extension of the invading strand using the sister chromatid as a repair template. Following extension, the newly synthesised strand is ligated to the original chromatid while a polymerase fills the gap generated (dotted line).

1.8 Role of p53-binding protein 1 (53BP1)

1.8.1 Structure and recruitment of 53BP1 to DNA

The DNA damage mediator protein 53BP1 has a number of distinct domains that mediate recognition and recruitment to sites of DNA damage, along with regions mediating protein-protein interactions that are critical for influencing the repair pathway choice and for the activation of associated checkpoint kinase signalling pathways.

The 'core' focus-forming region of 53BP1 comprises the oligomerisation domain (OD), a glycine-arginine rich (GAR) motif, a tandem Tudor domain and the ubiquitination-dependent recruitment (UDR) domain. As well as these domains, 53BP1 also contains a large N-terminal region containing 28 SQ/TQ phosphorylation motifs, which are capable of mediating several phosphorylation-dependent protein-protein interactions and lastly, at the C-terminus, there are tandem BRCA1 C-terminal (BRCT) domains [8] (figure 1.11).

The GAR domain was initially identified by immunoprecipitation of substrates with antibodies recognising methylated MRE11 in which 53BP1 was identified. It was observed that 53BP1 is methylated by PRMT1 within the GAR domain and it was then proposed that this region co-operated with the Tudor domains to mediate the recruitment of 53BP1 to ionising radiation-induced foci (IRIF) as pre-treatment with methylase inhibitors prevented recruitment of 53BP1 to sites of damage. Conversely, cells expressing 53BP1 with a mutant GAR domain were able to localise to damage normally [180]. This indicates a potential role for negative regulation of recruitment of 53BP1 to IRIF by methylation.

The tandem Tudor domains of 53BP1 specifically recognise and bind to di-methylated histone H4 on lysine-20 (H4K20me2). This interaction is critical for localisation of 53BP1 to sites of DNA damage. Recruitment of 53BP1 to IRIF via the Tudor domains is predominantly governed by methyltransferases MMSET and SETDB8, which have been shown to concentrate their activity at sites of DNA damage [181, 182]. However, as histone methylation is observed ubiquitously throughout the genome, it is also proposed that epitope masking by L3MBTL1, JMJD2A and polyubiquitin antagonises the recruitment of 53BP1. Following the generation of DSBs, methylated histones are unmasked facilitating 53BP1 recruitment [183-185]. Furthermore, the oligomerisation of 53BP1, via the OD domains, is required for its efficient recognition of methylated histones by the Tudor domains and for efficient recruitment into IRIF [186].

An additional level of complexity is introduced by the identification of the UDR domain, through which 53BP1 recognises mono-ubiquitinated H2A and H2AX on lysine-15 [155], which

is a DNA damage specific modification generated by the E3 ubiquitin ligase RNF168 [187]. The ubiquitin-binding activity of RNF168 was shown to be critical to for the retention of 53BP1 to sites of DNA damage [188]. Mutation of the UDR domain prevents focus formation by 53BP1 indicating a co-operative role for both ubiquitin and methylation recognition in localising 53BP1 to sites of DNA damage. Ubiquitin-dependent accumulation of 53BP1 to sites of DNA damage facilitated by the E3 ligases RNF8 and RNF168 is directly antagonised by the de-ubiquitinating enzyme, POH1, a component of the proteasome [184].

The SQ/TQ motifs are phosphorylation motifs located within the N-terminus of 53BP1, many of which are phosphorylated by the PI3-kinase ATM following its activation. Phosphorylation of these sites mediate further phospho-specific protein interactions with proteins such as Rif1 and PTIP, both of which have been shown to facilitate the downstream effects of 53BP1 (i.e. limiting DNA end resection and fusion of unprotected telomeres) [189-191]. However, many non-SQ/TQ motif residues within the N-terminus of 53BP1 may also be phosphorylated and have yet to be characterised. Furthermore, the replication-licensing factor and DNA damage response mediator TopBP1 (Topoisomerase IIβ-binding protein 1) is recruited to breaks by 53BP1, through its N-terminus, in a phosphorylation-dependent manner [192]. Interestingly, this particular interaction is also cell-cycle specific, integrating both damage response signalling and cell-cycle control [193].

Classically, BRCT domains are thought of as phosphorylation-dependent binding modules, which mediate protein-protein interactions between a phosphorylated peptide and the BRCT containing protein. However, the BRCT domains of 53BP1 can mediate a number of phosphorylation-independent interactions. The tumour suppressor protein p53 interacts directly with the BRCT domain of 53BP1 in a phosphorylation-independent manner [194, 195]. The BRCT domains also interact with Rad50 in complex with Mre11 and can also interact with the chromatin remodelling protein EXPAND1 [196, 197]. In *S. pombe* Crb2^{53BP1} and *S.cerevisiae* Rad9^{53BP1}, the BRCT domains have been shown to mediate phosphospecific interactions with γH2A.1 and γH2A respectively [198, 199]. Whether or not the BRCT domains of 53BP1 are capable of mediating phosphorylation-dependent protein interactions remains to be established and is the topic of chapter 5.

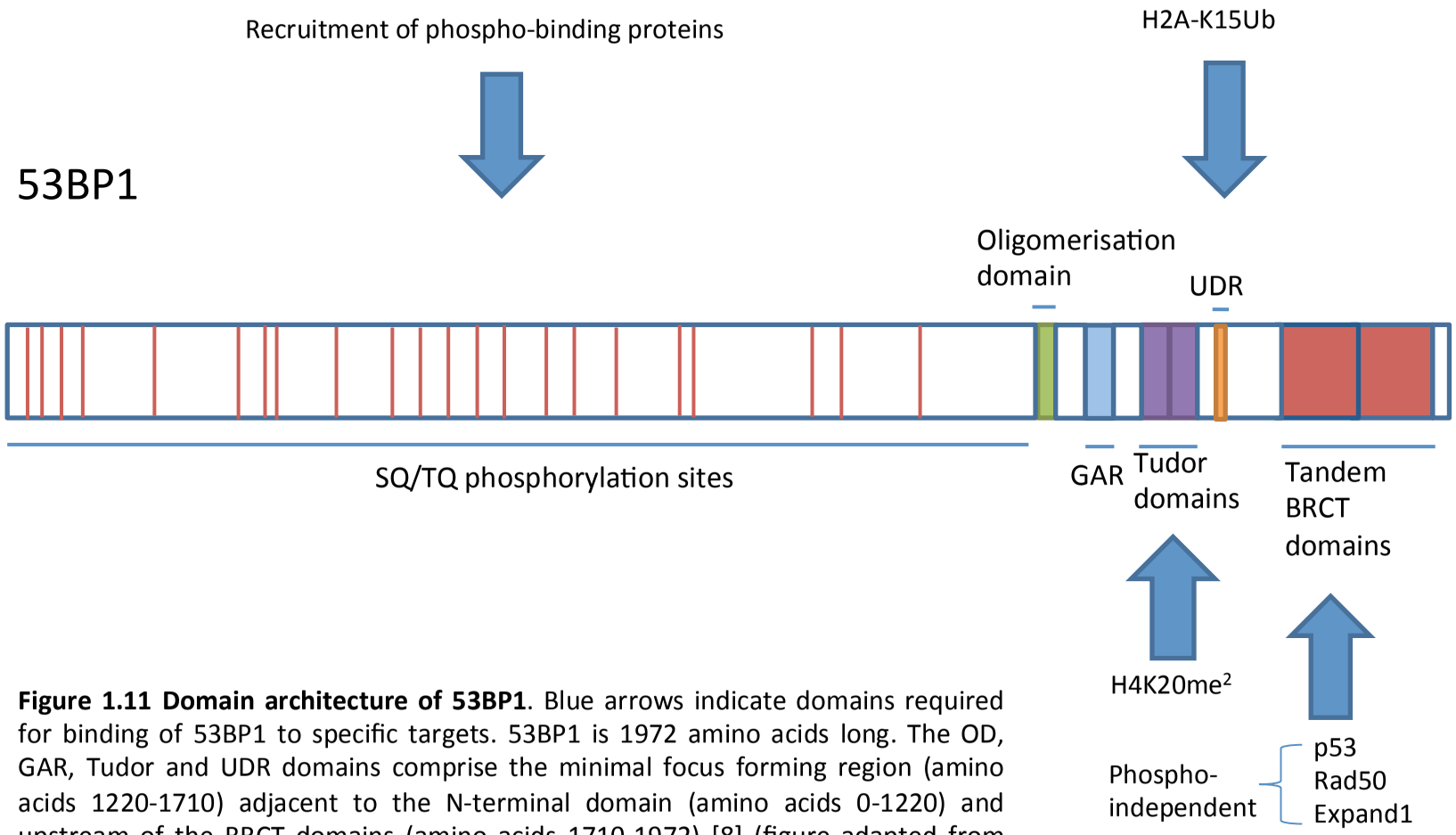

Figure 1.11 Domain architecture of 53BP1. Blue arrows indicate domains required for binding of 53BP1 to specific targets. 53BP1 is 1972 amino acids long. The OD, GAR, Tudor and UDR domains comprise the minimal focus forming region (amino acids 1220-1710) adjacent to the N-terminal domain (amino acids 0-1220) and upstream of the BRCT domains (amino acids 1710-1972) [8] (figure adapted from [176]).

1.8.2 Functions of 53BP1

53BP1 mediates several important functions in response to DNA damage. Firstly, 53BP1 regulates the repair pathway choice, favouring error prone NHEJ over HR by antagonising the resection of broken DNA ends [190]. Secondly, 53BP1 transduces the DNA damage response requiring ATM-dependent phosphorylation of its N-terminal domain in order to mediate interactions with downstream factors required for its function [200]. Furthermore, the activation of ATM serves as a critical signalling node, transducing the damage signal via phosphorylation to a vast number of downstream mediators and effector proteins including Chk2, which induces cell-cycle arrest [201]. Thirdly, the reorganisation of the chromatin structure in the region surrounding the DSB, often considered as a barrier to the repair process, requires 53BP1 and the damage response kinase ATM [202, 203]. The 53BP1-dependent reorganisation of chromatin has been studied further by analysing the mobility of unprotected telomeres, it has been demonstrated that 53BP1 is required for long-range NHEJ and to reorganise chromatin structure to allow increased telomere mobility (a feature proposed to explain increased telomere fusions observed in TRF2-/- conditional knock-out cells) [204]. In lymphocytes, 53BP1 and its downstream effectors have been shown to be required for Class-Switch Recombination (CSR) and V(D)J (Variable-Diversity-Joining)-recombination which are vital for the establishment of the immune system [205, 206].

53BP1 functions in the repair pathway choice by antagonising the resection of broken DNA ends promoted by BRCA1. In S- and G2-phase cells, BRCA1 displaces 53BP1 from DSB site in order to permit end resection initiated by CtIP and promote Homology-directed repair (HDR) [207, 208]. Both 53BP1 and BRCA1 elicit mutual antagonism of one another that is propagated by the recruitment of downstream factors. 53BP1 recruits Rif1 through phosphorylated SQ/TQ motifs within its N-terminus [190]. Loss of Rif1 phenocopies loss of 53BP1 at unprotected telomeres by preventing telomere fusions and failing to prevent end resection [190]. Conversely, BRCA1 has recently been shown to recruit an E3 ubiquitin ligase, UHRF1, through its BRCT domain in order to polyubiquitinate Rif1 and promote DNA end resection [209]. Downstream of the activity of BRCA1 at IRIF, 53BP1 is repositioned from the core of the focus to the periphery [208]. The physical repositioning of 53BP1 from the core of IRIF is achieved in two-phases. Firstly, by expansion of the 53BP1 focus followed by formation of a 53BP1-devoid core, the latter of which requires the de-ubiquitinating protein POH1, which has previously been shown to antagonise RNF8/RNF168-dependent polyubiquitination and recruitment of 53BP1 [184, 210]. The mechanism by which 53BP1 IRIF expand is of keen interest and likely reflects the initial selection and DSB processing required for the progression to HDR. Alongside

the requirement for POH1 to remove polyubiquitin chains from the core of IRIF, the expansion of 53BP1 IRIF requires BRCA1, CtIP and a number of chromatin repressive factors including Heterochromatin Protein 1 (HP1), the histone methyltransferases SETDB1 and SUV39 [210, 211]. This suggests the repositioning of 53BP1 requires the ability to modulate a highly dynamic chromatin environment.

Targeting proteins that govern DNA repair pathway choice have proved to be valuable therapeutic targets. BRCA1-deficient cells fail to repair DSBs by HR and as a subsequently cells resort to error prone and potentially mutagenic NHEJ for repair [212]. PARP inhibitors, such as Olaparib, have been very successful in sensitising BRCA1-deficient cells to ionising radiation by blocking the NHEJ repair pathway, creating a synthetic lethality with the failure to perform HR conferred by the loss of BRCA1 [213]. Interestingly, loss of 53BP1 was found to confer resistance to PARPi by restoring the ability for cells to perform HR [213]. The resistance to PARPi has been utilised to identify proteins that co-operate with 53BP1 to prevent end resection. For example, loss of PTIP confers resistance to PARPi indicating that it co-operates with 53BP1 to block HR [213]. PTIP is recruited to sites of DNA damage through ATM-dependent phosphorylation sites located within the N-terminus of 53BP1 [213]. Unlike Rif1, PTIP only appears to require the first 8 SQ/TQ motifs for its 53BP1-dependent function. PTIP also appears to be critical in order to limit end resection and to prevent fusion of unprotected telomeres [213]. Recently, PTIP has been shown to recruit the endonuclease Artemis to sites of damage in a phosphorylation-dependent manor and that remarkably, depletion of Artemis results in PARPi resistance in BRCA1-deficient cells [214]. This suggests that a key factor in protecting broken DNA ends from resection by nucleases is the generation of blunt DNA ends. Recent investigation has also identified REV7, a component of polymerase ζ, as a key factor acting downstream of 53BP1 in protecting broken DNA ends, it has been demonstrated that loss of REV7 restores HR and confers resistance to PARPi [215].

53BP1 is involved in mediating the cell-cycle checkpoint responses following DNA damage. In the absence of 53BP1 cells activate but fail to maintain a G2-M checkpoint arrest that would otherwise be propagated through sustained ATM-mediated phosphorylation of Chk2 [29]. Interestingly, in cells lacking Rif1, resection of DSBs leads to increased ATR activation following the generation of ssDNA [190]. One might expect that 53BP1 would indirectly suppress ATR activation given its role in preventing resection and the generation of ssDNA. However this is not the case, as 53BP1 is also required for ATR activation in order to establish G2-M phase checkpoint arrest [216]. Additionally, 53BP1 may also be required for G1-phase arrest and

preventing S-phase entry while DNA damage is present. The establishment of the G1-S phase checkpoint requires both 53BP1 and TopBP1 [193].

53BP1 is required for repair of DNA DSBs located in regions of heterochromatin. The heterochromatinised fraction of DSBs accounts for approximately 10-15% of breaks generated following exposure to ionising radiation. The resolution of these breaks specifically requires the BRCT domains of 53BP1, with the loss of these domains resulting in impaired MRN and pATM (pSer1981) localisation [202]. Furthermore, the repair of heterchomatinised DSB requires ATM-dependent phosphorylation of the repressor of transcription, KRAB-1 associated protein 1 (KAP-1) to promote chromatin relaxation [202]. The association of KAP-1 with chromatin is regulated by phosphorylation of serine-824 [217]. When KAP-1 is SUMOylated, it recruits the nucleosome remodeler, CHD3 [218]. Although phosphorylation of KAP-1 does not directly affect its SUMOylation, it changes the conformation of the binding region, preventing the association of CHD3 with KAP-1. Ultimately, phosphorylation of KAP-1 rapidly displaces CHD3 from chromatin to permit chromatin relaxation [203]. The ability of KAP-1 to associate with CHD3 to modulate the repair of heterochromatic breaks is also regulated by polySUMOylation as the SUMO protease, SENP7, is required to relax chromatin to permit repair by HR [218]. Despite determining the downstream events requiring the activated pATM, it remains to be established as to why deletion of the BRCT domains of 53BP1 results in a failure to localise both MRN and pATM to DSBs. Further characterisation of the specific interactions mediated by the BRCT domains will be required to address this question. Furthermore, the chromatin remodeler, EXPAND1 interacts with in a phosphorylation-independent manner through the BRCT domain of 53BP1 [197]. EXPAND1 associates with chromatin through histone H3 using its PWWP-domain. These interactions have also been shown to be required for the relaxation of chromatin surrounding DSBs and impacts upon sensitivity of cells to ionising radiation [197].

A number of research groups have demonstrated the extent to which 53BP1 governs chromatin mobility. By using fluorescently labelled TRF1, it has been shown that loss of 53BP1 prevents the increased telomere mobility observed at unprotected telomeres and that this mobility also requires ATM kinase [204]. The requirement for 53BP1 to mobilise chromatin is also applicable at DSBs and requires the nuclear envelope-bound LINC complex to promote chromatin reorganisation to facilitate repair [219]. This is a pivotal study as it suggests that the part of the driving force required to globally alter chromatin organisation may originate from the microtubules in the cytoplasm.

Finally, the role of 53BP1 in the cell is not limited to repair of DSBs, checkpoint signalling and chromatin mobility as detailed above, but also extends to the immune system. In specialised cells, 53BP1 has been shown to be required for CSR, a process by which B-cells switch immunoglobulin isotype by generating a controlled DSB [205]. Despite the requirement for both Rif1 and PTIP for long-range end joining of telomeres, failure to recruit PTIP (but not Rif1) by mutation of the N-terminus of 53BP1 does not affect CSR indicating that only Rif1 is required for this specialised process [213]. Alongside CSR, V(D)J-recombination (required for maturation of B and T cells as well as diversification of antibodies) was also found to be perturbed in 53BP1 deficient lymphocytes although, it remains to be established which factors acting downstream of 53BP1 are required for this process [206].

1.8.3 Role of TopBP1

TopBP1 is a large molecular scaffold protein that contains 9 BRCT domains that mediate many protein-protein interactions [220] (figure 1.12). As such, it has roles throughout the cell cycle, including the initiation of replication, the repair of DNA damage, transcriptional control, mediating checkpoint signalling and cell cycle arrest [221]. Predominantly, TopBP1 has been characterised as a critical factor required for the initiation of replication. In *S. cerevisiae*, $Dpb11^{TopBP1}$ bridges interactions between the replication pre-loading complex through Sld2 and MCM helicase via Sld3 and cdc45 to form the active helicase [222]. In mammalian cells, Treslin mediates the interaction of TopBP1 with cdc45 and the MCM complex, and as a result depletion of Treslin causes defective DNA replication [223].

Under conditions of replicative stress TopBP1 activates the checkpoint kinases ATR. Deacetylation of TopBP1 by SIRT1 facilitates suppression of replication origin firing [224]. In order to mediate its checkpoint activity, TopBP1 contains a conserved ATR-activation domain (AAD) located between BRCT domains 6 and 7 [225]. During replicative stress, the replication fork stalls at the site of damage, which causes the region of ssDNA on the lagging strand to become coated in RPA. RPA recruits ATR-interacting protein (ATRIP), which then recruits ATR kinase to the site of replicative stress. The heterotrimeric sliding clamp complex, Rad9-Rad1-Hus-1 (9-1-1) is loaded onto the DNA by the Rad17-RFC complex [226]. TopBP1 is then recruited to the stalled replication fork by interactions between TopBP1 BRCT domains 0, 1-2 and the phosphorylated C-terminus of Rad9 of the 9-1-1 complex [227]. Rad9-Rad1-Hus1 interacting nuclear orphan (RHINO) binds to both the 9-1-1 complex and TopBP1 to fully activate ATR [228]. The ATR-activation domain of TopBP1 contacts the PI3K regulatory domain (PRD) of ATR to stimulate its activity [229]. Activated ATR kinase phosphorylates a number of downstream targets including the checkpoint kinase Chk1 to promote intra S-phase checkpoint

arrest [230]. Recently, ATR-dependent Chk1 signalling was demonstrated to require post-translational modification of ATRIP by SUMO2/3. Generation of an unSUMOylatable mutant by mutation of two lysine residues impaired localisation of ATRIP to sites of replicative stress [231].

Interestingly, it was recently proposed that the MRN complex is responsible for recruitment of TopBP1 to stalled replication forks, although the downstream activation of ATR still requires the 9-1-1 complex [232]. Furthermore, it has been demonstrated that early MRN recruitment to IR-induced damage occurs independently of MDC1, through interactions with Rad17 [233]. It will of future interest to determine whether Rad17 is required for MRN and TopBP1 recruitment to stalled replication forks.

Unusually, TopBP1 has also been identified as a transcriptional repressor. Its role in suppressing the transcriptional activity of E2F1 requires oligomerisation of TopBP1, which in turn is governed by phosphorylation of serine-1159 [234]. TopBP1 also has a role in suppressing the transcriptional activity of the tumour suppressor, p53 [235].

TopBP1 also mediates interactions with BLM helicase a component of the BTR complex that suppresses crossover events during HR. Previously, TopBP1 had been demonstrated to regulate the stability of BLM [236], although this now appears not to be the case as virally-induced degradation of TopBP1 does not influence the stability of BLM [237]. Despite this, the TopBP1-BLM interaction is required for maintenance of genome stability as measured by increased sister chromatid exchanges (SCEs) [237]. Additionally, TopBP1 is required for V(D)J recombination in lymphocytes [145]. The mechanism by which TopBP1 regulates the BLM helicase in the resolution of DHJs remains to be established.

In *S. pombe*, $Rad4^{TopBP1}$ has been demonstrated to interact in a phosphorylation-dependent manner with $Crb2^{53BP1}$ [238]. In humans, TopBP1 is recruited to 53BP1 through BRCT domains 0, 1-2 and 4-5 in G1-phase. This contrasts with S-phase, as recruitment of TopBP1 to stalled DNA replication forks requires BRCT domains 0, 1-2 and 7-8. Furthermore, in stable cell lines expressing TopBP1 lacking BRCT domains 4-5 a G1-S checkpoint defect is observed, comparable to that observed by depletion of 53BP1 or TopBP1 alone [193]. Moreover, G1-phase cells are sensitised to IR-induced killing following treatment with an ATR inhibitor, indicating a potential role for ATR-dependent checkpoint signalling in G1-phase cells [239]. Additionally, TopBP1 BRCT domain 5 has been shown to interact with phosphorylated MDC1

[240]. As a result, further work will be required to determine which sets of interactions mediated by these domains are required for checkpoint activation.

Due to the complex interactions mediated by TopBP1 and given its diverse functions, it is difficult to dissect the importance of individual interactions mediated by this protein. For example, deletion of a single set of BRCT domains may result in the abolition of several interactions. As a result, it becomes necessary to examine the binding target to determine which specific interactions are required for its function and in the case of BRCT domains, whether they are phosphorylation-dependent.

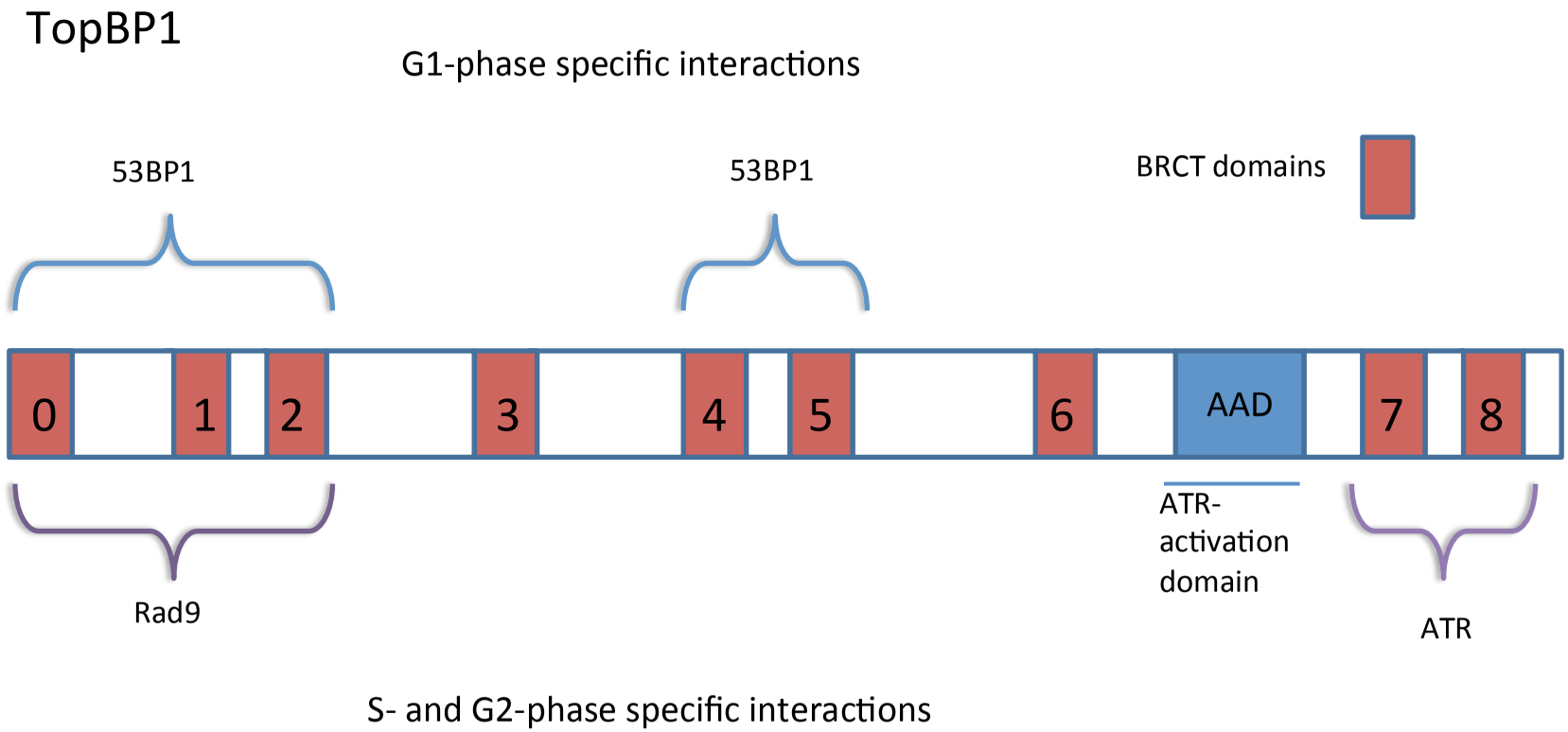

Figure 1.12 Domain architecture of TopBP1. (Adapted from [221])

1.9 Aims

The overall aim of this project was to investigate mechanisms associated with the roles of certain post-translational modifications in response to stresses, including response to arsenite and ionising radiation.

Firstly, following the identification of many eukaryotic initiation factors in proteomic screens undertaken to identify SUMOylated substrates, the initial aim of the project was to determine whether the eukaryotic initiation factor 4A, a component of the eIF4F complex, is a true SUMOylation target *in vivo*. If so, the aim was then to identify the residue(s) that is/are SUMOylated, and finally, by mutating the SUMOylated residue(s), to characterise the intracellular role of this modification and to determine whether it forms part of the cellular response to stress.

Secondly, following the identification of two phosphorylated residues within the N-terminus of 53BP1 that interact with TopBP1 BRCT domain 0, 1-2 and 4, 5 *in vitro*, the aim of this project was to determine whether these sites are phosphorylated *in vivo*. If so, the aim was then to determine whether failure to phosphorylate these residues disrupts the interaction between 53BP1 and TopBP1. Finally, by generating an unphosphorylatable mutant of 53BP1, the aim was to characterise the role of the 53BP1-TopBP1 interaction in mediating the response to genotoxic stress.

Thirdly, following identification of a phosphorylation specific interaction between recombinant 53BP1-BRCT domains and a γH2AX phospho-peptide, the aim was then to determine whether this interaction occurs, *in vivo,* in mammalian cells. By making specific point mutations within the BRCT domain, the project then aimed to identify the downstream effects of a failure to mediate this interaction and whether it is required to mediate the response to genotoxic stress.

2. Materials and Methods

2.1 Bacterial Methods

2.1.1 Media

LB

10g/l Tryptone

10g/l NaCl

5g/l Yeast extract

LB Agar plates

10g/l Tryptone

10g/l NaCl

5g/l Yeast extract

15g/l Agar

2.1.2 Antibiotics

Bacterial plasmids contained resistance genes to a range of antibiotics. Antibiotics were added to the media prior to use. Stock concentrations of antibiotics were stored at -20^{o}C.

Table 2.1 Bacterial antibiotics and concentrations used.

Antibiotic	Stock concentration (mg/ml)	Final concentration (µg/ml)
Ampicillin	100	100
Kanamycin	100	100
Chloramphenicol	34 in ethanol	34

2.1.3 *E. coli* strains

NM522 *E. coli* strain was used for all bacterial based methodologies excluding cultures used for DNA midi-preps and protein overexpression.

F' *proA*$^{+}$*B*$^{+}$ *lacI*^{q} *Δ(lacZ)M15/ Δ(lac-proAB) glnV thi-1 Δ(hsdS-mcrB)5* (NEB)

DH5α *E. coli* strain was used for bacterial culture for DNA midi-preps.

F- *80dlacZ M15 (lacZYA-argF) U169 recA1 endA1hsdR17(rk-, mk+) phoAsupE44 -thi-1 gyrA96 relA1* (MCLAB)

BL21 C+ *E. coli* strain was used for culturing bacteria for protein overexpression and purification.

F-, *omp*T, *hsd*S_B (r_B–, m_B–), *dcm*, *gal* λ(DE3), pLysS, Cm^{r}. (Promega)

2.1.4 Transformations

E. coli transformation was carried out by thawing the cells on ice. 2ng of plasmid DNA was added to 100µl of competent cells and incubated on ice for 20 minutes. After this incubation the cells were heat shocked at 37°C for 90 seconds. 1ml of LB was added to the cells before returning them to the 37°C for a further 60 minutes. After the second incubation the cells were collected by centrifugation at 3,000rpm for 3 minutes and most of the supernatant removed. Approximately 100µl of the remaining supernatant was used to re-suspend the cell pellet and cells were plated onto pre-warmed and dried LB agar plates containing the appropriate antibiotic.

2.1.5 Competent cell preparation

TRNS1

100mM RbCl

50mM $MnCl_2 \bullet 4H_2O$

10mM $CaCl_2 \bullet 2H_2O$

35mM Sodium Acetate

6.6% Glycerol

Adjusted to pH 5.8 using 0.2M acetic acid and filtered through a 0.22µm filter.

TRNS2

100mM RbCl

10mM $CaCl_2 \bullet 2H_2O$

10mM MOPS

6.6% Glycerol

Adjusted to pH 6.8 using potassium hydroxide and filtered through a 0.22µm filter.

A single colony of NM522 cells were cultured overnight in 5ml of LB at 37°C with shaking at 180rpm. This culture was then used to inoculate 1l of LB and incubated for a further 2-4 hours at 37°C with shaking at 180rpm. The culture was grown to an optical density of between 0.5-0.6 as determined by spectrophotometric measurements taken at 595nm. Once the cells had reached the optimum density the culture was cooled on ice for approximately 60 minutes before being collected by centrifugation at 5,000rpm for 5 minutes at 4°C. The supernatant was discarded and the pelleted cells were re-suspended in 25ml of TRNS1 and incubated on ice for 60 minutes. Cells were collected again by centrifugation at 5,000rpm for 5 minutes at 4°C.

After the supernatant was removed the cells were re-suspended in 12ml of TRNS2 solution and incubated on ice for a further hour. Finally, the cells were pipetted into 300µl aliquots and were snap frozen in liquid nitrogen before being stored at -80°C ready for use.

2.1.6 Blue/White colony selection

Blue/White colony selection was used to select for colonies that had successfully integrated the DNA insert into the pGEM-T Easy plasmid backbone. Ligation into the linearized cloning vector disrupts the LacZα peptide ORF, resulting in white colonies on agar plates containing X-GAL and IPTG along with the ampicillin selection marker. X-GAL is an analogue of galactose that can be metabolised by β-galactosidase and isopropyl β-D-1-thiogalactopyranoside (IPTG) is used to induce the expression of the lacZ gene.

2.1.7 Bacterial protein expression

BL21 C+ *E. coli* were inoculated into 1l of LB media and allowed to grow at 37°C for ~5 hours until they reached an optical density of between 0.5-0.6. Cells were then placed on ice for 30 minutes before adding IPTG to a final concentration of 0.2mM. Induced cells were then incubated overnight at 16°C. Cells were harvested by ultracentrifugation at 4°C and the pellet was collected and frozen at -20°C until purification.

2.2 DNA Methods

2.2.1 Qiagen Minipreps

Cells from a 10ml bacterial culture were collected by centrifugation at 3000rpm for 5 minutes at 4°C. The supernatant was removed and the cell pellet was re-suspended in 250µl of buffer P1 containing RNAse A. 250µl of buffer P2 was added and mixed by inversion. 350µl of buffer N3 was added and mixed by inversion to precipitate protein from the solution. The resultant mixture was centrifuged at 13,000rpm for 10 minutes at room temperature. The supernatant was then transferred to QIAprep spin column and passed through the column by centrifugation at 13,000rpm for 1 minute. The flow-through was then discarded before washing the column with 500µl of PB buffer. A second wash was performed this time with buffer PE, which precipitates the DNA from solution. As before the flow through was discarded. The column was centrifuged again without the addition of any buffers to remove excess buffer from the filter within the column. Finally, 50µl of H_2O was added to the column and incubated at room temperature for 2 minutes. Eluted DNA was collected into a clean Eppendorf tube by centrifugation.

2.2.2 DISH Minipreps

DISH minipreps were used to screen white colonies from white/blue selection plates for the integration of the DNA insert into pGEM-T easy cloning vector.

DISH1

50mM Glucose

10mM EDTA

25mM Tris (pH 8.0)

DISH2

0.2mM NaOH

1% SDS

DISH3

3M KOAc

8M Glacial Acetic acid

TE

10mM Tris-HCl pH 8.0

1mM EDTA

2ml Cultures were grown for a period of 4 to 5 hours before being transferred to a microcentrifuge tube and spun down. The supernatant was removed leaving just the cell pellet, which was then re-suspended in 100µl of DISH1 solution. 200µl of DISH2 solution was then added to the tube to lyse the cells. Finally 300µl of ice-cold DISH3 solution was added to precipitate proteins from the solution. The resultant mixture was centrifuged for 5 minutes at 13,000rpm.

Once the debris had been pelleted, the supernatant was transferred to a new microcentrifuge tube containing an equal volume of phenol chloroform. The solutions were mixed and again centrifuged at 13,000rpm for 5 minutes. The top layer was transferred to a new microcentrifuge tube containing 1ml of 100% ethanol. This was mixed and left for 30 minutes to allow the precipitation of DNA from the solution. The DNA was isolated by centrifugation as

before and the supernatant removed. The pelleted DNA was dried in a vacuum desiccator for 5 minutes before resuspension in 50µl of TE.

2.2.3 Qiagen Midipreps

100ml of LB was inoculated with DH5α cells from a smaller pre-culture and containing the plasmid to be propagated. The culture was grown overnight at 37°C and harvested by centrifugation the following morning. After the removal of the LB media the bacterial pellet was resuspended in 4ml of buffer P1 containing RNase A. Buffer P2 was added and incubated at room temperature for 5 minutes to lyse the cells. Buffer P3 was added to precipitate the proteins from solution. The mixture was then centrifuged at 4,000rpm for 30 minutes to remove cell debris from the solution.

A QiaTip was equilibrated with 4ml of buffer QBT before the addition of the cell lysate. The lysate passed through the column by gravity flow. The tip was then washed with 20ml of buffer QC before eluting the plasmid DNA from the tip in buffer QF. The elution was collected in a clean falcon tube. The DNA was precipitated from solution with the addition of 3.5ml of isopropanol. The tube was then centrifuged at 4,000rpm for 45 minutes. The supernatant was carefully removed and the DNA pellet was resuspended in 1ml of 70% ethanol and transferred to a microcentrifuge tube. The solution was centrifuged for 10 minutes at 13,000rpm and the supernatant was again removed. The pellet was then dried in a vacuum desiccator for 10 minutes before resuspension in 100µl of TE buffer.

The concentration of plasmid midipreps was determined using a nano-drop spectrophotometer. Plasmid midipreps produced DNA concentrations ranging from 1-2µg/µl.

2.2.4 Ethanol precipitation

Solutions:

3M NaAc

100% Ethanol (-20^{o}C)

70% Ethanol (Room temperature)

Sodium acetate was added to the sample equal to 1/10 of the total volume of the sample. The sample was mixed by vortex. Two volumes of 100% ethanol were added to the sample before mixing and centrifugation at 13,000rpm for 10 minutes. The supernatant was removed and the pelleted DNA was re-suspended in 500µl of 70% ethanol. The sample was again centrifuged,

supernatant removed and pellet dried in a vacuum desiccator for 10 minutes. The DNA was then re-suspended in water or an appropriate buffer.

2.2.5 Agarose Gel electrophoresis

1x TBE buffer:

100mM Tris base

100mM Boric acid

2mM EDTA

6x Loading dye:

2.5% Ficoll-400

11mM EDTA

3.3mM Tris-HCl (pH7.6)

0.017% SDS

0.015% Bromophenol blue

30% Glycerol

DNA samples were analysed by agarose gel electrophoresis. Most DNA samples were run on a 0.8% agarose gel. The gel was prepared by the addition of 1.6g of agarose to 200ml of 1x TBE buffer. The resultant mixture was heated to melt the agarose before being allowed to cool at room temperature. Before the gel had set 10µl of ethidium bromide was added to the mixture before pouring into a prepared gel tray complete with a gel comb. The gel was allowed to set at room temperature for approximately 20 minutes. Once set the gel was submerged in a gel tank containing 1x TBE buffer. Sample buffer was added to each of the DNA samples at the appropriate concentration before running for approximately 30 minutes –dependent upon the mass of the DNA in the sample. With ethidium bromide intercalated between the bases of the DNA the sample was visualised by excitation with ultraviolet light.

2.2.6 Site-directed Mutagenesis

Mutagenesis primers were designed to mutate as few bases as possible while still achieving the required codon change. Depending on the number of bases to be changed flanking regions

of homology were included varying in length and ending with a cytosine or guanine base. The primers were diluted to 100pmol/µl concentration.

A typical PCR reaction was set up as follows:

5µl KOD hot start DNA polymerase buffer

1.5mM $MgSO_4$

50ng DNA Template

0.2mM dNTPs

0.3µM Forward primer

0.3µM Reverse primer

0.02U/µl KOD hot start DNA polymerase

Each reaction was made up to a total volume of 50µl in distilled water. The reaction was run for between 20 and 30 cycles as well as at a range of annealing temperatures ranging from 40°C to 60°C to optimise DNA product synthesis. Extension time was also altered relative to the size of the template plasmid.

After the reaction the DNA product was digested with *Dpn*I, which recognises methylated residues only found on the template strand. The remaining product can then be transformed into competent cells to propagate the DNA allowing for subsequent sequence analysis.

2.2.7 Sequencing

DNA sequencing was carried out by Sourcebioscience.

2.2.8 PCR amplification

A typical PCR reaction was set up as follows:

5µl KOD hot start DNA polymerase buffer

1.5mM $MgSO_4$

50ng DNA template

0.2mM dNTPs

0.3µM Forward primer

0.3µM Reverse primer

0.02U/µl KOD hot start DNA polymerase

Each reaction was made up to a total volume of 50µl in distilled water. The reaction was run for between 20 and 30 cycles as well as a range of annealing temperatures ranging from 40°C to 60°C to optimise DNA product synthesis. Extension time was also altered relative to the size of the DNA to be amplified.

2.2.9 Restriction digestion

A typical restriction digest was set up as follows:

5µl of 10x Cutsmart restriction digest buffer

1µg of DNA

10U/µl of Restriction enzyme

The reaction was carried out in a total volume of 50µl for the duration of 1 hour at 37°C. Restricted DNA fragments were analysed by agarose gel electrophoresis to confirm the efficiency of the digest.

2.2.10 DNA gel extraction

DNA fragments were purified from agarose gels firstly by careful excision of the DNA fragment using a clean blade and a UV light box. The excised fragment was transferred to an Eppendorf tube. 300µl of Easypure® Salt solution along with 50µl of Melt solution were added to the sample which was then incubated at 50°C for approximately 10 minutes until the gel pieces had completely melted. 8µl of Easypure DNA binding beads were added to the mixture and incubated at room temperature for 5 minutes. Centrifugation was used to isolate the beads bound to the purified DNA fragment. A series of 2 further washes were used to remove residual melted agarose and contaminants. Finally the beads were re-suspended in 20µl of water to elute the DNA from the beads.

Purified fragment concentration was determined by nanodrop spectrophotometry.

2.2.11 Ligations

Purified digested fragments were ligated into destination vectors using quick ligase. Below shows a typical ligation reaction:

50ng of destination vector

DNA insert*

10µl of 2x Quick ligase buffer

5% Quick ligase

*concentration of DNA insert was calculated using a molar ratio of 3:1 (insert:vector).

The reaction was carried out in a total volume of 20µl for 15 minutes at room temperature. 5µl of the ligation mixture was transformed into competent cells and plated on agar plates containing the appropriate antibiotic.

2.2.12 Cloning

DNA fragments were cloned by PCR amplification with the addition of appropriate endonuclease restriction sites for both the 5' and 3' ends of the designed primers. The PCR product was analysed by agarose gel electrophoresis and purified using the agarose gel extraction protocol to remove the DNA template from the mixture.

The purified fragment was ligated into an intermediate destination vector (pGEM-T easy) before transformation into competent cells. White/blue colony selection was used to establish whether the colonies formed had integrated the insert into the vector. Clones were validated by restriction digest and sequencing. More of the insert was digested from the pGEM-T vector and ligated into the destination vector. The destination vector had been digested with the same restriction enzymes and pre-treated with calf intestinal phosphatase to prevent re-ligation of the vector to itself.

Finally colonies were screened the following day using gel electrophoresis and validated by sequencing.

2.2.13 Designing guide RNAs/ssODN template for CRISPR

Guide RNAs were designed using a function build into Benchling®. Oligonucleotides were identified by searching for 20 base pair sequences adjacent to a protospacer adjacent motif (PAM) site marked by 5' NGG 3'. Oligonucleotides were scored for both on-target and off-target effect probabilities. The 3 highest scoring (i.e. highest on-target with the lowest off-target scores) in a defined region were used to test cutting efficiency.

The DNA oligonucleotides had additional bases added to the 5' and 3' ends of each to create sticky ends (red) that would anneal to the ends generated by cutting the pSpCas9 backbone and to facilitate cloning. For example to target exon 10 of the *TP53BP1* gene:

5’ CACCGGGACTGCTAGGAACGATAAA 3’

3’ CCCTGACGATCCTTGCTATTTCAAA 5’

Once the oligonucleotides had been cloned into the pSpCas9 plasmid it would synthesize the gRNA along with Cas9 in mammalian cells. DNA oligonucleotides were ordered from Eurofins Genomics®.

2.2.14 Cloning DNA oligonucleotides into pSpCas9(BB)-neo

The synthesised DNA oligonucleotides were suspended in distilled water to a final concentration of 100pmol/µl. The oligonucleotides were incubated with T4 Polynucleotide kinase to phosphorylate the 5’ and 3’ ends prior to ligation. Finally, the oligonucleotides were heated and cooled gradually to allow the complementary strands to anneal.

Table 2.2 Example reaction for the preparation of the heteroduplex DNA.

Component	Volume
gRNA top	1µl (100pmol)
gRNA bottom	1µl (100pmol)
10x T4 PNK buffer with ATP	1µl
T4 Polynucleotide Kinase (10,000U/ml)	1µl
H_2O	6µl

A 10µl total reaction volume was then subjected to the following program in a PCR machine.

Temperature	**Time**
37°C	30 minutes
95°C	5 minutes
25°C	>5°c/min

The newly formed heteroduplex DNA was diluted 1:200 with distilled water before setting up the ligation reaction with the Cas9 vector.

Table 2.3 Example reaction for the ligation of the guide into the Cas9 vector.

Component	Volume
pSpCas9(BB)-neo	1µl (100ng)
Diluted oligonucleotide duplex	2µl
10x Fastdigest Buffer	2µl

Dithriothreitol (DTT) (10mM)	1µl
ATP (10mM)	1µl
Fastdigest BpiI	1µl
T7 DNA ligase	0.5µl
H_2O	11.5µl

The ligation mix was subjected to the following program on a PCR machine.

Temperature	**Time**
37°C	5 minutes
21°C	5 minutes

Cycle above 6 times

Hold at 4°c

Next, PlasmidSafe® exonuclease was used to digest any remaining linearised pSpCas9 vector.

Table 2.4 Example reaction for the digestion of unligated backbone vector.

Component	Volume
Ligation mix	11µl
10x PlasmidSafe buffer	1.5µl
10mM ATP	1.5µl
PlasmidSafe exonuclease	1µl

The digestion mix was then subjected to the following program on a PCR machine.

Temperature	**Time**
37°C	30 minutes
70°C	30 minutes

Finally, 5µl of the final mix was transformed into 100µl of competent bacterial NM522. The following day colonies were selected for validation by sequencing using the U6 forward primer.

2.2.15 Mammalian Genomic miniprep

The Cas9-gRNA constructs were transfected into cells using an appropriate transfection method. The cells were incubated for a further 5 days, on the 2nd day the media was supplemented with 1mg/ml G418 disulfate antibiotic to select for transformed cells. Following this the cells were collected by trypsinisation and centrifugation.

Genomic preps were obtained using Sigma GenElute™ Mammalian Genomic DNA miniprep kit following the manufacturer's protocol.

2.2.16 Gibson assembly fusion of PCR fragments

Gibson Assembly was used to create generate a 53BP1 repair template to incorporate *EmeraldGFP* gene at the N-terminus of 53BP1. The repair template included homology arms of 500 bases upstream and 500 bases downstream of the start codon. *EmGFP* was included after the start codon in exon 1 of 53BP1. The repair template was cloned into pUC19, a bacterial cloning vector.

Primers for Gibson Assembly were designed using the online NEBuilder tool (New England Biolabs). Primers were designed to create overlapping homology between the PCR products to be fused together.

The homology arms were then amplified using PCR of U2OS genomic DNA. *EmGFP* was amplified from a template vector and pUC19 was linearized with EcoRI restriction digestion. The PCR products and target vector were gel purified to remove template DNA (i.e. either genomic or undigested vector).

The gel purified DNA fragments were supplemented at a vector: insert ratio of 1:1 before the addition of the Gibson Assembly master mix. The maser mix contained all three components required for the reaction (an exonuclease, a polymerase and a ligase). The reaction was incubated for 60 minutes at 37°C. After incubation, 2µl of the final mixture was transformed into competent bacteria and plated onto agar plates containing ampicillin (ampicillin-resistance gene contained by pUC19 vector).

The reaction generated ~300 bacterial colonies. 10 where picked, cultured before isolating the DNA using a Qiagen miniprep kit. Purified DNA was analysed by agarose gel electrophoresis. 2 out of the 10 colonies screened contained the 4.4Kb product rather than pUC19 alone (3.3Kb). Sequencing by Sourcebioscience was then used to validate the generation of the repair templates.

2.3 Protein Methods

2.3.1 Nickel affinity purification from bacteria

Binding buffer:

5mM imidazole

500mM NaCl

20mM Tris HCl (pH 7.0)

Protease cocktail inhibitors

Wash buffer:

20mM imidazole

500mM NaCl

20mM Tris HCl (pH 7.0)

Elution buffer:

500mM imidazole

500mM NaCl

20mM Tris HCl (pH7.0)

The pellet was thawed in 15ml of binding buffer followed by sonication at amplitude 27% for 2 minutes in 5 second pulses. Cell debris was removed by centrifugation at 15,000rpm for 20 minutes. 1ml of nickel agarose or cobalt resin was equilibrated in binding buffer before being added to the lysate. After 1 hour of incubation at 4^{o}C, the lysate was run through a column and washed with 10ml of wash buffer. Purified protein was eluted by addition of 300µl of elution buffer into a clean microcentrifuge tube. Samples were stored in 10% glycerol, snap frozen and stored at -80°C.

2.3.2 GST-tagged protein purification

NETN buffer:

0.5% NP-40

20mM Tris pH 8.0

100mM NaCl

1mM EDTA

Wash buffer:

100mM Tris pH 8.0

120mM NaCl

Elution buffer:

100mM Tris pH 8.0

120mM NaCl

20mM Glutathione

The pelleted bacteria were re-suspended in 15ml of NETN buffer with protease inhibitors. The suspension was then sonicated on ice at 27% amplitude for 5 second pulses for a total of 1 minute. The homogenous mixture was then centrifuged at 4°C at 15,000rpm for 20 minutes to remove cell debris. The supernatant was then allowed to flow through a column containing GST beads previously equilibrated in NETN buffer. Once the supernatant had passed through the column it was washed 3x with 10ml of wash buffer. Finally, protein was eluted from the beads in 5x 300µl aliquots in elution buffer. The purified protein was snap frozen in 10% glycerol and stored at -80°C until use.

2.3.3 Nickel affinity purification from Mammalian cells (denaturing conditions)

Buffer A:

6M guanidinium hydrochloride

100mM sodium dihydrophosphate

10mM Tris-HCl pH8

Buffer C:

8M urea

100mM sodium dihydrophosphate

10mM Tris-HCl pH 6.3

HU Buffer:

8M urea

200mM Tris-HCl pH6.8

1mM EDTA

5% w/v SDS

0.1% bromophenol blue

1.5% w/v DTT

Cells were lysed using 1.85M NaOH/7.5% β-mercaptoethanol. Protein was then precipitated using 20% TCA. The mixture was then centrifuged and the supernatant was removed to retain the denatured proteins. The pelleted protein was re-suspended in Buffer A and allowed to solubilise for a further hour. 20µl/sample aliquots of nickel agarose were equilibrated in Buffer A with 0.05% Tween. Nickel beads were added to the protein solution and incubated overnight at 4°C. The following morning the samples were washed twice more with Buffer A, a further four washes with Buffer C and two more times with Buffer C with 0.05% tween and 50mM Imidazole. After the final wash the nickel beads were re-suspended in 42µl of HU buffer and boiled for 5 minutes to elute bound protein. Samples were centrifuged and run on SDS-PAGE as above.

2.3.4 Concentrating protein samples

Protein samples were concentrated using centrifugal filters from Milipore®. Samples were spun at 3,000rpm for variable lengths of time dependent on the degree of concentration required.

2.3.5 Bradford Assay

Bradford assay was performed using a pre-made 5x concentration solution. The reagent was diluted and 1ml was added to each cuvette. 1µl of the protein sample was added to the cuvette before inverting with parafilm. The resultant absorption at 595nm was compared to a standard curve of a known set of concentrations of bovine serum albumin to calculate the concentration of the protein sample.

2.3.6 SDS-PAGE

5x Sample buffer:

60mM Tris-HCl pH 6.8

25% Glycerol

2% SDS

5% β-mercaptoethanol

0.01% Bromophenol Blue

4x Separating gel buffer:

1.5M Tris-HCl pH 8.8

0.4% SDS

4x Stacking gel buffer:

0.5M Tris-HCl pH 6.8

0.4% SDS

10% Separating gel:

33% Protogel (0.8% Acrylamide)

25% Separating gel buffer

0.1% Ammonium Persulfate (APS)

0.001% TEMED

6% Stacking gel:

20% Protogel

12.5% Stacking gel buffer

0.25% APS

0.0005% TEMED

Samples for analysis by SDS-PAGE were prepared by the addition of sample buffer to the final 1x concentration. Samples were then boiled for 5 minutes using a heating block and centrifuged at 13,000rpm for 5 minutes before being loaded into the gel. The gel was run at 150V for approximately 1 hour.

2.3.7 Coomassie staining

The presence of protein bands was detected using Coomassie InstantBlue stain. 10ml was added to a petri dish containing the polyacrylamide gel and incubated for 60 minutes at room temperature on an orbital shaker. Blue protein bands present within the gel could then excised and prepared for mass spectrometry.

2.3.8 Western Blotting

Semi-dry transfer buffer:

48mM Tris-base

39mM Glycine

0.04% SDS

20% Methanol

2 x 6 pieces of filter paper were cut to the same size as the polyacrylamide gel and soaked in semi-dry transfer buffer. A section of PVDF transfer membrane was also cut to a similar size and soaked in methanol. The gel was placed carefully on top of the transfer membrane and sandwiched between the two sets of soaked filter paper in the semi-transfer tank. The transfer was run at 150mA for between 35-50 minutes dependent upon the size of the protein to be investigated.

After the transfer had completed the membrane was removed and incubated for 30 minutes in 4% (w/v) milk in PBS on an orbital shaker. The primary antibody was then added directly to the milk solution to the desired concentration before incubating overnight at 4°C.

The next morning the primary antibody solution was removed and the transfer membrane was washed 3x in PBS-Tween with each wash lasting between 5-10 minutes. After washing, the appropriate secondary antibody coupled to horseradish peroxidase (HRP) was added to 4% milk in PBS and incubated with the membrane for 1 hour. After this incubation period the membrane was washed 3 times as before, followed by 1 additional wash in PBS without tween.

2.3.9 Chemilluminescence detection

The transfer membrane was then incubated with 2ml of Pierce western blotting substrate. Chemilluminescence was analysed by exposing the membrane to an Amersham hyperfilm X-ray film and developed in a Xograph film developer. X-ray film exposure times were varied from 4 seconds to 60 minutes to optimise clarity of bands present.

2.3.10 Immunoprecipitation

Immunoprecipitation was performed using Sigma HA-immunoprecipitation kit. Cells were lysed using Sigma lysis buffer. Sigma Lysis buffer was supplemented with additional inhibitors to prevent protein degradation and de-phosphorylation.

Lysis buffer was supplemented with:

2mM EGTA

50mM NaF

0.1mM Sodium vanadate

25mM β-glycerolphosphate

150mM NaCl

PhosStop® phosphatase inhibitor cocktail

Protease inhibitor cocktail with EDTA

The cells were incubated for 15 minutes at room temperature with 1 ml of the lysis buffer before scraping the cells into a microcentrifuge tube. Following this the cells were sonicated for 5 second pulses at amplitude 27% for 1 minute. 1µl of Benzonase and 1µl of 2M $MgCl_2$ was added to the lysates and incubated for 60 minutes on ice. Treated lysates were transferred to a spin column before the addition of 10µl of the HA- antibody resin. The mixture was incubated overnight at 4°C on a rotating wheel.

The following morning the column was spun in a microcentrifuge at 4°C to remove unbound protein from the HA- resin. The resin was washed a further 6 times in 1 x IP buffer. The IP buffer was also supplemented with additional inhibitors.

IP buffer was supplemented with:

2mM EGTA

50mM NaF

0.1mM Sodium vanadate

25mM β-glycerolphosphate

150mM NaCl

PhosStop® phosphatase inhibitor cocktail

Protease inhibitor cocktail with EDTA

One final wash was performed with 0.1% IP buffer before the addition of 100µl Laemmli buffer. The samples were boiled for 5 minutes in a heating block before eluting the protein by centrifugation into a clean microcentrifuge tube. Samples were analysed by SDS-PAGE and Western Blot.

2.3.11 *In vitro* SUMOylation Assay

Protein components for the *in vitro* assay were prepared by purifying protein from a 1l culture of *E. coli* as described above. Purified protein was snap frozen in 10% glycerol and stored at -80°C ready for use.

The *in vitro* assay was prepared with the controls shown below. Components added are in µl.

Table 2.5 Shows an example set up for the *in vitro* SUMOylation assay.

Reaction Tube No.	1	2	3	4	5	6	7	8
	eIF4A	No SAE	Assay	A+ pli1	eIF4A	eIF4A+ Pli1	eIF4A	eIF4A+Pli1
Substrate	10	10			10	10	20	20
10x Buffer		4	4	4	4	4	4	4
E2 (Ubc9/Hus5) [1.5mg/ml]		2	2	2	2	2	2	2
Sumo-GG (Pmt3) [5mg/ml]		4	4	4	4	4	4	4
E1 (SAE; Rad31/Fub2) [0.5mg/ml]			4	4	4	4	4	4
CPK [3.5mg/µl]		2	2	2	2	2	2	2
PPI [0.12 mg/µl]		2	2	2	2	2	2	2
E3 (pli1) [1.5mg/ml]				2		2		2
Water	30	16	22	20	12	10	2	0

The reaction mix was incubated at 30°C for 2 hours before the direct addition of 8µl of 5xSDS sample buffer. Samples were then run on SDS-PAGE.

2.3.12 In-gel trypsin digestion

Bands were cut from the SDS-PAGE gel and de-stained by washing gel pieces in 25mM NH_4HCO_3 in 50% MeCN (acetonitrile) solution. This was repeated 3 times to remove Coomassie stain and dehydrate the gel pieces. The gel pieces were then reduced by addition of 10mM DTT in 25mM NH_4HCO_3 and incubation at 50°C for 45 minutes. This solution was then replaced with 50mM iodoacetamide in 25mM NH_4HCO_3 and incubated for a further 45 minutes in the dark for alkylation to occur. Samples were then digested with trypsin (10ng/µl) overnight. The

following day peptides were recovered in 5% tetrafluoroacetic acid (TFA) to a final volume of ~8µl. Samples were then stored at -20°C until analysis by mass spectrometry.

2.3.13 Mass spectrometry

Protein samples were analysed by SDS-PAGE. Bands of interest were excised and digested with trypsin following the 'in-gel' digestion protocol outlined above. Peptides were analysed by liquid chromatography tandem mass spectrometry (LC-MS/MS) in which digested peptides were eluted in order of mass and ionised by electrospray ionisation before acceleration, deflection and finally detection. Mass to charge ratios were plotted and the resultant spectra was BLAST searched against a database of known eukaryotic proteins using Mascot Daemon software. The software was also used to identify a shift in mass corresponding to that of Lysine conjugated to di-glycine to signify a modified residue.

2.4 Mammalian Tissue culture methods

2.4.1 Media

Mammalian cell lines used were cultured in Dulbecco's Modified Eagle's Medium (DMEM). Media was supplemented with 10% fetal calf serum (FCS). L-glutamine along with penicillin/streptomycin was also added to the media prior to use.

2.4.2 Antibiotics

G418 was used to select for mammalian cells that had integrated a plasmid containing the neomycin resistance gene.

2.4.3 Cell lines

Table 2.6 details the cell lines used in experiments.

Cell Line	Special requirements
HeLa	
U2OS	
U2OS-DR-GFP	U2OS cell line with an integrated cassette that produces a GFP signal if DSB repair occurs by HR. Contains an I-SceI restriction site.
HeLa YFP-BRCT WT	HeLa cell line with an integrated YFP plasmid containing the BRCT domains of 53BP1. Culture in 400µg/µl G418.
HeLa YFP-BRCT R1811E	HeLa cell line with an integrated YFP plasmid containing the BRCT domains of 53BP1. Culture in 400µg/µl G418.
+/+ H2AX Mouse Embryonic Fibroblast (MEF)	
-/- H2AX Mouse Embryonic Fibroblast (MEF)	

2.4.4 Trypsinisation

0.0025% (w/v) in PBS was filter sterilised using a 0.22µm filter.

Cells were cultured in T175 flasks. Cells were trypsinised firstly by the removal of media containing FCS. The cells were then washed with 10ml of PBS. After removal of the PBS, 10ml of trypsin solution was added. The trypsin was incubated for 5 minutes to allow digestion of the adhesive proteins utilised by the cells. Media containing serum was added to the cells to ablate the activity of the trypsin. The cells were then counted and collected by centrifugation before re-suspension in new media. Finally the cells were seeded into a new flask to passage the cells and/or seeded for experiments in 35mm dishes.

2.4.5 Cell counting

The number of cells per ml of media was calculated using a haemocytometer.

2.4.6 Total cell extracts

Total cell extracts were prepared by addition of 50µl of 1xSDS-Sample buffer to a 35mm plate. Cells were then removed by scraping and transferred to an Eppendorf tube. The samples were sonicated at amplitude 27% for 30 seconds in 5 second pulses. Samples were then boiled and centrifuged ready for analysis by SDS-PAGE.

2.4.7 RNA interference

SiRNA oligonucleotides were obtained from Life Technologies.

RNA oligonucleotide transfections were set up as follows for each plate:

50µl OptiMEM (Serum free media)

5µl Hiperfect transfection reagent

2µl of 20µM siRNA oligonucleotides

The solution was mixed and incubated at room temperature for 10 minutes to allow complex formation. Cells were trypsinised as described above and $2x10^5$ cells were seeded per plate. The cells were reverse transfected (i.e. while still in suspension) with the prepared transfection solution. siRNA oligonucleotides were diluted to a final concentration of 20nM. Typically cells were incubated for a further 48 hours to allow RNA interference (RNAi) to occur. The efficacy of RNAi was assessed by both western blot analysis and immunofluorescence where appropriate.

2.4.8 Mammalian cell transfection (calcium phosphate)

2x HBS

0.0162% NaCl (w/v)

0.0004% $Na_2HPO_4 \bullet 7H_2O$ (w/v)

0.013% HEPES (w/v)

Adjusted to pH 7.0

2M $CaCl_2$

The calcium phosphate transfection method was used to transfect HEK293 cells. Prior to transfection the cells were trypsinised and seeded at low confluency (20-30%) on 10cm plates two hours before transfection to allow the cells to re-attach to the plate.

For the transfection, 2x HBS was thawed at room temperature before preparing the $CaCl_2$/HBS/DNA mixture. For each 10cm dish, 10µg of DNA was diluted in 500µl of 244mM $CaCl_2$. The DNA/$CaCl_2$ was then added dropwise to 500µl of 2xHBS. Finally, the prepared mixture was added dropwise evenly to the media of the 10cm plate and incubated at 37°C for 24 hours. The media was changed the following day and the cells were cultured for a further 60 hours before being lysed.

2.4.9 Mammalian cell transfection (lipid-based)

After incubating cells with the siRNA transfection reagent the cells were washed with PBS and new media added. Cells were then transfected with plasmids constructs containing either the wild type protein or a mutant version.

Plasmid transfections were set up as follows for each plate:

50µl OptiMEM

2.75µl Nanojuice transfection booster

1.5µl Nanojuice core transfection reagent

1.5µg Plasmid DNA

Reagents were briefly vortexed before the addition of the plasmid DNA.

2.4.10 Mammalian cell transfection (Electroporation)

Due to the requirement for high transfection efficiency, electroporation was performed using Invitrogens' NEON® transfection system. Cells were trypsinised and counted. $2x10^5$ cells were transfected per plate. Cells were isolated and pelleted before re-suspension in buffer R. 500µg of plasmid DNA was added to the cell suspension. The cell suspension was drawn up into a NEON transfection tip before placing in a cuvette containing electrolytic buffer. The cells were electroporated at a set voltage, time and number of pulses recommended for each cell type by the manufacturer's database.

Finally, the cells were expelled from the pipette tip into a 35mm plate containing 2ml of media. The following day the transfection efficiency was assessed using a GFP reporter construct. Typically transfection efficiencies higher than 95% were achieved using this protocol.

2.4.11 Irradiation

In order to generate DNA DSBs cells were exposed to gamma radiation from a Caesium-137 source.

For larger samples, for example those in 96-well plates, an X-ray machine was used to generate DNA damage.

2.4.12 Fluorophores

Fluorophores used for immunofluorescence experiments include:

DAPI – Blue

FITC – Green

Cy3 – Orange

Cy5 – Far Red

The graph below illustrates the excitation and emission spectra of each fluorophore. The distribution of the spectra allows the use of all 4 fluorophore channels in one experiment. (Dotted lines denote excitation spectra and solid lines denote excitation spectra).

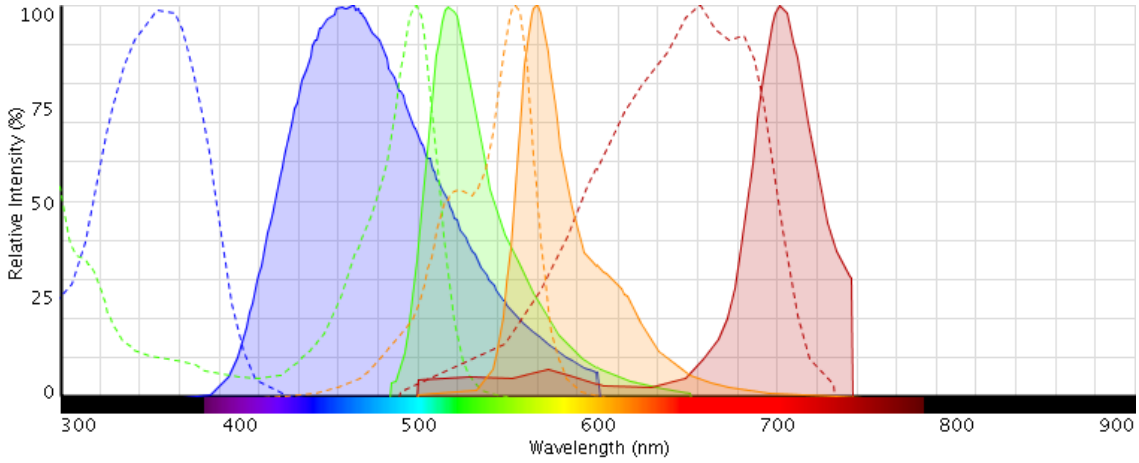

(Life Technologies 2015)

2.4.13 Immunofluorescence

Mammalian cells were cultured on glass coverslips. Following RNAi and plasmid transfections cells were treated as indicated and processed by either fixation using 4% paraformaldehyde before permeabalisation with 0.1% Triton X100 or the reverse for triton extraction. Methanol fixation was used for immunofluorescence experiments staining for TopBP1. Coverslips were washed with PBS three times between each step. Antibodies were diluted in 4% Bovine serum albumin (BSA) in PBS to assay specific concentrations ranging from 1:1000 to 1:100 (see table below for further details) and incubated on the glass coverslips for 1 hour at room temperature.

Table 2.7 Details the antibodies and concentrations used in experiments.

Primary Antibody	Dilution factor for IF	Host
α-HA	1:200	Mouse monoclonal
α-53BP1	1:400	Rabbit polyclonal
α-pATM (S1981)	1:400	Rabbit monoclonal
α-NBS1	1:1,000	Rabbit polyclonal
α-γH2AX (S139)	1:400	Rabbit polyclonal
α- γH2AX (S139)	1:800	Mouse monoclonal
α-BRCA1	1:100	Rabbit polyclonal
α-TopBP1	1:1,000	Rabbit polyclonal

After the primary antibody was removed the coverslips were washed 3 more times with PBS before the addition of the secondary antibody coupled to a fluorophore. The secondary antibody was diluted in 4% BSA and incubated on the coverslips for 30 minutes at room temperature. The secondary antibody was removed by 3 further washes in PBS before

mounting the coverslips onto slides with Prolong gold mounting media with DAPI. Slides were left overnight at 4°C to allow the mounting media to set. Immunofluorescence slides were imaged using an Imsol Deltavision IX70 microscope.

2.4.14 ScanR

Analysis of foci co-localisation was achieved using ScanR microscopy. Initially cells were cultured as before on 35mm dishes. Cells were seeded at $2x10^5$ cells per well and were reverse transfected with 53BP1 siRNA oligonucleotides. Cells were incubated for 24 hours before washing with PBS and transfection with plasmid constructs containing either wild-type 53BP1 or one of the serine/threonine mutants. Cells were incubated for a further 24 hours before being trypsinised and re-seeded onto a 96-well scanR plate. Cells were seeded at $2x10^4$ cells per well.

The following day cells were exposed to 8Gy of IR using an X-ray machine. The cells were allowed to recover for 4 hours before fixation using -20°C methanol for 15 minutes. Cells were processed for immunofluorescence as before using antibodies for TopBP1 and HA at their appropriate concentrations. Primary antibodies were incubated for 1 hour and secondary antibodies for 30 minutes at room temperature. Finally cells were stained with DAPI at a 5µg/ml concentration for 10 minutes at room temperature.

Analysis by scanR microscopy was assisted by Dr V. Savic (University of Sussex). 6x6 images were taken per well. DAPI intensity stain was analysed to produce a cell cycle profile on the contents of each well. The resulting images were analysed for both 53BP1 and TopBP1 foci. Co-localisation was assessed by the production of a database listing the X,Y coordinates of each focus along with its size only in G1 cells. G1 phase cells were scored for either having co-localised foci or not.

2.4.15 Homologous recombination assay

A U2OS cell line with an integrated plasmid cassette was used to analyse changes in global homologous recombination (HR). The integrated cassette contains an inactive GFP molecule due to a direct repeat (DR) adjacent to an I-SceI restriction site. When an I-SceI expressing plasmid is transfected into these cells it generates one DSB per cell. Downstream of the inactive GFP is a C-terminal fragment capable of being used as a template to restore the GFP to the active form i.e. without the DR. If the repair occurs by homologous recombination using the downstream template a GFP signal is produced. Un-repaired breaks or breaks repaired by non-homologous end joining (NHEJ) do not produce any GFP signal.

U2OS DR-GFP cells were treated as before by depleting endogenous 53BP1 using RNAi. 48 hours after reverse transfection with the siRNA oligonucleotides the cells were transfected with either the wild-type 53BP1 or one of the mutants alongside an I-SceI plasmid. After transfection the cells were incubated for a further 48 hours to allow for the induction of a DSB and to allow time for repair to occur. After the incubation period the cells were trypsinised and analysed by fluorescence activated cell sorting (FACS).

2.4.16 Fluorescence activated cell sorting

U2OS-DR-GFP (direct repeat) cells were seeded onto 35mm dishes and transfected with siRNA oligonucleotides targeting 53BP1. 48 hours later cells were transfected with both siRNA resistant constructs alongside a pCBASceI construct designed to create a double strand break in the DR-GFP construct. Cells that repair the damage using homologous recombination produce and active GFP signal.

To analyse the samples by FACS the cells were trypsinised from 35mm dishes and centrifuged before being concentrated into 500µl of PBS with 1mM EDTA. Cells were vortexed briefly to prevent clumping. Once the fluidics had pressurised and the lasers were at an operational temperature the samples could then be analysed for GFP fluorescence.

2.4.17 Generation of stable transfected cell lines

Stable cell lines were generated by initially seeding $2x10^5$ HeLa cells per 35mm dish before transfecting the cells when they had reached approximately 70-80% confluence. The plasmid transfected contained a resistance neomycin resistance gene that confers resistance to G418 disulfate. 48 hours after the initial transfection the cells were checked for transfection efficiency under a fluorescent light microscope. After checking the transfection efficiency the media was changed and supplemented with 700µg/ml of G418. The cells were continually treated with media containing this selection marker at this concentration for a further 14 days. Cells that had failed to retain and integrate the plasmid had undergone apoptosis and surviving colonies were all expressing the protein of interest. After the initial selection the G418 concentration was decreased to 400µg/ml.

Due to the nature of the following experiments the cell line was cultured as a polyclonal population with a range of different expression profiles.

2.4.18 Cross-sectional analysis of foci

$1x10^5$ HeLa cells were seeded per plate and reverse transfected with siRNA oligonucleotides targeting 53BP1. 48 hours later the cells were either left untransfected or transfected with the wild-type protein or one of the mutant constructs. The cells were then exposed to ionising

radiation. Mock-treated and wild-type cells were exposed to 3Gy while mutants were exposed to 1Gy to generate similar foci numbers after 8 hours. 8 hours post-IR exposure cells were fixed in 4% paraformaldehyde and permeablised using 0.1% Triton X100. Cells were processed for immunofluorescence staining for BRCA1 and 53BP1 for mock-treated and si53BP1 whereas the wild-type and mutant constructs were stained for BRCA1 and HA. Coverslips were mounted on glass slides using prolong gold mounting media containing DAPI.

A series of non-overlapping de-convolved z-stack images were obtained using an IMSOL Deltavision IX70 inverted microscope. 20 images were taken per stack with a z distance of 0.2µm between each image. Each image was subjected to 10 de-convolution cycles.

Intensity profiles were measured across individual foci using SoftworXs image analysis software. Profiles of 20 foci were generated per slide. Intensity values were normalised to the highest intensity read on that particular channel. The average of the relative foci intensities were plotted with error bars representing 1 standard deviation.

2.4.19 Laser track micro-irradiation and spinning disc confocal microscopy

$2x10^5$ HeLa cells were seeded onto MatTek 35mm glass bottom dishes and reverse transfected with siRNA oligonucleotides for 53BP1. 48 hours later cells were transfected with YFP-tagged constructs containing either the tandem BRCT domains of 53BP1 fused to a nuclear localisation signal (NLS) one of the mutants or just the YFP-NLS. Cells were incubated for a further 16 hours before the addition of Hoechst 34580 diluted to a final concentration of 10µg/ml. The Hoechst stain was allowed to intercalate with the DNA for 20 minutes at 37°C. Following pre-sensitisation with Hoechst a 405nm wavelength laser was used to generate DSBs. Fluorescence intensity on the 488nm scanning laser was tracked over 2 minutes. Slidebook6 reader software was used to quantify the change in intensity normalised to an un-damaged control. Tracking experiments were repeated 3 times and the average plotted with error bars showing 1 standard deviation.

For experiments using MEFs cells were seeded at $1x10^6$ cells per well and incubated with siRNA for only 24 hours before transfection.

2.4.20 EdU/BrdU dual pulse labelling to assess G1-S phase entry

$1x10^5$ U2OS cells were seeded and reverse transfected as previously described with siRNA oligonucleotides targeting 53BP1. Following a 48 hour incubation period the cells were washed and transfected using Nanojuice® transfection reagents using the protocol described previously. 16 hours following the transfection the cells were pre-incubated with EdU-

containing media for 1 hour at 37°C. The cells were then washed twice with PBS to remove residual EdU before irradiation with 2Gy of ionising radiation using a caesium^{137} source. After irradiation the cells were supplemented with media containing another nucleotide analogue, BrdU. The cells were incubated for a further 7 hours before fixation and permeabalisation for ClickiT chemistry and immunofluorescence.

The DNA was denatured by adding 2ml of 4M HCl to each well followed by incubation for 20 minutes at room temperature. This is critical to allow the BrdU antibody to bind its target. Following on from this the cells were washed five times using a neutralising buffer (phosphate/citric acid buffer). The cells were washed a further two times using a PBS/ 0.1% Triton X100/ 1% BSA (antibody-stain) solution.

Table 2.8 Details preparation of the ClickiT reaction.

Reagent	Amount (v/v)
1x ClickIt EdU reaction buffer	86%
$CuSO_4$	0.4%
Alexa Fluor 647 azide	0.025%
10x ClickIt EdU buffer additive	10%
Total volume	10ml

500µl of the ClickiT mixture was added to each well and incubated for 30 minutes at room temperature in the dark. Following on from this the cells were washed two times using the antibody-stain solution. After washing, the anti-BrdU and anti-HA antibodies were diluted into the antibody stain solution and 100µl was spotted onto each of the coverslips. The coverslips were incubated for a further 60 minutes at room temperature. After incubation, the antibodies were washed off the coverslips three times with the antibody stain solution. A secondary, fluorophore coupled antibody, was used to stain for the HA tag and was incubated with the coverslips for a further 30 minutes at room temperature.

Finally, the secondary antibody was washed off the coverslips a further three times using the antibody stain solution. Note that the BrdU antibody does not require a secondary antibody as the primary antibody is already coupled to alexa fluor 488. The coverslips were washed two further times in PBS before mounting onto glass slides using Prolong gold mounting media with DAPI.

2.4.21 Dilution and clonal expansion of mammalian cells for CRISPR

Following transfection with the Cas9 containing the targeting gRNA and incubation G418 disulfate for 5 days, the polyclonal cells were trypsinised and serially diluted to a final

concentration of 1 cell/ml. 200µl of the diluted cell solution was added to each well of a 96-well plate and cultured for 3-weeks or until each well became confluent. Cells were then cultured on larger plates and screened for deletion of the targeted gene.

3. Investigating the role of SUMOylation of eukaryotic translation initiation factors (eIFs)

3.1 Introduction

The eukaryotic initiation factors, eIF4A1 and eIF4A2, belong to the RNA DEAD-box helicase family. Despite their striking structural conservation these helicases have distinct roles in regulating cellular metabolism [84]. eIF4A1 has been shown to directly impact upon translation by affecting the ability of the assembling ribosome to traverse secondary structures located within the 5' UTR of the mRNA [241]. Conversely, eIF4A2 has been shown to be required for miRNA-mediated mRNA silencing [85, 242].

The RNA helicase activity of eIF4A1 has been shown to be highly inefficient and dependent upon interactions with other initiation factors such as eIF4G and eIF4B to promote efficient unwinding activity [81, 243, 244]. Consequently, post-translational modification of this protein holds the potential to tip the balance and globally alter translation either directly by altering its helicase activity or indirectly by affecting its availability within the cell. Furthermore, eIF4A1 and eIF4A2 have been identified in proteomic screens designed to identify SUMOylated proteins [4, 5].

3.2 Results

3.2.1 eIF4A1 and eIF4A2 are SUMOylated *in vitro* on K225 and K226 respectively

In order to test whether or not the translation initiation factors eIF4A1 and eIF4A2 can be SUMOylated *in vitro*, 6x His-tagged eIF4A1 and GST-tagged eIF4A2 proteins (plasmid constructs provided by Professor Simon Morley) were expressed and affinity purified from bacteria. Expression of the proteins was induced in *Escherichia coli* and then recombinant His-eIF4A1 protein was affinity purified using nickel beads. Separately, glutathione-coupled beads were used to affinity purify GST-tagged eIF4A2 protein. The purified proteins were eluted in 300µl aliquots following protocols described in sections 2.3.1 and 2.3.2. Purified protein eluates were analysed by SDS-PAGE and staining with Coomassie instant blue protein stain (figure 3.1a and b).

Purified eIF4A1 ran at the expected molecular mass of ~46kDa. eIF4A2 has a similar molecular mass to that of eIF4A1, however due to the addition of a GST-tag, its mass is increased by approximately 25kDa so that it migrates closer to ~61kDa as seen on the gel. Each eluted fraction was divided into 50µl aliquots in 10% glycerol, snap frozen in liquid nitrogen and stored at -80°C until use.

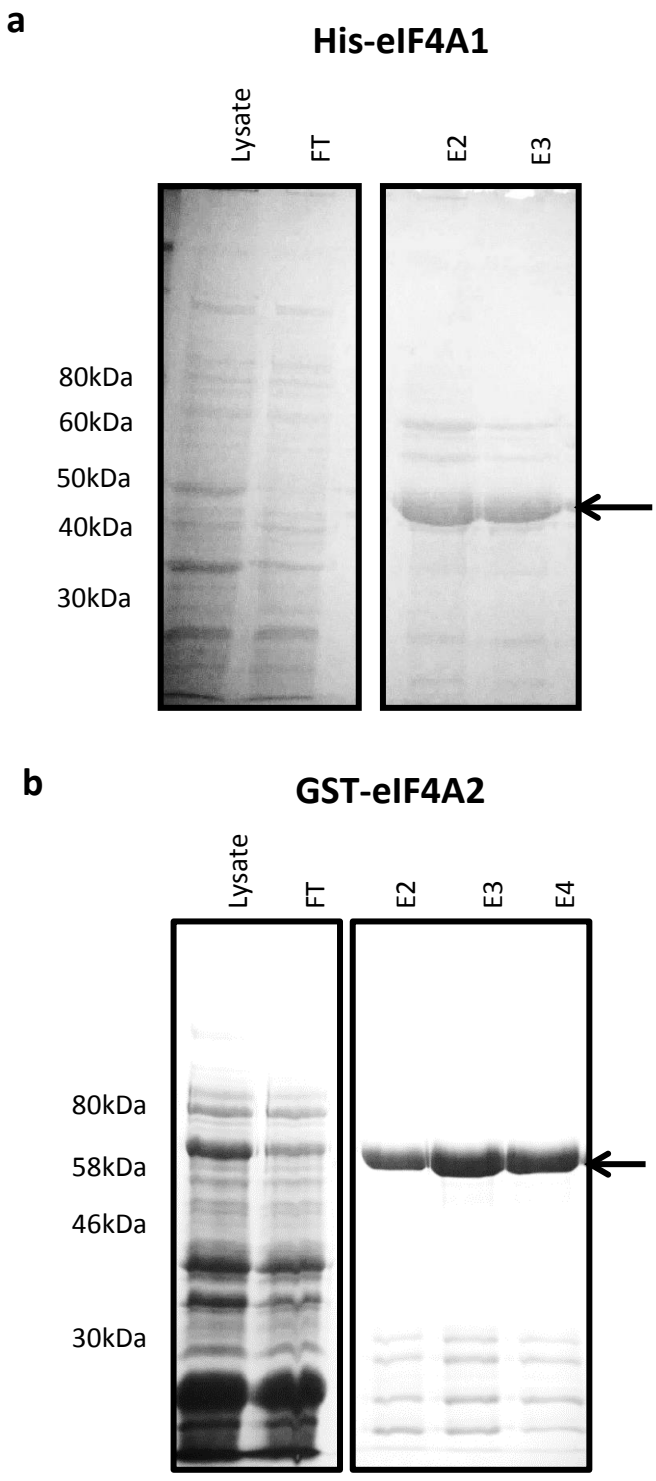

Figure 3.1 Affinity purification of His-eIF4A1 and GST-eIF4A2. a) Shows coomassie stained polyacrylamide gel of affinity purified His-eIF4A1 eluted from nickel beads following expression in *Escherichia coli.* FT = Flow through. E2, E3 = Elution fractions. b) Coomassie stained polyacrylamide gel of affinity purified GST-eIF4A2 eluted from GST beads following expression in *Escherichia coli*. FT = Flow through. E2, E3, E4 = Elution fractions.

Recombinant eIF4A1 and eIF4A2 were then tested for the ability to be SUMOylated in an *in vitro* SUMOylation assay. This assay includes an E1 activating enzyme (Rad31 and Fub2) and an E2 conjugating enzyme (Hus5) with or without an E3 ligase (Pli1). Additionally, it uses a SUMO construct with an additional trypsin-cleavage site. His-SUMO-tr-GG has an additional trypsin-cleavage site (lysine residue) engineered immediately adjacent to the diglycine motif as used in the identification of SUMOylation sites in eIF4G [76]. This enables the generation of peptides with a smaller mass/charge ratio (m/z) shift after trypsin digestion and improves target identification by mass spectrometry. Following incubation with the SUMOylation machinery the eIF4A proteins were analysed by SDS-PAGE and Coomassie Instantblue® staining to identify additional bands corresponding to SUMOylated species (figures 3.2a and b). The conjugation of SUMO to a modified lysine should produce a characteristic shift of 20kDa or multiples thereof for polySUMOylated products.

In vitro SUMOylation of recombinant eIF4A1 protein did not produce any additional bands. However the possibility remained that other proteins used in the assay with a comparable relative mobility could mask a SUMOylated species. Additionally, the quantity of SUMOylated protein could be such that the Coomassie staining might not detect smaller quantities of modified proteins. As a result, the indicated segments (figure 3.2a and b) were excised from the gel and the protein digested with trypsin to produce short peptide sequences as illustrated in figure 3.3a. The resulting peptides were analysed by LC-MS/MS using an LTQ-Orbitrap mass spectrometer.

In vitro SUMOylation of recombinant eIF4A2 did show an additional band potentially representing a SUMOylated product. The band identified (marked by * on figure 3.2b) has a higher relative mobility than expected for a SUMOylated species, running at approximately 58kDa rather than the expected 86kDa. As before, the possibility remained that other proteins included in the assay could also mask the presence of SUMOylated eIF4A2. Groups of bands, excised in segments including that marked by *, were excised from the gel and analysed by LC-MS/MS.

The spectra generated were used to identify peptides cleaved by trypsin using Mascot daemon software (i.e. peptides cleaved on the C-terminal side of lysine and arginine residues). A basic local alignment search tool (BLAST) was used to identify which protein the peptides belonged to. The software was also able to identify post-translational modifications characterised by a shift in the m/z ratio.

Mascot software was able to identify a single peptide within eIF4A1 that showed a characteristic mass shift (represented by di-glycine conjugated to a lysine residue)(figure 3.3b). This peptide mapped to the N-terminal region of eIF4A1 at amino acid residue K225. Similarly, a single SUMOylation site was identified in eIF4A2 (figure 3.3c). The modified lysine in eIF4A2, K226, mapped to an equivalent region of eIF4A1, within the N-terminal portion of the protein.

The positions of these SUMOylated residues were then identified on the available crystal structures for both eIF4A1 and eIF4A2 [245, 246] (figure 3.4a and b). The modified residues project out from the main structures on an alpha helix. This suggests that the sites would be accessible for SUMOylation *in vivo*.

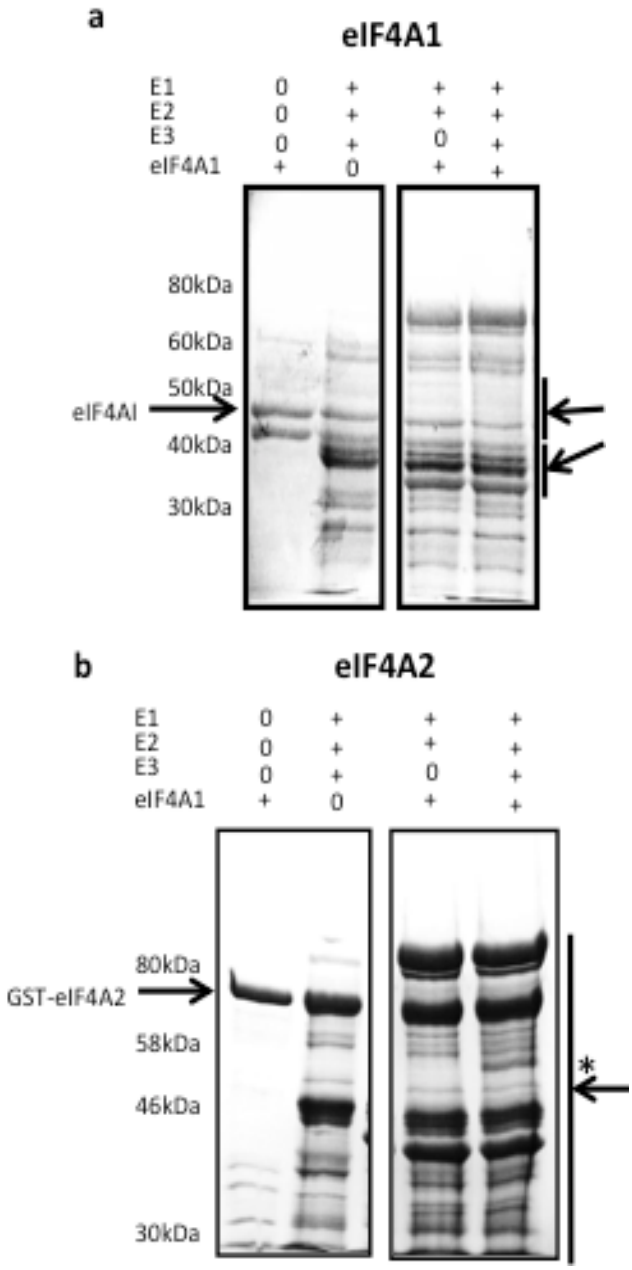

Figure 3.2 *In vitro* SUMOylation of recombinant eIF4A1 and eIF4A2. a) Shows a coomassie-stained polyacrylamide gel of samples run on a gel following the *in vitro* SUMOylation assay of His-eIF4A1 (vertical bars indicate bands excised for analysis by mass spectrometry). + marks the addition of *S. pombe* E1 (SUMO activating enzyme, Rad31/Fub2 heterodimer); E2 (SUMO conjugating enzyme, Hus5) and E3 (SUMO ligase, Pli1). Arrows indicate the regions/bands excised for mass spectrometric analysis. Arrows indicate segments containing the SUMO-modified form. b) *In vitro* SUMOylation of GST-eIF4A2 (vertical bars indicate regions analysed by mass spectrometry). Arrows indicate the regions/bands excised for mass spectrometric analysis. *indicates SUMOylated eIF4A2 species

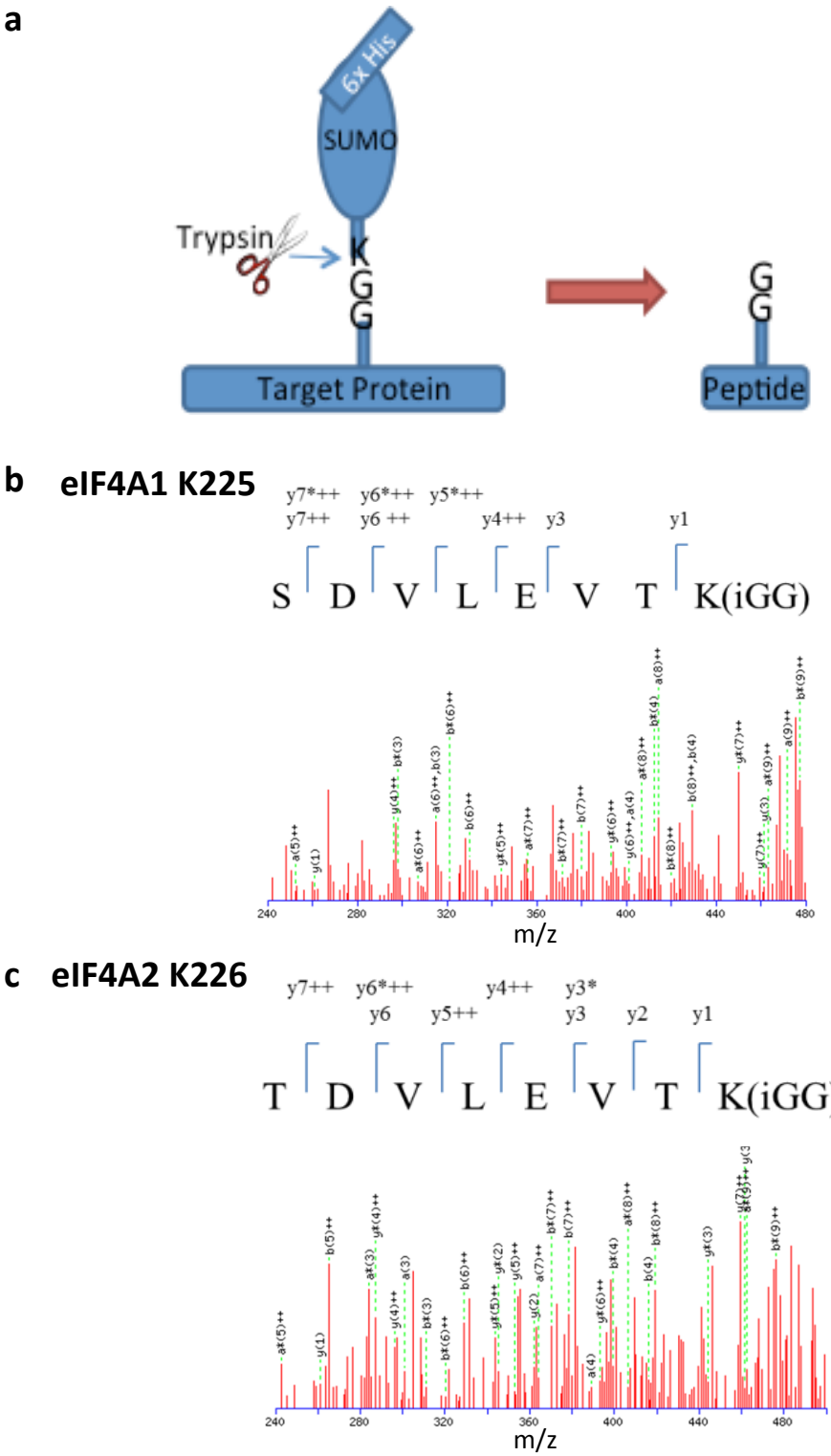

Figure 3.3 eIF4A1 and eIF4A2 are SUMOylated *in vitro* on K225 and K226 respectively. a) diagrammatic representation of tryptic digestion of SUMOylated proteins to generate diglycine-conjugated peptides. Figure shows cleavage of the C-terminal side of Lysine adjacent to diglycine. 6x His = Histidine tag. b) Mass spectra showing the detection of the SUMOylated peptide identified in eIF4A1 following tryptic digestion. c) Mass spectra showing the detection of the SUMOylated peptide identified in eIF4A2 following tryptic digestion.

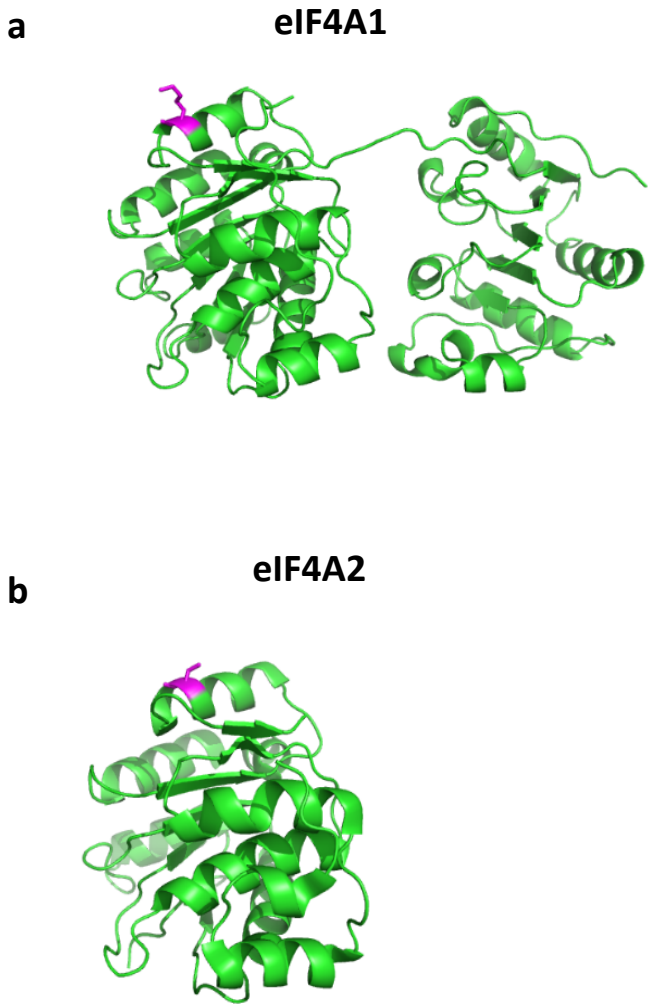

Figure 3.4 SUMOylation sites identified using the *in vitro* SUMOylation assay map to an external face of the available crystal structures of eIF4A1 and eIF4A2. a) Crystal structure of eIF4A1 was obtained from the protein data bank and adapted from [245] with the SUMOylated lysine (K225) highlighted in magenta. b) Crystal structure of the N-terminal portion of of eIF4A2 obtained from the protein data bank and adapted from [246] with the SUMOylated lysine (K226) highlighted in magenta.

3.2.2 eIF4A1 and eIF4A2 are SUMOylated *in vivo*

After the identification of these SUMOylation sites *in vitro* using *S. pombe* purified components, it was necessary to establish whether or not eIF4A1 and eIF4A2 are in fact SUMOylated *in vivo*, in mammalian cells.

In order to analyse this, HeLa cells stably expressing His-SUMO1 and His-SUMO2 (kindly provided by Prof. R Hay) were cultured and used for affinity purification studies. Nickel affinity purification and Western blot analysis of His-SUMO1 and His-SUMO2 from these cells reveals a range SUMO of conjugates with various molecular weights (figure 3.5a). The SUMO conjugates purified from these cells were probed for eIF4A and eIF4A2 (figure 3.5b) to reveal the presence of SUMO1-modified eIF4A and SUMO1- and 2-modified eIF4A2. The specificities of the two antibodies used in this assay were tested against recombinant proteins with the eIF4A antibody reporting on both isoforms (eIF4A1 and 2) and the eIF4A2 antibody solely reporting on recombinant eIF4A2 (Figure 3.6a). Dr. Jirapas Jongjitwimol performed these experiments.

Despite there being no clear additional eIF4A species purified from the His-SUMO2 expressing cells in figure 3.5b the likelihood of eIF4A being modified by SUMO2/3 is quite high given the substantial shift in molecular weight observed for eIF4A purified from His-SUMO1 expressing cells i.e. indicating the indicating the presence of a polySUMOylated species with SUMO1 as a chain terminator. This is supported by the fact that when the same affinity purified lysates are analysed using the eIF4A2 specific antibody a modified eIF4A2 species is observed for both SUMO1 and SUMO2 conjugates.

Having established that SUMOylated species of eIF4A2 could be identified in mammalian cells, it then became possible to test whether the amino acid residues identified by mass spectrometry were indeed genuine sites targeted for post-translational modification. The modification of eIF4A2 by SUMO1 on K226 was examined further as this modified species was the one most easily identified by Western analysis.

By depleting the endogenous protein by RNAi and transfecting cells with flag-eIF4A2 and flag-eIF4A2(K226R) constructs, Dr. Jirapas Jongjitwimol was able to show that mutation of K226 abolishes SUMOylation of eIF4A2 in cells expressing his-SUMO1 (figure 3.6b).

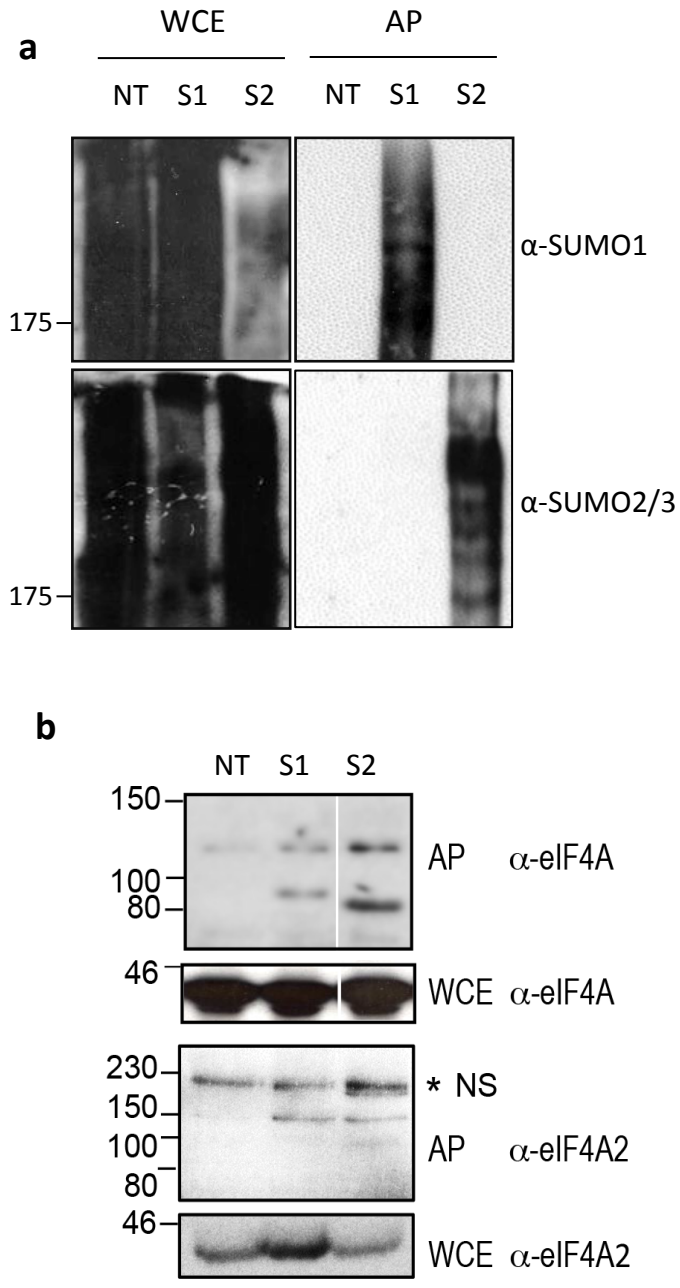

Jirapas Jongjitwimol

Figure 3.5 eIF4A1 and eIF4A2 are SUMOylated *in vivo* by SUMO1 and SUMO2/3. (Performed by Dr. Jiripas Jongjitwimol). HeLa cells either not-transfected (NT) or stably expressing his-SUMO1 (S1) and his-SUMO2/3 (S2) were cultured and SUMOylated proteins were affinity purified (AP) using Nickel agarose beads. WCE = Whole cell extracts. a) Shows a western blot probed with anti-SUMO1 and anti-SUMO2/3 antibodies following affinity purification b) Affinity purified lysates were analysed by western blot for the presence of eIF4A and eIF4A2.

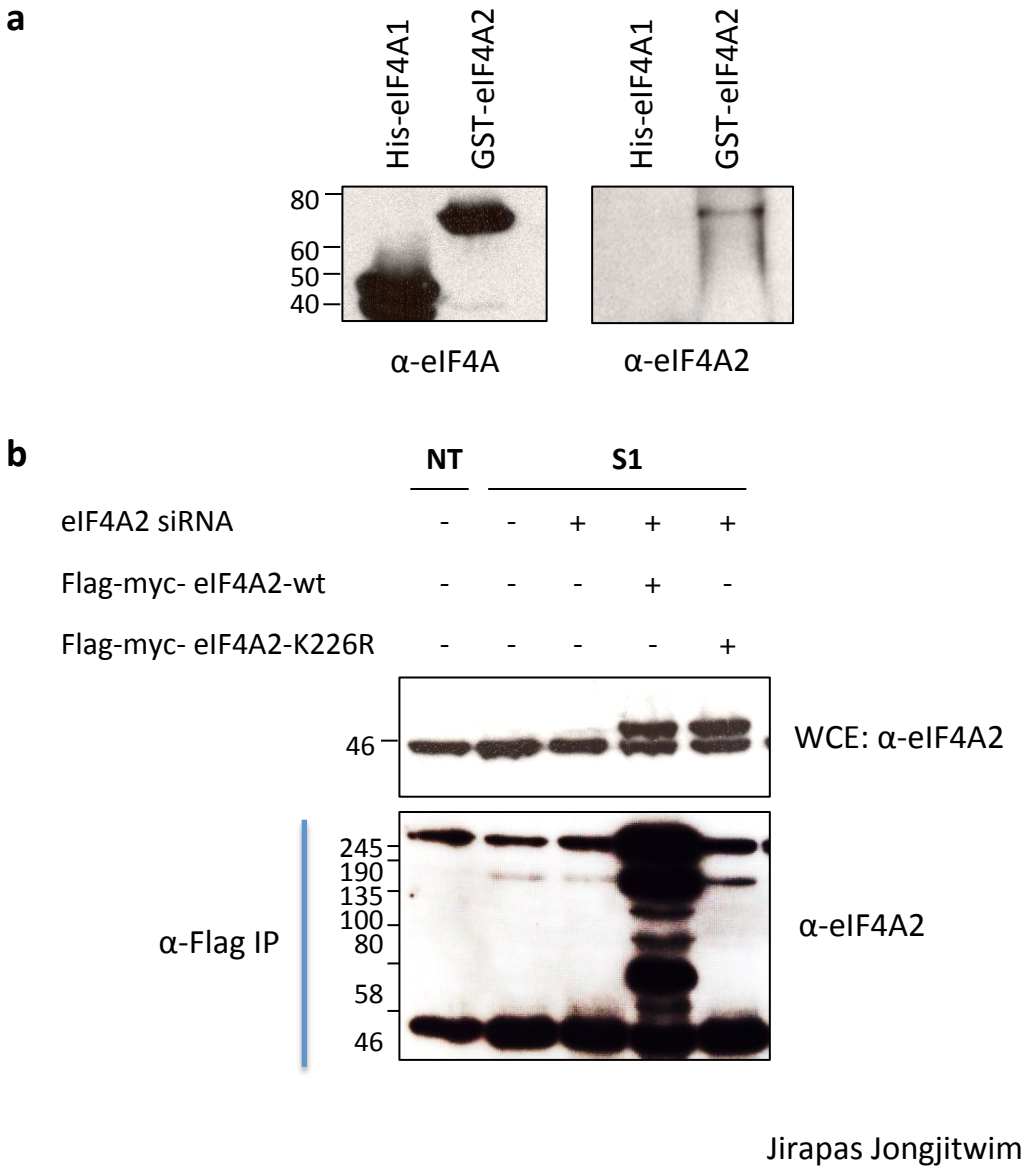

Figure 3.6 eIF4A2 is SUMOylated on K226 *in vivo*. (Performed by Dr. Jiripas Jongjitwimol). a) Western blot analysis of recombinant eIF4A1 and eIF4A2 protein was used to demonstrate the specificity of eIF4A and eIF4A2 antibodies. b) HeLa cells stably expressing his-SUMO1 (S1) cells were depleted of eIF4A2 by RNA interference over 24 hours before transfection with siRNA resistant constructs expressing either wild-type Flag-myc-eIF4A2-wt or a K226R mutant. Flag-myc-eIF4A2 was immunoprecipitated from whole cell extracts (WCE) using α-Flag-coupled agarose beads and IP-lysates were analysed by western blot for the presence of higher-molecular weight species of eIF4A2.

3.2.3 Mutation of K226 affects the formation of stress granules after treatment with arsenite

Having demonstrated that the eukaryotic initiation factor eIF4A2 is SUMOylated on K226 by SUMO1, we were interested to determine whether failure to post-translationally modify this residue results in an observable defect or cellular change. One of the roles of SUMOylation is to regulate protein trafficking and localisation. For example, SUMOylation of PML promotes the formation of PML bodies which are discrete nuclear protein aggregates that form in response to cellular stress [19].

In contrast to the role of SUMO in controlling nuclear compartmentalisation we wanted to test whether the same level of control could be exhibited by SUMO over cytoplasmic proteins i.e. altering their sub-cellular localisation and affecting their recruitment to cytoplasmic aggregates. This is particularly relevant with respect to the cytoplasmic formation of stress granules and processing bodies (P-bodies). Stress granules form when translation is blocked and is proposed to be a protective response leading to either the degradation or recycling of mRNA [247]. There are two mechanisms that are thought to facilitate the formation of stress granules by phosphorylation of eIF2α, either by preventing its association with the charged tRNA, or by targeting eIF4A1 and eIF4G directly [247]. As eIF4G has recently been shown to be SUMOylated, investigating the role of SUMOylation of eIF4A2 on stress granule formation could provide a link between these two observations [76].

In order to test this, cells were transfected with siRNA oligonucleotides targeting eIF4A2. Following transfection with the siRNAs, cells were then transiently transfected with either wild-type Flag-eIF4A2 or the K226R unSUMOylatable mutant. After expression of the plasmids the cells were then treated with either ionising radiation to induce DNA damage or sodium arsenite to induce oxidative stress, which in turn induces stress granule formation [248] (figure 3.7). The results provisionally indicated that the incorporation of eIF4A2 into stress granules was impaired when K226 was mutated to arginine. To further investigate this we repeated the experiment to model the volume of the stress granules using images taken across a z-range.

Image analysis was performed by taking deconvolved z-stacks images over a z-plane of 4µm at 0.05µm slices. 10 cells were imaged per sample with surface mapping and volume analysis using Imaris microscopy software. Example surface mapping is shown in figure 3.8a.

Immunofluorescence analysis of flag-eIF4A2 and flag-eIF4A2(K226R) incorporation into stress granules reveals that mutation of eIF4A2 results in an increase in the number of stress granules with smaller volumes following treatment with arsenite (figure 3.8b and c).

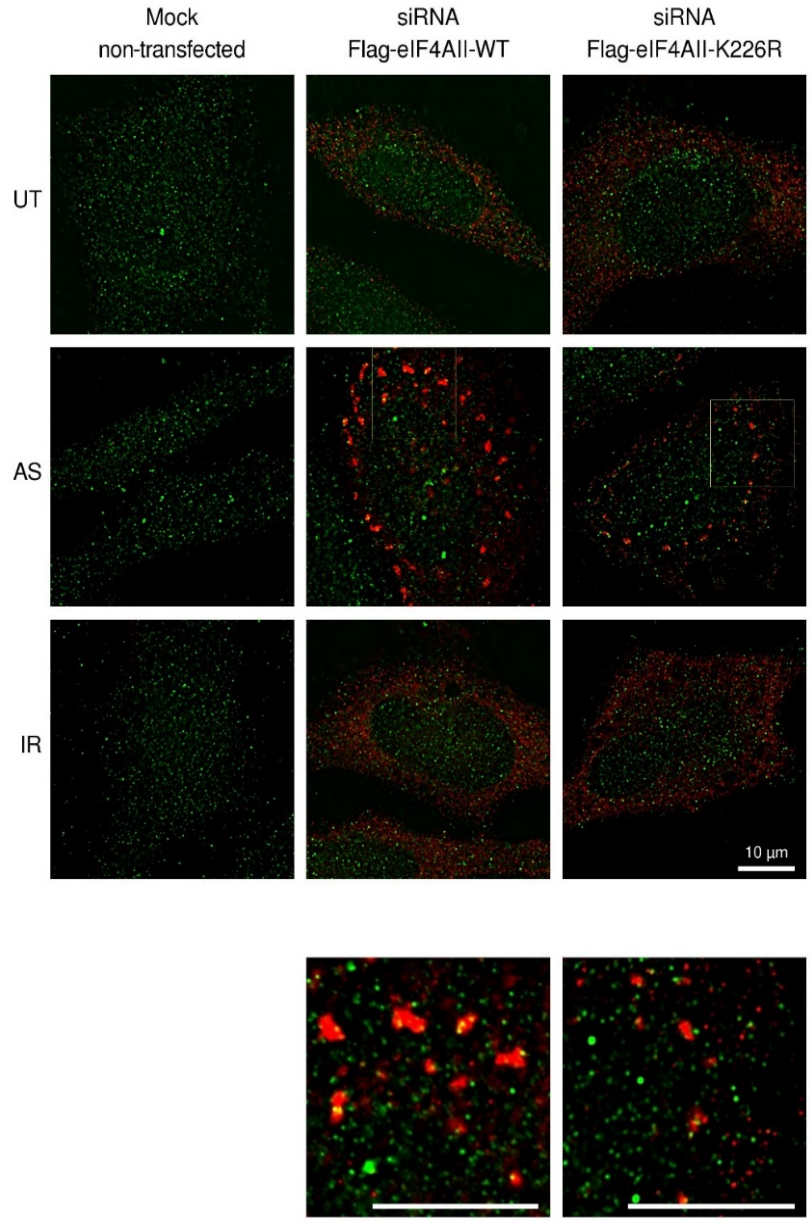

Jirapas Jongjitwimol

Figure 3.7 Localisation of Flag-eIF4A2 wild-type and K226R mutant in response to different stress conditions. (Performed by Dr. Jirapas Jongjitwimol). HeLa cells were depleted of eIF4A2 by transfection with siRNA oligonucleotides. 24 hours following transfection, cells were transfected with either wild-type Flag-eIF4A2 or the K226R mutant. The cells were then either left untreated (UT), treated with 1mM sodium arsenite (AR) for 30 minutes or exposed to 3Gy of ionising radiation and allowed to recover for 30 minutes. Following treatment the cells were fixed and immunostained for SUMO-1 (green) and eIF4A2 via a Flag antibody (red). Yellow boxes indicate regions of the image magnified in the bottom two panels. Scale bars show 10µm.

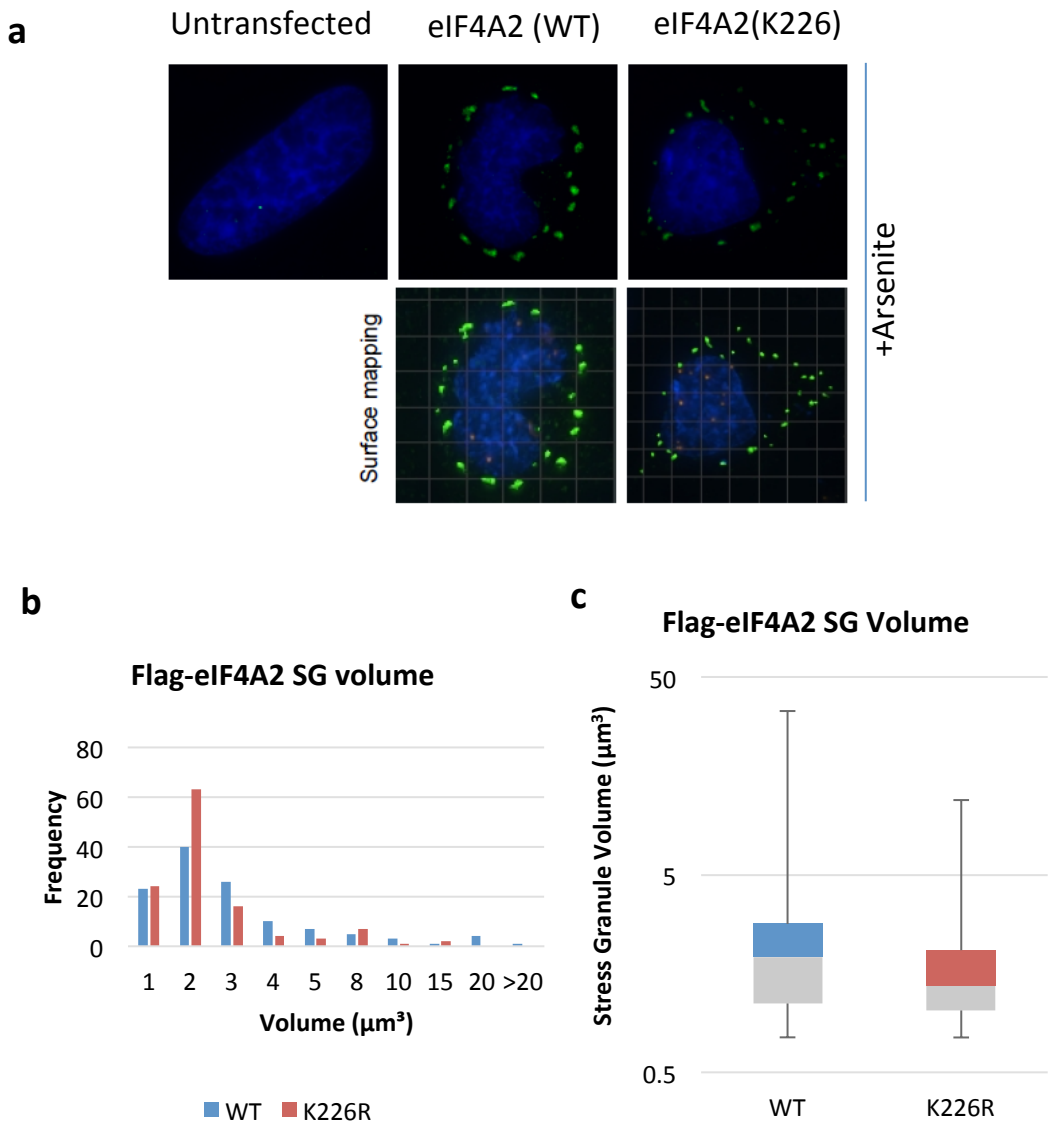

Figure 3.8 Mutation of K226 results a larger population of stress granules with smaller volumes after treatment with arsenite. HeLa cells were depleted of eIF4A2 by transfection with siRNA oligonucleotides. 24 hours following transfection cells were transfected with either wild-type Flag-eIF4A2 or the K226R mutant followed by treatment with 1mM sodium arsenite for 30 minutes. High resolution z-stack (z=4µm 0.05µm/slice) images were taken and deconvolved using Softworx software suite. Cells were fixed and immunostained with an anti-Flag antibody. Volumetric analysis was carried out on 120 stress granules using Imaris software. a) shows example images eIF4A2 stress granules (green). Two-panels below shows identification of stress granules by surface mapping using Imaris. b) Histogram showing the frequency of stress granule volumes (n=120 stress granules analysed for each sample). c) Box and whisker plot shows skewed distribution of stress granule volumes median, upper and lower quartiles of stress granule volumes (n=120).

3.2.4 Mutant eIF4A2 forms smaller stress granules although eIF4A2 and TIA1 co-localise normally

Following on from the identification of a larger population of smaller eIF4A2 stress granules in cells transfected with the K226R mutant, it was necessary to determine whether the amount of eIF4A2 being incorporated into stress granules is reduced by this mutation or whether the overall volume of the stress granules is affected. Additionally, it was necessary to confirm that the cytoplasmic bodies to which eIF4A2 was being incorporated are stress granules as opposed to P-bodies, which contain different translation factors and components.

In order to this, the above experiment was repeated with additional co-immunostaining for a known component of stress granules, TIA1 [249]. As before, high-resolution z-stack images were taken and deconvolved before being analysed by Imaris. Flag-eIF4A2 co-localises with TIA1 indicating that eIF4A2 is incorporated into stress granules following treatment with arsenite (figure 3.9a). Co-localisation of Flag-eIF4A2 and TIA1 was further analysed by Imaris software. The software calculates the fluorescence signal overlap between two channels above a threshold. The threshold was determined by a non-transfected control and would therefore represent only transfected cells and not background fluorescence. Co-localisation of Flag-eIF4A2 and TIA1 was not affected by mutation of K226 to arginine indicating that SUMOylation of K226 is not required for recruitment of eIF4A2 to stress granules (figure 3.9b).

Finally, it was possible to analyse the average stress granule volume across all 3 experiments for each sample. There was a slight decrease in stress granule volume between Flag-eIF4A2 wild-type and the K226R mutant indicating that despite the fact that SUMOylation of eIF4A2 was not absolutely required for localisation to stress granules, SUMOylated eIF4A2 might mediate interactions with other proteins located in stress granules which also may be SUMOylated (figure 3.9c).

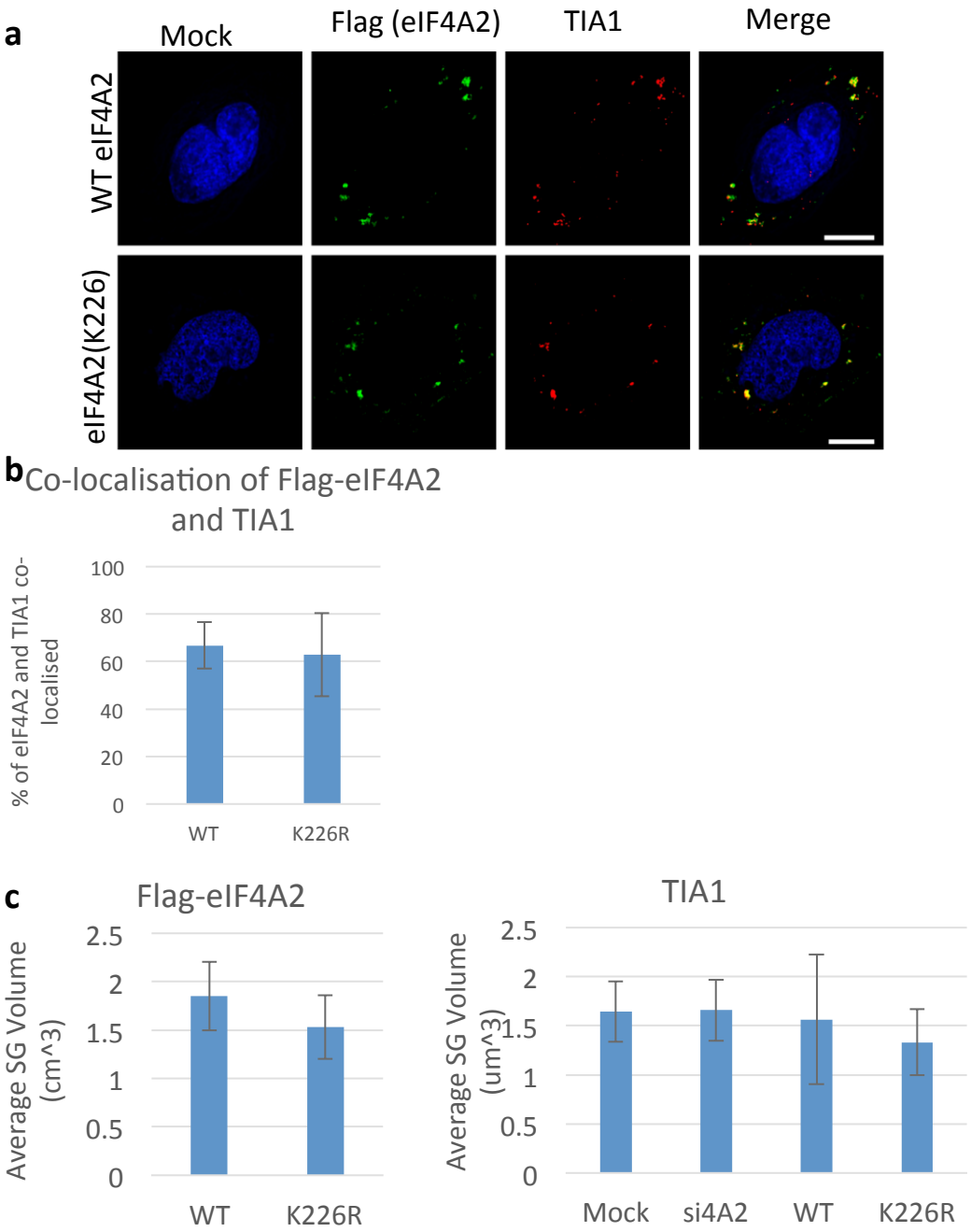

Figure 3.9 Mutation of K226 results in a slight reduction in overall stress granule volume after treatment with arsenite. HeLa cells were depleted of eIF4A2 by transfection with siRNA oligonucleotides. Following this cells were transfected with either wild-type Flag-eIF4A2 or the K226R mutant. Cells were fixed and stained for both Flag-eIF4A2 and TIA1. a) Example image showing high resolution z-stack (z=4µm 0.05µm/slice) images deconvolved using Softworx software suite. b) Co-localisation analysis was performed using Imaris software suite. Results show percentage of overlapping fluorescence signal averaged over 3 experiments. c) Average stress granule volume per image was calculated by mapping surfaces to fluorescence signal using Imaris software suite. Average of 3 experiments. Error bars show 1 standard deviation.

3.3 Discussion

Using recombinant proteins purified from *E. coli,* it was demonstrated that both eIF4A1 and eIF4A2 are SUMOylated *in vitro* using recombinant proteins affinity purified from *E. coli*. Additionally, K225 in eIF4A1 and K226 in eIF4A2 were identified as SUMOylation sites using LC-MS/MS. There are some limitations to these results, one of the foremost being the use of SUMOylation protein components purified from *S. pombe*. It is possible that the yeast SUMO conjugation machinery is not representative of the specificity and individual complexity that is present in mammalian cells. Mammals possess several SUMO E3 ligases that are each capable of dictating SUMO target specificity and which may result in SUMOylation of other lysine(s) [250].

Consideration also has to be made for the ability of *E. coli* to correctly fold mammalian proteins. *In vitro* SUMOylation artefacts could be identified by the incorrect folding/unmasking of lysine residues not present on the external face of the protein structure. Although these additional sites can be SUMOylated they are unlikely to represent genuine target sites due to their location within the correctly folded protein. To answer this latter point, the sites identified on both eIF4A1 and eIF4A2 map to an external face of the available crystal structures of both eIF4A1 and the N-terminal domain of eIF4A2, supporting the conclusion that they are true SUMOylation sites [245, 246].

In order to confirm the *in vitro* results, we went on to show that SUMOylated isoforms of eIF4A1 and eIF4A2 can be identified *in vivo* in mammalian cells by utilising HeLa cells stably expressing His-SUMO1 and His-SUMO2. One of the limitations of using these cell types is that the overexpression of SUMO within the cell could dramatically alter the physiology of the cells. However, analysis of these cell lines reveals a comparable level of protein expression and minimal change to the quantity of SUMO conjugates [251, 252]. This likely reflects the availability of the rate limiting SUMOylation machinery required for the conjugation of SUMO to target proteins. However, the generation of stable cell lines relies on random genomic integration of the His-SUMO plasmid. This occurs without disruption to the endogenous SUMO gene, the result of which produces a mixture of potentially competing tagged and untagged protein being present within the cell. This could also be in part why we fail to observe additional bands signifying eIF4A modification with SUMO2/3 i.e. if His-tagged SUMO2 is not expressed as highly as the endogenous SUMO2 and SUMO3 genes.

By focusing on SUMO1 modification of eIF4A2 we were able to show that the lysine residue (K226) identified by mass spectrometry was the sole lysine residue SUMOylated *in vivo* by

creating a un-SUMOylatable mutant, K226R. Mutation of this residue results in an increase in smaller stress granules after treatment with arsenite. Care has to be taken however to account for the inevitable variation in over-expression of the construct produced by transiently transfecting cells with this construct. In order to account for the potential variation of expression of eIF4A2 by transient transfection, the stress granule volumes of TIA-1 were also analysed, revealing that both eIF4A2 and TIA-1 stress granule volumes decrease following transfection with the eIF4A2-K226R mutant. Alternatively, a larger scale experiment using automated SCANR microscopy could be used to assess the volumes of a much larger samples size. An additional advantage is that the volumes could be normalised to the total internal FITC intensity within each of the transfected cells. This would allow us to account for the variation in expression following transient transfection.

Finally, one might expect that if SUMOylation of eIF4A2 is required for the re-localisation of eIF4A2 to stress granules, over-expression of an unSUMOylatable mutant would fail to form stress granules altogether. This is not the case however as we still see that both TIA1, a known component of stress granules and eIF4A2 still localise to discrete cytoplasmic bodies. This is likely to result from similarities with PML body formation, during which SUMO creates a large binding surface and essentially acts like a ‘glue’ to hold PML and its binding partners together [49]. If the same is true for stress granules we may continue to see recruitment to stress granules while other eIFs within stress granules, such as eIF4G and eIF4E, are still modified. To fully identify the role of SUMO in stress granule formation, it may be necessary to identify and mutate all of the SUMOylation sites in the proteins contained in the eIF4F complex and analyse the defects produced. However, due to the relatively minor defects observed by mutating the SUMOylation site of eIF4A2 alone, the direction of the project was switched at this point.

4. Characterisation of the phospho-specific interactions between 53BP1 and TopBP1

4.1 Introduction

The N-terminus of 53BP1 contains 28 SQ/TQ phosphorylation site motifs [213]. Phosphorylation of 53BP1 within this region has been shown to mediate several protein-protein interactions, only a few of which have been demonstrated to be critical for the function of 53BP1. For example, the role of 53BP1 to promote repair by NHEJ relies on the ability to protect broken DNA ends from being resected by nucleases. This is achieved through a set of phospho-specific interactions between the phosphorylated SQ/TQ motifs located within N-terminal region of 53BP1 and other proteins such as Rif1 [190] and PTIP [213]. Additionally, in G1-phase cells, 53BP1 has also been shown to interact with TopBP1 [193] in a phosphorylation-dependent manner. These interactions appear to be at least partly conserved between species as this phosphorylation-dependent interaction has previously been observed in *Schizosaccharomyces pombe* between Crb2^{53BP1} and Rad4^{TopBP1} [238].

TopBP1 is a BRCT-containing protein that has 9 BRCT domains [220, 221] (figure 1.12) and acts predominantly during S-phase in the initiation of DNA replication [192, 253]. TopBP1 is also recruited to sites of replicative stress through interactions between the C-terminus of the Rad9 subunit of the Rad9-Hus1-Rad1 (9-1-1) complex [254]. Localisation of TopBP1 is required for the activation of the checkpoint kinase, ATR [255]. This activation requires the ATR activation domain (AAD) located within the C-terminal portion of TopBP1, just upstream of BRCT domains 7-8 [256]. Despite its predominant function in S-phase during replication, the role of the recruitment of TopBP1 to DSBs in G1-phase cells remains largely uncharacterised and suggests that TopBP1 has additional, cell-cycle dependent functions.

By cloning segments of TopBP1 and analysing the co-localisation with 53BP1, Cescutti et al demonstrated that the 53BP1-TopBP1 interaction in G1-phase is mediated by two sets of BRCT domains within TopBP1, BRCT domains 1-2 and 4-5 [193]. However in S- and G2-phase cells, TopBP1 localises at sites of damage through a separate combination of BRCT-dependent interactions: in S- and G2-phase cells TopBP1 BRCT domains 1-2 and 7-8 are required for co-localisation of TopBP1 with RPA [193].

4.1.1 53BP1 phosphopeptides, pSer366 and pThr760, interact specifically with BRCT domains 4-5 and 1-2 *in vitro*

Previous work from the Pearl laboratory identified the requirement for CDK-dependent phosphorylation of Crb2^{53BP1} to promote interaction with the BRCT domains of Rad4^{TopBP1} [238].

In order to identify the phosphorylation sites within the N-terminus of 53BP1 that mediate the phospho-specific interaction with TopBP1, M. Day (Pearl Lab) identified a consensus peptide sequence that was required to mediate the phosphorylation-dependent interaction between the N-terminus of $Crb2^{53BP1}$ and BRCT domains 1,2 of $Rad4^{TopBP1}$. Using the consensus identified in figure 4.1a (where Φ is either alanine, valine, isoleucine, leucine or methionine and x is any amino acid) M.Day identified four candidate phosphopeptides. M. Day performed fluorescence polarisation experiments with each of the candidate phosphopeptides and recombinant TopBP1-BRCT domains.

Of the four candidate sites identified, two showed a specific interaction with the BRCT domains of TopBP1 (highlighted in green in figure 4.1a). 53BP1 phosphoserine-366 peptide specifically interacts with TopBP1 BRCT domains 4-5 (figure 4.1b) and phosphothreonine-670 peptide specifically interacts with TopBP1 BRCT domains 0, 1-2 (figure 4.1c). From these data, dissociation constants (K_d) were calculated. The interaction between BRCTs 4-5 and pSer366 has an affinity of 31.35 μM. The interaction between BRCTs 0, 1-2 and pThr670 displayed a much stronger affinity of 1 μM.

a

BRCT1	**Φ Φ Φ x x T/S P**
BRCT2	**Φ x x T/S P**
Thr 334	G G C S L A S T P A T
Ser 366	S S D L V A P S P D A
Ser 380	T P F I V P S S P T E
Thr 670	E V E E I P E T P C E

Φ=A,V,I,L,M
x=Any amino acid

b

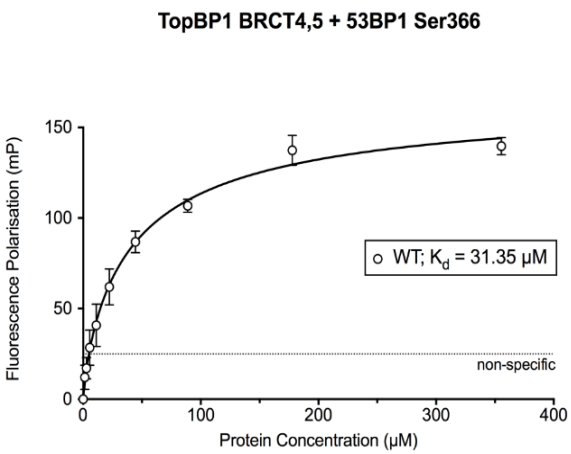

Fluorescein-GYG-SSDLVAPpSPDAFRSTP

c

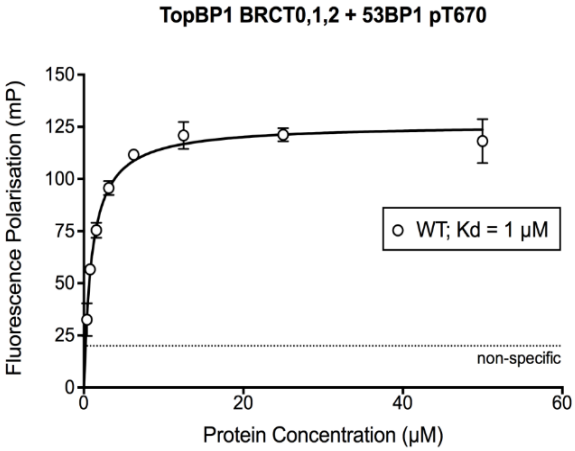

Fluorescein-GYG-VEEIPEpTPCESQGEE

Matthew Day

Figure 4.1 BRCT domains 4-5 and BRCT domains 0, 1 and 2 interact with phospho-serine 366 and phospho-threonine 670 *in vitro*. a) Consensus phosphopeptide motifs are in bold. Four candidate phosphopeptides from 53BP1 predicted to interact with TopBP1-BRCT1,2- predicted phosphorylated residue is highlighted in red. Phospho-peptides found to interact with TopBP1 are highlighted in green. Fluorescence polarisation performed by M. Day (Pearl lab) shows b) specific interaction of a phospho-serine 366 phosphopeptide labelled with fluoroscein when titrated against BRCT domains 4 and 5 of TopBP1. c) specific interaction of a phospho-threonine 670 phosphopeptide labelled with fluoroscein with BRCT domains 0, 1 and 2 of TopBP1. Fluorescence values below the dotted line indicate non-specific fluorescence.

4.2 Results

4.2.1 Ser366 and Thr670 of 53BP1 are phosphorylated in response to DNA damage

Having identified interactions between 53BP1-pSer366 and pThr670, and TopBP1 BRCTs 4-5 and 0, 1-2 *in vitro* using fluorescence polarisation, it was then necessary to establish whether these residues are in fact phosphorylated *in vivo.*

In order to do this, custom rabbit polyclonal antibodies were generated by ImmunoKontact® to target phosphorylated Ser366 and phosphorylated Thr670 phospho-peptides. To test the specificity of the antibodies, HeLa cells were either transfected with siRNA oligonucleotides targeting 53BP1 or transfected with a non-targeting control. 48 hours following transfection the cells were either exposed to 8Gy of ionising radiation or left untreated before incubating for a further 4 hours. Whole cell extracts were prepared by lysing cells in SDS-PAGE sample buffer followed by sonication. The lysates were analysed by Western blot for 53BP1, tubulin and the two phospho-specific antibodies.

The results indicated that both of the phospho-specific antibodies, pSer366 and pThr670, recognise 53BP1 as shown by the absence of bands in cells depleted of 53BP1 (figure 4.2). Furthermore, both Ser366 and Thr670 only appear to be phosphorylated following DNA damage suggesting that these interactions may form part of a DNA damage-specific response.

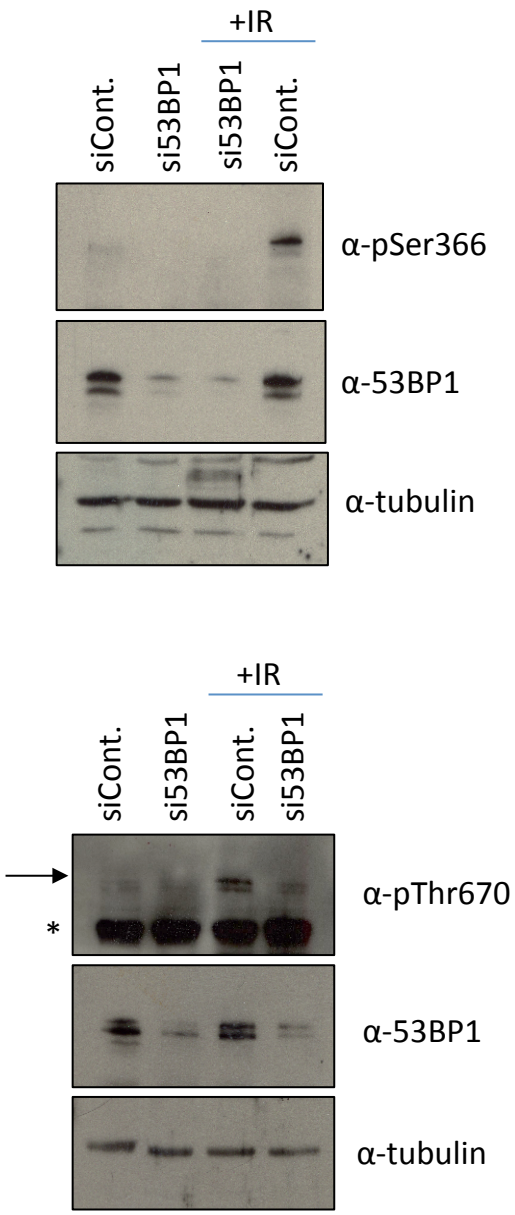

Figure 4.2 53BP1 is phosphorylated on Serine-366 and Threonine-670 in response to ionising radiation. HeLa cells were reverse transfected with either siRNA targeting 53BP1 or a non-targeting control and incubated for 48 hours. After which, cells were exposed to 8Gy IR and allowed to recover for 4 hours before lysing the cells processing for western blotting by sonication. Whole cell extracts were analysed by Western blot and probed for phospho-Ser366, phospho-Thr670, 53BP1 and tubulin. *Indicates non-specific bands. Arrow indicates 53BP1 phosphorylated on T670.

4.2.2 TopBP1 fails to co-immunoprecipitate with 53BP1 phospho-binding site mutants

After demonstrating that the phosphorylation sites that facilitate interaction between 53BP1 and TopBP1 *in vitro* are genuine phosphorylation sites used *in vivo*, it was important to test whether failure to phosphorylate either of these sites disrupted the 53BP1-TopBP1 interaction.

In order to do this, Dr O. Wilkinson (Watts Lab) used site-directed mutagenesis to generate unphosphorylatable mutants in a HA-53BP1 cDNA construct: a serine to alanine substitution mutation at residue 366 (S366A) and a threonine to alanine mutation at residue 670 (T670A). A double-mutant was also made containing both S366 and T670 to alanine mutations (SATA).

HEK293 cells were transfected by calcium phosphate transfection protocol. Following transfection the cells were incubated for a further 60 hours. The cells were either exposed to 8Gy of ionising radiation using an X-ray machine or left untreated. The cells were incubated for 4 hours following irradiation before processing for immunoprecipitation. Samples were analysed by Western blotting using anti-HA (53BP1) and TopBP1.

TopBP1 co-immunoprecipitated with HA-53BP1 in cells transfected with the wild-type 53BP1 cDNA construct (figure 4.3). This indicates that these two proteins interact *in vivo* in mammalian cells. However, when the cells were transfected with either S366A, T670A or the double-mutant, the amount of TopBP1 that co-immunoprecipitates with 53BP1 is reduced. Unexpectedly, TopBP1 co-immunoprecipitates with the wild-type 53BP1 regardless of whether the cells were exposed to ionising radiation prior to harvesting. The reason for this is not clear, but could be indicative of stress induced by the overexpression of 53BP1 within these cells. Overall, these results indicate that inability to phosphorylate either S366 or T670, within the N-terminus of 53BP1, impairs the interaction between 53BP1 and TopBP1.

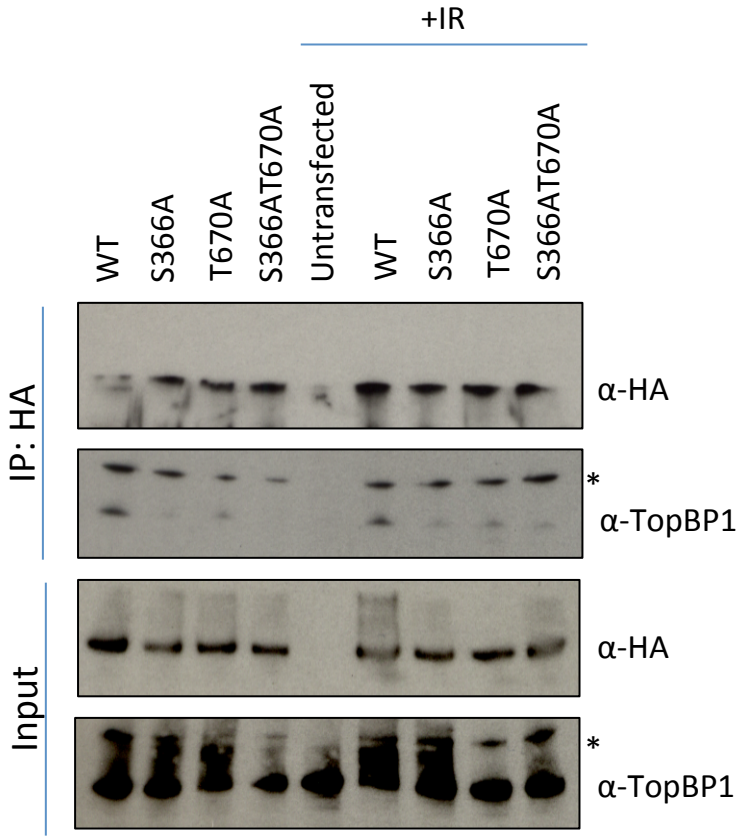

Figure 4.3 Mutation of S366 or T670 to alanine impairs co-immunoprecipitation of HA-53BP1 and TopBP1. HEK293FT cells were cultured and transfected with HA-53BP1 constructs (wild-type or mutant) using calcium phosphate protocol and incubated for a further 60 hours. Cells were then exposed to 9Gy IR and allowed to recover for 4 hours before lysis. IP was performed using HA-IP kit (Sigma) using provided buffers supplemented with cocktail protease and phosphatase inhibitors. Samples were analysed by Western blot for HA and TopBP1. *marks non-specific antibody binding of TopBP1 antibody.

4.2.3 53BP1 phosphorylation mutants fail to co-localise with TopBP1 following DNA damage in G1-phase cells

Having established that the mutation of either 53BP1-S366 or -T670 decreases the interaction between 53BP1 and TopBP1, it was then important to analyse the localisation of these proteins within the cells. Firstly, it was necessary to identify whether either of these mutations prevented 53BP1 from localising to sites of damage and secondly, whether TopBP1 was also still recruited to sites of DNA damage and if so, whether the two proteins co-localised. Additional markers were employed to identify G1-phase cells prior to co-localisation analysis as previous investigation has demonstrated that the interaction of 53BP1 with TopBP1 is limited to G1-phase cells [193].

In order to do this, immunofluorescence was performed on cells depleted of endogenous 53BP1 and transfected with the HA (53BP1) cDNA constructs. Following on from transfection, the cells were treated with 8Gy of ionising radiation and left to recover for 4 hours, following the experimental methods outlined by Cescutti et al [193], before analysis by immunofluorescence. The cells were immuno-stained for HA (53BP1), TopBP1 and CENPF a marker expressed only in S- and G2-phase cells.

The results demonstrate that the 53BP1-S366A or -T670A mutants disrupt co-localisation of 53BP1 and TopBP1 in G1-phase cells (figure 4.4). Perfect co-localisation between 53BP1 and TopBP1 is observed following damage in cells transfected with the wild-type 53BP1 cDNA. Mutation of the phosphorylation site with the weaker affinity for TopBP1 BRCTs 4-5, S366, still appears to allow the formation of TopBP1 foci. However, these do not co-localise with 53BP1. In contrast, mutation of the phosphorylation site with the stronger affinity for TopBP1 BRCTs 0, 1-2, T670, drastically impairs TopBP1 focus formation in G1-phase cells.

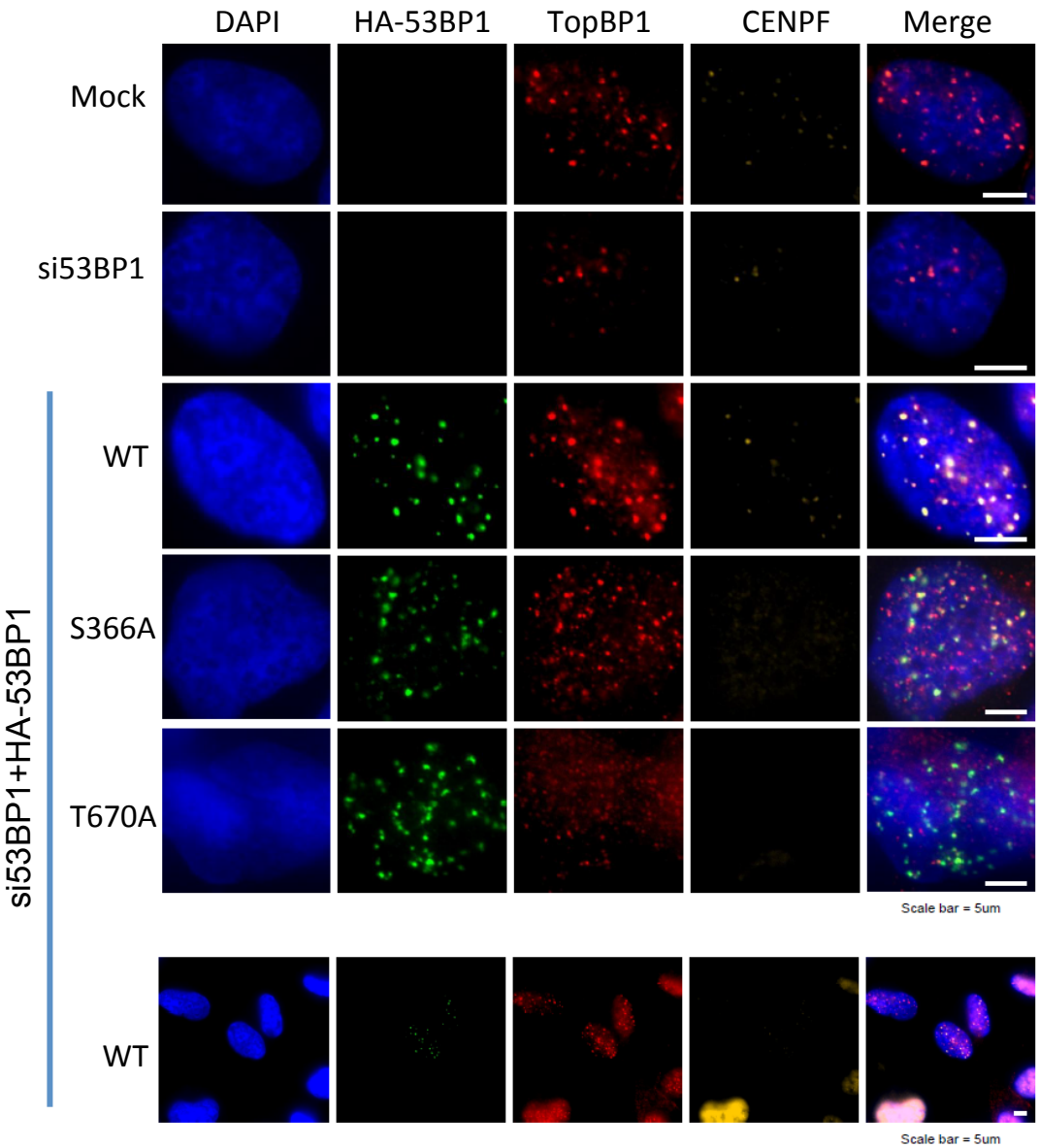

Figure 4.4 53BP1 phosphorylation sites, S366 and T670, are required for co-localisation of 53BP1 with TopBP1 in G1-phase cells. U20S cells were reverse transfected with 53BP1 siRNA. 48 hours later cells were transfected with an siRNA resistant construct containing either wild-type HA-53BP1 or one of the phosphorylation site mutants. 16 hours after this cells were exposed to 8Gy ionising radiation Cells were allowed to recover for 4 hours before fixation in methanol for 20 minutes and staining for HA, TopBP1 and CENPF. Bottom panel shows example of G1-phase cell identification by analysing cells negative for CENPF. Scale bar = 5 µm.

4.2.4 Quantitative analysis of 53BP1-TopBP1 co-localisation using SCANR microscopy

Given that the mutation of two phosphorylation sites in 53BP1 appears to affect co-localisation with TopBP1, it was important to further analyse this phenotype and quantify this defect. With support from Dr. Velibor Savic (University of Sussex), SCANR automated microscopy was employed to image and analyse large numbers of cells to further investigate the co-localisation. The same experimental set up was used as before: 53BP1-depleted cells were transfected with the cDNA constructs and seeding them into a 96-well SCANR plate. Following irradiation the cells were fixed and stained as before.

The SCANR microscope was programmed to take 36x 3-channel images per well at a 20x magnification. Each image was analysed for total internal DAPI intensity to generate a cell cycle profile to which each cell could then be characterised as either G1- S- or G2-phase. This would enable the isolation and analysis of just the G1-phase population of cells. Following this, each of the cells was analysed for 53BP1 and TopBP1 foci based on a set of criteria determined by analysing several example images. For example, the minimum and maximum size and intensity of each focus was set to include as many foci as possible but also to exclude any staining artefacts. Finally, the X and Y co-ordinates along with their size and reference to which cell they belong was exported.

Using this equipment and methodology it was possible to analyse over 91,000 cells over 4 biological repeats in which over 670,000 TopBP1 foci and over 50,000 53BP1 foci were identified.

In order to analyse such a vast array of data, G1-phase population of cells were identified based on the cell cycle profile generated before. Next, the transfected population of cells were identified and plotted on X and Y co-ordinates in Microsoft Excel along with the data for each TopBP1 and 53BP1 focus including the radius of each. From this it was possible to score each G1-phase transfected cell as to whether TopBP1 and 53BP1 IRIF were co-localised.

One of the limitations of this experimental format was the transfection efficiency in which the number of transfected cells ranged from 1 to 5% of the total population of cells. In order to minimise the number of cells excluded from analysis based on the variable expression level of 53BP1, a cell was scored as having co-localised foci if one or more 53BP1 foci overlapped with a TopBP1 focus. Overlap was defined as the centre of 1 focus intersected by the perimeter of another.

Finally, over 350 cells were counted per sample and defined as either having or not having 53BP1-TopBP1 co-localised foci. The results show that mutation of either S366 or T670 to alanine disrupts the co-localisation of 53BP1 and TopBP1 in G1-phase cells (figure 4.5a and b). As co-localisation of 53BP1 and TopBP1 has been demonstrated to be limited to G1-phase cells whereby in G2-phase cells TopBP1 co-localises with RPA [193], G2-phase cells transfected with the wild-type 53BP1 cDNA construct were also analysed for co-localisation. Approximately 18% of the G2-phase cells analysed were still scored as having co-localised foci even in G2-phase, this gave an indication the background level of co-localisation reported using these parameters. Having analysed the background co-localisation observed in G2-phase cells, it can be seen that mutation of 53BP1-S366 and -T670 impairs co-localisation of 53BP1 and TopBP1 to near background levels.

After having demonstrated that the co-localisation of TopBP1 to sites of DNA damage required phosphorylation of 53BP1 on both S366 and T670, it was necessary to test whether the number of TopBP1 foci was affected by the loss of 53BP1. Provisionally, it looked as if the number of TopBP1 foci in these cells decreased as seen in figure 4.4.

In order to further examine whether this was indeed the case, the SCANR data generated above was used to calculate the average number of TopBP1 foci identified per cell in both mock-treated cells and those transfected with siRNA oligonucleotides targeting 53BP1. Additionally, it was possible to segregate the populations of both G1- and G2-phase cells. The results indicate that 53BP1-depleted G1-phase cells have fewer TopBP1 foci following DNA damage than those mock-treated (figure 4.6). Additionally, it can also be seen that the number of TopBP1 foci per cell in G2-phase cells remains unchanged between the mock-treated and 53BP1-depleted cells following damage. This serves to consolidate the notion that the localisation of TopBP1 in G1-phase cells is at least in part a 53BP1-dependent event.

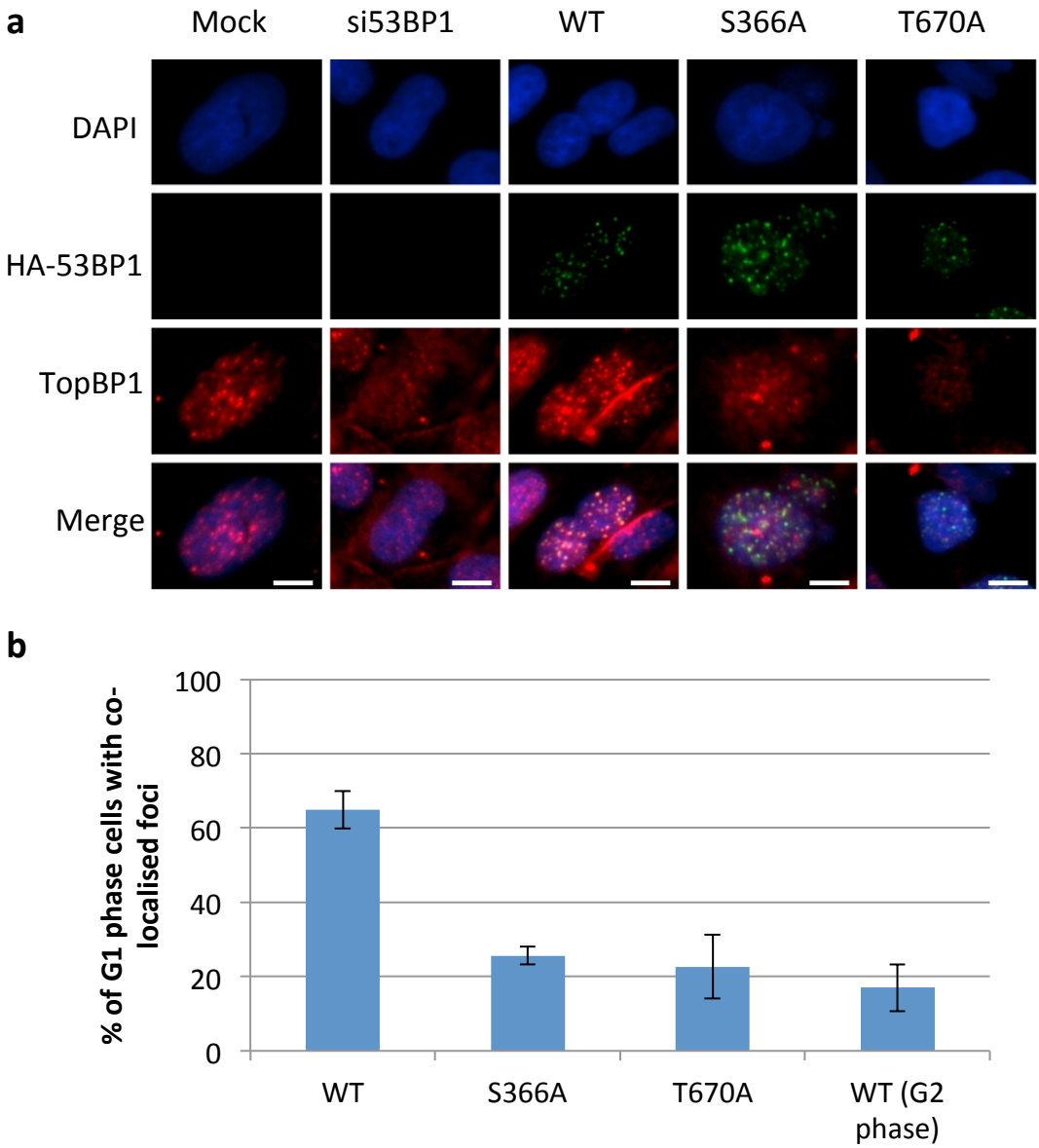

Figure 4.5 53BP1 phosphorylation sites, S366 and T670, are required for TopBP1 binding. U20S cells were reverse transfected with 53BP1 siRNA. 24 hours later cells were transfected with an siRNA resistant construct containing wild-type HA-53BP1 or one of the BRCT mutants. 24 hours after this cells were re-plated into a 96-well SCANR plate and after a further 24 hours were exposed to 8Gy ionising radiation Cells were permitted to recover for 4 hours before staining for HA and TopBP1. SCANR software was used to take 36 images per well at 20x magnification. a) shows example images taken by the SCANR microscope. b) Each image was analysed for 53BP1, TopBP1 foci and DAPI intensity. DAPI intensity was used to create cell cycle profiles and gate for G1 phase cells. The resulting population of cells were scored for co-localisation (co-localised foci ≥ 1 per cell). N>345 transfected cells analysed for each sample over 4 experimental repeats. Error bars represent 1 standard deviation.

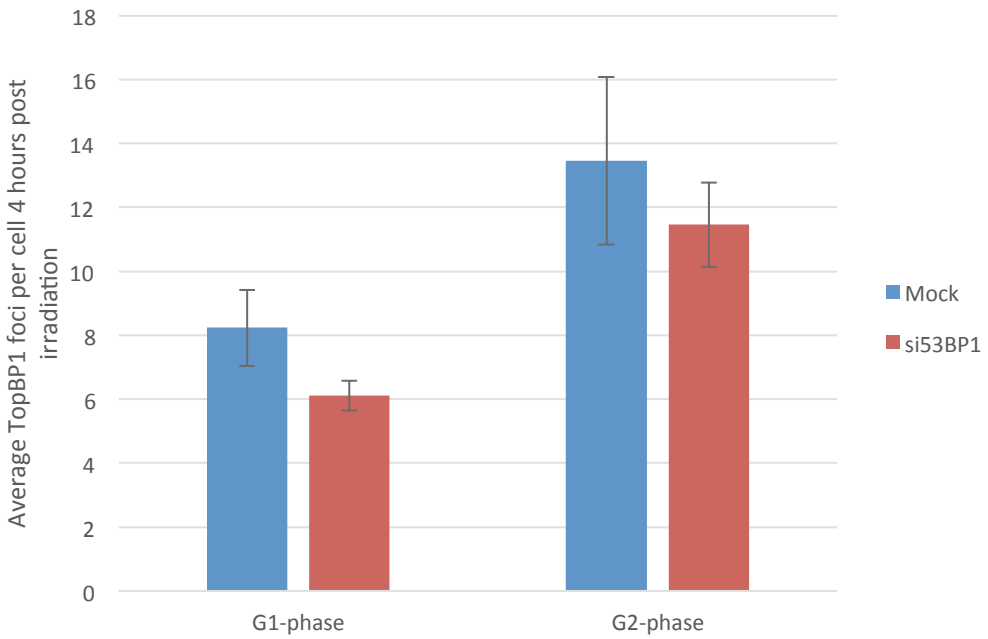

Figure 4.6 Depletion of 53BP1 reduces the number of TopBP1 foci in G1 phase cells. U20S cells processed as in figure 4.5 were analysed by SCANR 4 hours after exposure to 8Gy ionising radiation either with or without prior depletion of 53BP1 by RNAi. 36 images per well were analysed to calculate the number of TopBP1 foci per cell in G1-phase and G2-phase cells based on DAPI intensity. Once cells had been categorised the number of TopBP1 foci per cell was calculated for each population. N>59000 foci were analysed per sample over 4 experimental repeats.

4.2.5 S366A and T670A mutants display altered cell cycle profiles

After having demonstrated that both 53BP1-S366 and -T670 are phosphorylated *in vivo* and that inability to phosphorylate 53BP1 results in a failure to co-localise TopBP1 in G1-phase cells, it was necessary to identify and characterise any physiological defect that may occur as a consequence.

Previous work from Cescutti et al [193] demonstrated that both TopBP1 and 53BP1 are required for sustained G1-S phase arrest of cells following DNA damage and that a stable cell line expressing TopBP1 lacking the BRCT domains 4-5 also fails to sustain a G1-S phase checkpoint. In their study, they did not test mutant TopBP1 lacking BRCT domains 0, 1-2 although from our co-immunoprecipitation and immunofluorescence data, it seems likely that failure of 53BP1 to interact with TopBP1-BRCT domains 0, 1-2 may also produce a comparable defect.

In order to determine whether an inability to phosphorylate 53BP1 on either of these phosphorylation sites results in a checkpoint defect, the SCANR data were re-analysed. This involved determination of the cell-cycle status of each cell analysed based on total internal DAPI intensity. The cell-cycle status of each cell transfected with either wild-type 53BP1 or one of the mutants, could then be compared to determine whether there were more cells in a particular phase of the cell-cycle 8 hours following the introduction of DNA damage. Although this would provide only a single snap-shot of the cell cycle profiles following damage, it would give some indication as to whether there was any alteration in the cell cycle profile with the unphosphorylatable 53BP1 mutants. Additionally, in order to account for cells that may still express the cDNA constructs but not necessarily form foci, total internal fluorescence intensity was also measured for each cell. Fluorescence intensity above a threshold determined by examining mock-transfected cells was used to examine the transfected population of cells.

Following the introduction of DNA damage, it would be expected that cells would initiate a cell-cycle arrest. If a cell-cycle checkpoint defect is present, in the hours following irradiation the population of cells may be skewed towards either G1- or G2- phase depending on the stage in which the cell-cycle the defect occurs. By analysing the number of cells in each stage of the cell-cycle 8 hours following the introduction of DNA damage, cells transfected with either the 53BP1-S366A or -T670A mutant show altered cell cycle profiles characterised by a larger G2-phase population of cells compared to those cells transfected with the wild-type cDNA (figure 4.7). The larger proportion of G2-phase cells observed following damage in the

samples transfected with the phosphorylation mutants, compared to those transfected with the wild-type 53BP1, suggests that there is a cell-cycle checkpoint defect.

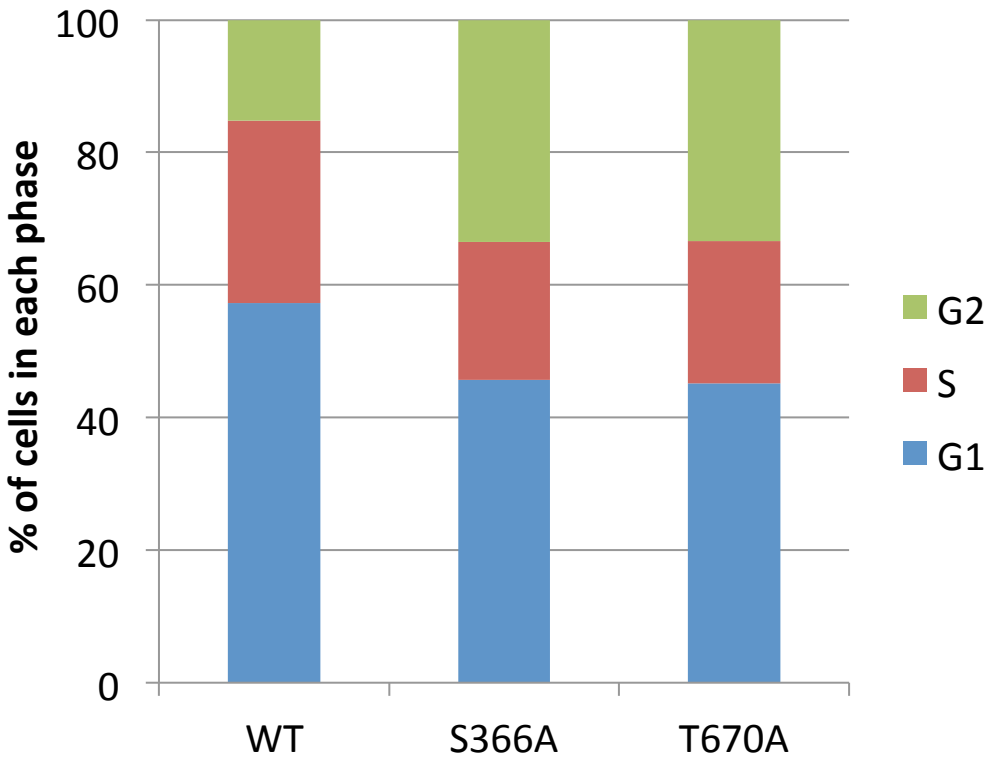

Figure 4.7 53BP1 phosphorylation mutants show altered cell cycle profiles. U20S cells processed as in figure 4.5 were analysed by SCANR 4 hours after exposure to 8Gy ionising radiation. Only cells expressing either wild-type 53BP1 (WT) or the phosphorylation site mutants (S366A and T670A) were compared. 36 images per well were analysed for DAPI intensity and total internal FITC intensity to generate a cell cycle profile of transfected cells. N>1325 cells were analysed per sample. Chart shows the proportion of transfected cells 4 hours post irradiation in each stage of the cell cycle (either G1, S or G2-phase).

4.2.6 53BP1 phosphorylation mutants fail to maintain the S-phase entry checkpoint following damage

To further investigate whether phosphorylation of 53BP1 was required for G1-S cell cycle arrest following damage, it was necessary to employ a more accurate assay to test whether the cells could arrest in G1-phase and prevent premature entry into S-phase following damage.

In order to do this cells were treated as before by depleting endogenous 53BP1 in U2OS cells before transfecting the cells with either wild-type 53BP1, 53BP1-S366A, -T670A or the double mutant. The cells were seeded at low confluence to allow them to continue cycling throughout treatment. After transfection the cells were pulse-labelled with the nucleotide analogue, EdU, for 1 hour at 37°C. This enabled the identification of cells that were already in S-phase prior to irradiation. Following EdU-labelling, the cells were washed in PBS and irradiated. After irradiation the cells were treated with media supplemented with a second nucleotide analogue, BrdU, for a further 7 hours at 37°C (figure 4.8a). By utilising this series of pulse labelling experiments it was possible to determine whether cells were progressing through G1 into S phase following damage.

Firstly, by examining the number of EdU-negative cells (i.e. cells not already in S-phase at the time of irradiation) and BrdU positive cells (i.e. cells entering s-phase following damage) it can be seen that in mock-treated cells exposed to 2Gy ionising radiation there is a decrease in the number of BrdU positive cells following ionising radiation, which is indicative of a G1-S phase arrest (figure 4.8b). Furthermore, by depleting 53BP1 by RNAi comparable numbers of BrdU positive cells can be observed in both the un-treated and those exposed to ionising radiation, confirming that these cells fail to sustain a G1-S phase cell cycle arrest. This is consistent with the observations made by Cescutti et al [193].

Having confirmed that there is a G1-S phase checkpoint defect in a 53BP1-depleted background, it was necessary to establish whether the cell-cycle defect was attributable to the phosphorylation sites identified earlier. To do this, the experiment was repeated with the additional transfection of the 53BP1-depleted U2OS cells with either the wild-type or mutant cDNA constructs, either 53BP1-S366A, -T670A or the double mutant. Additional immunostaining for HA was used to identify transfected cells.

By analysing the transfected population of cells and assessing whether or not they had incorporated the 2nd DNA label, it was possible to see examples of cells transfected with the mutant 53BP1 that continued into S-phase despite the presence of damage (figure 4.8c). Furthermore, it was possible to quantify the number of EdU negative; BrdU positive cells

transfected with either the wild-type 53BP1 cDNA or the phosphorylation mutants as a percentage of the total EdU negative cells (figure 4.8d). These results demonstrate that 53BP1-depleted cells expressing wild-type 53BP1 are capable of sustaining G1 arrest, whereas the cells transfected with either 53BP1-S366A, -T670A or the double mutant are not capable of sustaining G1 arrest (figure 4.8e).

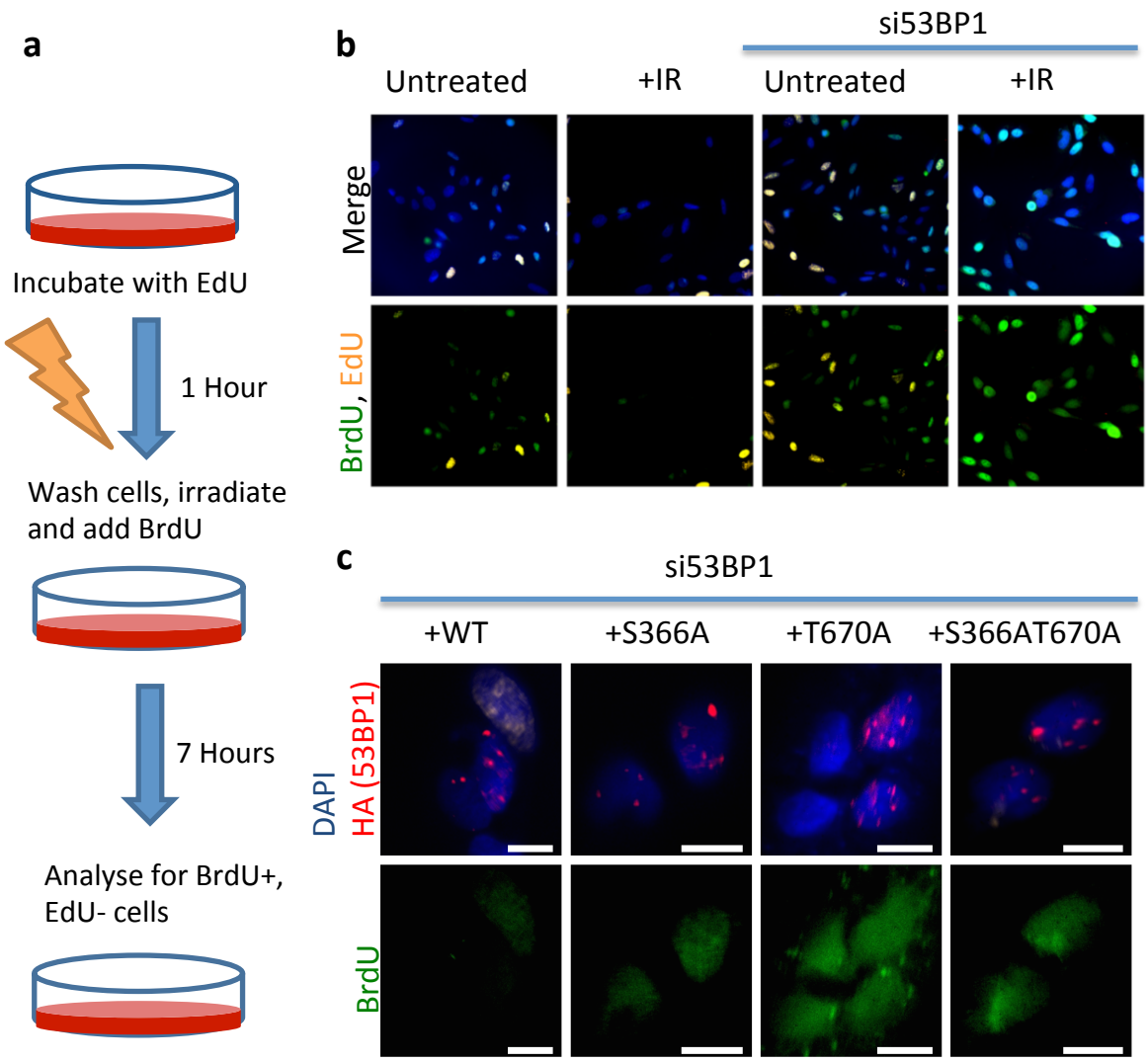

Figure 4.8 Phosphorylation of S366 and T670 are required for maintenance of the G1-S phase checkpoint. a) Diagrammatic representation of treatment. U20S cells were reverse transfected with 53BP1 siRNA. 48 hours later cells were transfected with an siRNA resistant construct containing wild-type HA-53BP1 or one of the phosphorylation mutants. 15 hours later cells were incubated for 1 hour with EdU before washing, irradiated with 2Gy ionising radiation and the addition of BrdU and nocodazole. Cells were incubated for a further 7 hours before fixation and staining for HA, EdU and BrdU. EdU+ cells (Yellow) were ignored for analysis. S-phase entry after damage was analysed by counting BrdU+ cells (Green). b) shows effect of siRNA depletion of 53BP1 on G1-S phase entry by incorporation of BrdU following damage. c) shows example images of BrdU incorporation in transfected cells. d) shows quantification of EdU negative; BrdU positive cells following IR with and without depletion of 53BP1. e) shows quantification of EdU negative; BrdU positive cells following IR with depletion of endogenous 53BP1 and transfection with either wild-type or mutant 53BP1.

d

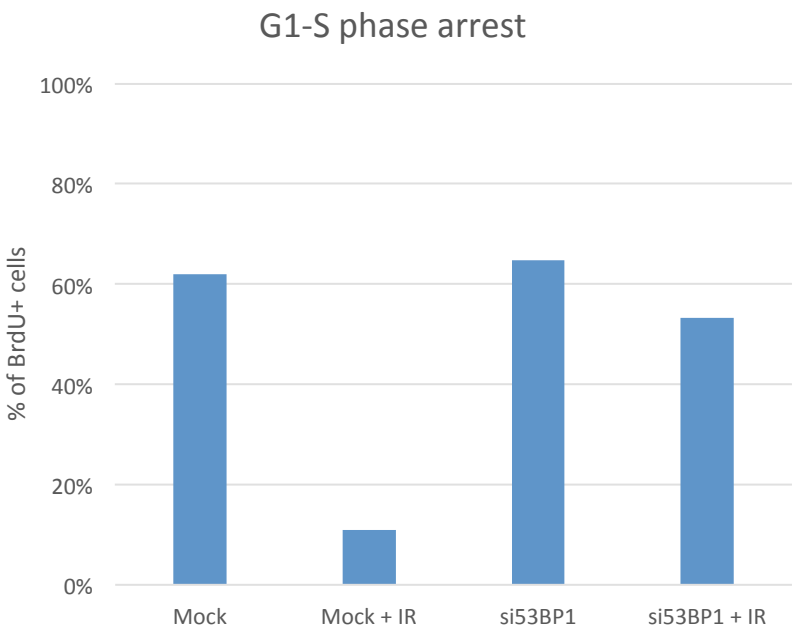
G1-S phase arrest
100%
80%
60%
40%
20%
0%
% of BrdU+ cells
Mock
Mock + IR
si53BP1
si53BP1 + IR

e

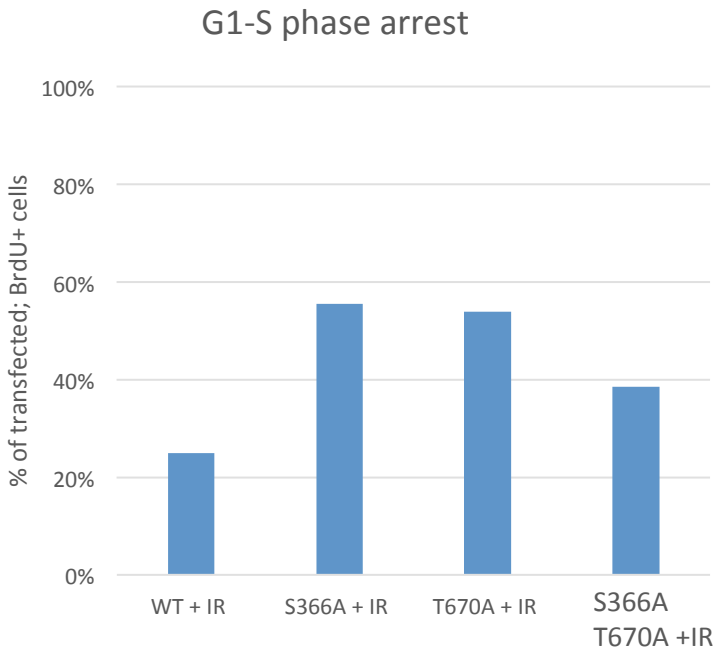
G1-S phase arrest
100%
80%
60%
40%
20%
0%
% of transfected; BrdU+ cells
WT + IR
S366A + IR
T670A + IR
S366A
T670A +IR

4.2.7 53BP1 phosphorylation mutants show a 'slow' kinetic repair defect

Having determined that mutation of either S366 or T670 within the N-terminus of 53BP1 confers a checkpoint defect, it was necessary to analyse whether these mutations result in a failure to repair DNA breaks following DNA damage.

To investigate this, HeLa cells were reverse transfected with siRNA oligonucleotides targeting 53BP1 as before. Following this, the cells were transfected with either the wild-type 53BP1 construct or one of the phosphorylation mutants. Cells were then exposed to 5Gy ionising radiation and allowed to recover for the indicated time before fixation and immunostaining for HA (53BP), γH2AX and CENPF. The γH2AX foci were enumerated in cells negative for CENPF i.e. cells in G1-phase.

A repair defect was observed 16 and 24 hours following irradiation in cells transfected with 53BP1-S366A, -T670A or the double mutant (figure 4.9). These cells appear to show a 'slow' kinetic repair defect. Previous investigations have shown these types of defects to result from a failure to resolve complex breaks or those dependent on the chromatin environment [202, 203].

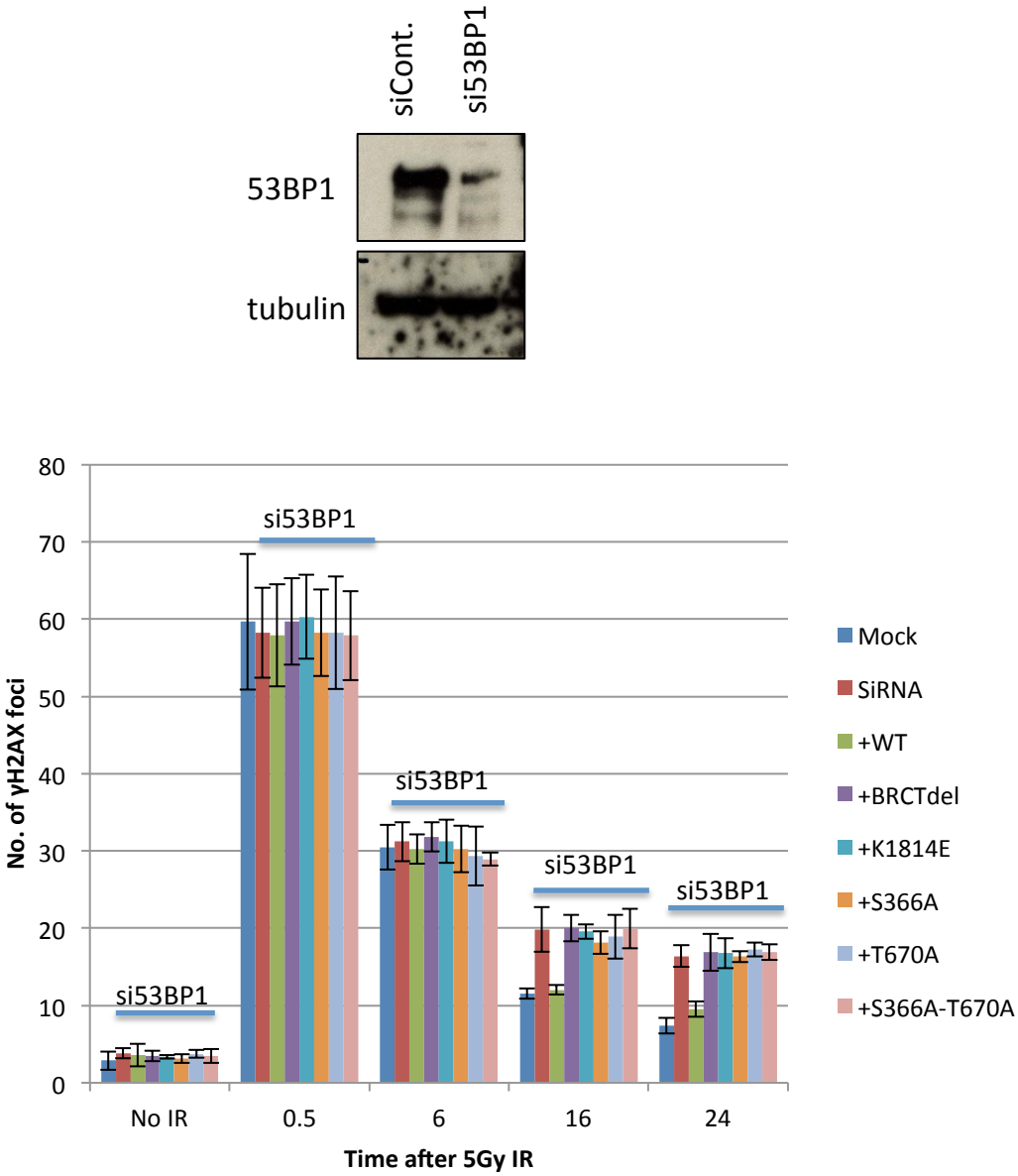

Figure 4.9 53BP1 phosphorylation mutants show a 'slow' kinetic repair defect. HeLa cells were reverse transfected with 53BP1 siRNA. 48 hours later cells were transfected with an siRNA resistant construct containing wild-type HA-53BP1 or one of the phosphorylation mutants. 16 hours later cells were exposed to 5Gy ionising radiation and allowed to recover for the indicated time before staining for HA, γH2AX and CENPF. The number of γH2AX foci per cell was enumerated n=25 CENPF negative cells. Graph shows average of 3 experiments. Error bars represent 1 standard deviation. Horizontal blue bars show samples depleted of 53BP1 by RNAi.

4.2.8 The late stage repair defect can be rescued by depletion of KAP-1

KRAB-associated protein 1 (KAP-1) is a key regulator of chromatin structure and remodelling in response to DNA damage. Previous investigation has indicated a role for pATM-dependent phosphorylation of KAP-1 on S824 in facilitating the 'slow' kinetic repair of complex or DSBs [202, 203]. Phosphorylation of KAP-1 acts to promote chromatin relaxation and accessibility to DSB sites. It was therefore decided to test whether the 'slow' kinetic repair defect is due to an inability to phosphorylate KAP-1 to promote chromatin relaxation.

To investigate this, HeLa cells were either depleted of 53BP1 as before or double-depleted of both 53BP1 and KAP-1. As described above, siRNA resistant constructs were transfected into either 53BP1-depleted or double-depleted (si53BP1/siKAP1) backgrounds. Cells were then exposed to 3Gy ionising radiation, allowed to recover for the indicated time before fixing and staining for HA (53BP1) and γH2AX. Finally, γH2AX foci were enumerated to indicate the number of breaks remaining within the cell at that time.

Enumeration of γH2AX foci in cells double-depleted of 53BP1 and KAP-1 reveals that the additional depletion of KAP-1 bypasses the 'slow' kinetic repair defect produced by depletion of 53BP1 or transfection with 53BP1-S366A, -T670A or the double mutant (figure 4.10). This indicates that these persistent DSBs result from a failure to repair breaks in regions of heterochromatin.

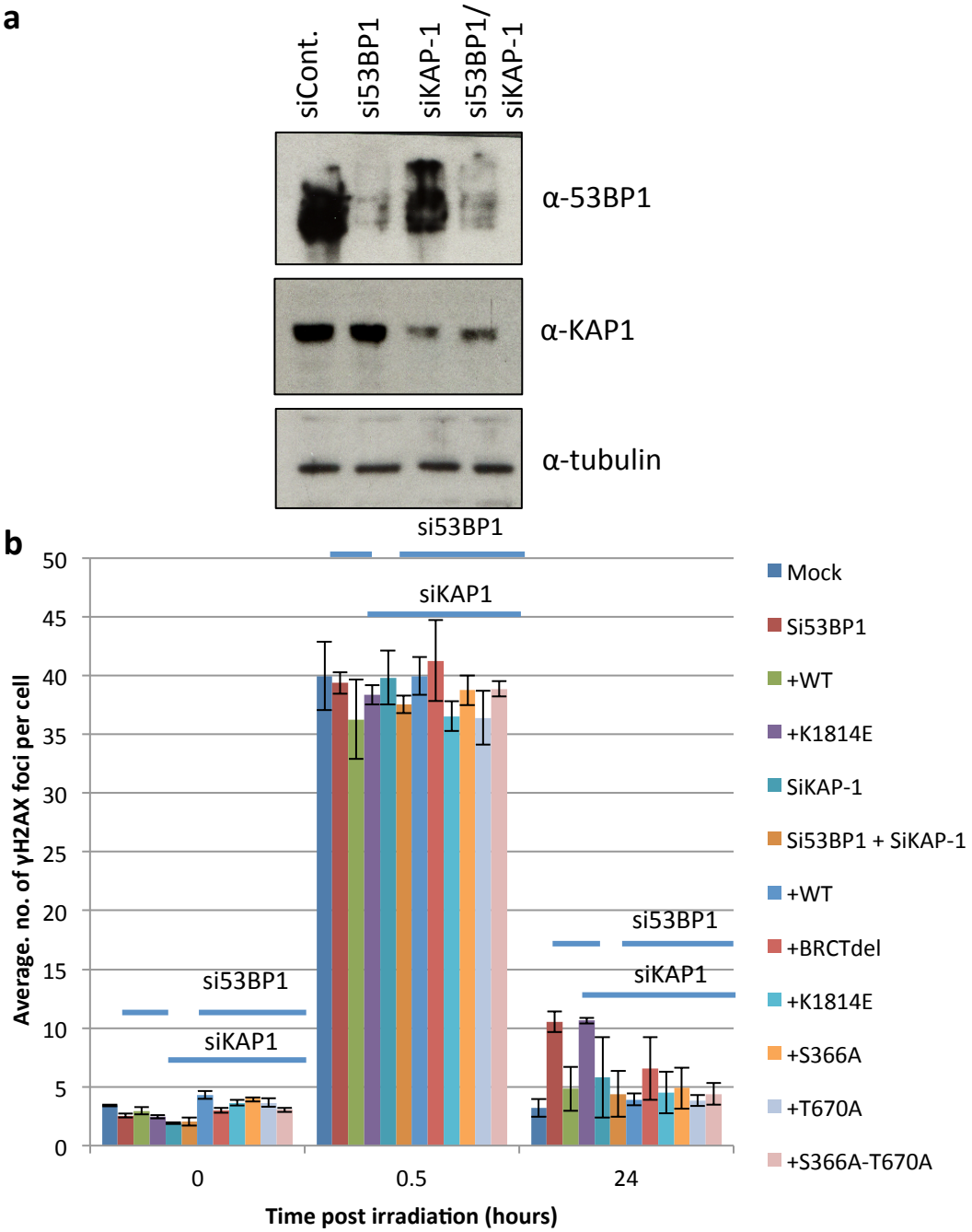

Figure 4.10 siRNA depletion of KAP-1 rescues the 'slow' kinetic repair defect in 53BP1 phosphorylation mutants. HeLa cells were reverse transfected with 53BP1 and/or KAP-1 siRNA. 48 hours later cells were transfected with an siRNA resistant construct containing wild-type HA-53BP1 or one of the BRCT mutants. 16 hours later cells were exposed to 3Gy ionising radiation and allowed to recover for the indicated time before staining for HA and γH2AX. a) Western blot of whole cell extracts showing siRNA depletion of 53BP1 and KAP-1. b) Graph shows the average number of γH2AX foci per cell (average of 3 experiments, error bars show 1 standard deviation). Horizontal blue bars show samples depleted of 53BP1 and/or KAP-1.

4.2.9 53BP1 phosphorylation mutants show normal repositioning of 53BP1 in S- and G2-phase cells

Having identified that the 53BP1 phosphorylation site mutants, S366A and T670A, have G1, G1/S checkpoint defects and fail to repair a fraction of the total number of breaks, it then became necessary to determine if the defects observed were limited solely to G1-phase cells.

53BP1 plays a pivotal role in the choice of DSB repair mechanism- favouring NHEJ over HR by preventing resection of the broken DNA ends [190]. 53BP1 does this by antagonising BRCA1 in S-and G2-phase cells [212]. Previously it has been observed that 53BP1 is physically repositioned to the periphery of the IRIF several hours following exposure to ionising radiation and that this repositioning is critical for the progression to HR-mediated repair [210].

In order to examine whether repositioning of 53BP1 was altered, the localisation of BRCA1 relative to 53BP1 was assessed in S- and G2-phase cells following the introduction of DNA damage. This was achieved by exposing cells to 3Gy ionising radiation before allowing them to recover for a period of 8 hours. The cells were then fixed and immunostained for BRCA1 and 53BP1. High-resolution z-stack images were taken on a z-range of 2µm at 0.1µm intervals. The images were deconvolved and IRIF intensity profiles were measured across both channels to determine the relative distance of 53BP1 from BRCA1.

No repositioning defect was observed as the 53BP1 phosphorylation mutant proteins, 53BP1-S366A, - T670A and the double mutant were repositioned normally, relative to BRCA1, towards the periphery of IRIF in S- and G2-phase cells (figure 4.11). This indicates that this S- and G2-phase specific function of 53BP1 does not require these phosphorylation sites.

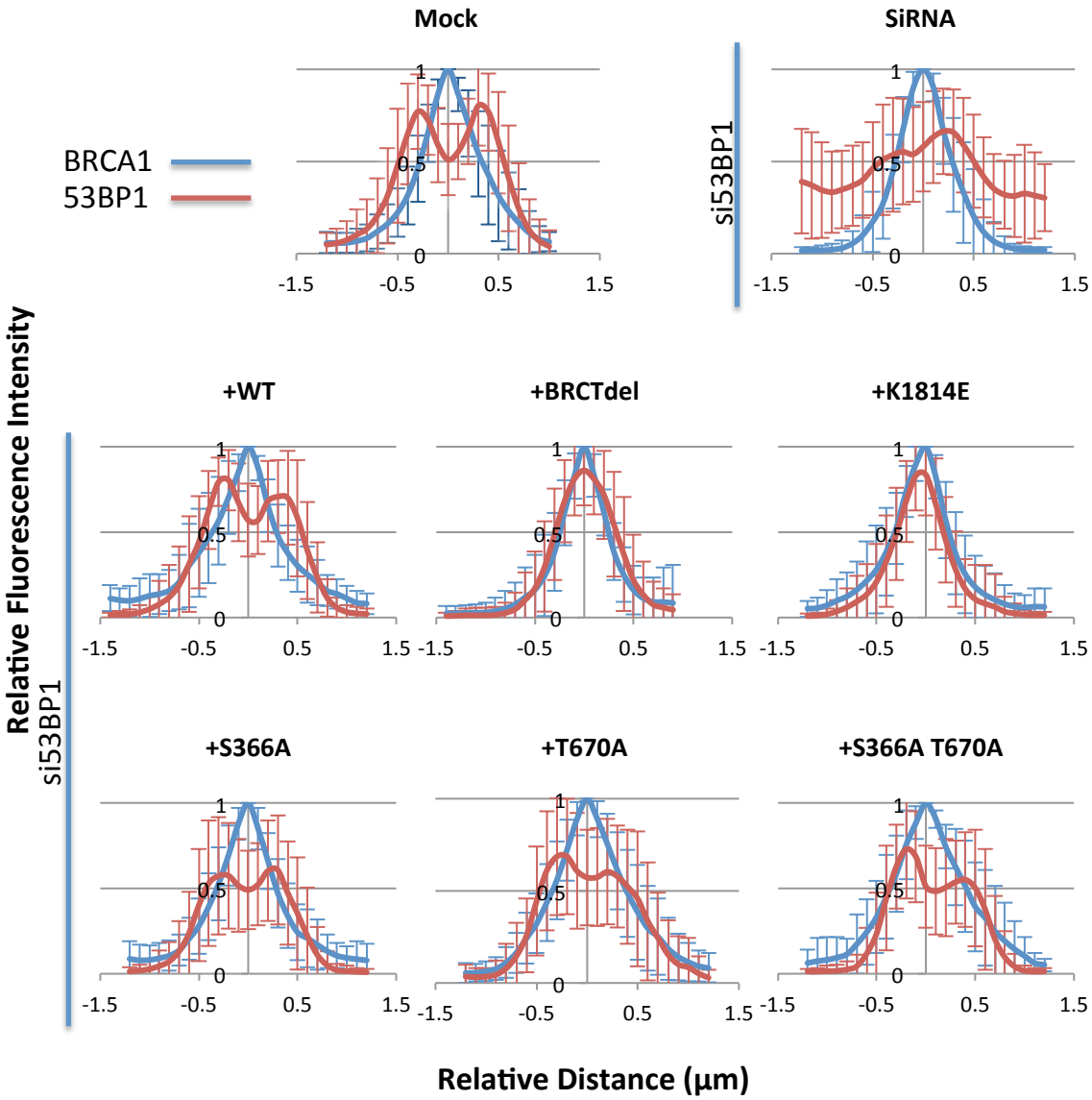

Figure 4.11 53BP1 phosphorylation site mutants show normal displacement by BRCA1 in G2 cells. HeLa cells were reverse transfected with 53BP1 siRNA. 48 hours later cells were transfected with an siRNA resistant construct containing wild-type HA-53BP1 or one of the BRCT mutants. 16 hours after this cells were exposed to either 3Gy (Mock and WT) or 1Gy IR for mutants and allowed to recover for 8 hours before staining for HA and BRCA1. High resolution, deconvolved Z-stack images were obtained. Quantitative measurements of intensity across foci were generated using softWoRx software (n>20 foci) error bars show 1 standard deviation. Vertical blue bars show samples depleted of 53BP1 by RNAi.

4.3 Discussion

In vitro analysis of two phospho-peptides from the N-terminus of 53BP1 revealed a specific interaction between phosphorylated 53BP1 and the BRCT domains of TopBP1. A phosphoserine366-containing 53BP1 peptide interacts with BRCT domains 4-5 of TopBP1 with a dissociation constant of 31.35µM. A second interaction was also identified, specifically between a phosphothreonine670-containing 53BP1 peptide and BRCT domains 0, 1-2 of TopBP1. Interestingly, this second interaction had a much higher affinity with a dissociation constant of 1µM. Furthermore, it was possible to establish that these sites were genuine phosphorylation targets and were phosphorylated *in vivo* following DNA damage using custom antibodies generated against the phosphopeptides.

Western analysis of whole cell extracts taken from HeLa cells with and without RNAi depletion of 53BP1 indicates that both of the custom antibodies are specific to 53BP1. Further work is required to test whether there is any cross-reactivity with the un-phosphorylated peptide. This could be achieved by Western analysis of lysates pre-treated with λ-phosphatase. Despite this, the lack of reactivity with lysate from HeLa cells without exposing the cells to ionising radiation prior to lysing does indicate a degree of specificity. Finally, although these antibodies are suitable for studying the phosphorylation of 53BP1 when proteins can be resolved based on their molecular weight, non-specific activity of the antibodies with proteins with a lower molecular weight, revealed by Western analysis, indicate that these antibodies may not be suitable for immunofluorescence-based experiments.

By mutating either S366 or T670 to alanine, it was possible to demonstrate that inability to phosphorylate either residue individually, affects the ability of TopBP1 to co-immunoprecipitate with 53BP1 (figure 4.3). TopBP1 also co-immunoprecipitates with HA-53BP1 even in the absence of DNA damage. This contrasts with the results from figure 4.2 which demonstrate that these residues are only phosphorylated following DNA damage. This might occur as a result of excess HA-53BP1 overexpression of the cDNA constructs within these cells. Calcium phosphate transfection of HEK293 cells is optimised to allow for the production of large quantities of protein. The overexpression itself could stress the cells and result in increased phosphorylation of these residues. Further, Western analysis of total cell extracts from these cells, probing for pSer-366 and pThr-670 could be used to test whether overexpression of 53BP1 in increases 53BP1 phosphorylation in the absence of DNA damage.

Alternatively, it is also possible that there is a basal level of 53BP1 phosphorylation, perhaps allowing 53BP1 and TopBP1 to co-operate within the cell, even in the absence DNA of damage.

This seems less likely however, as there was no increase observed in the quantity of TopBP1 co-immunoprecipitated from cells following exposure to ionising radiation compared to those without damage.

The failure of 53BP1 phosphorylation site mutants to co-localise with TopBP1 was quantified using SCANR microscopy. This automated approach allowed the analysis of a large number of cells and foci across different channels. Additionally, by generating profiles based on total internal DAPI staining intensity, the individual cell-cycle status of each cell could be determined. The data analysis using this method does have some limitations however, since analysis of the number of foci generated per cell is likely to be an underestimate of the true number, due to the way in which the data are analysed. A focus has to be defined by a clear set of criteria i.e. minimum intensity, minimum area and maximum area based on the exposure times for each image. These thresholds aim to prevent misinterpretation of background fluorescence and concurrently, antibody staining artefacts from being interpreted as additional foci. In order to prevent misidentification the thresholds are set slightly above the minimum requirement for focus identification based on manual analysis of several images. The assigned criteria are then applied to all of the images for analysis. The result is that some weaker foci or larger, more intense foci may not have been accounted for.

Analysis of the number of transfected cells identified in each phase of the cell cycle reveals a larger S- and G2-phase population of cells following DNA damage in cells transfected with 53BP1-S366A and -T670A. Although these data indicate a marked difference in the cell-cycle profiles 4 hours following DNA damage there are some limitations to these results. These results only provide a single snapshot of cell-cycle status following DNA damage. It is possible that these cells had entered S-phase prior to irradiation and had subsequently entered G2-phase by the time the cells were fixed. Additionally, G2-phase cells were not prevented from proceeding through mitosis during the experiment. Further controls would be needed to confirm that the cell cycle changes occur specifically in response to DNA damage i.e. including the cell cycle profiles of un-irradiated controls. As a result, it was necessary to analyse this phenotype in a more controlled environment. In order to do this, dual-pulse labelling experiments were employed to examine the G1-S checkpoint.

Utilising the dual-pulse labelling assay, it was possible to determine that consistent with previous observations, loss of 53BP1 results in a failure to sustain the G1-S phase checkpoint [193]. This experimental format allowed the identification only of cells that had entered S-phase following irradiation and allowed us to exclude the population of cells that had already

entered S-phase before irradiation, as determined by the incorporation of the first DNA analogue EdU. Secondly, transfected cells could be identified by the presence of HA (53BP1) foci for the wild-type and mutant constructs. However, this experiment is limited as transfected cells can only be identified in the presence of DNA damage i.e. the formation of HA (53BP1) foci. Ideally, it would be necessary to identify transfected cells in the presence and absence of damage to confirm that the cell-cycle defect, caused by mutation of 53BP1, only occurs in response to DNA damage. This could be achieved using fluorescence activated cell sorting to identify transfected cells irrespectively of HA-53BP1 IRIF formation.

With any cell-cycle analysis the choice of cell line utilised is critical. Some cell lines, such as HeLa cells, are very highly transformed and as a result intricate regulation of the cell cycle is lost. In fact it is questionable as to whether HeLa cells display any cell-cycle control at all. Often this ability to regulate the cell cycle stems from mutated p53, a common feature in cancerous/immortalised cell lines. In order to study the G1-S phase checkpoint, U2OS cells were used as they are a transfectable isogenic cell line with an intact p53 response and are capable of sustaining a G1-S phase arrest following the introduction of DNA damage as shown in Figure 4.8a.

Although more representative than HeLa cells, U2OS cells might not accurately represent the physiological response to damage. This may be better represented using different cell lines such as *hTERT*-immortalised retinal pigment epithelium (RPE) cells. These cells are more physiologically representative of uncancerous cells and are immortalised via the expression of telomerase allowing indefinite proliferation. Further analysis of several cell lines under the same test conditions would help to confirm whether a cell-cycle defect is occurring and would negate any cell line-specific traits that may affect the results.

Further work will be required to establish whether under these experimental conditions there is a risk that the HeLa cells are still cycling following on from the introduction of damage. In order to be confident that only G1-phase cells were being analysed, CENPF a marker of S- and G2-phase cells was used as a selection marker. Despite this, there is also the possibility that at the longest time point i.e. 24 hours following irradiation, the cells may have continued through the cell-cycle. If that is the case, it is possible that cells that were analysed could have passed through S-, G2- and M-phase back to G1 prior to the enumeration of foci.

In order to try and account for this a number of steps could be taken. Firstly, U20S or another cell line capable of confluence arrest could be utilised for these experiments to analyse non-

cycling cells. Secondly, nocodazole could be used to block cells from cycling from G2-phase through mitosis and back through to G1-phase. This could be performed in combination with CENPF staining to identify only non-cycling G1-phase cells.

To further characterise the DNA DSBs that persist at late stages following irradiation, dual depletion of KAP-1 and 53BP1 was demonstrated to bypass the 53BP1-dependent repair kinetics indicating that this subset of breaks require phosphorylation of KAP-1 to allow relaxation of heterochromatin in order to resolve these breaks. As before, care has to be taken to account for any disruption to the cell cycle using these experimental formats and additionally, to determine if depletion of KAP-1 has ramifications beyond repair of DSBs.

In order to account for this, dual-depletion of 53BP1 and KAP-1 followed by a double knock-in of 53BP1 could be used with a phospho-mimetic and un-phosphorylatable mutant of KAP-1. This would determine whether the bypassing of the repair defect by depletion of KAP-1 is synonymous with ATM-dependent phosphorylation of KAP-1.

5. Determining the phospho-specific interactions of the BRCA-1 C-terminal (BRCT) domains of 53BP1

5.1 Introduction

In a previous collaboration between the Watts and Pearl labs it was shown that in *S. pombe*, the BRCT domains of Crb2, the orthologue of 53BP1, interact directly with γH2A [205]. Conservation of this interaction is suggested by the fact that the *S. cerevisiae* orthologue Rad9, also interacts with phosphorylated H2A [199]. To build on this we wished to establish whether mammalian 53BP1 is capable of mediating the same interaction and if so, to determine the functional role of this interaction in DNA repair.

Previously, Noon et al [257] showed that deletion of the BRCT domains of 53BP1 results in a 'slow' kinetic repair defect as shown by enumeration of γH2AX foci following exposure to IR. These breaks are proposed to represent approximately 15% of the total number of breaks i.e. those generated in regions of heterochromatin. In order for the DNA repair machinery to gain access to the break site and facilitate repair, extensive chromatin remodeling and reorganization is required. As this phenotype was observed by deleting the entire region encoding the BRCT domains it remained unclear as to which set(s) of specific interactions, mediated by these domains, are required for the correct processing of complex breaks. For example, the BRCT domains have been shown to mediate a phosphorylation-independent interaction with the tumor suppressor protein p53, as well as a phosphorylation-independent interaction with one of the heterotrimeric subunits of the MRN complex, Rad50 [258, 259].

Several groups have suggested that recruitment of 53BP1 to sites of DNA damage is dependent on phosphorylation of H2AX. In the experiments performed by Ward et al, H2AX +/+ and H2AX -/- embryonic stem cells were transfected with either wild-type H2AX or H2AX-S139A mutant (i.e. an unphosphorylatable H2AX mutant). As expected, they observed that formation of 53BP1 foci had been restored in the H2AX -/- cells that had been transfected with the wild-type histone variant. However, mutant cells transfected with the H2AX-S139A mutant failed to form 53BP1 foci, potentially reflecting the requirement for γH2AX at early time-points following damage [260]. More recently, Kocylowski et al used a similar experimental format to dissect the role of ubiquitination in 53BP1 recruitment. They studied RNF8 -/- MEFs, which fail to ubiquitinate histone H2A and failed to form 53BP1 foci. By transfecting the cells with a ubiquitin-H2A fusion protein they were able to restore the ability to form 53BP1 foci. Interestingly, introduction of the H2AX-S139A mutation failed to rescue the defect in 53BP1 focus formation despite the presence of ubiquitin [261].

Both of these experiments suggest an as yet uncharacterised role for phosphorylated H2AX in the localisation of 53BP1 into foci (i.e. other than methylation- and ubiquitination-dependent recruitment through the Tudor and UDR domain of 53BP1). Our aim was to establish whether 53BP1 directly interacts with γH2AX through its tandem BRCT domains.

5.1.1 Fluorescence polarisation reveals a phospho-specific interaction between the BRCT domains of 53BP1 and γH2AX

To begin to investigate the interaction of 53BP1 and γH2AX, Matthew Day (Pearl lab, University of Sussex) performed fluorescence polarisation with a fluorescein-coupled γH2AX phosphopeptide titrated against concentrations of purified recombinant BRCT domains from 53BP1 (figure 5.1a). He found that there was a specific interaction between the BRCT domains of 53BP1 and the γH2AX phosphopeptide. In addition to this, he was able to calculate a dissociation constant of 1.4μM for the interaction. He then went on to test whether this interaction was dependent on the peptide being phosphorylated. Pre-treatment of the γH2AX phosphopeptide with λ-phosphatase prior to *in* vitro analysis abolished its interaction. Since H2AX is phosphorylated on S139 in response to DNA damage [262], the significance of this phosphorylation-dependent interaction indicates a potential role for the interaction in the DNA damage response and more specifically in response to DSBs.

M. Day went on to further test the specificity exhibited by the BRCT domains of 53BP1 by performing the same experiment with another phosphopeptide, phospho-KAP-1. KAP-1 is phosphorylated on S821 by pATM in response to DNA damage and facilitates chromatin remodelling to allow repair. The BRCT domains of 53BP1 showed no interaction with the KAP-1 phosphopeptide (figure 5.1b) indicating that the BRCT domains display at least some degree of specificity.

It was proposed that the location of the 'pSQEY' motif at the C-terminal end of the phosphopeptide might be important for dictating the specificity exhibited by the BRCT domains. This contrasts with the KAP-1 phosphopeptide, in which three additional residues follow the 'pSQEL' motif, 'SGG' masking the otherwise exposed carboxyl group. Interestingly, amidation of the tyrosine or the addition of a single glycine residue at the C-terminal side of the γH2AX phosphopeptide significantly reduced the interaction of the BRCT domains of 53BP1 with the phosphopeptide (figure 5.1c). This indicates that the exposed C-terminal carboxyl group of the tyrosine is important for the interaction to occur and likely forms the basis of a unique biochemical signature that is specifically recognised by 53BP1.

In order to fully characterise this interaction, M. Day also analysed a known γH2AX interacting protein, MDC1 [263]. By performing fluorescence polarisation experiments using the γH2AX phosphopeptide, this time titrated against the BRCT domains of MDC1, he demonstrated that the BRCT domains of MDC1 specifically recognise γH2AX (figure 5.1d). The BRCT domains of MDC1 show a 3.5-fold higher affinity for γH2AX than those of 53BP1 with a calculated dissociation constant (K_d) of 0.4μM ± 0.05.

M. Day also solved the X-ray crystal structure of the BRCT domains of 53BP1 bound to the last four amino acids of the γH2AX phosphopeptide (figure 5.2a). Arginine 1811 of the BRCT domains of 53BP1 mediates polar contacts between the amine-containing functional group and the carboxyl-terminus of the γH2AX phosphopeptide, whilst lysine 1814 mediates contact between the amine-containing functional group and the phospho-serine residue (figure 5.2b). Having identified the residues critical for mediating this interaction, M. Day was able to show that by making either one of two charge reversal mutations (R1811E or K1814E), the specific interaction observed by fluorescence polarisation, was abolished (figure 5.1d).

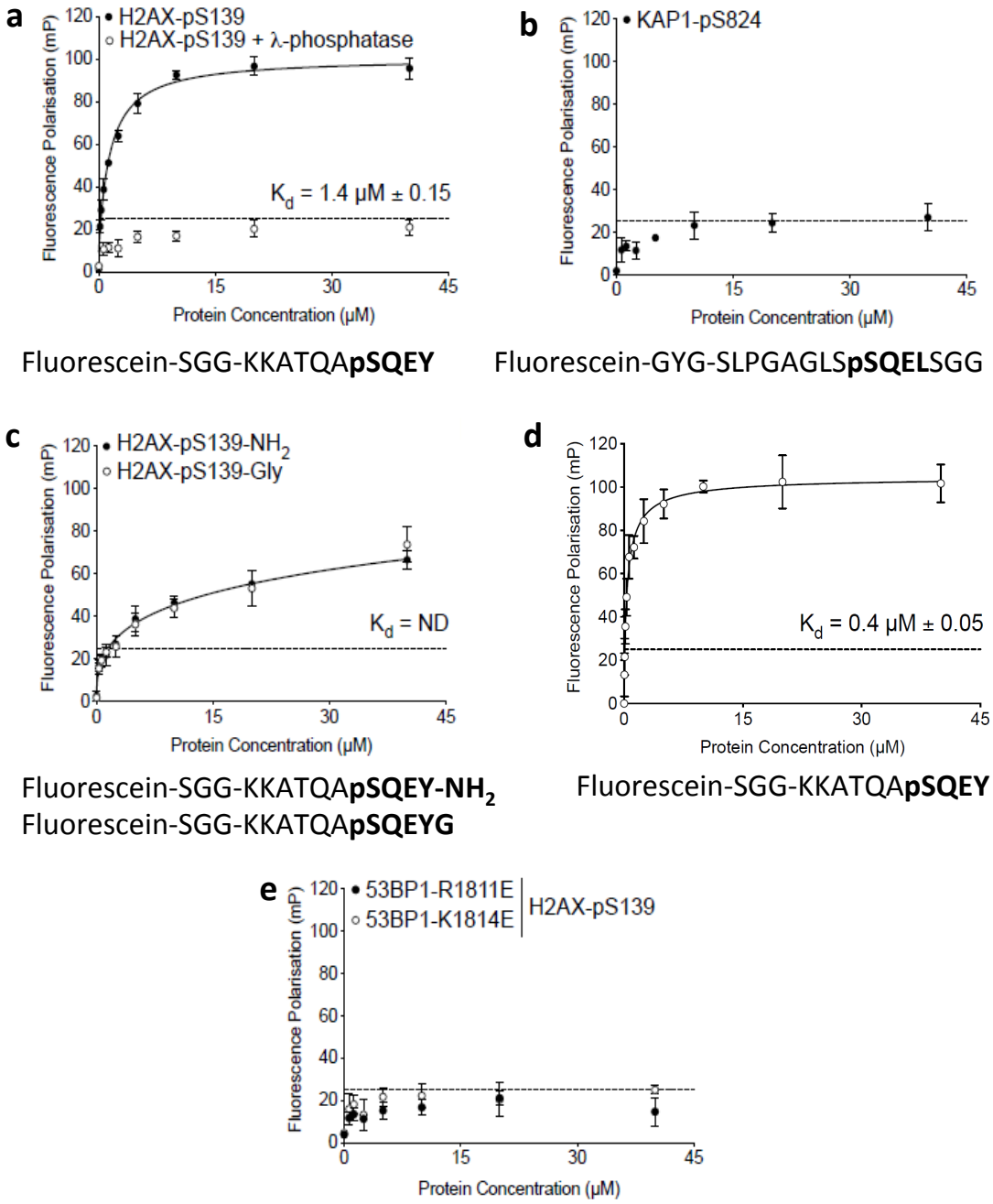

Matthew Day

Figure 5.1 53BP1 BRCT domains interact specifically with γH2AX phosphopeptide *in vitro.* Fluorescence polarisation performed by M. Day (Pearl Lab) shows a) 53BP1 BRCT domain interaction with γH2AX phosphopeptide with and without pre-treatment with λ-phosphatase. b) Interaction with KAP1 phosphopeptide. c) Interaction with charge reversal of the C-terminal tyrosine or charge neutralisation with glycine. d) Interaction of the BRCT domains of MDC1 with the γH2AX phosphopeptide d) BRCT mutants R1811E and K1814E with the γH2AX phosphopeptide.

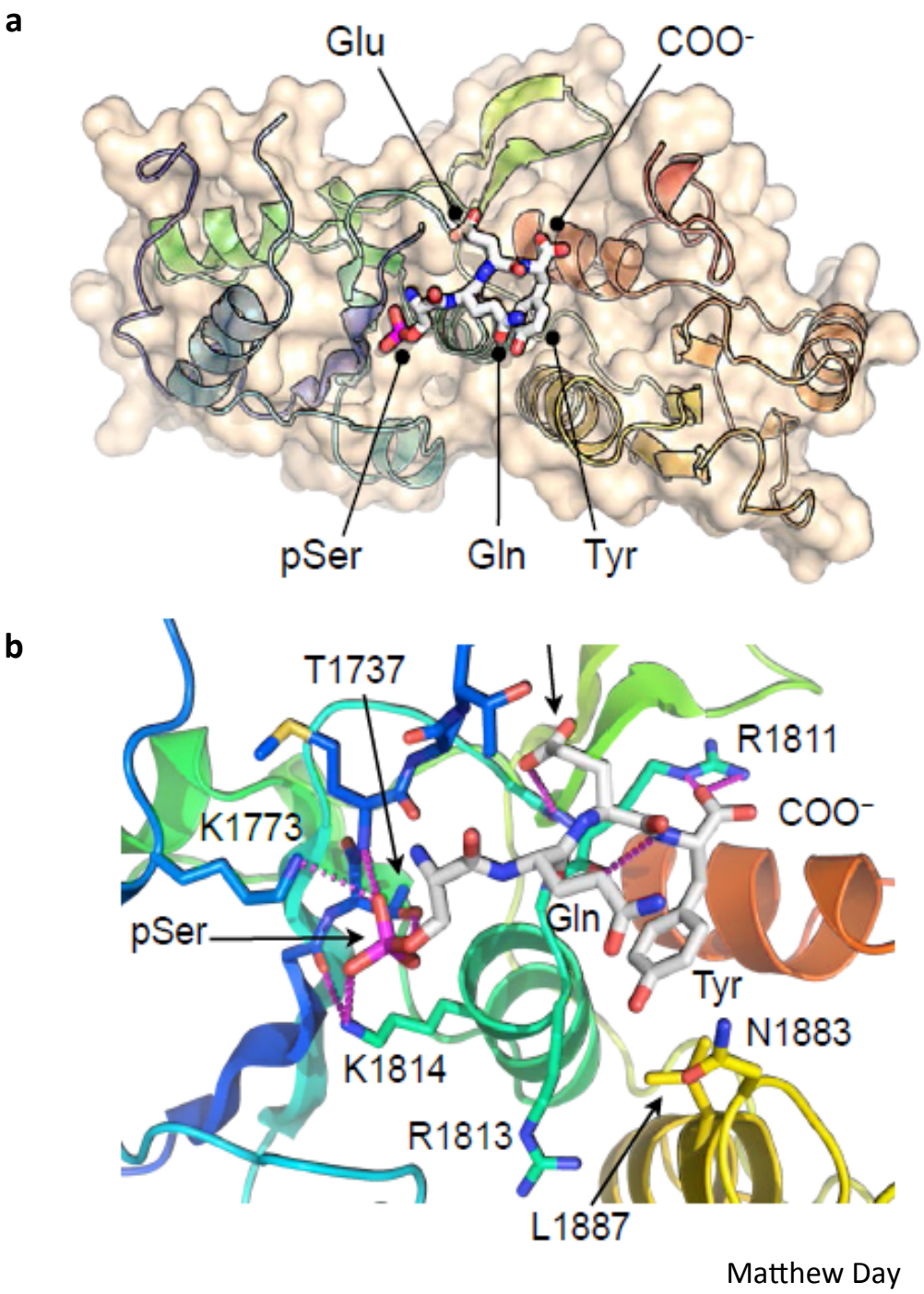

Figure 5.2 Crystal structure of γH2AX phosphopeptide bound to the BRCT domains of 53BP1. X-ray crystallography performed by Matthew Day**.** a) shows space filling model of the tandem BRCT domains of 53BP1 bound to the pSQEY peptide. b) shows detailed interaction between the phosphate group and K1814 of the BRCT domain as well as the carboxyl-group of the tyrosine and R1811.

5.2 Results

5.2.1 The BRCT domains of 53BP1 co-purify with γH2AX

Once it had been established that the BRCT domains of 53BP1 directly bind γH2AX *in vitro*, it was necessary to demonstrate this interaction *in vivo*. In order to do this the BRCT domains were cloned into an eYFP-tagged vector downstream of a nuclear localisation signal (cloning was performed by Dr Anthony Oliver). The two charge reversal mutants, R1811E and K1814E, were also introduced into the same vector. The constructs along with an empty vector control with just the eYFP and NLS alone, henceforth referred to as eYFP-NLS-BRCT (WT, R1811E or K1814E), were transfected into HeLa cells with the aim of generating stable transfected cell lines.

Stable cell lines expressing the YFP-tagged constructs were generated by culturing cells in selective medium 48h after transfection. The constructs used contained a neomycin-resistance gene and the medium was supplemented with G418 disulphate antibiotic 48 hours after transfection. As a result, any surviving cells that could proliferate in the medium approximately 14 days following transfection would have retained the plasmid and should express the YFP-NLS-BRCT domain. Stable cell lines were generated for both YFP-NLS-BRCT (WT) and YFP-NLS-BRCT (R1811E).

The stable cell lines were cultured and exposed to 30Gy of ionising radiation and incubated for a further hour before lysing. Dr Oliver performed a GFP-trap experiment to purify the recombinant BRCT domains from the mammalian cells. This enabled the analysis of proteins co-purifying with the BRCT domains under native conditions. Western analysis revealed that γH2AX co-purifies with the wild-type BRCT domains but not with the R1811E mutant (figure 5.3). The abolition of this interaction as shown by co-IP is consistent with and supplemented by the earlier structural and *in vitro* data.

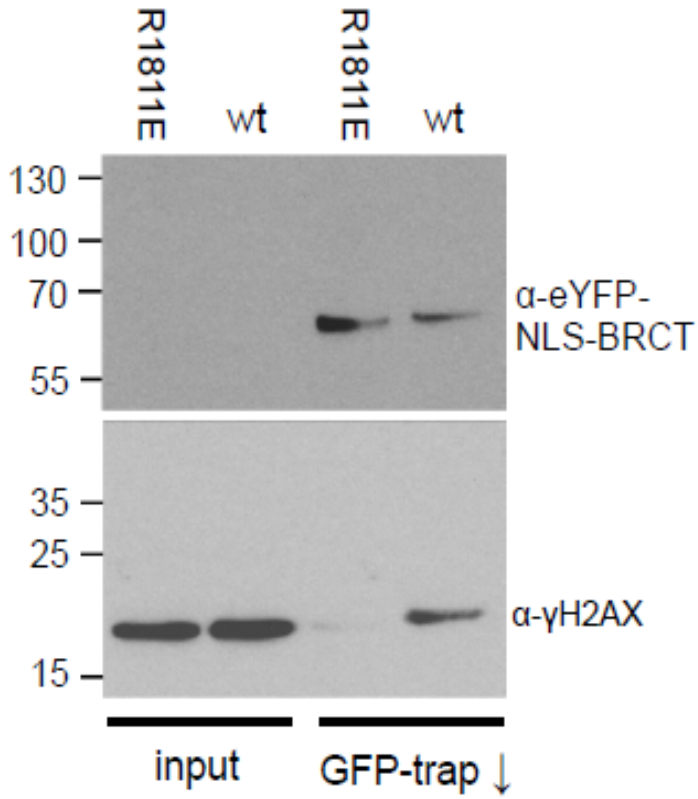

Antony Oliver

Figure 5.3 BRCT domains of 53BP1 can pull-down γH2AX following damage. Stable HeLa cell lines expressing YFP-NLS-BRCT wild type and R1811E were generated by G418 antibiotic selection. Cell lines were cultured in 4x 20cm dishes before irradiation with 30Gy IR. Cells were allowed to recover for 30 minutes before harvesting by scraping. Performed by Dr A Oliver, the cell lysates were incubated with GFP-trap resin along with protease and phosphatase inhibitors. Retained protein was analysed by SDS-PAGE and Western blot probed for YFP using a polyclonal GFP antibody and for γH2AX.

5.2.2 The BRCT domains in isolation can localise to sites of DNA damage

Once the interaction of the BRCT domains and γH2AX had been identified biochemically by co-purification from mammalian cells, it was then necessary to determine whether the BRCT domains alone could localise to sites of DNA damage.

In order to test this, cells were transiently transfected with the BRCT domain constructs eYFP-NLS-BRCT (WT, R1811E, K1814E or empty vector). The cells were pre-treated for 30 minutes at 37°C with Hoechst stain. Hoechst intercalates between stacked base pairs in double stranded DNA via the minor groove [264]. The dye was then excited using a high-power UVA laser to induce DNA damage in a highly localised region within the cell nucleus. Following the induction of damage, using a spinning-disc confocal microscope, it was possible to track and record changes in fluorescence intensity in real-time.

Using this approach, it was established that 53BP1-BRCT domains alone are capable of localising to sites of laser-induced damage independently of domains required for recognition of histone methylation and ubiquitination (figure 5.4a). In order to confirm that double strand breaks were generated by the laser, a control vector expressing the BRCT domains of MDC1, eYFP-NLS-BRCT (MDC1) (previously shown to interact with γH2AX [263]), was included. As demonstrated earlier, the BRCT domains of MDC1 have a 3.5-fold higher affinity for the γH2AX phosphopeptide. Interestingly, this increased affinity is apparent using this live-cell assay, the change in fluorescence intensity of MDC1-BRCTs is nearly 3-fold higher than that of 53BP1-BRCTs (figure 5.4b).

Furthermore, cells transfected with either of the two BRCT mutant constructs (YFP-NLS-R1811E or K1814E) fail localise to sites of damage as indicated by the negligible change in fluorescence intensity following the introduction of DNA damage (figure 5.4b). Failure of the two mutant BRCT domains (R1811E and K1814E) to localise to sites of damage strongly supports the hypothesis that this interaction is phosphorylation dependent and specifically requires the interaction with the carboxyl group on the phosphopeptide.

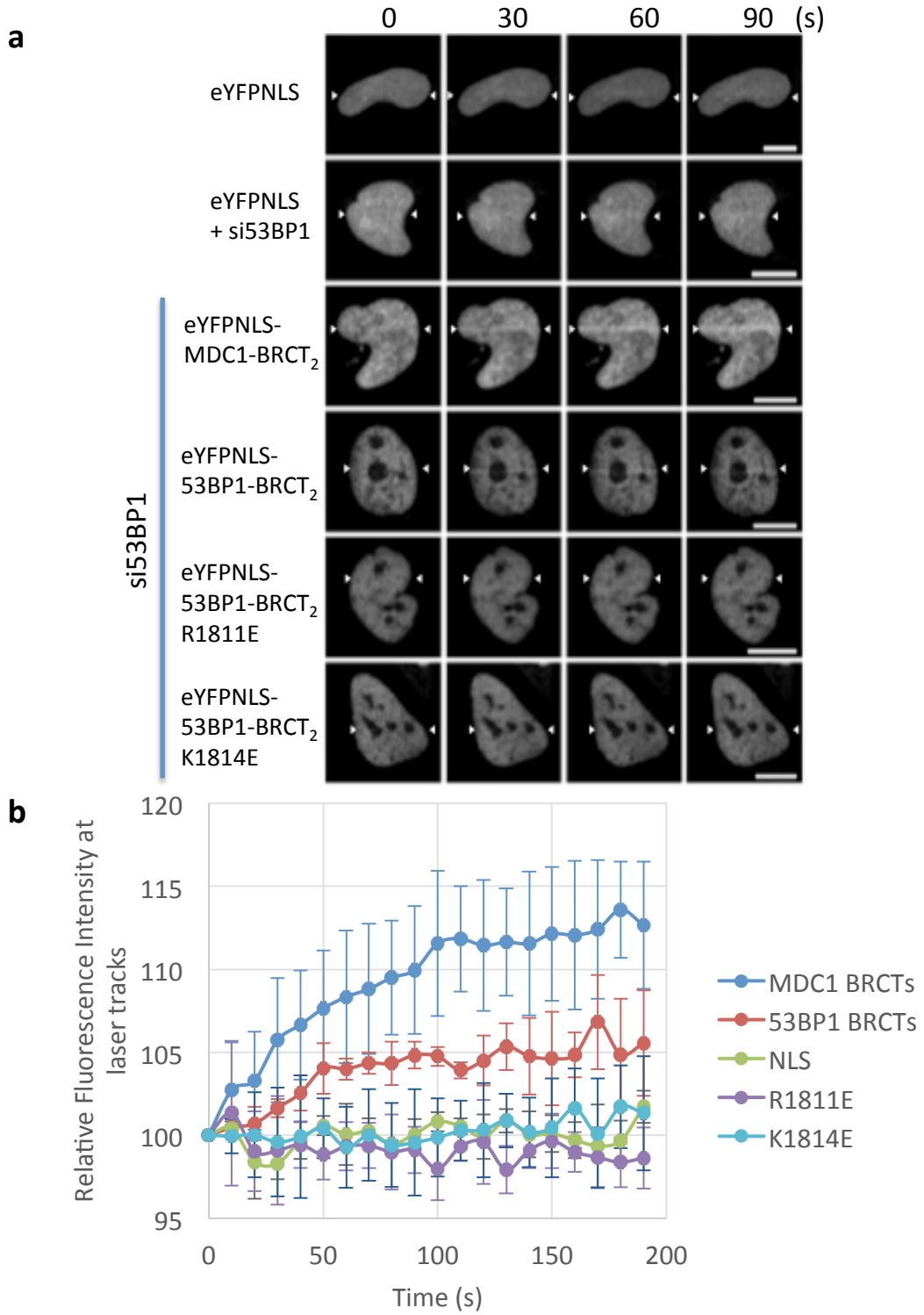

Figure 5.4 53BP1 BRCT domains localise to DNA damage. a) HeLa cells were reverse transfected with 53BP1 siRNA. 48 hours later cells were transfected with YFP-NLS-BRCT constructs containing either wild-type BRCT domains from 53BP1 or MDC1, an empty vector containing a nuclear localisation signal (NLS) or one of the 53BP1-BRCT point mutants. 16 hours after this and after pre-sensitisation with Hoechst stain cells were damaged using laser micro-irradiation. YFP was tracked over 2 minutes to observe localisation to laser tracks. b) YFP was tracked over 2 minutes to observe localisation. Fluorescence intensity profiles were generated using Slidebook6 software (n=30 from 3 experimental repeats. Error bars show 1 standard deviation).

5.2.3 The BRCT domains localisation is dependent on kinase activity

To analyse the dependence of the localisation of the BRCT domains on phosphorylation, the laser track experiments were repeated in cells that had been pre-treated with caffeine 1 hour prior to micro-irradiation. High concentrations of caffeine have previously been shown to inhibit the kinases required to phosphorylate γH2AX [265]. Pre-treating cells with 8mM caffeine prior to irradiation inhibits H2AX phosphorylation (figure 5.5a).

Caffeine pre-treatment of cells prior to laser-induced irradiation prevented localisation of eYFP-NLS-BRCT (WT) to regions of laser-induced damage (figure 5.5b). In order to characterise this further, the checkpoint kinases ATM and DNA-PK that are responsible for phosphorylating H2AX in response to damage, were targeted using specific inhibitors.

These two kinases display functional redundancy since in the absence of ATM, DNA-PK is able to phosphorylate H2AX, albeit to a lesser extent than in the presence of ATM [266]. Additionally, inhibition of DNA-PK alone does not to affect γH2AX focus formation [267]. In order to analyse the effect of inhibiting these kinases HeLa cells were treated with either DMSO (control), KU99533 (ATMi), NU 7441 (DNA-PKi) or treated with both. Simultaneous inhibition of ATM and DNA-PK prevents phosphorylation of histone H2AX in response to ionising radiation. A partial decrease in phosphorylation was observed after ATM inhibition alone (figure 5.6a).

Having established the concentrations of both inhibitors required to prevent the phosphorylation of H2AX, it was then necessary to test whether, under conditions where phosphorylation of H2AX is inhibitied, YFP-NLS-BRCT (WT) was still able to localise to sites of damage induced by laser-microirradiation.

Cells were treated as before with the additional pre-treatment with specific inhibitors. The results clearly indicate that when the kinases required for γH2AX generation are inhibited, the BRCT domains of 53BP1 fail to localise to sites of damage (figure 5.6b). Addition of the DNA-PKi does not affect localisation of the BRCT domains to sites of damage. However the addition of ATMi alone significantly impairs localisation of YFP-NLS-BRCT (WT). Finally, by adding a combination of both DNA-PKi and ATMi localisation of the wild-type BRCT domains to regions of damage is completely abolished. These results are consistent with the earlier observations that implicate γH2AX as a possible 53BP1 BRCT domain-interacting candidate.

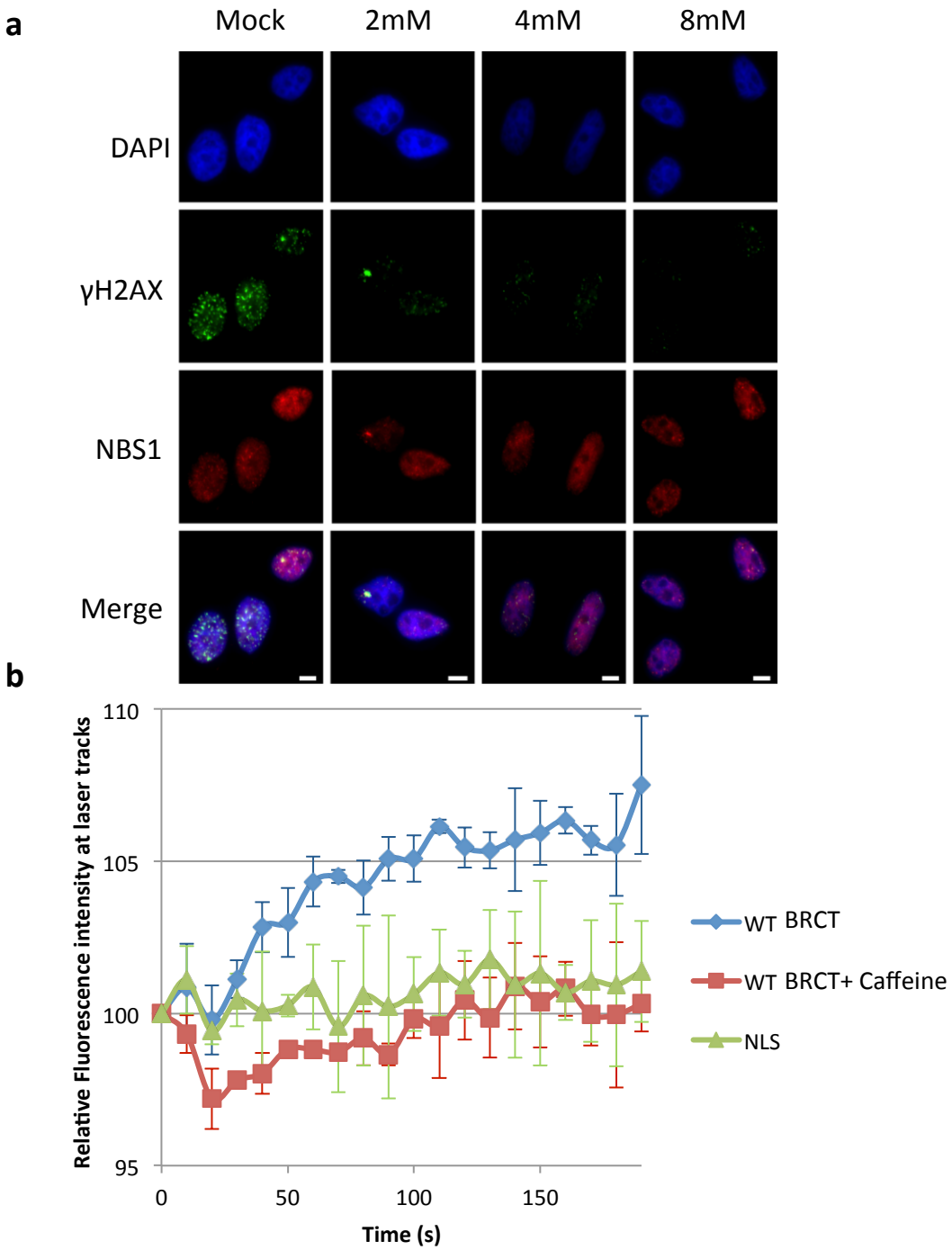

Figure 5.5 YFP-BRCT constructs fail to localise to caffeine treated cells. a) HeLa cells were treated with the indicated concentration of caffeine 1 hour prior to irradiation with 3Gy IR. Cells were allowed to recover for 30 minutes after IR before 0.1% Triton extraction and fixation in 0.4% PFA. Cells were immuno-stained for γH2AX and NBS1. b) HeLa cells were reverse transfected with 53BP1 siRNA. 48 hours later cells were transfected with either an empty vector containing a nuclear localisation signal (NLS) or YFP-NLS-53BP1-BRCT constructs. 15 hours after this cells were incubated with 8mM caffeine for 1 hour prior to laser micro-irradiation. YFP was tracked over 2 minutes to observe localisation. Fluorescence intensity profiles were generated using Slidebook6 software (n=30 from 3 experimental repeats. Error bars show 1 standard deviation).

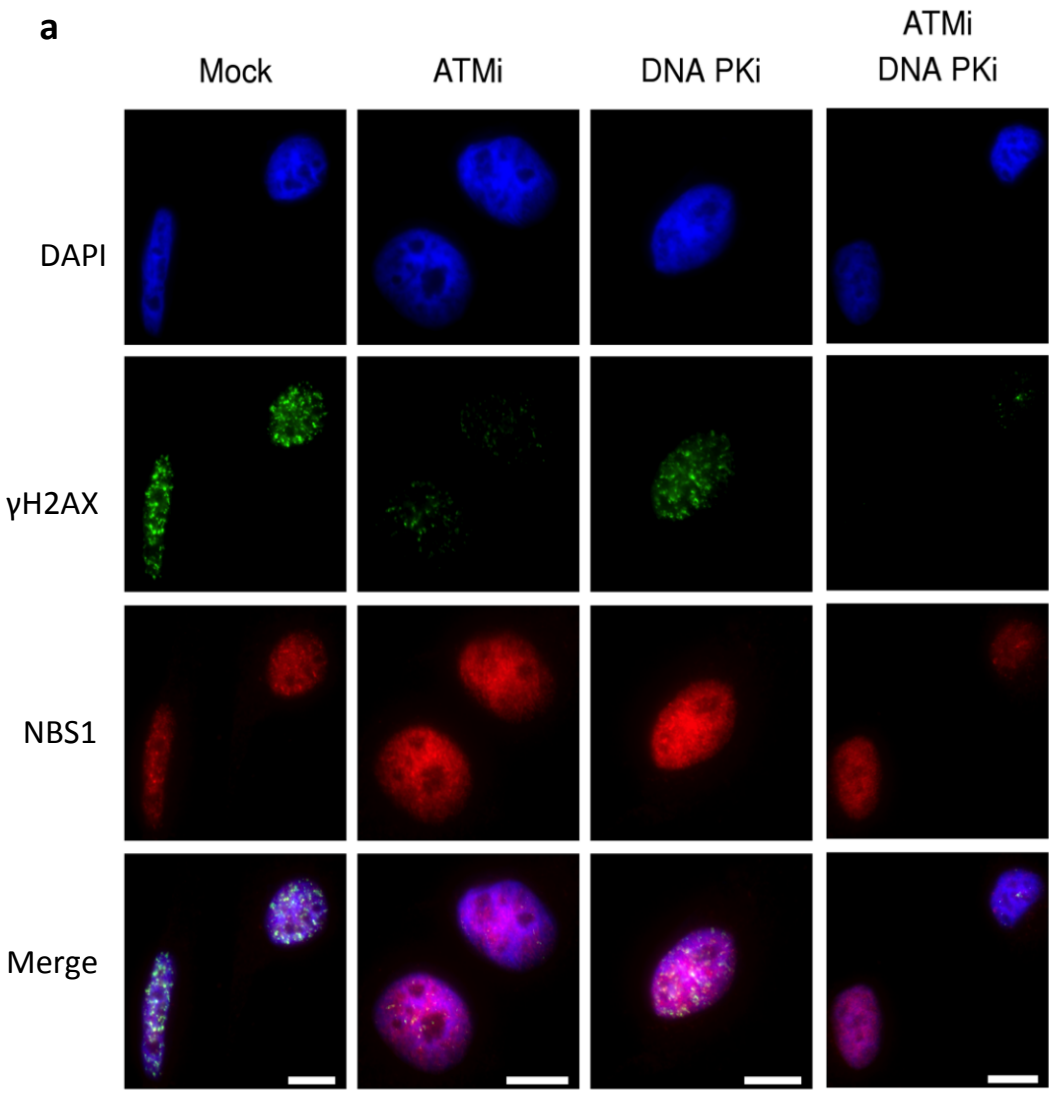

Figure 5.6 53BP1 BRCT domains localise to DNA damage dependent on kinase activity of ATM and DNA-PK. a) HeLa cells were treated with either DNA-Pki, ATMi or both before fixing and staining for γH2AX and NBS1 b) HeLa cells were reverse transfected with 53BP1 siRNA. 48 hours later cells were transfected with YFP-NLS-BRCT constructs containing either a nuclear localisation signal alone (NLS) or wild-type 53BP1-BRCT domains (WT). 15 hours after this cells were treated with either DNA-Pki, ATMi or both for 1 hour prior to laser micro-irradiation following pre-sensitisation with Hoechst stain. YFP was tracked over 2 minutes to observe localisation. Fluorescence intensity profiles were generated using Slidebook6 software (n=30 from 3 experimental repeats. Error bars show 1 standard deviation).

b

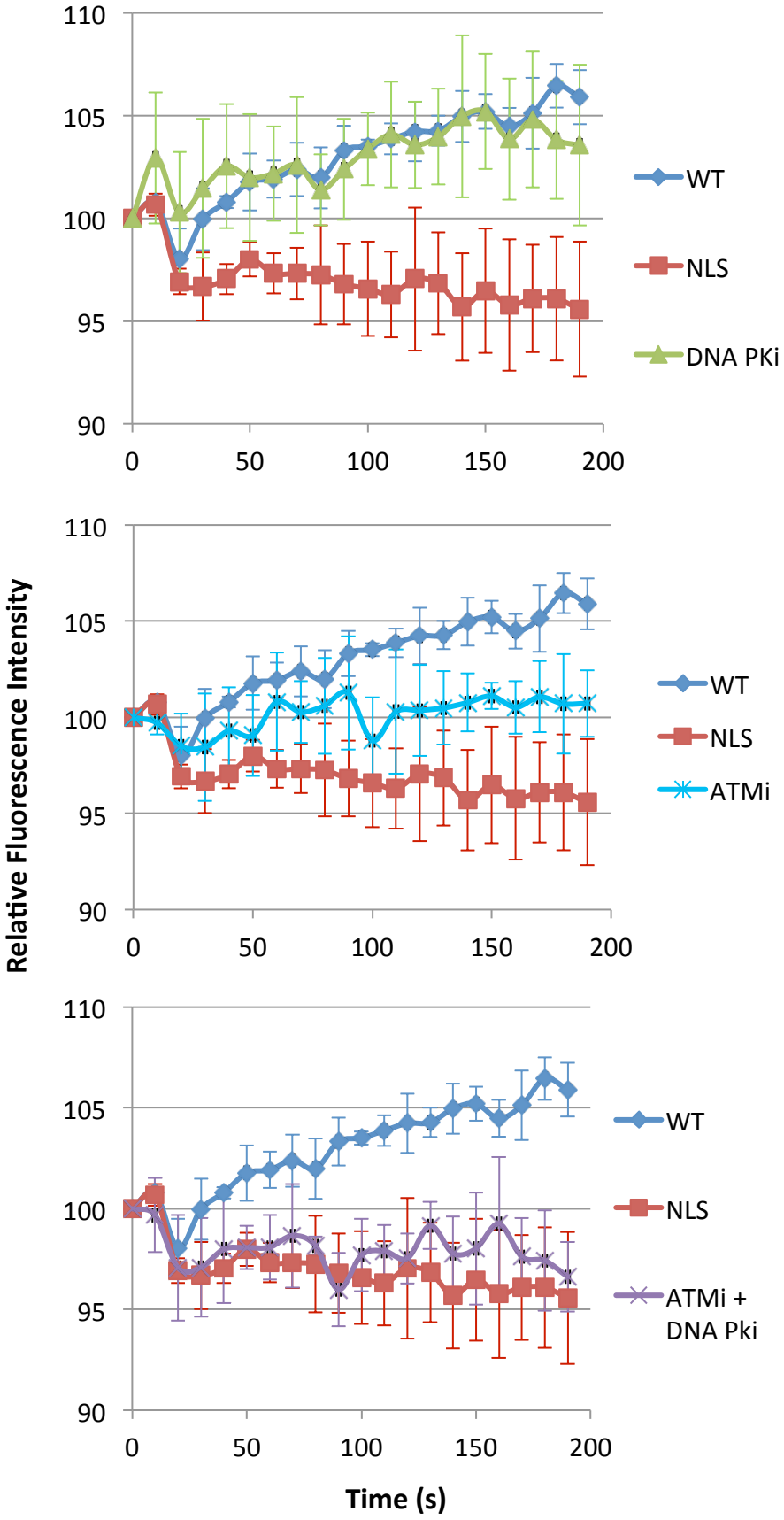
110
105
100
95
90
0
50
100
150
200
WT
NLS
DNA PKi
WT
NLS
ATMi
WT
NLS
ATMi +
DNA Pki
Relative Fluorescence Intensity
Time (s)

5.2.4 The localisation of the BRCT domains of 53BP1 to sites of DNA damage are dependent on the presence of the Histone variant H2AX

Having shown that the localisation of the BRCT domains, in isolation, to sites of damage is dependent on both specific recognition of a phosphopeptide and the activity of the kinases required for phosphorylating H2AX in response to damage, it was then important to show whether this localisation was also dependent on the histone variant H2AX. The laser micro-irradiation experiments with YFP-NLS-BRCT (WT) were repeated using H2AX -/- and H2AX +/+ mouse embryonic fibroblasts (MEFs). In the absence of the histone variant H2AX, and without affecting any of the cellular kinases, the wild-type 53BP1 BRCT domains fail to localise to tracks produced by laser micro-irradiation (figure 5.7a and b).

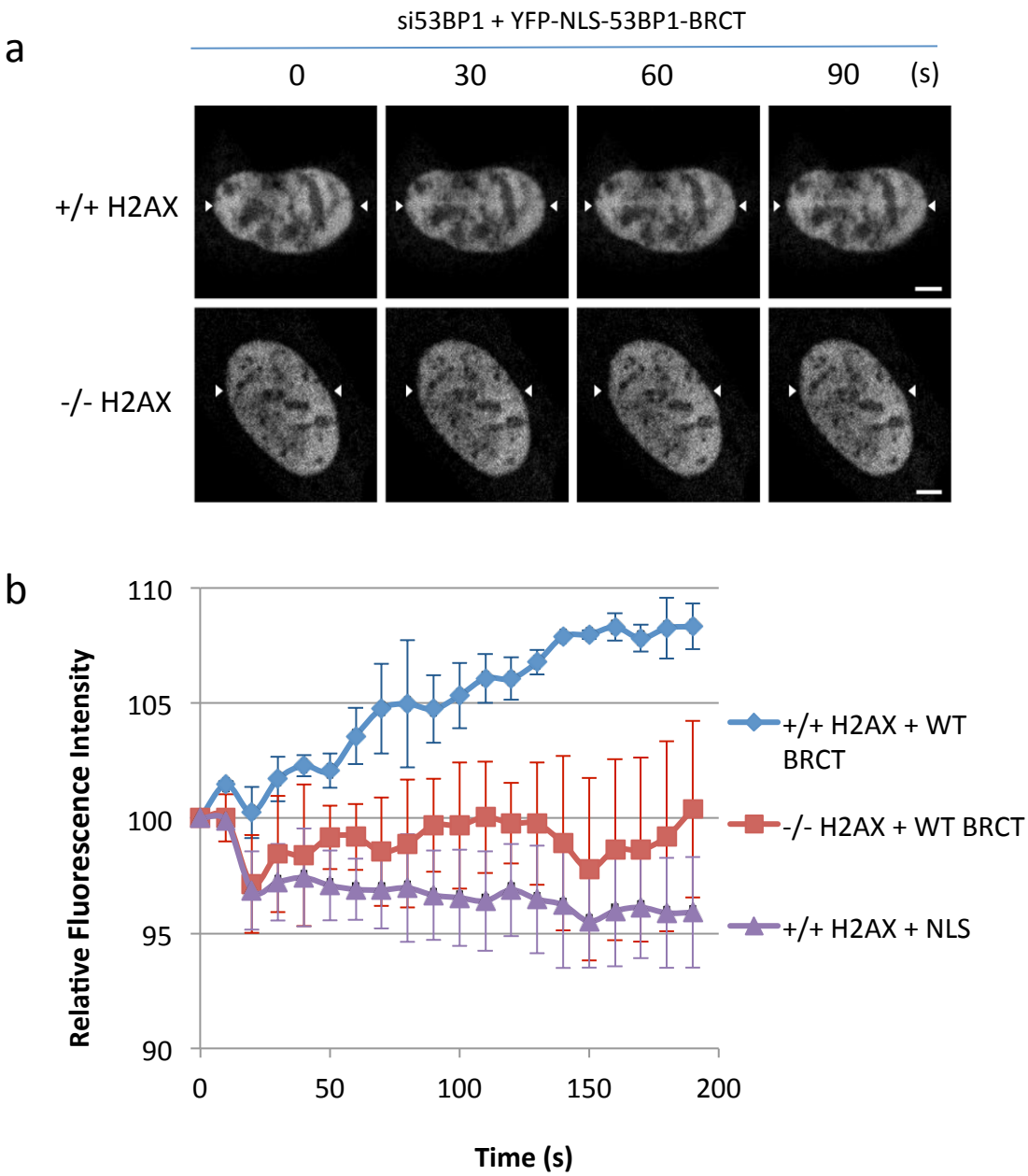

Figure 5.7 Loss of H2AX abolishes 53BP1 BRCT localisation to DSBs. a) H2AX +/+ and H2AX -/- MEFs were reverse transfected with 53BP1 siRNA. 24 hours later cells were transfected with YFP-NLS-BRCT constructs containing either wild-type BRCT domains (WT) or a nuclear localisation signal alone (NLS). 16 hours after this cells were damaged using laser micro-irradiation. YFP was tracked over 2 minutes to observe localisation. b) Fluorescence intensity profiles were generated using Slidebook6 software (n=30 from 3 experimental repeats. Error bars show 1 standard deviation).

5.2.5 Localisation of the BRCT domains does not result from dimerization with endogenous 53BP1

53BP1 has been demonstrated to oligomerize through its oligomerization domain- a region upstream of the domains required for focus formation [268]. However, the ability of the Crb2^{53BP1} BRCT domains to co-purify in *S. pombe* indicates that in yeast 53BP1 oligomerizes through its BRCT domains [269]. In mammalian cells, Lee et al demonstrated that the BRCT domains of 53BP1 are also required for dimerization in addition to the oligomerization domain [196]. Importantly, they were also able to demonstrate that GST-BRCT could oligomerize with full-length 53BP1. As a result, it was necessary to test whether the localisation that was observed using the YFP-NLS-BRCT construct occurred as a result of oligomerization of the BRCT domains with endogenous 53BP1.

All of the YFP-NLS-BRCT experiments were performed under conditions where 53BP1 was depleted using RNAi. However, as RNAi is not 100% effective the possibility remained that the BRCTs could localise with the residual levels of the endogenous protein. It was hypothesised that, if this were the case, the ability of the BRCT domains to localise to damage would be enhanced when 53BP1 was not depleted as there would be more protein available to interact with. In order to test this, HeLa cells were either depleted of 53BP1 by RNAi or left untreated. 48 hours after this the cells were transfected with the YFP-NLS-BRCT (WT or Empty Vector) as before. Protein localisation was analysed for 3 minutes following laser-induced DNA damage.

The results indicate that there was no difference in the ability of the BRCT domains to localise to damage when 53BP1 is depleted using RNAi versus untreated controls (figure 5.8). This indicates that localisation of the BRCT domains to damage was not a result of oligomerization with the endogenous full-length 53BP1.

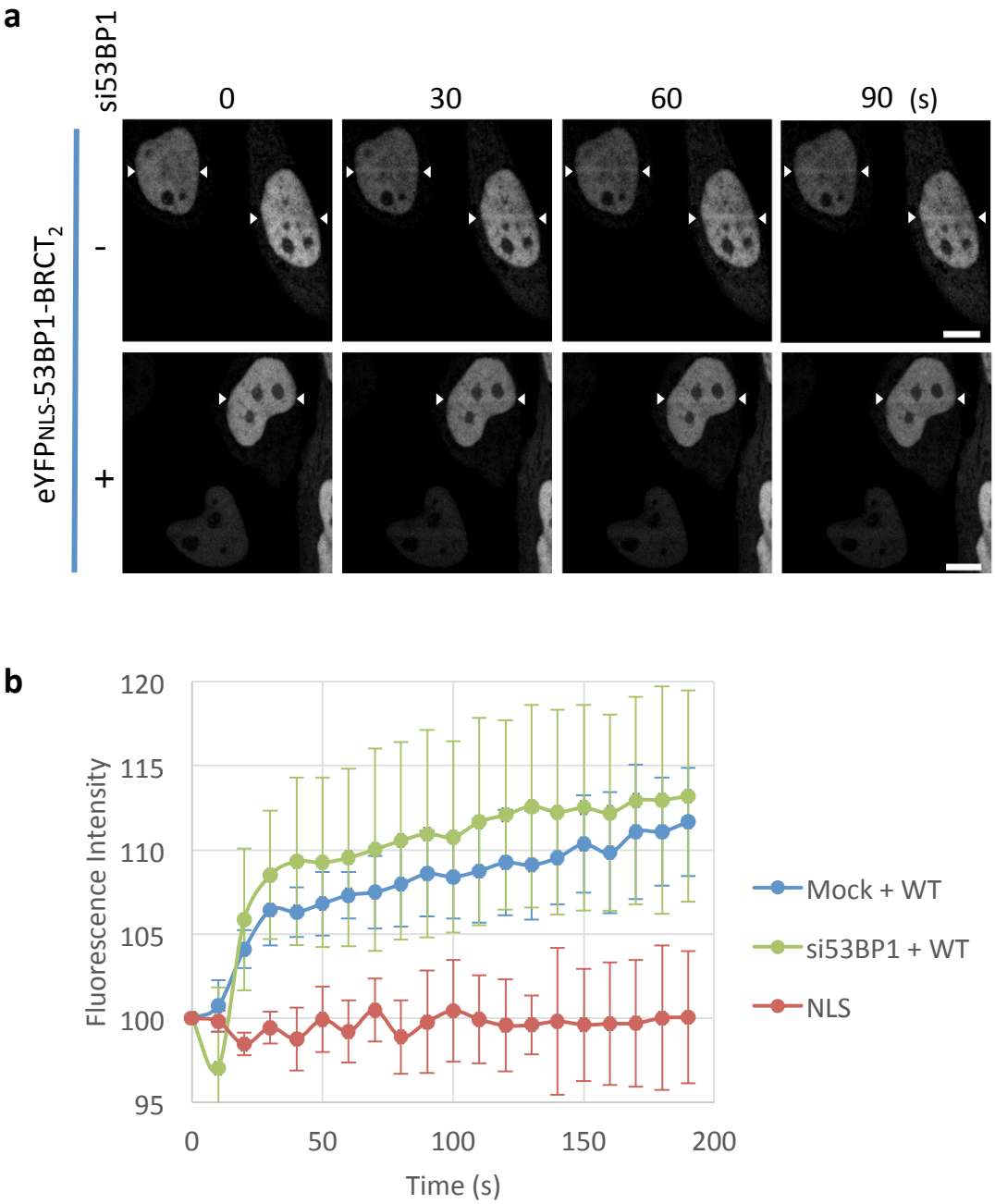

Figure 5.8 Localisation of the BRCT domains does not result from oligomerization with endogenous 53BP1. a) HeLa cells were either reverse transfected with 53BP1 siRNA or a non-targeting control. 48 hours later cells were transfected with YFP-NLS-BRCT constructs containing either wild-type BRCT domains (WT) or a nuclear localisation signal alone (NLS). Cells were pre-treated with Hoechst stain prior to laser micro-irradiation. YFP was tracked over 3 minutes to observe localisation. b) Fluorescence intensity profiles were generated using Slidebook6 software (n=30 from 3 experimental repeats. Error bars show 1 standard deviation).

5.2.6 Mutation of the BRCT domain of 53BP1 by single point mutations causes a late stage repair defect

Having shown that 53BP1 BRCT domains are capable of interacting with γH2AX both *in vitro* and *in vivo*, experiments were undertaken to characterise any role that this interaction has in the context of 53BP1-dependent DNA repair.

To do this, Dr Oliver Wilkinson (Watts lab) made two point mutations using site directed mutagenesis within the BRCT domains of a full length HA-53BP1 siRNA-resistant cDNA construct (R1811E and K1814E). He utilised HeLa cells seeded at high confluence and depleted them of endogenous 53BP1 using RNAi. Following this he transfected the cells with either the wild-type 53BP1 or one of the BRCT mutants. After the cells were allowed to express the cDNA they were either left untreated or exposed to 3Gy of ionising radiation. γH2AX foci were then enumerated to study the repair kinetics of these cells.

Mutation of the BRCT domain of 53BP1 results in a 'slow' kinetic repair defect as characterised by a persistence of γH2AX foci at 16 and 24 hours following irradiation (figure 5.9a)(performed by Dr O. Wilkinson). It is proposed that these breaks represent a subset of DNA DSBs that require more complex repair, occurring with slow repair kinetics [202, 203]. Dr Ross Cloney (Watts Lab) consolidated these findings using U2OS cells (figure 5.9b). These data corroborate the findings by Noon et al [202] who demonstrated that deletion of the BRCT domain produces a 'slow' kinetic repair defect. Our data shows that this defect is attributable to the failure to mediate a phospho-specific interaction between 53BP1-BRCTs and their likely binding partner, γH2AX.

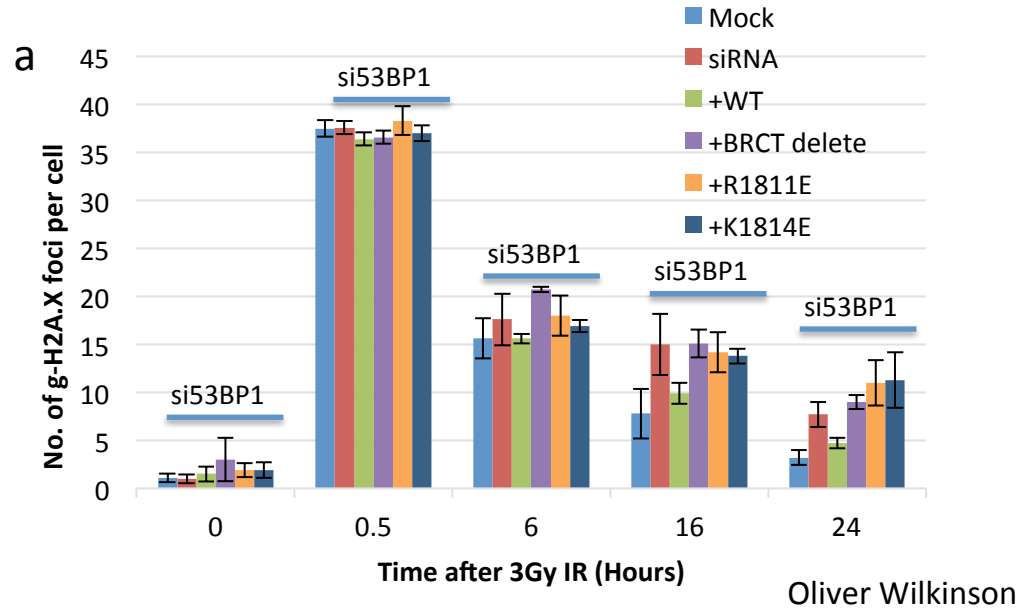

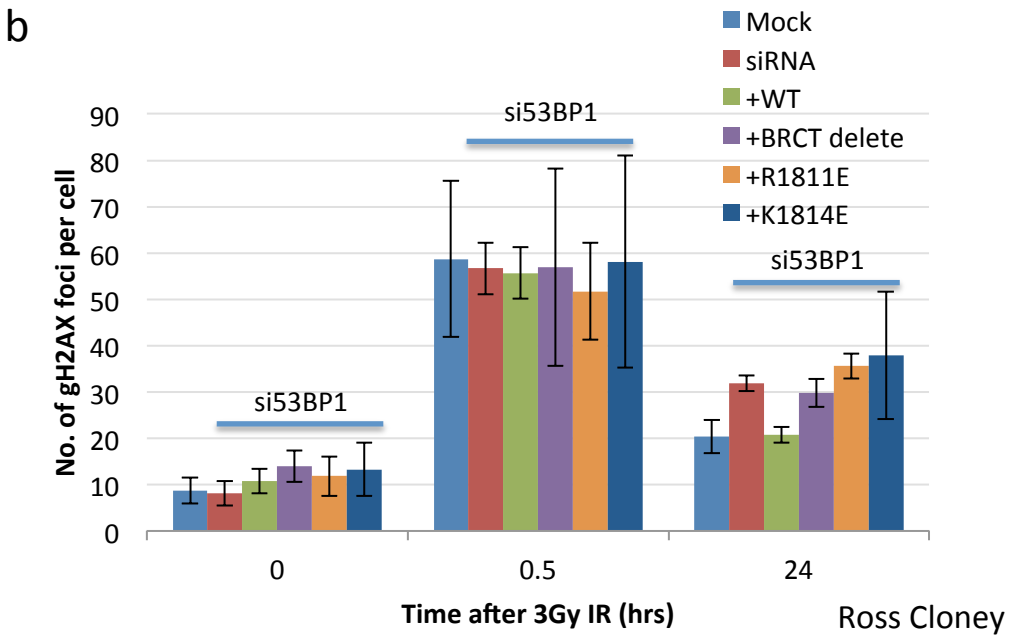

Figure 5.9 53BP1 BRCT domain mutants show a 'slow' kinetic repair defect. (Performed by Dr. Oliver Wilkinson). a) HeLa cells were reverse transfected with 53BP1 siRNA. 48 hours later cells were transfected with an siRNA resistant construct containing wild-type HA-53BP1 or one of the BRCT mutants. 16 hours later cells were exposed to 3Gy ionising radiation and allowed to recover for the indicated time before fixing and staining for HA and γH2AX. γH2AX foci were enumerated for 25 cells. Error bars show 1 standard deviation over 3 experimental repeats b) U2OS cells processed as in a. (Performed by Dr. Ross Cloney) (n=25 error bars represent 1 standard deviation over 3 experimental repeats. Horizontal blue bars show samples depleted of 53BP1 by RNAi.

5.2.7 53BP1 BRCT domain mutants do not affect localisation of the MRN complex at late stage timepoints

A single point mutation (either R1811E or K1814E) within the BRCT domain of 53BP1 recapitulates the 'slow' repair defect observed by Noon et al [202]. In order to investigate possible implications of disrupting this interaction, it was necessary to test the localisation of other key mediators in the DNA damage response. Deletion of the BRCT domains has previously been shown to disrupt the localisation of both pATM and the MRN complex [202].

The MRN complex (comprising Mre11, Rad50 and Nbs1) is recruited rapidly to DSBs and recognises broken DNA ends directly [270]. The MRN complex is recruited to DSBs prior to the recruitment of 53BP1 and the generation of γH2AX. After initial DSB recognition, the MRN complex is capable of mediating several further interactions with mediator proteins to facilitate the DNA damage response. The MRN complex activates the checkpoint kinase, triggering autophosphorylation of ATM [271], which in turn phosphorylates γH2AX. MDC1 recognises γH2AX through its BRCT domains [263] and in turn, MDC1 recruits more of the MRN complex. This cycle facilitates the spreading of the γH2AX along the chromatin, flanking the regions surrounding the break. Following on from this, 53BP1 is recruited by histone post-translational modifications- ubiquitination of histone H2A and dimethylation of histone H3 [9, 181].

Given the importance of these two mediators (MRN and pATM) for the progression of DNA damage repair, immunofluorescence was used to analyse whether the localisation of these mediators was affected in cells transfected with the 53BP1 BRCT domain mutants. The BRCT domains of 53BP1 have been shown to be involved in phospho-independent interactions with the MRN complex through Rad50 [259]. Since the MRN is complex required prior to the recruitment of pATM, it was necessary to test whether the interaction of 53BP1 with Rad50 is disrupted by mutation of the BRCT domains of 53BP1.

HeLa cells were treated as before by depleting the endogenous 53BP1 using RNAi followed by transfection with either the 53BP1 wild-type or one of the mutants (R1811E, K1814E or Y1502L-Tudor domain) constructs. A HA-53BP1 construct with a point mutation located within the Tudor domain was also included: mutation of the Tudor domain abolishes localisation of 53BP1 to IRIF. In order to generate comparable numbers of γH2AX foci after 24 hours, due to the repair defect observed in figure 5.9, both the mock-treated and cells transfected with the wild-type construct were exposed to 8Gy ionising radiation, whereas the mutants were exposed to just 3Gy as used by Noon et al [202]. This was to ensure that all samples had

between 5 and 10 breaks per cell 24 hours after irradiation. The cells were immunostained for HA (53BP1) to identify transfected cells and NBS1.

Localisation of the MRN complex was not disrupted by the introduction of the 53BP1 BRCT-R1811E or K1814E mutants (figure 5.10). This contrasts with the deletion of the BRCT domain or transfection with the Tudor domain mutant, which does impair MRN localisation. This shows that the mutations are specific to the phosphorylation-dependent interactions of the BRCT domains.

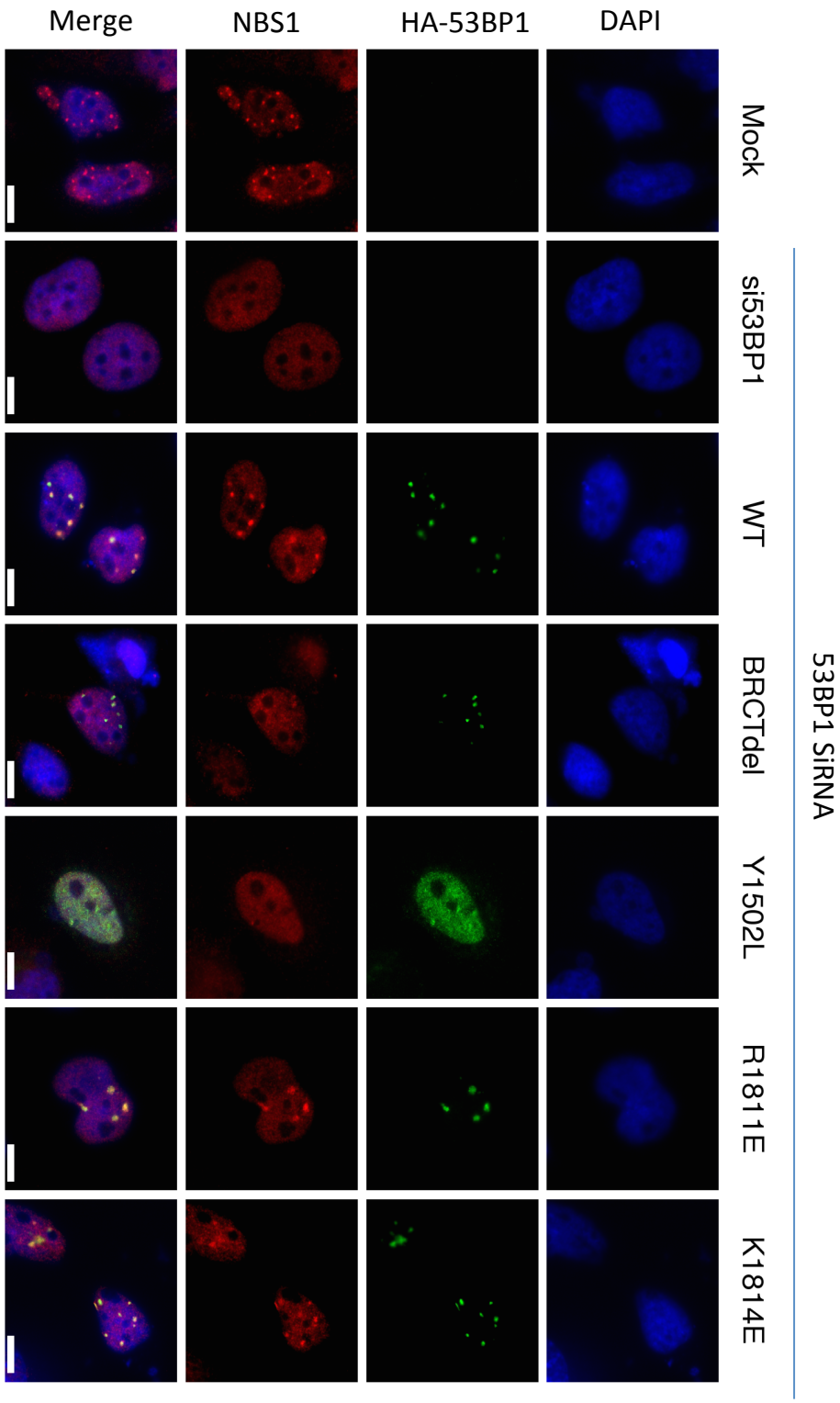

Figure 5.10 53BP1 BRCT domain mutants co-localise to sites of damage recognised by the MRN complex. HeLa cells were reverse transfected with 53BP1 siRNA. 48 hours later cells were transfected with an siRNA resistant construct containing either wild-type HA-53BP1 or one of the BRCT or Tudor domain mutants. 16 hours after this cells were exposed to either 8Gy for Mock and WT or 3Gy ionising radiation for the mutants and allowed to recover for 24 hours before staining for HA and NBS1. Scale bar = 10µm.

5.2.8 53BP1 BRCT domain mutants fail to localise pATM at late stage timepoints

Having established that the MRN complex localised normally to sites of DNA damage with the 53BP1 BRCT domain mutants, it was necessary to examine whether pATM localisation was disrupted. The experiment was repeated with staining for HA (53BP1) and pATM. Interestingly, both point mutations result in a failure to localise pATM at late stage time-points (figure 5.11). It can be seen that despite normal 53BP1 focus formation, pATM completely fails to localise to sites of damage and phenocopies the 53BP1-depleted cells and those transfected with the 53BP1 Tudor domain mutant Y1502L (which fails to form foci).

In order to quantify the localisation of both pATM and MRN, the fluorescence intensity of each was measured at loci in the cell marked by the presence of a 53BP1 focus, via the HA tag (figure 5.12). Furthermore, to account for the variability in expression produced by transient transfections intensities of the HA- (53BP1) foci were also measured. All three fluorescence channels were normalised to the average focus intensity of the cells transfected with the wild-type 53BP1 construct. The intensities of HA foci were consistent across all experiments and all foci analysed, indicating that there were similar levels of expression of the exogenous constructs. The pATM localisation defect produced by the 53BP1 BRCT domain mutants resulted in ~50% reduction in fluorescence intensity at sites marked by a HA (53BP1) focus. The 53BP1 BRCT point mutants (R1811E and K1814E) fail to localise pATM but do still localise the MRN complex. Finally, as noted before, depletion of 53BP1 alone or transfection with the 53BP1 tudor domain mutant does impair MRN complex localisation.

To investigate this further it was important to establish the time following irradiation at which phosphorylated ATM is no longer localised at the site of damage. Due to there being no defect in γH2AX foci formation it was thought that pATM was likely to be concentrated and localised at the sites of damage early on before displaying the defective pan-nuclear distribution. 53BP1-depleted HeLa cells were transfected with either the wild-type or K1814E mutant constructs and were fixed and stained for HA and pATM 30 minutes and 1 hour following irradiation. The results indicate that pATM fails to localise to damage as early as 30 minutes following damage when the BRCT domain is mutated (figure 5.13). This suggests that the recruitment and activation of pATM to in order to phosphorylate H2AX is highly transient and that the retention of the kinase to chromatin is likely achieved by a separate BRCT-dependent set of interactions.

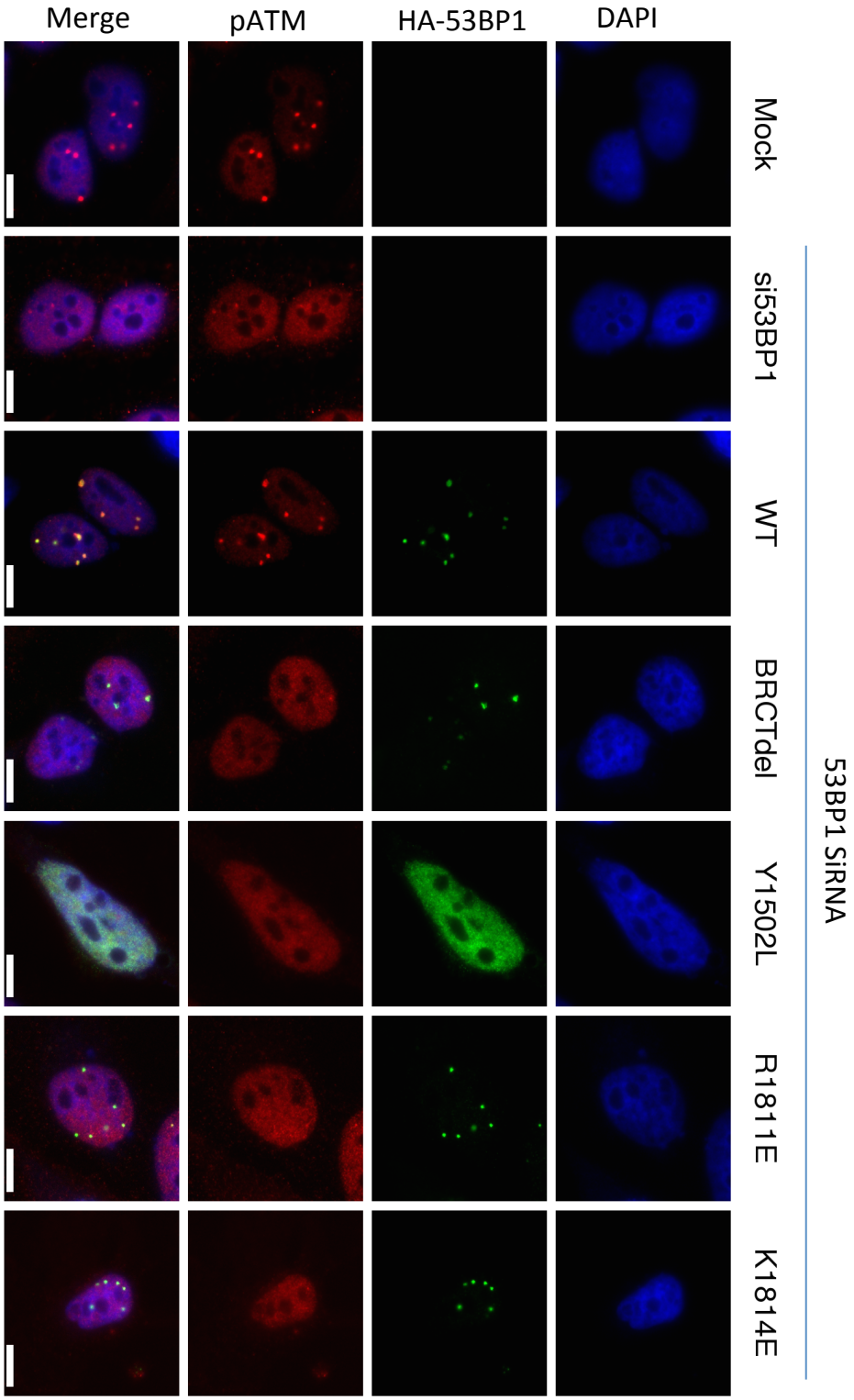

Figure 5.11 53BP1 BRCT domain mutants fail to localise pATM to sites of DNA damage. HeLa cells were reverse transfected with 53BP1 siRNA. 48 hours later cells were transfected with an siRNA resistant construct containing either wild-type HA-53BP1 or one of the BRCT or Tudor domain mutants. 16 hours after this cells were exposed to either 8Gy for Mock and WT or 3Gy ionising radiation for the mutants and allowed to recover for 24 hours before staining for HA and pATM. Scale bar = 10μm.

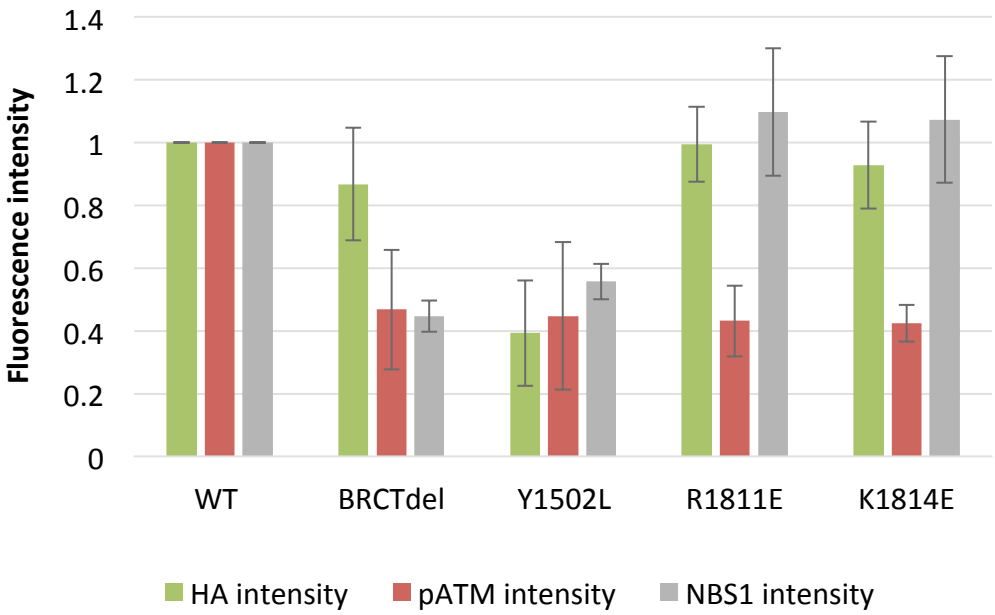

Figure 5.12 53BP1 BRCT domain mutants co-localise to sites of damage recognised by the MRN complex but fail to localise pATM. Cells were processed as in 5.9 and 5.10 with cells stained for HA, pATM and NBS1. Foci intensity was measured using Softworx software suite. Foci were marked by the presence of 53BP1 via the HA tag. Intensity values were normalised to wild-type foci intensity for NBS1, pATM and HA. Graph shows average intensities of 30 foci from 3 experiments with error bars showing 1 standard deviation.

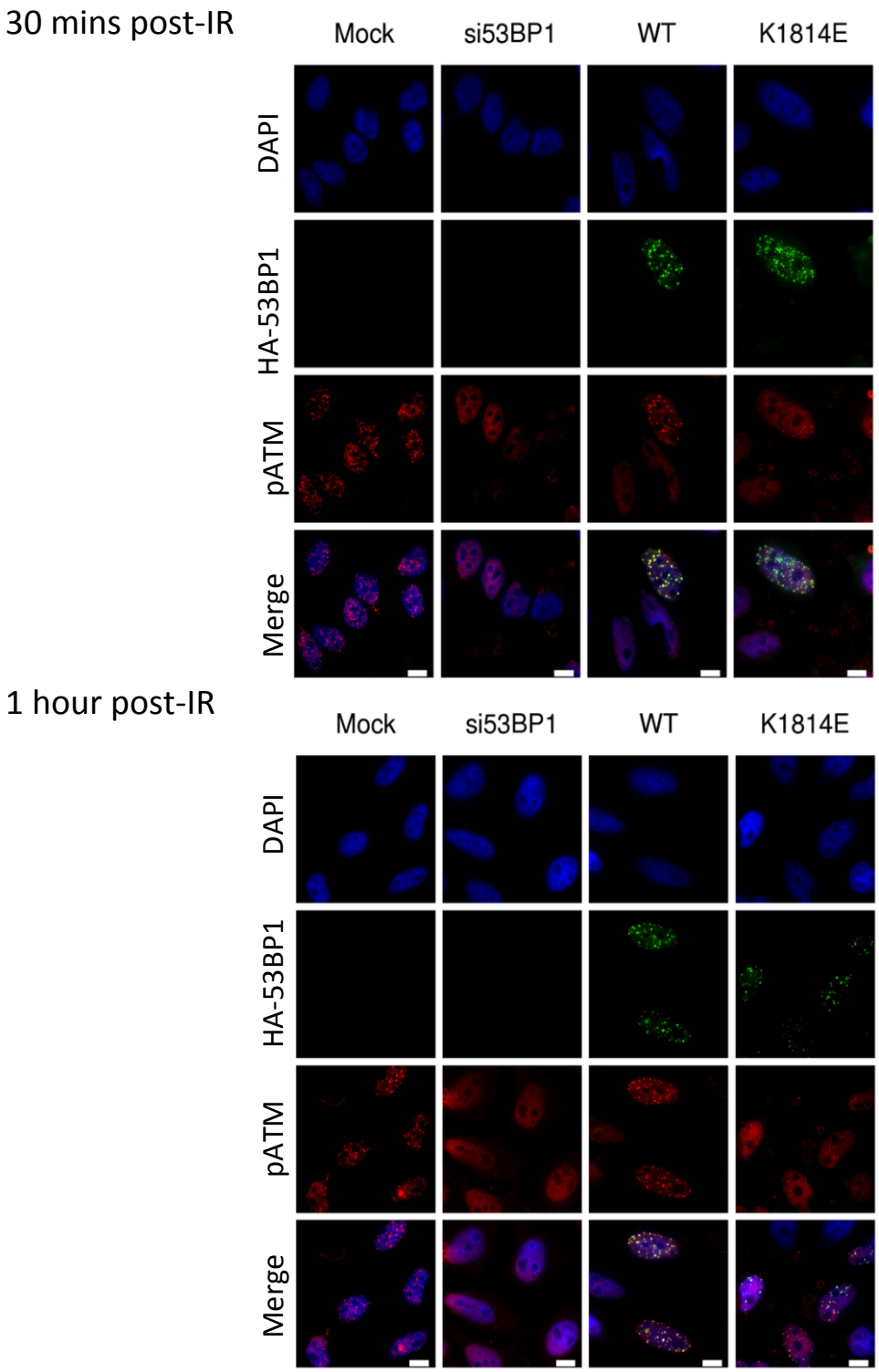

Figure 5.13 53BP1 BRCT domain mutants fail to localise pATM to sites of damage as early as 30 minutes after irradiation. HeLa cells were reverse transfected with 53BP1 siRNA. 48 hours later cells were transfected with an siRNA resistant construct containing wild-type HA-53BP1 or one of the BRCT mutants. 16 hours after this cells were exposed 3Gy ionising radiation and allowed to recover for the indicated time before staining for HA and pATM. Scale bar = 10μm.

5.2.9 Depletion of KAP-1 by RNAi rescues the 'slow' kinetic repair defect caused by BRCT domain mutants

As mentioned in section 4.2.9 in order to repair complex breaks, via 'slow' kinetic repair, pATM-dependent phosphorylation of KAP-1 on S824 is required [202, 203]. Phosphorylation of KAP-1 acts to promote chromatin relaxation and accessibility to DSB sites. It was therefore decided to test whether the 'slow' kinetic repair defect produced by the 53BP1 BRCT mutants that results in a failure to localise pATM described above, is due to an inability to phosphorylate KAP-1 to promote chromatin relaxation.

HeLa cells were either depleted of 53BP1 as before or dual depleted of both 53BP1 and KAP-1. As described above, siRNA resistant constructs were transfected into either 53BP1 only-depleted or double-depleted backgrounds. Cells were then exposed to 3Gy ionising radiation, allowed to recover for the indicated time before fixing and staining for HA (53BP1) and γH2AX. Finally, γH2AX foci were enumerated to indicate the number of breaks present within the cell at that time.

Depletion of KAP-1 rescues the 'slow' kinetic repair defect produced by mutation of the BRCT domains of 53BP1 (figure 5.14). As before, 53BP1-depleted cells and those transfected with the 53BP1 BRCT-K1814E mutant show a 'slow' kinetic repair defect. This is overcome by the additional depletion of KAP-1 as the number of persistent γH2AX foci is close to wild-type or untreated levels. This supports the hypothesis that the heterochromatin structure acts as a barrier to repair for a subset of breaks that require BRCT-dependent pATM localisation.

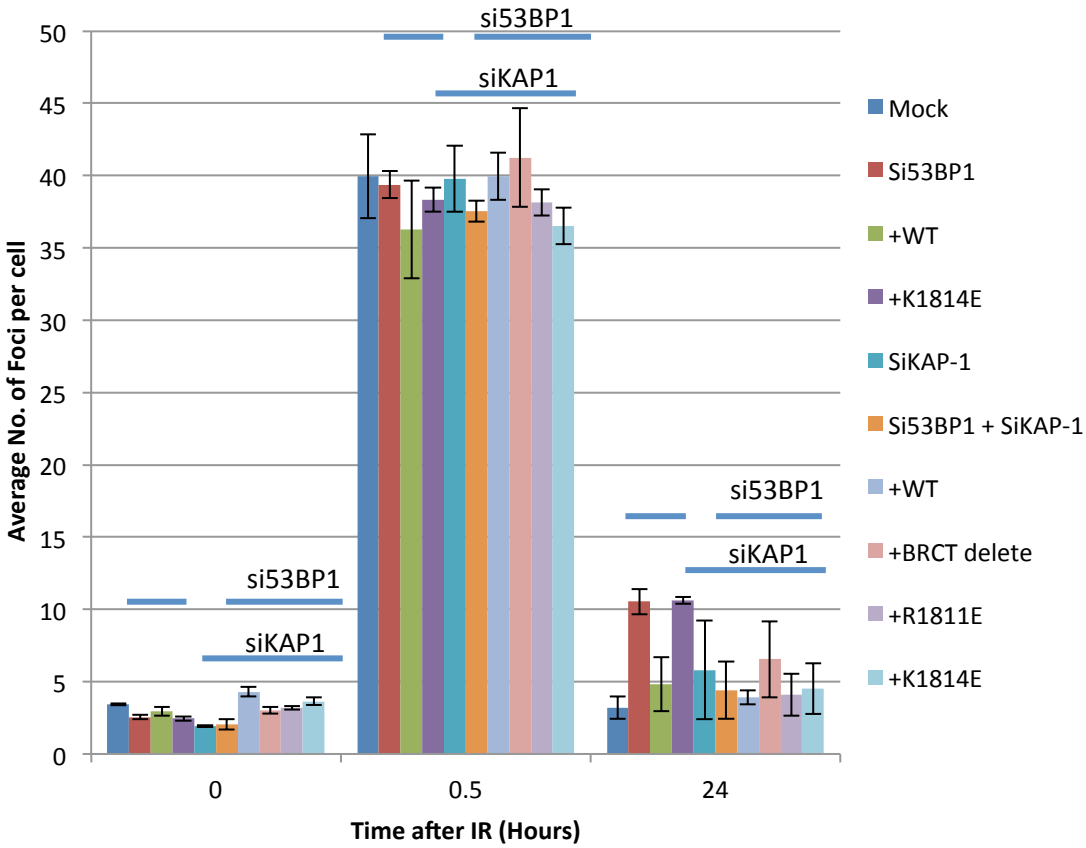

Figure 5.14 siRNA depletion of KAP-1 rescues the 'slow' kinetic repair caused by mutation of the BRCT domains of 53BP1. HeLa cells were reverse transfected with 53BP1 and/or KAP-1 siRNA. 48 hours later cells were transfected with an siRNA resistant construct containing wild-type HA-53BP1 or one of the BRCT mutants. 16 hours later cells were exposed to 3Gy ionising radiation and allowed to recover for the indicated time before staining for HA and γH2AX. The graph shows average number of γH2AX foci per cell (n=25). Error bars show 1 standard deviation over 3 experimental repeats. (note: This experiment was performed at the same time as figure 4.10 with the same controls). Horizontal blue bars show samples depleted of 53BP1 and/or KAP-1.

5.2.10 53BP1 BRCT domain localisation to damage is independent of the chromatin environment

Given the influence of KAP-1 on chromatin structure and how this affects the kinetics of repair, it was important to test whether the chromatin environment has any bearing on the 53BP1 BRCT-γH2AX interaction. To investigate this, HeLa cells were either depleted of 53BP1 only or dual-depleted of 53BP1 and KAP-1. Next, the cells were transfected with the YFP-NLS-BRCT (WT) constructs used earlier. Cells were pre-sensitised with Hoechst before the induction of damage using a high-power UVA laser.

Depletion of KAP-1 did not affect the ability of the YFP-NLS-BRCT (WT) to localise to sites of damage (figure 5.15). Both with and without KAP-1 RNAi, the change in intensity measured at sites of damage was approximately 7% indicating that the interaction between the BRCT domain of 53BP1 and γH2AX occurs irrespective of the chromatin structure surrounding the break site.

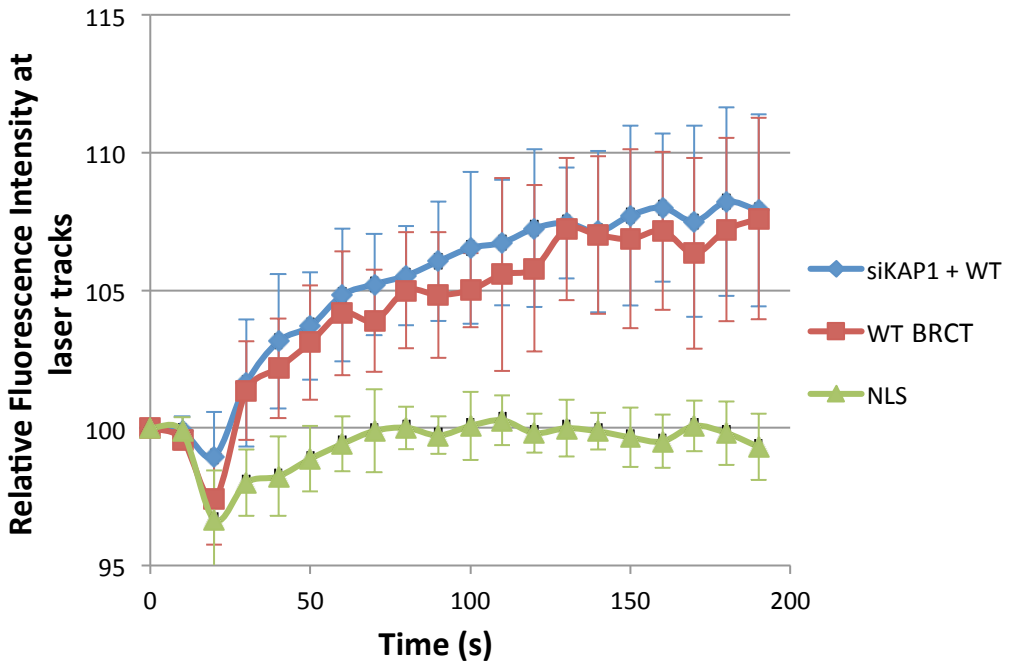

Figure 5.15 YFP-BRCT domains of 53BP1 localise to damage irrespective the of chromatin environment. HeLa cells were reverse transfected with either 53BP1 or 53BP1 and KAP1 siRNA. 48 hours later cells were transfected with either YFP-NLS or YFP-NLS-BRCT constructs. 16 hours later cells were pre-sensitized with Hoechst stain and exposed to laser micro-irradiation. YFP was tracked over 2 minutes to observe localisation to laser tracks. Fluorescence intensity profiles were generated using Slidebook6 software (n=30 from 4 experimental repeats. Error bars show 1 standard deviation).

5.2.11 53BP1 BRCT domain mutants fail to re-position 53BP1 to the periphery of the IRIF during S and G2-phase

53BP1 is physically repositioned to the periphery of IRIF relative to BRCA1 to allow end resection in S- and G2-phase cells [210]. Experiments were undertaken to test whether mutations within the γH2AX binding site in the BRCT domains of 53BP1 affect the antagonistic relationship between 53BP1 and BRCA1. More specifically, given the newly identified interaction of the BRCT domains and γH2AX, the relative positions of 53BP1 and BRCA1 in IRIF were analysed.

To test this R Cloney (Watts lab) used a similar experimental format as before, depleting HeLa cells of endogenous 53BP1 by RNAi followed by transfection with either the wild-type or mutant 53BP1 BRCT constructs. The cells were then exposed to 1Gy ionising radiation. Following irradiation, the cells were incubated for a further 8 hours to allow DSB repair progression. High-resolution z-stack images were taken. The images were then deconvolved using SoftworX software suite. Imaris software was used to render z-stacks into 3-dimentional images (figure 5.16a).

Fluorescence intensity profiles were measured from deconvolved z-stack images by drawing a single line intersecting the middle of the IRIF. 30 profiles over three experiments were normalised to their highest intensity and positioned such that the highest intensity of BRCA1 was positioned at zero. Endogenous and wild-type transfected 53BP1 show focal expansion of ~0.5µm in both directions from the IRIF centre 8 hours following irradiation. Analysis of individual focus examples reveals that the wild-type 53BP1 construct does not create a precise ring surrounding BRCA1. Instead, expanded 53BP1 lobes can be observed on either side of BRCA1. Further work will be required to determine the significance of this observation.

As can be seen from the analysis, 53BP1 fails to reposition at the periphery of IRIF when the phospho-specific binding activity of the BRCT domain is disrupted (figure 5.16a and b). Instead, 53BP1 remains localised to the core of the IRIF.

As 53BP1 is not removed from the core of the IRIF in cells transfected with the BRCT mutants, it was proposed that this might hinder progression from NHEJ to HR-driven repair. In order to test whether HR was affected by mutation of the BRCT domain, R Cloney used U2OS cells stably expressing a DR-GFP construct.

After depletion of 53BP1, the cells were co-transfected with both the wild-type or mutant 53BP1 constructs along with an ISce-I expression plasmid. ISce-I introduces a double strand

break within the inactive *GFP* gene. As before, if the cell attempts to repair this break by HR the inactive *GFP* is resected, thereby removing an in-frame stop codon from the *GFP* gene. The downstream repair template, a N- and C-terminally truncated variant of the *GFP* gene can be used to restore the active *GFP* gene, which is under the control of a promoter [272]. Repair by HR can then be analysed by fluorescence activated cell sorting.

R Cloney found that despite a failure to reposition 53BP1 containing a mutation in the phospho-peptide binding site, there was not a defect in HR (figure 5.17). However, given the influence of the chromatin environment on the efficacy of repair, using a reporter construct that is likely integrated in a region of euchromatin is probably not a suitable method to characterise this type of homology-mediated repair.

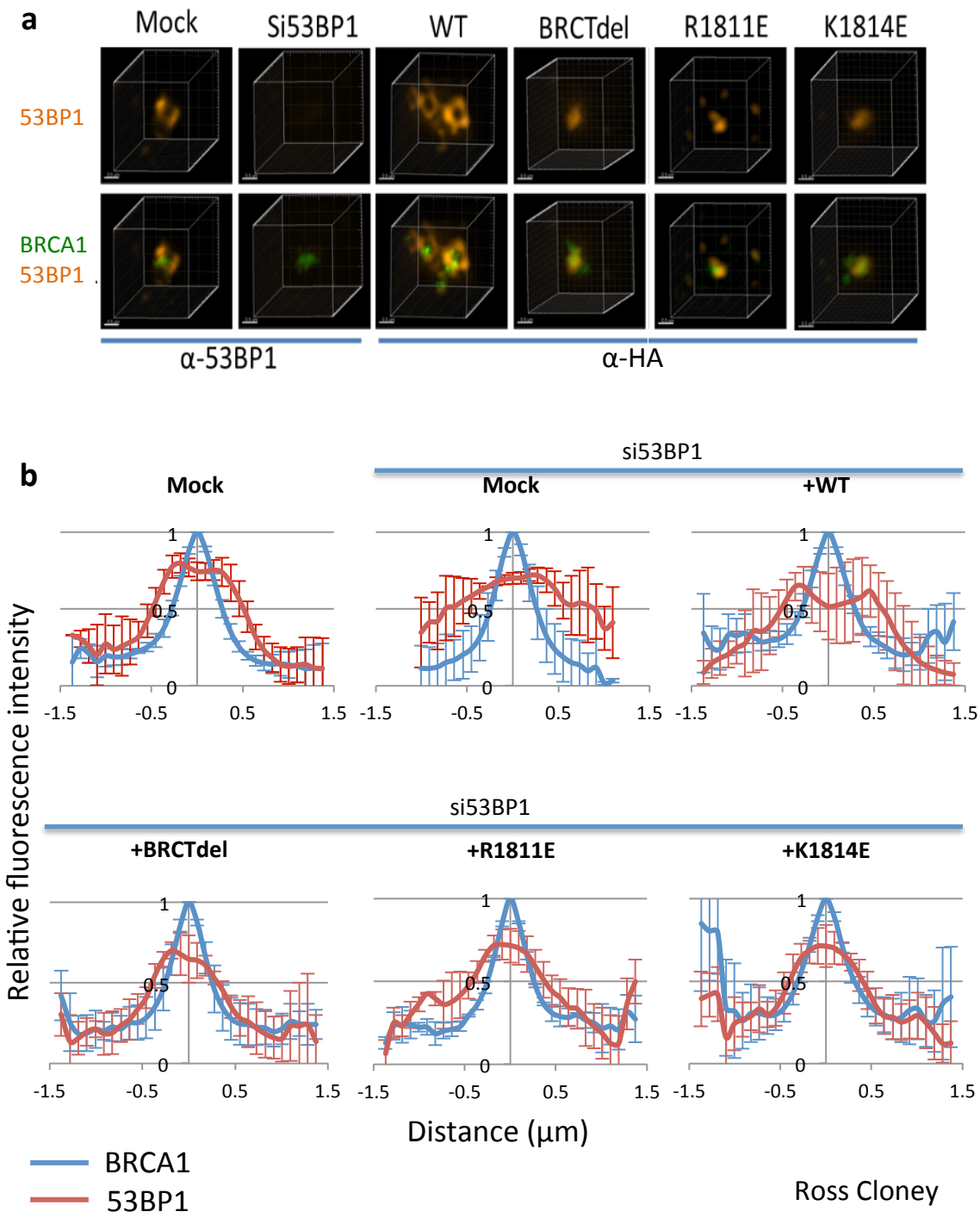

Figure 5.16 53BP1 BRCT mutants are not displaced by BRCA1 and fail to reposition to the periphery of IRIF in G2 cells. HeLa cells were reverse transfected with 53BP1 siRNA. 48 hours later cells were transfected with an siRNA resistant construct containing wild-type HA-53BP1 or one of the BRCT mutants. 16 hours after this cells were exposed to either 3Gy (Mock and WT) or 1Gy IR for mutants and allowed to recover for 8 hours before staining for HA and BRCA1. a) High resolution, deconvolved Z-stack images were obtained and rendered using Imaris. b) Quantitative measurements of intensity across foci were generated using softWoRx software (n>25) average of 3 experiments.

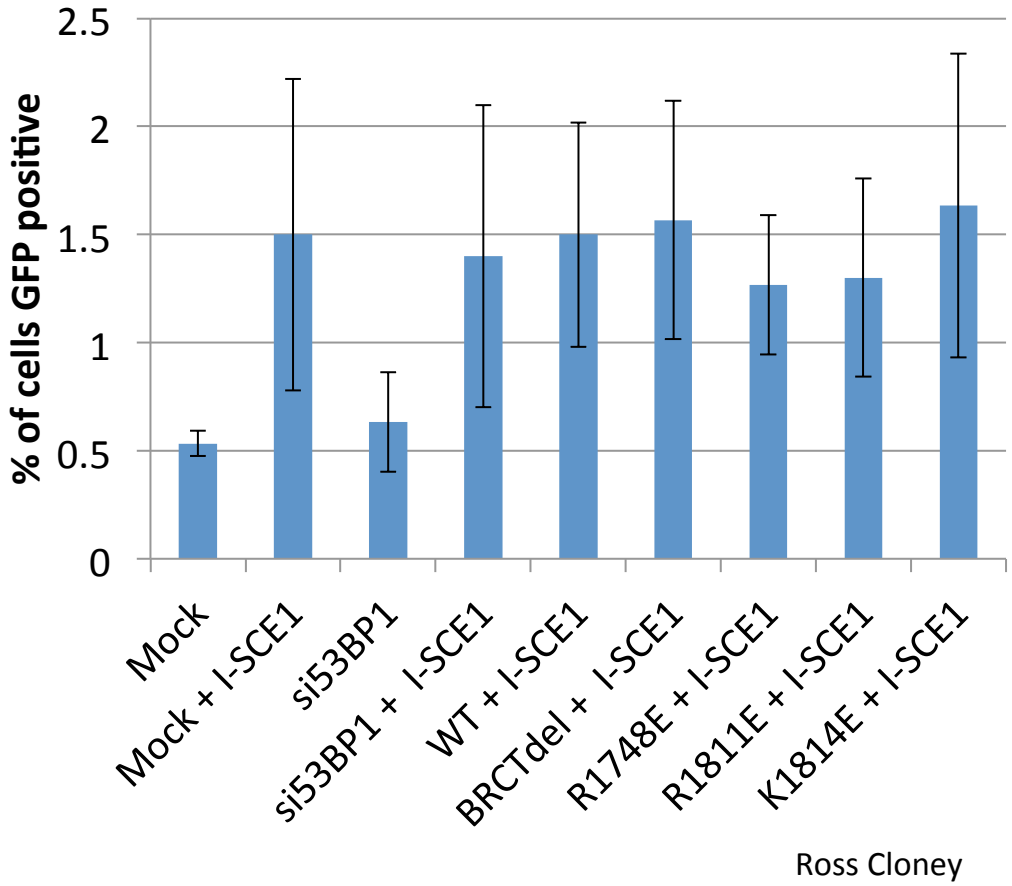

Figure 5.17 53BP1 BRCT mutants do not show a HR defect. (Performed by Dr. Ross Cloney). U20S cells with a stably integrated DR-GFP construct with an Isce-I cut site were reverse transfected with 53BP1 siRNA. 24 hours later cells were transfected with an siRNA resistant construct containing wild-type HA-53BP1 or one of the BRCT mutants alongside a plasmid encoding Isce-I. Cells were incubated for 48 hours before trypsinisation and analysis by flow cytometry. Results show % of cells that are GFP positive (average of 3 experiments, error bars show 1 standard deviation).

5.2.12 Re-positioning of 53BP1 in S and G2 phase is dependent on ATR kinase activity

Having demonstrated that disruption of the phospho-specific binding activity of the BRCT domains of 53BP1 affected its re-localisation, it was necessary to further characterise the role of phosphorylation in mediating this repositioning event. Since the repositioning occurs several hours after the creation of the damage, it was hypothesised that there might be a secondary phosphorylation event that directs 53BP1 away from the focus core. Caffeine was added to cells after the initial phosphorylation event, required to phosphorylate γH2AX, to determine if the repositioning of 53BP1 requires a secondary phosphorylation event.

In order to do this the HeLa cells were exposed to ionising radiation to introduce double strand breaks. The cells were treated with 8mM caffeine to block any further H2AX phosphorylation. The addition of caffeine was staggered from 30 minutes (i.e. after the initial wave of H2AX phosphorylation) to 6 hours after irradiation. The cells were allowed to recover for a period of 8 hours before fixing and staining for 53BP1 and BRCA1. Unlike, previous experiments 53BP1 was visualised using an antibody directed to the endogenous protein, rather than via a HA-tag on an exogenously introduced construct. Deconvolved high-resolution z-stack images were taken and as before intensity profiles were measured from 30 foci over 3 experiments.

The results show that repositioning of 53BP1 from the core of the focus in S- and G2-phase cells is firstly a kinase-dependent event and secondly, that this kinase-dependent phosphorylation event occurs after the initial wave of phosphorylation observed immediately following damage (figure 5.18a and b). Additionally, the repositioning of 53BP1 occurs between 6 to 8 hours following the introduction of DNA damage. As demonstrated earlier, the majority of DSBs generated were repaired, using fast kinetics, between 6 and 16 hours following irradiation. The results indicate that the majority of 53BP1 focal expansion occurs between 6-8 hours after irradiation.

Finally, we wanted to identify the kinase responsible for the second wave of phosphorylation. The above experiment was repeated using either an ATMi (Ku55933) or an ATRi (ATR kinase inhibitor II) in place of the caffeine used before.

Unexpectedly the ATM inhibitor, which had been previously demonstrated to significantly reduce γH2AX foci formation after DNA damage, did not affect 53BP1 repositioning after irradiation. However, treatment with an ATR inhibitor did prevent the repositioning of 53BP1 in S- and G2-phase cells (figure 5.19 and figure 5.20). This suggests that there is a role for ATR

in the reorganisation of IRIF at later time points following irradiation but does not rule out the possibility of ATR-dependent phosphorylation of H2AX to facilitate the repositioning of 53BP1.

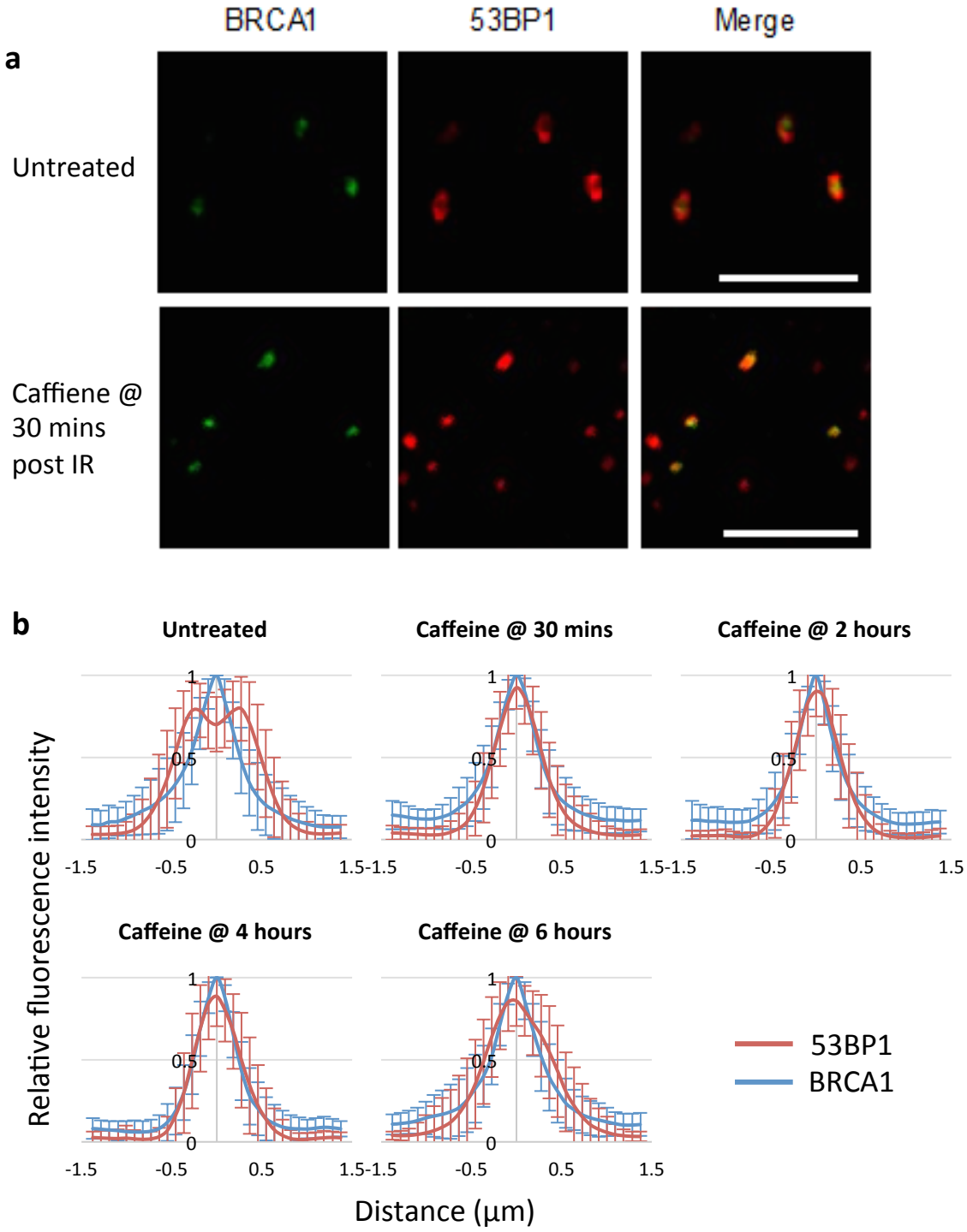

Figure 5.18 Repositioning of 53BP1 in G2-phase cells is a kinase dependent event. HeLa cells were exposed to 3Gy ionising radiation. Cells were allowed to recover for the indicated time before the addition of 8mM caffeine. 8 hours after the initial damage cells were fixed and immunostained for 53BP1 and BRCA1. a) Deconvolved z-stack images were obtained b) intensity profiles across foci were generated using softWoRx software (n=30 average shown over 3 experiments with 1 standard deviation). Scale bar = 5µm.

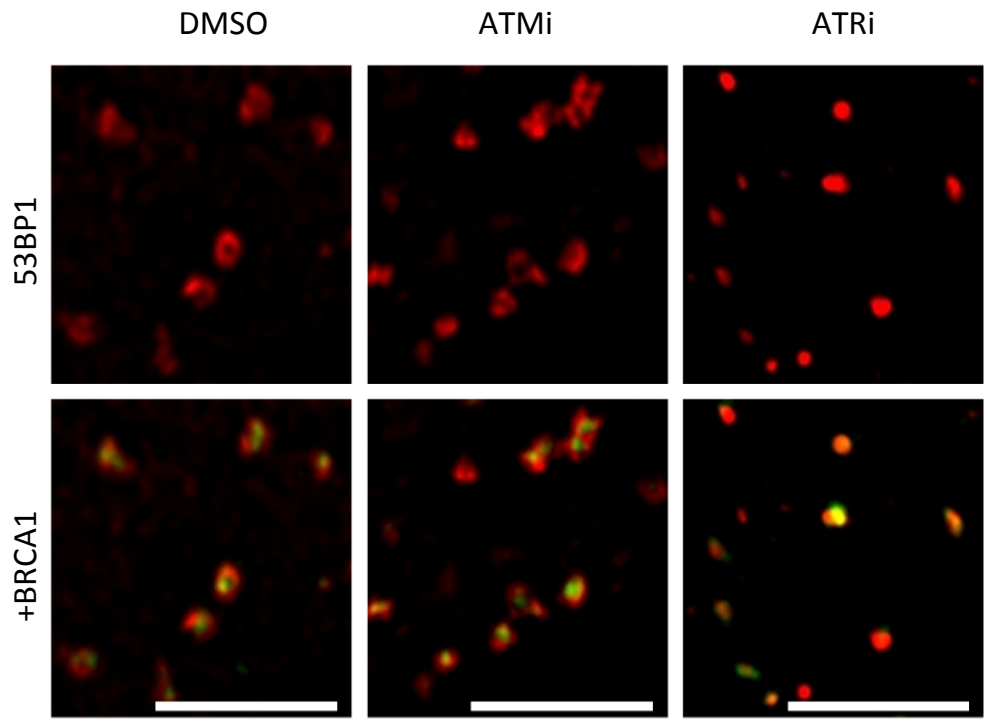

Figure 5.19 ATR kinase activity is required for 53BP1 repositioning in G2 phase cells. HeLa cells were exposed to 1Gy of ionising radiation. Cells were allowed to recover for the 30 minutes before the addition of either Ku55933 (ATMi) or ATR kinase inhibitor II. 8 hours after the initial damage cells were fixed and immunostained for 53BP1 (red) and BRCA1 (green). High-resolution z-stack images were taken and deconvolved using softWoRx software suite. Scale bar = 5µm.

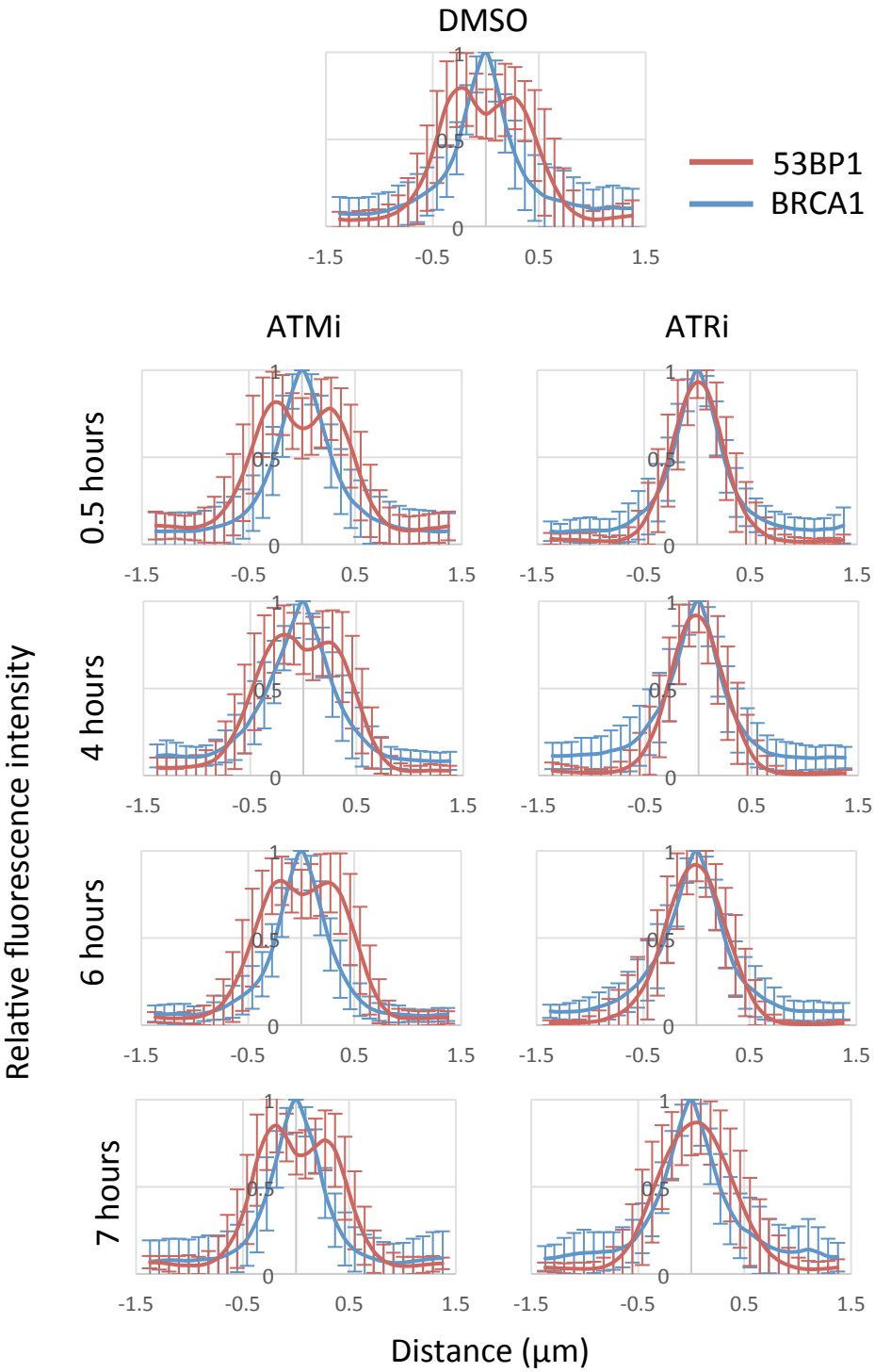

Figure 5.20 ATR kinase activity is required immediately prior to 53BP1 repositioning in G2 phase cells. HeLa cells were processed as in 5.18 inhibitors were added at the indicated times. 8 hours following irradiation cells were fixed and stained for BRCA1 and 53BP1. IRIF intensity profiles were measured across foci using softWoRx software suite (n=30 average shown over 3 experiments with 1 standard deviation).

5.3 Discussion

Our investigations have shown that the BRCT domains of 53BP1 interact specifically and directly with γH2AX *in vitro* using a combination of fluorescence polarisation and X-ray crystallography. Using the X-ray crystal structure it was possible to identify residues critical for mediating this interaction and as a result, make specific point mutations to abolish this interaction.

Furthermore, by isolating the BRCT domains of 53BP1 fused to an eYFP-fluorescent reporter it was possible to observe and quantify the intrinsic ability of the BRCT domains to localise to sites of laser-induced damage. Importantly, this localisation was not the result of dimerization of the BRCT domain with residual endogenous 53BP1. Additionally, by making one of two point mutations or by targeting the kinases responsible for phosphorylating H2AX, the localisation was abolished and demonstrates that the *in vivo* interaction is also phosphorylation dependent.

Although these data allude to γH2AX being the interacting partner with which the BRCT domains of 53BP1 interact, the failure of the mutant BRCT domains to localise to laser-induced damage only indicates dependence on a phosphorylated target, but does not indicate which target protein. The same is true when the activity of the checkpoint kinases, ATM and DNA-PK, are inhibited. The failure to localise the BRCT domain to sites of damage indicates that phosphorylation by ATM and DNA-PK is required, but as these kinases are responsible for phosphorylating hundreds of proteins within the cell, it does not rule out another phosphorylated target being responsible for the localisation.

Furthermore, the failure to localise YFP-NLS-BRCT (WT) in H2AX -/- MEFs clearly indicates a dependence of H2AX, however the possibility remains that loss of this histone variant may result in the additional loss of multiple protein interaction networks associated with the γH2AX which could ultimately prevent the localisation of the BRCT domains.

One of the limitations of using the YFP-NLS-BRCT reporter constructs is the overexpression produced by the CMV promoter used to drive expression. This promoter caused the entire nucleus to display a fluorescent signal. As a result, it was not possible to visualise localisation of the constructs using damage induced by ionising radiation, this is likely due to the expression level of the YFP-NLS-BRCT (WT) being far higher than the endogenous level. This could also result from the competition of 53BP1 with MDC1 as mentioned earlier. As a result, more concentrated damage was generated using a high power UVA laser. Even with the more

highly concentrated damage, the change in localisation of the YFP signal was very small (as low as 5-7%).

In order to establish whether the competition with MDC1 was the reason for the small change in localisation, it would be necessary to deplete MDC1 by siRNA prior to analysing the recruitment kinetics of YFP-NLS-BRCT (WT). However, depletion of MDC1 would disrupt the MDC1-MRN-ATM-γH2AX positive feedback loop required for γH2AX spreading along the chromatin, it would therefore be unlikely that the wild type BRCT domains would localise to sites laser-induced damage under these conditions.

Further work will be required to analyse the interactions of the BRCT domains of both MDC1 and 53BP1 at endogenous expression levels and fully characterise the competition between these two proteins. Genome editing techniques, such as CRISPR, could be used to create mutations in the *TP53BP1* gene under the control of the endogenous promoter. The same techniques could also be employed to tag the gene with a *GFP* reporter gene to analyse recruitment kinetics in real-time.

Thirdly, by knocking down endogenous 53BP1 and transfecting cells with constructs containing our mutants we were able to demonstrate that the phospho-specific interactions of the BRCT domains are required for repair of 'slow' kinetic or complex DSBs. The repair defect occurs due to a failure to retain pATM at the sites of damage independently of MRN localisation. Using dual RNAi depletion we were able rescue the repair defect by targeting the downstream chromatin effector, KAP-1.

Following the generation of CRISPR engineered cell lines, it would be necessary to confirm that the same repair defects and localisation defects are still observed. Given the varied range of important roles mediated by KAP-1 in regulating and protecting the genome [273] it would be important to confirm that the rescue produced by the depletion of KAP-1, results directly from phosphorylation of KAP-1 by pATM. By using genome engineering techniques, an un-phosphorylatable mutant (S824A) and a phosphomimetic mutant (S824D/E) could be generated under the control of the endogenous promoters. Enumerating γH2AX as before, with these new cell lines would indicate whether the repair defect is solely due to the defective KAP-1 phosphorylation by pATM.

Finally, by analysing the repositioning of 53BP1 in S- and G2-phase IRIF it has been demonstrated that a phospho-specific interaction, mediated by the BRCT domains of 53BP1, is required for repositioning of 53BP1 from the core of the IRIF to the periphery. Further to this,

it was possible to show that this defect is phenocopied by the inhibition of ATR kinase following damage. As ATR potentially regulates a number of downstream proteins by post-translational modification, it will be necessary to further characterise the role of this kinase in the repositioning of 53BP1 and whether this acts downstream of the BRCT-γH2AX interaction.

6. Discussion

6.1 Investigating the role of SUMOylation of eukaryotic translation initiation factors

As the role of SUMOylation in regulating eIFs is discussed predominantly in section 3.3, this section will focus on the future directions of this project in relation to further characterisation of the role of SUMOylation in mediating the response to cellular stress.

Looking at the future direction for this project it would be important establish whether the introduction of an unSUMOylatable mutant affects miRNA-mediated mRNA silencing. Collaborative work from M. Bushell (University of Leicester) has since shown that mutation of K226 in eIF4A2 does not impair miRNA-mediated mRNA silencing using a let7 luciferase reporter assay. In order to further characterise the role of SUMO, it would be useful to create unSUMOylatable eIF4A mutants under the control of their endogenous promoters using gene-editing techniques. The generation of these cell lines would be an invaluable tool to characterise any changes, while more importantly not producing any artificial change due to the over- or under-expression of exogenously introduced plasmid constructs.

Firstly, it would need to be established whether or not K216 is the sole target of SUMOylation of eIF4A1 in mammalian cells. Following on from this, and the generation of a mutant using gene editing, polysome fractionation and mRNAseq could be used to identify which transcripts within the cell are being actively translated. Further to this, any change in the mRNAs being targeted for translation in response to stress granule formation could be quantified and normalised to the cellular mRNA levels. Additionally, any decrease in the number of actively translated genes between the mutant and wild-type eIF4A1 with and without pre-treatment with a stress granule inducing agent would help elucidate whether SUMOylation of translation factors acts to promote stress granule formation.

In the case of eIF4A2, given that the unSUMOylatable mutant does not affect miRNA-mediated mRNA silencing, a polySUMO-eIF4A2 fusion protein could be introduced into mammalian cells. Analysis of how readily this fusion protein is incorporated into stress granules under stress conditions could further consolidate this function of SUMO. As mentioned earlier, the mild phenotype observed may result from group protein interactions by a number of SUMOylated proteins. As a result, mutation of all of the SUMOylation sites identified in the eIF4F complex might yield a more severe phenotype further indicating any role played by SUMO in this process.

6.2 Characterisation of the phospho-specific interactions between 53BP1 and TopBP1 and their role in DNA DSB repair

In this project, it has been determined that two phosphorylation sites within the N-terminal region of 53BP1, S366 and T670, are required for interaction between 53BP1 and TopBP1 in G1-phase cells. Both S366 and T670 are phosphorylated in response to damage *in vivo.* Furthermore, failure to phosphorylate either site disrupts co-localisation between 53BP1 and TopBP1 in G1-phase cells, as observed by immunofluorescence and impairs the direct physical interaction of these two proteins, as observed by immunoprecipitation. Cells that cannot mediate the interaction between 53BP1 and TopBP1 fail to sustain G1-phase arrest and prevent entry into S-phase while DNA damage persists (figure 6.1). Concomitantly, cells expressing these phosphorylation site mutants fail to repair a subset of DNA breaks representative of the heterochromatic proportion of DNA DSBs. However, no defect was observed in localisation of the checkpoint kinase, pATM or in the S- and G2-phase repositioning of 53BP1.

By analysing the co-localisation of 53BP1 with TopBP1, it was possible to determine that mutation of either phosphorylation site within 53BP1, mutation of either S366A or T670A, resulted in impaired recruitment of TopBP1 to DNA DSBs. The 53BP1-S366A mutation appears to abolish co-localisation with TopBP1 foci present within the cells, however the 53BP1-T670A mutation appears to disrupt TopBP1 foci formation altogether. This is consistent with the observations of Cescutti et al [193] who showed that the removal of the BRCT domains 0, 1-2 from the N-terminus of TopBP1 prevented its co-localisation with both 53BP1 and RPA. Furthermore, they also demonstrated that deletion of TopBP1 BRCT domains 4-5 did not prevent focus formation in response to damage, but did significantly impair co-localisation of TopBP1 and 53BP1. This suggests that despite both phosphorylation sites being required for interaction of 53BP1 with TopBP1 there may yet be some functional difference of phosphorylating each residue.

Furthermore, it remains to be determined which kinase(s) are required for phosphorylation of S366 and T670A. As the phosphopeptide sequence is comprised of a phosphorylated-serine/threonine followed by a proline residue, the kinase responsible for phosphorylating these residues is potentially a cyclin-dependent kinase [274]. This would also be consistent with the observations made in *S. pombe*, whereby $Crb2^{53BP1}$ is phosphorylated on threonine-187 by CDK in order to interact with $Rad4^{TopBP1}$ [238]. This could be analysed by pre-treating cells with specific kinase inhibitors to determine which kinase is required to phosphorylate these sites following damage. It will be of importance to note whether the same kinase is

responsible for the phosphorylation of S366 and T670 or whether phosphorylation of these residues requires the activity of two separate protein kinases. Furthermore, it could also be the case that phosphorylation of one residue may be dependent on the prior phosphorylation of the other, as is the case in *S. pombe*, whereby the phosphorylation of T187 by CDK requires prior phosphorylation of both T215 and T235 [238].

One interesting point to note is that despite a failure to recruit TopBP1 to IRIF when 53BP1-T670 is mutated to alanine, cells treated with siRNA oligonucleotides targeting 53BP1 alone are still able to form TopBP1 foci. One explanation for this phenomenon is that in cells where endogenous 53BP1 has been depleted, the cells are unable to protect the broken DNA ends from being resected [190]. This in turn would allow RPA to bind to any newly generated single stranded regions of DNA [275]. In these examples, TopBP1 may still be recruited through the conventional interaction with ATR through ATRIP and RPA [221]. This RPA-dependent recruitment of TopBP1 to sites of damage may be distinct from circumstances in which 53BP1 is present and prevents generation of ssDNA, but cannot associate with TopBP1 in a phosphorylation-dependent manner. This may also serve to account for the decreased number of TopBP1 foci present in 53BP1-depleted cells, as TopBP1 localisation may be limited to breaks that have undergone extensive end resection. In order to determine whether this is in fact the case, co-localisation of TopBP1 foci with RPA in 53BP1-depleted G1-phase cells could be analysed.

Alternatively, in cells with 53BP1 present, it would be interesting to determine whether TopBP1, 53BP1 and RPA co-localise to DNA damage in G1-phase cells. If RPA is not present in IRIF where 53BP1 and TopBP1 co-localise, it would suggest that the role of this interaction is to recruit TopBP1 in the absence of RPA-coated ssDNA.

Additionally, by analysing the number of γH2AX foci per cell in HeLa cells following exposure to ionising radiation, it was demonstrated that 53BP1-depleted cells transfected with either of the phosphorylation site mutants (53BP1-S366A, -T670A or double mutant) display a defect in DSB repair. A subset of the total number of breaks (~15%) remained unrepaired 24 hours following exposure to ionising radiation. The defect observed reflects the failure to complete the ‘slow’ kinetic DSB repair representative of the heterochromatic proportion of DSBs [202]. Further to this, additional depletion of KAP-1, the downstream mediator required for chromatin relaxation, bypasses the ‘slow’ kinetic repair defect. This suggests that there is a requirement for TopBP1 localisation for repair of 53BP1-dependent DSBs comparable to those requiring ATM for repair, but not acting through ATM localisation [203].

Interestingly, TopBP1 has been shown to localise ATM through interactions with the MRN complex in Xenopus egg extracts. In these extracts, ATM-dependent phosphorylation of S1131 is required for full activation of ATR by TopBP1, however the interaction with MRN has not been demonstrated in humans [221, 276]. In mammalian cells however, TopBP1 is required for full activation of ATR via its ATR-activation domain [229]. As a result it would also be important to analyse whether ATR, or its downstream target Chk1, are activated in response to damage in G1-phase cells with the phosphorylation site mutants. Research has only tentatively suggested a role for ATR in G1-phase cells as treatment with ATR inhibitors increases cell sensitivity to ionising radiation-induced killing [239]. Furthermore, ATR foci have been observed in G1-phase cells following exposure to ionising radiation. Analysis of the recruitment kinetics of ATR show its accumulation over two hours, comparable to that of TopBP1 recruitment, which appears 1-2 hours following damage and peaking at approximately 4 hours after DNA damage [193, 277].

The interaction of 53BP1 with TopBP1 is also required to mediate G1-S phase checkpoint arrest in response to DNA damage. Although the exact role of TopBP1 in this process remains to be established, it has been demonstrated that TopBP1 regulates replication origin firing during S-phase and that TopBP1 is required for intra-S phase checkpoint arrest by suppressing the firing of 'late' replication origins [223, 224]. It is possible that localisation of TopBP1 to IRIF in G1-phase cells serves to deplete the available pool of TopBP1 capable of licencing DNA replication and thereby preventing entry into S-phase. However, this is unlikely as depletion of TopBP1 alone results in a failure to maintain G1-phase cell-cycle arrest following DNA damage [193].

There is second mechanism by which TopBP1 may regulate S-phase entry. Conventionally, CDK2 bound to cyclin-E governs entry into S-phase by phosphorylating Rb (Retinoblastoma protein), which would otherwise suppress the activity of the transcription factor, E2F-1 [278]. E2F-1 activates transcription of a number of genes required to promote entry into S-phase [279]. Furthermore, it has been demonstrated that overexpression of E2F-1 alone is enough to stimulate cells to enter S-phase [280]. Importantly, TopBP1 interacts directly with E2F-1 through TopBP1-BRCT domain 6 and suppresses the transcriptional activity of E2F-1 by re-localising it to IRIF [281]. Ultimately this suggests that in G1-phase cells, phosphorylation of 53BP1 on S366 and T670 are required for recruitment of TopBP1 to IRIF in order to re-localise and suppress the transcriptional activity of E2F-1 and prevent entry into S-phase while DSBs are present. In order to determine if this is the case, it would be necessary to deplete E2F-1 from cells expressing the 53BP1 phosphorylation site mutants. If G1-S phase arrest is

dependent on downstream regulation of E2F-1 by TopBP1, the additional depletion of E2F-1 should restore the G1-S phase checkpoint in cells expressing the 53BP1 phosphorylation mutants.

Finally, by analysing 53BP1 repositioning in G2-phase cells and the ability to perform HR using a GFP-reporter assay it was possible to demonstrate that neither of these phosphorylation mutants appears to impair the progression towards HR-mediated repair, or HR itself, following exposure to ionising radiation. This further strengthens the idea that the G1-phase specific interaction between 53BP1 and TopBP1 is limited to the repair of complex of breaks solely by NHEJ.

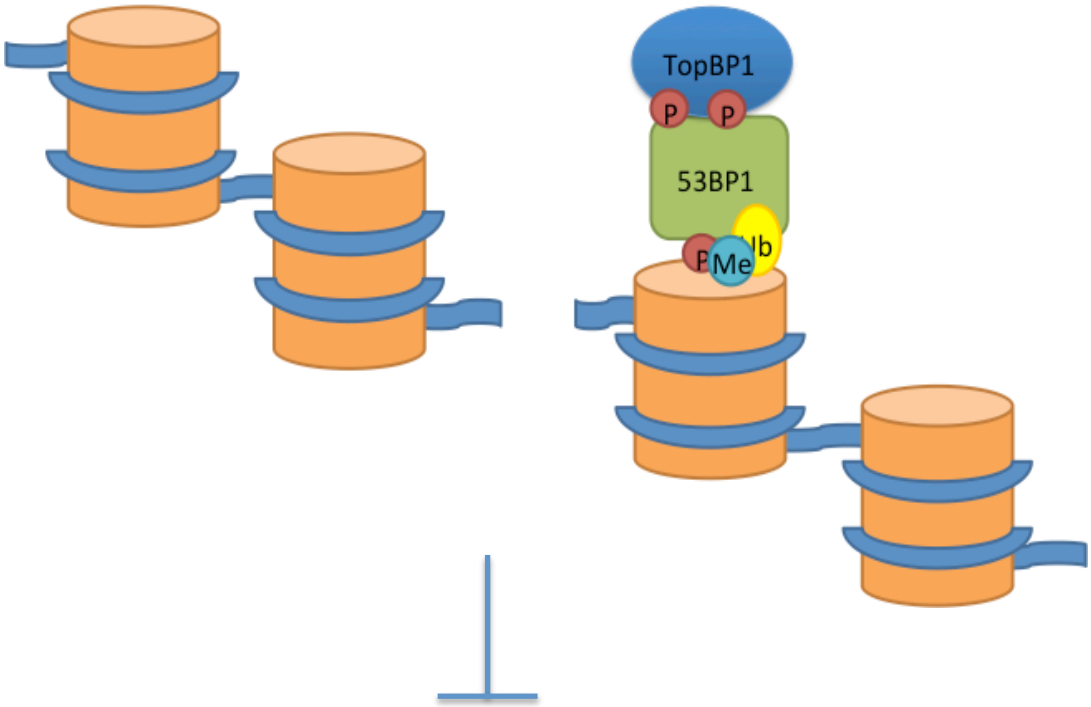

Figure 6.1 Proposed model for the role of the G1-phase phosphorylation-dependent interaction between 53BP1 and TopBP1.

6.3 Determining the phospho-specific interactions of the BRCT domains of 53BP1 and their role in DNA damage repair

In this project, it has been demonstrated that the BRCT domains of 53BP1 interact specifically and directly with γH2AX *in vitro*. *In vivo*, localisation of the BRCT domains to sites of damage is phosphorylation-dependent, requires the histone variant H2AX and the kinase activity of both ATM and DNA-PK following damage.

While this work was being undertaken, the 53BP1 BRCT-γH2AX interaction was also identified by another research group by performing the reciprocal experiments i.e. co-purification of proteins with a γH2AX peptide. Further validation of this interaction by this research group, suggested that mutation of K1814 to methionine impairs recruitment of full-length 53BP1 to sites of laser induced damage, although the affect was less severe than in cells lacking MDC1 (which would fail to propagate the γH2AX signal) [282, 283]. This suggests that the recruitment of full-length 53BP1 to sites of DNA damage may be directly influenced by the ability to recognise γH2AX. However the decrease in the rate of 53BP1 recruitment when the BRCT domains are mutated is quite small and potentially difficult to detect without analysing large numbers of cells.

The *in vitro* interaction data indicate that the BRCT domains of MDC1 have a 3.5-fold higher affinity for the γH2AX phosphopeptide than those of 53BP1 (K_d=0.4μM ± 0.05 for MDC1-BRCTs and 1.4μM ± 0.14 for 53BP1-BRCTs). This suggests that at the molecular level MDC1 is capable of out-competing 53BP1 for γH2AX. This is not surprising given that the interaction of MDC1 with γH2AX is required, prior to 53BP1 recruitment, for the spreading of the γH2AX signal along the chromatin via additional recruitment of MRN and pATM [263, 283, 284]. It is only after this that 53BP1 is recruited through a combination of histone methylation and damage-induced ubiquitination [9, 10]. Given the weaker affinity of the BRCT domains of 53BP1 for γH2AX it may be that this interaction only becomes physiologically important at this later stage.

Further investigation could be undertaken to establish the specific dynamics of both 53BP1 and MDC1 to elucidate the potential antagonism. This could be analysed by transfecting cells with fluorescently labelled MDC1 and 53BP1. Live-cell imaging could be utilised to determine, in real-time, whether MDC1 is retained at the break following damage or if there is a handover to allow 53BP1 access to the chromatin via γH2AX binding.

The BRCT domains of 53BP1 mediate multiple phosphorylation-independent interactions with p53, Rad50 and EXPAND1 [196, 197, 258, 285]. Having characterised further interaction with

γH2AX, it would be necessary to determine whether this interaction is mutually exclusive or whether the BRCT domains are capable of mediating several phosphorylation-dependent and -independent interactions simultaneously.

Mutations that impair the γH2AX-binding of the BRCT domains of 53BP1 also disrupt pATM but not MRN localisation. This is significant as previously it has been shown that deletion of the BRCT domains impair the localisation of both ATM and MRN [202]. Interestingly, it has been demonstrated that ATM can localise to IRIF in the absence of MRN and Ku70 [286]. This suggests that multiple interactions may be possible within the cell to localise ATM to the sites of damage without the requirement for the conventional MDC1-MRN-ATM interaction and could also begin to explain why localisation of pATM, but not MRN, is affected [283].

In this project, it has also been established that an inability to mediate the phosphorylation-dependent interactions of the BRCT domains of 53BP1 results in a persistence of γH2AX foci at later time points, comparable to inhibition of ATM and representative of the heterochromatic proportion of DSBs [202]. Furthermore, these breaks are repaired by downregulation of KAP-1 (figure 6.2). ATM-dependent phosphorylation of SUMOylated KAP1 is required to release CHD3, a chromatin remodeler, from regions of heterochromatin in order to promote relaxation of heterochromatin [203]. Interestingly, Artemis the DNA endonuclease is also required for resolution of DSBs that display 'slow' kinetics repair, but acts independently of KAP-1 phosphorylation [267]. These results suggest that although repair of heterochromatic breaks requires signalling though 53BP1 and ATM, there may be a number of downstream effector proteins required to both remodel chromatin and process the broken DNA ends in preparation for repair.

In addition to the role of repair of heterochromatic DSBs in G1-phase cells, it has been demonstrated that there is a defect in 53BP1 repositioning in S- and G2-phase cells, a defect that is recapitulated by the inhibition of ATR checkpoint kinase following on from early break processing events (figure 6.3). Further work will be required to demonstrate whether a failure to reposition 53BP1 to the periphery of BRCA1 marked IRIF confers a repair defect. Using a DR-GFP reporter assay no defect in HR was observed. It is likely however, that using a reporter construct upstream of the repair template may not reflect the complexity required for complete homology-mediated repair, which under normal physiological conditions may be hindered by the chromatin environment. One way of visualising the progression to HR would be stain for Rad51 foci using immunofluorescence. If a failure to reposition 53BP1 blocks the progression towards HR-mediated repair, it would be expected that Rad51 foci would fail to

form. Furthermore, it would be possible to correlate any failure to form Rad51 foci with the chromatin environment by co-immunostaining for other markers of heterochromatin such as HP1α [287].

Given that both deletion of the BRCT domains of 53BP1 and the inhibition of ATR produce the same repositioning defect, it would be important to examine whether the roles of these proteins are epistatic. If inhibition of ATR in combination with the 53BP1 BRCT mutant did not result in synthetic lethality or a more severe defect, it could be concluded that these proteins function in the same repair pathway. This would also suggest that one of two scenarios exist within the cell, either ATR phosphorylates H2AX in response to damage in S- and G2 phase or the BRCT domains of 53BP1 are required for additional processing of DSBs prior to activation of ATR following damage.

Although phosphorylation of H2AX in response to ionising radiation primarily occurs by ATM, ATR has been shown to be required for H2AX phosphorylation during replicative stress [288]. If the role of ATR in this process is to phosphorylate H2AX, it would suggest that there may be cross-talk between these apparent damage-specific responses.

Alternatively, the requirement for ATR kinase could be further downstream. Previous investigation has shown that a handover event exists between ATM and ATR kinase in response to DNA damage that is dependent on the presence of single stranded DNA [289]. As demonstrated in figure 5.10, mutation of the BRCT domain of 53BP1 prevents localisation of pATM following damage. As a result, it would be necessary to test whether the repositioning of 53BP1 requires pATM for early break processing. Previous investigation has shown that ATM is required to stimulate nucleases MRE11 and CtIP [290]. Furthermore, DNA end resection is a prerequisite for full ATR activation via the recruitment of ATRIP to RPA which binds unprotected single stranded DNA [291]. The ability of the cells to resect DNA ends could also be analysed by RPA focus formation. If the BRCT domain mutants block end resection by preventing the repositioning of 53BP1, it would be expected that RPA foci would fail to form in these cells. This would theoretically contrast with depletion of endogenous 53BP1 alone, in where the cells would be unable to protect the DNA ends from resection and would show RPA foci. Additionally, as the nuclease activity of Mre11 is regulated by phosphorylation, Western analysis could also be used to investigate phosphorylation of Mre11 in cells transfected with the mutant 53BP1 BRCT domains and those treated with an ATR inhibitor [148]. This would help to determine whether the repair of heterochromatic breaks in S- and G2-phase are a two-phase process requiring initial processing with ATM followed by later activity by ATR.

To further examine the role of 53BP1 and ATR and to establish whether the activity of ATR is downstream of 53BP1, it would be necessary to use immunofluorescence to assess whether ATR is still recruited to these sites of damage when the BRCT domain is mutated. It is possible that a failure to reposition 53BP1 at the periphery of the IRIF would block end-resection and subsequent ATR recruitment. Further work would be required to elucidate the ATR-dependent process required for DSB resolution in S- and G2-phase cells.

Interestingly, in *D. melanogaster*, researchers have shown that that depletion of ATR results in a persistence of H2Av foci within DAPI-bright regions of nuclei. The DAPI-bright regions of DNA, co-stained with HP1a, mark areas of heterochromatin. Following damage, DSBs are resected and repositioned to the periphery of the region by expansion of the HP1a domain prior to Rad51 foci formation and additional processing for repair [292]. This suggests that ATR may have some role in regulating factors required for repositioning the DSBs to the periphery of the heterochromatic regions.

As ATR checkpoint kinase phosphorylates a number of downstream target proteins, it is important to consider, if not H2AX, which proteins acting downstream are phosphorylated by ATR kinase. A number of downstream factors have been shown to be required for 53BP1 IRIF expansion, including BRCA1, CtIP, SETDB1, SUV39 and HP-1 [210, 211]. The requirement for CtIP, a known target of ATR kinase, indicates that 53BP1 IRIF expansion is concomitant with long-range DNA end resection and suggests a role for ATR immediately prior to 53BP1 IRIF expansion, as seen in figure 5.20 by delaying ATR inhibitor addition [293]. Further work will be required to establish which of the chromatin remodelling proteins, if any, require phosphorylation by ATR kinase and discern the individual and collective contributions of both chromatin compaction and relaxing factors in promoting DSB repair. If chromatin-remodelling factors required for repair of heterochromatic DSBs are regulated by ATR, this could suggest a mechanism by which TopBP1 is required for the 'slow' kinetic repair in G1-phase cells.

Ultimately, the future direction of this project will concern piecing together the networks of interactions between 53BP1, MDC1 and pATM in order to understand why the 53BP1-BRCT-γH2AX interaction is required to retain phosphorylated ATM at sites of DSBs. Further work will be required to establish the requirement for TopBP1 in the resolution of heterochromatic breaks. Lastly, in S- and G2-phase cells further work will also be required to establish the sequence of events in the preparation of DSBs marked for repair by HR and the potential role of the BRCT domains of 53BP1 and ATR in regulating this repair pathway.

‘Slow’ kinetic DSB repair

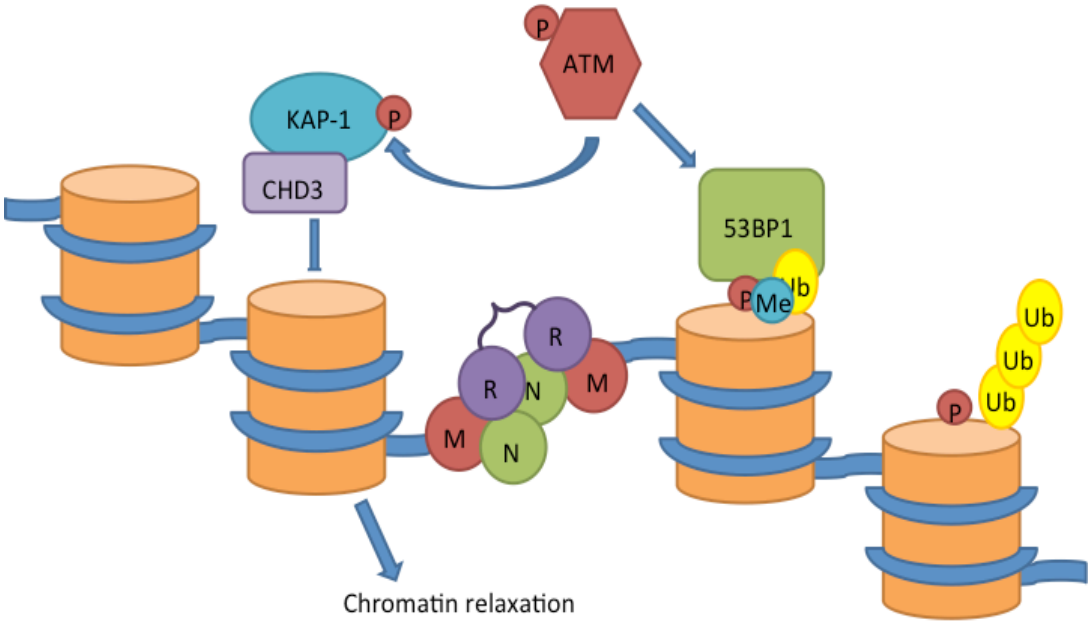

Figure 6.2 Proposed model for resolution of heterochromatic breaks requiring the phospho-specific interactions between 53BP1 BRCT domain and γH2AX.

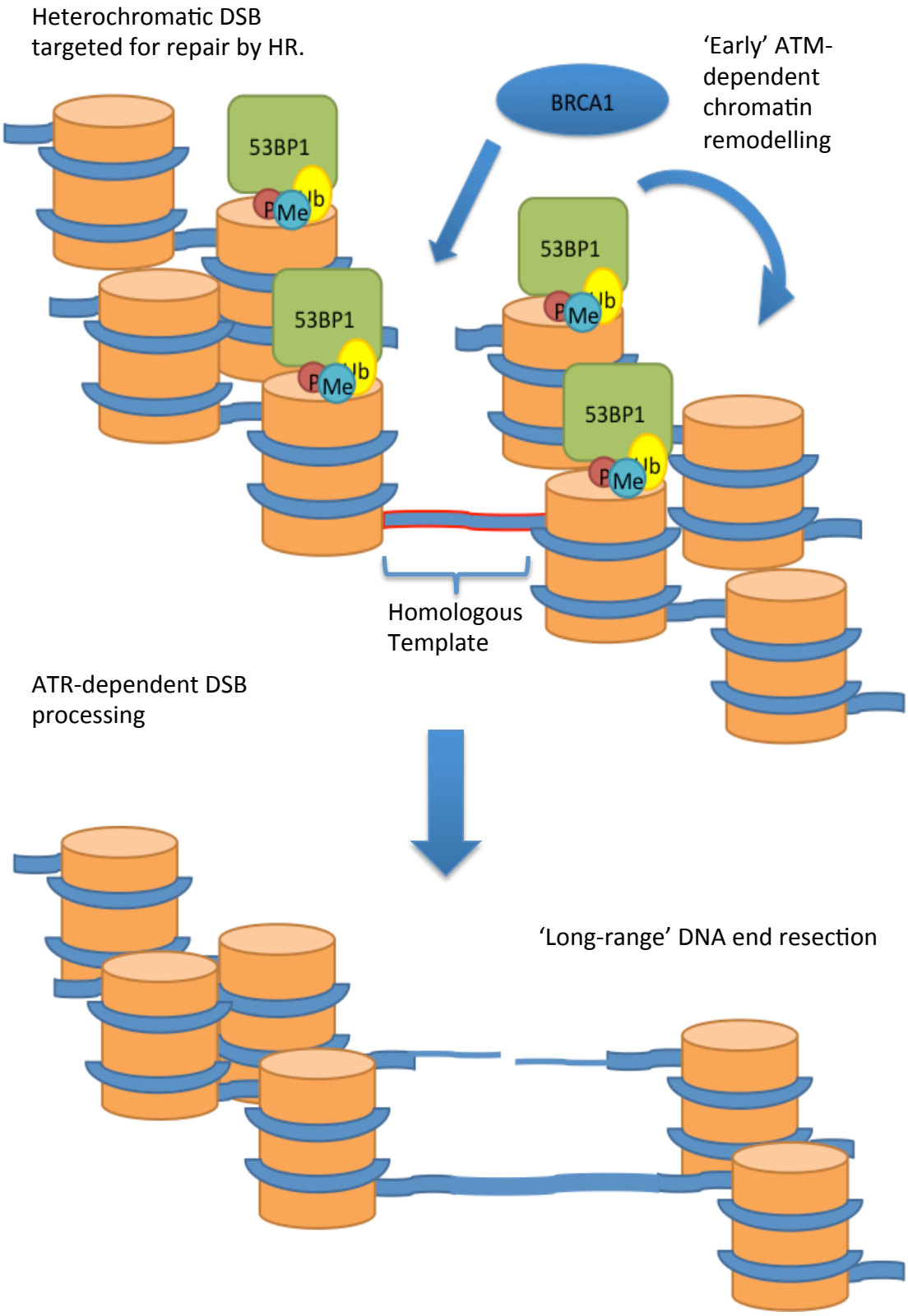

Figure 6.3 Proposed model for resolution of S- and G2- phase heterochromatic breaks destined for repair by HR. 53BP1 needs to be repositioned relative to BRCA1 to permit long-range end resection. DNA outlined in red marks the template for repair.

7. References

1. Sonenberg, N. and A.G. Hinnebusch, *Regulation of translation initiation in eukaryotes: mechanisms and biological targets.* Cell, 2009. **136**(4): p. 731-45.
2. Becker, J., et al., *Detecting endogenous SUMO targets in mammalian cells and tissues.* Nat Struct Mol Biol, 2013. **20**(4): p. 525-31.
3. Blomster, H.A., et al., *In vivo identification of sumoylation sites by a signature tag and cysteine-targeted affinity purification.* J Biol Chem, 2010. **285**(25): p. 19324-9.
4. Bruderer, R., et al., *Purification and identification of endogenous polySUMO conjugates.* EMBO Rep, 2011. **12**(2): p. 142-8.
5. Matafora, V., et al., *Proteomics analysis of nucleolar SUMO-1 target proteins upon proteasome inhibition.* Mol Cell Proteomics, 2009. **8**(10): p. 2243-55.
6. Yang, W., et al., *Analysis of oxygen/glucose-deprivation-induced changes in SUMO3 conjugation using SILAC-based quantitative proteomics.* J Proteome Res, 2012. **11**(2): p. 1108-17.
7. Roukos, V., B. Burman, and T. Misteli, *The cellular etiology of chromosome translocations.* Current opinion in cell biology, 2013. **25**(3): p. 357-364.
8. Panier, S. and S.J. Boulton, *Double-strand break repair: 53BP1 comes into focus.* Nat Rev Mol Cell Biol, 2014. **15**(1): p. 7-18.
9. Fradet-Turcotte, A., et al., *53BP1 is a reader of the DNA-damage-induced H2A Lys 15 ubiquitin mark.* Nature, 2013. **499**(7456): p. 50-54.
10. Hartlerode, A.J., et al., *Impact of histone H4 lysine 20 methylation on 53BP1 responses to chromosomal double strand breaks.* PLoS One, 2012. **7**(11): p. e49211.
11. Beltrao, P., et al., *Evolution and functional cross‐talk of protein post‐translational modifications.* Molecular Systems Biology, 2013. **9**(1).
12. Sudhakar, A., et al., *Phosphorylation of serine 51 in initiation factor 2 alpha (eIF2 alpha) promotes complex formation between eIF2 alpha(P) and eIF2B and causes inhibition in the guanine nucleotide exchange activity of eIF2B.* Biochemistry, 2000. **39**(42): p. 12929-38.
13. Heesom, K.J. and R.M. Denton, *Dissociation of the eukaryotic initiation factor-4E/4E-BP1 complex involves phosphorylation of 4E-BP1 by an mTOR-associated kinase.* FEBS Lett, 1999. **457**(3): p. 489-93.
14. Haupt, Y., et al., *Mdm2 promotes the rapid degradation of p53.* Nature, 1997. **387**(6630): p. 296-299.
15. Hornbeck, P.V., et al., *PhosphoSitePlus: a comprehensive resource for investigating the structure and function of experimentally determined post-translational modifications in man and mouse.* Nucleic Acids Research, 2012. **40**(Database issue): p. D261-D270.
16. Zhu, X., et al., *Adhesion-dependent cell cycle progression linked to the expression of cyclin D1, activation of cyclin E-cdk2, and phosphorylation of the retinoblastoma protein.* The Journal of Cell Biology, 1996. **133**(2): p. 391-403.
17. Wilkinson, K.D., *Ubiquitination and deubiquitination: Targeting of proteins for degradation by the proteasome.* Seminars in Cell & Developmental Biology, 2000. **11**(3): p. 141-148.
18. Neo, S.H., et al., *TRIM28 Is an E3 Ligase for ARF-Mediated NPM1/B23 SUMOylation That Represses Centrosome Amplification.* Mol Cell Biol, 2015. **35**(16): p. 2851-63.
19. Sahin, U., H. de The, and V. Lallemand-Breitenbach, *PML nuclear bodies: assembly and oxidative stress-sensitive sumoylation.* Nucleus, 2014. **5**(6): p. 499-507.
20. Guo, L., et al., *A Cellular System that Degrades Misfolded Proteins and Protects against Neurodegeneration.* Molecular Cell, 2014. **55**(1): p. 15-30.
21. Song, J.G., et al., *SUMO-specific protease 6 promotes gastric cancer cell growth via deSUMOylation of FoxM1.* Tumour Biol, 2015.

22. Schimmel, J., et al., *Uncovering SUMOylation Dynamics during Cell-Cycle Progression Reveals FoxM1 as a Key Mitotic SUMO Target Protein.* Molecular Cell, 2014. **53**(6): p. 1053-1066.
23. Wieland, T., et al., *Reversible histidine phosphorylation in mammalian cells: a teeter-totter formed by nucleoside diphosphate kinase and protein histidine phosphatase 1.* Methods Enzymol, 2010. **471**: p. 379-402.
24. Traven, A. and J. Heierhorst, *SQ/TQ cluster domains: concentrated ATM/ATR kinase phosphorylation site regions in DNA-damage-response proteins.* Bioessays, 2005. **27**(4): p. 397-407.
25. Lovejoy, C.A. and D. Cortez, *Common mechanisms of PIKK regulation.* DNA repair, 2009. **8**(9): p. 1004-1008.
26. Murr, R., et al., *Orchestration of chromatin-based processes: mind the TRRAP.* Oncogene, 2007. **26**(37): p. 5358-5372.
27. Kashima, I., et al., *Binding of a novel SMG-1–Upf1–eRF1–eRF3 complex (SURF) to the exon junction complex triggers Upf1 phosphorylation and nonsense-mediated mRNA decay.* Genes & Development, 2006. **20**(3): p. 355-367.
28. Brown, J.A.L., et al., *A Novel Role for hSMG-1 in Stress Granule Formation.* Molecular and Cellular Biology, 2011. **31**(22): p. 4417-4429.
29. Shibata, A., et al., *Role of ATM and the Damage Response Mediator Proteins 53BP1 and MDC1 in the Maintenance of G2/M Checkpoint Arrest.* Molecular and Cellular Biology, 2010. **30**(13): p. 3371-3383.
30. Ball, H.L., J.S. Myers, and D. Cortez, *ATRIP Binding to Replication Protein A-Single-stranded DNA Promotes ATR–ATRIP Localization but Is Dispensable for Chk1 Phosphorylation.* Molecular Biology of the Cell, 2005. **16**(5): p. 2372-2381.
31. DeFazio, L.G., et al., *Synapsis of DNA ends by DNA ‐ dependent protein kinase.* The EMBO Journal, 2002. **21**(12): p. 3192-3200.
32. Nigg, E.A., *Cellular substrates of p34cdc2 and its companion cyclin-dependent kinases.* Trends in Cell Biology, 1993. **3**(9): p. 296-301.
33. Ye, X., et al., *The Cyclin E/Cdk2 Substrate p220(NPAT) Is Required for S-Phase Entry, Histone Gene Expression, and Cajal Body Maintenance in Human Somatic Cells.* Molecular and Cellular Biology, 2003. **23**(23): p. 8586-8600.
34. Sherr, C.J., *Mammalian G₁ cyclins.* Cell, 1993. **73**(6): p. 1059-1065.
35. Reinhardt, H.C. and M.B. Yaffe, *Phospho-Ser/Thr-binding domains: navigating the cell cycle and DNA damage response.* Nat Rev Mol Cell Biol, 2013. **14**(9): p. 563-580.
36. Hoege, C., et al., *RAD6-dependent DNA repair is linked to modification of PCNA by ubiquitin and SUMO.* Nature, 2002. **419**(6903): p. 135-141.
37. Turcu, F.E.R., K.H. Ventii, and K.D. Wilkinson, *Regulation and Cellular Roles of Ubiquitin-specific Deubiquitinating Enzymes.* Annual review of biochemistry, 2009. **78**: p. 363-397.
38. Moudry, P., et al., *Ubiquitin-activating enzyme UBA1 is required for cellular response to DNA damage.* Cell Cycle, 2012. **11**(8): p. 1573-1582.
39. Zhao, G.Y., et al., *A Critical Role for the Ubiquitin-Conjugating Enzyme Ubc13 in Initiating Homologous Recombination.* Molecular Cell, 2007. **25**(5): p. 663-675.
40. Berndsen, C.E. and C. Wolberger, *New insights into ubiquitin E3 ligase mechanism.* Nat Struct Mol Biol, 2014. **21**(4): p. 301-307.
41. Hurley, James H., S. Lee, and G. Prag, *Ubiquitin-binding domains.* Biochemical Journal, 2006. **399**(Pt 3): p. 361-372.
42. Yang, W., *An overview of Y-Family DNA polymerases and a case study of human DNA polymerase eta.* Biochemistry, 2014. **53**(17): p. 2793-803.
43. Eifler, K. and A.C. Vertegaal, *Mapping the SUMOylated landscape.* Febs j, 2015. **282**(19): p. 3669-80.

44. Mendes, A.V., et al., *Evaluation of the activity and substrate specificity of the human SENP family of SUMO proteases.* Biochim Biophys Acta, 2016. **1863**(1): p. 139-47.
45. Owerbach, D., et al., *A proline-90 residue unique to SUMO-4 prevents maturation and sumoylation.* Biochem Biophys Res Commun, 2005. **337**(2): p. 517-20.
46. Lamoliatte, F., et al., *Large-scale analysis of lysine SUMOylation by SUMO remnant immunoaffinity profiling.* Nat Commun, 2014. **5**: p. 5409.
47. Palvimo, J.J., *PIAS proteins as regulators of small ubiquitin-related modifier (SUMO) modifications and transcription.* Biochemical Society Transactions, 2007. **35**(6): p. 1405-1408.
48. Burkovics, P., et al., *Srs2 mediates PCNA-SUMO-dependent inhibition of DNA repair synthesis.* EMBO J, 2013. **32**(5): p. 742-55.
49. Psakhye, I. and S. Jentsch, *Protein Group Modification and Synergy in the SUMO Pathway as Exemplified in DNA Repair.* Cell, 2012. **151**(4): p. 807-820.
50. Lallemand-Breitenbach, V., et al., *Role of Promyelocytic Leukemia (Pml) Sumolation in Nuclear Body Formation, 11s Proteasome Recruitment, and as(2)O(3)-Induced Pml or Pml/Retinoic Acid Receptor α Degradation.* The Journal of Experimental Medicine, 2001. **193**(12): p. 1361-1372.
51. Tatham, M.H., et al., *RNF4 is a poly-SUMO-specific E3 ubiquitin ligase required for arsenic-induced PML degradation.* Nat Cell Biol, 2008. **10**(5): p. 538-46.
52. Xu, Y., et al., *Structural insight into SUMO chain recognition and manipulation by the ubiquitin ligase RNF4.* Nat Commun, 2014. **5**: p. 4217.
53. Rojas-Fernandez, A., et al., *SUMO chain-induced dimerization activates RNF4.* Mol Cell, 2014. **53**(6): p. 880-92.
54. Enserink, J.M., *Sumo and the cellular stress response.* Cell Division, 2015. **10**(1): p. 1-13.
55. Schimmel, J., et al., *Uncovering SUMOylation dynamics during cell-cycle progression reveals FoxM1 as a key mitotic SUMO target protein.* Mol Cell, 2014. **53**(6): p. 1053-66.
56. Galanty, Y., et al., *RNF4, a SUMO-targeted ubiquitin E3 ligase, promotes DNA double-strand break repair.* Genes Dev, 2012. **26**(11): p. 1179-95.
57. Panse, V.G., et al., *A proteome-wide approach identifies sumoylated substrate proteins in yeast.* J Biol Chem, 2004. **279**(40): p. 41346-51.
58. Westman, B.J., et al., *A proteomic screen for nucleolar SUMO targets shows SUMOylation modulates the function of Nop5/Nop58.* Mol Cell, 2010. **39**(4): p. 618-31.
59. Dever, T.E. and R. Green, *The Elongation, Termination, and Recycling Phases of Translation in Eukaryotes.* Cold Spring Harbor Perspectives in Biology, 2012. **4**(7).
60. Saibil, H., *Chaperone machines for protein folding, unfolding and disaggregation.* Nat Rev Mol Cell Biol, 2013. **14**(10): p. 630-642.
61. Passmore, L.A., et al., *The eukaryotic translation initiation factors eIF1 and eIF1A induce an open conformation of the 40S ribosome.* Mol Cell, 2007. **26**(1): p. 41-50.
62. des Georges, A., et al., *Structure of mammalian eIF3 in the context of the 43S preinitiation complex.* Nature, 2015. **525**(7570): p. 491-495.
63. Lee, S.H., et al., *Poly(A) RNA and Paip2 act as allosteric regulators of poly(A)-binding protein.* Nucleic Acids Res, 2014. **42**(4): p. 2697-707.
64. Eulalio, A., et al., *Deadenylation is a widespread effect of miRNA regulation.* Rna, 2009. **15**(1): p. 21-32.
65. Villa, N., et al., *Human eukaryotic initiation factor 4G (eIF4G) protein binds to eIF3c, -d, and -e to promote mRNA recruitment to the ribosome.* J Biol Chem, 2013. **288**(46): p. 32932-40.
66. Fekete, C.A., et al., *N- and C-terminal residues of eIF1A have opposing effects on the fidelity of start codon selection.* The EMBO Journal, 2007. **26**(6): p. 1602-1614.
67. Hussain, T., et al., *Structural Changes Enable Start Codon Recognition by the Eukaryotic Translation Initiation Complex.* Cell, 2014. **159**(3): p. 597-607.

68. Saini, A.K., et al., *Eukaryotic translation initiation factor eIF5 promotes the accuracy of start codon recognition by regulating Pi release and conformational transitions of the preinitiation complex.* Nucleic Acids Res, 2014. **42**(15): p. 9623-40.
69. Shin, B.-S., et al., *rRNA Suppressor of a Eukaryotic Translation Initiation Factor 5B/Initiation Factor 2 Mutant Reveals a Binding Site for Translational GTPases on the Small Ribosomal Subunit.* Molecular and Cellular Biology, 2009. **29**(3): p. 808-821.
70. Hinnebusch, A.G., *The Scanning Mechanism of Eukaryotic Translation Initiation.* Annual Review of Biochemistry, 2014. **83**(1): p. 779-812.
71. Korneeva, N.L., et al., *Inhibition of MAP Kinase-Interacting Kinase (MNK) Preferentially Affects Translation of mRNAs Containing both a 5'-Terminal Cap and Hairpin.* J Biol Chem, 2015.
72. Dennis, M.D., L.S. Jefferson, and S.R. Kimball, *Role of p70S6K1-mediated Phosphorylation of eIF4B and PDCD4 Proteins in the Regulation of Protein Synthesis.* Journal of Biological Chemistry, 2012. **287**(51): p. 42890-42899.
73. Martineau, Y., et al., *Control of Paip1-eukayrotic translation initiation factor 3 interaction by amino acids through S6 kinase.* Mol Cell Biol, 2014. **34**(6): p. 1046-53.
74. Tourrière, H., et al., *The RasGAP-associated endoribonuclease G3BP assembles stress granules.* The Journal of Cell Biology, 2003. **160**(6): p. 823-831.
75. Xu, X., et al., *Sumoylation of eIF4E activates mRNA translation.* EMBO Rep, 2010. **11**(4): p. 299-304.
76. Jongjitwimol, J., et al., *The <italic>S. pombe</italic> Translation Initiation Factor eIF4G Is Sumoylated and Associates with the SUMO Protease Ulp2.* PLoS ONE, 2014. **9**(5): p. e94182.
77. Zaborske, J.M., et al., *Selective control of amino acid metabolism by the GCN2 eIF2 kinase pathway in Saccharomyces cerevisiae.* BMC Biochem, 2010. **11**: p. 29.
78. Grosso, S., et al., *Sensitivity of global translation to mTOR inhibition in REN cells depends on the equilibrium between eIF4E and 4E-BP1.* PLoS One, 2011. **6**(12): p. 22.
79. Kubacka, D., et al., *Investigating the consequences of eIF4E2 (4EHP) interaction with 4E-transporter on its cellular distribution in HeLa cells.* PLoS One, 2013. **8**(8): p. e72761.
80. Nishimura, T., et al., *The eIF4E-Binding Protein 4E-T Is a Component of the mRNA Decay Machinery that Bridges the 5' and 3' Termini of Target mRNAs.* Cell Rep, 2015. **11**(9): p. 1425-36.
81. Andreou, A.Z. and D. Klostermeier, *eIF4B and eIF4G Jointly Stimulate eIF4A ATPase and Unwinding Activities by Modulation of the eIF4A Conformational Cycle.* J Mol Biol, 2013.
82. Wolfe, A.L., et al., *RNA G-quadruplexes cause eIF4A-dependent oncogene translation in cancer.* Nature, 2014. **513**(7516): p. 65-70.
83. Barbosa, I., et al., *Human CWC22 escorts the helicase eIF4AIII to spliceosomes and promotes exon junction complex assembly.* Nat Struct Mol Biol, 2012. **19**(10): p. 983-90.
84. Galicia-Vazquez, G., et al., *A cellular response linking eIF4AI activity to eIF4AII transcription.* RNA, 2012. **18**(7): p. 1373-84.
85. Meijer, H.A., et al., *Translational repression and eIF4A2 activity are critical for microRNA-mediated gene regulation.* Science, 2013. **340**(6128): p. 82-5.
86. Yoshida, M., et al., *Poly(A) binding protein (PABP) homeostasis is mediated by the stability of its inhibitor, Paip2.* Embo j, 2006. **25**(9): p. 1934-44.
87. Hinnebusch, A.G., *Translational regulation of GCN4 and the general amino acid control of yeast.* Annu Rev Microbiol, 2005. **59**: p. 407-50.
88. Pelletier, J. and N. Sonenberg, *Internal initiation of translation of eukaryotic mRNA directed by a sequence derived from poliovirus RNA.* Nature, 1988. **334**(6180): p. 320-5.

89. Thakor, N. and M. Holcik, *IRES-mediated translation of cellular messenger RNA operates in eIF2alpha- independent manner during stress.* Nucleic Acids Res, 2012. **40**(2): p. 541-52.
90. Lozano, G. and E. Martinez-Salas, *Structural insights into viral IRES-dependent translation mechanisms.* Curr Opin Virol, 2015. **12**: p. 113-20.
91. Yamamoto, H., et al., *Structure of the mammalian 80S initiation complex with initiation factor 5B on HCV-IRES RNA.* Nat Struct Mol Biol, 2014. **21**(8): p. 721-7.
92. Muhs, M., et al., *Cryo-EM of ribosomal 80S complexes with termination factors reveals the translocated cricket paralysis virus IRES.* Mol Cell, 2015. **57**(3): p. 422-32.
93. Marnef, A., B.E. Jady, and T. Kiss, *Human polypyrimidine tract-binding protein interacts with mitochondrial tRNAThr in the cytosol.* Nucleic Acids Res, 2015.
94. Morris, M.J., et al., *An RNA G-Quadruplex Is Essential for Cap-Independent Translation Initiation in Human VEGF IRES.* Journal of the American Chemical Society, 2010. **132**(50): p. 17831-17839.
95. Cammas, A., et al., *Stabilization of the G-quadruplex at the VEGF IRES represses cap-independent translation.* RNA Biol, 2015. **12**(3): p. 320-9.
96. Anderson, P., N. Kedersha, and P. Ivanov, *Stress granules, P-bodies and cancer.* Biochimica et Biophysica Acta (BBA) - Gene Regulatory Mechanisms, 2015. **1849**(7): p. 861-870.
97. Chang, C.T., et al., *The activation of the decapping enzyme DCP2 by DCP1 occurs on the EDC4 scaffold and involves a conserved loop in DCP1.* Nucleic Acids Res, 2014. **42**(8): p. 5217-33.
98. Tomecki, R., et al., *The human core exosome interacts with differentially localized processive RNases: hDIS3 and hDIS3L.* The EMBO Journal, 2010. **29**(14): p. 2342-2357.
99. Barnes, T., et al., *Identification of Apurinic/apyrimidinic endonuclease 1 (APE1) as the endoribonuclease that cleaves c-myc mRNA.* Nucleic Acids Research, 2009. **37**(12): p. 3946-3958.
100. Fabian, M.R., et al., *Structural basis for the recruitment of the human CCR4-NOT deadenylase complex by tristetraprolin.* Nat Struct Mol Biol, 2013. **20**(6): p. 735-9.
101. Piao, X., et al., *CCR4-NOT Deadenylates mRNA Associated with RNA-Induced Silencing Complexes in Human Cells.* Molecular and Cellular Biology, 2010. **30**(6): p. 1486-1494.
102. Zhang, X., et al., *PARN deadenylase is involved in miRNA-dependent degradation of TP53 mRNA in mammalian cells.* Nucleic Acids Res, 2015. **43**(22): p. 10925-38.
103. Nomakuchi, T.T., et al., *Antisense oligonucleotide-directed inhibition of nonsense-mediated mRNA decay.* Nat Biotech, 2015. **advance online publication**.
104. He, F. and A. Jacobson, *Nonsense-Mediated mRNA Decay: Degradation of Defective Transcripts Is Only Part of the Story.* Annu Rev Genet, 2015. **49**: p. 339-66.
105. Yao, B., et al., *Mapping of Ago2-GW182 functional interactions.* Methods Mol Biol, 2011. **725**: p. 45-62.
106. Eystathioy, T., et al., *The GW182 protein colocalizes with mRNA degradation associated proteins hDcp1 and hLSm4 in cytoplasmic GW bodies.* Rna, 2003. **9**(10): p. 1171-3.
107. Sidrauski, C., et al., *The small molecule ISRIB reverses the effects of eIF2 α phosphorylation on translation and stress granule assembly.* eLife, 2015. **4**.
108. Buchan, J.R. and R. Parker, *Eukaryotic Stress Granules: The Ins and Outs of Translation.* Molecular Cell, 2009. **36**(6): p. 932-941.
109. Emara, M.M., et al., *Hydrogen peroxide induces stress granule formation independent of eIF2alpha phosphorylation.* Biochem Biophys Res Commun, 2012. **423**(4): p. 763-9.
110. Moutaoufik, M.T., et al., *UVC-induced stress granules in mammalian cells.* PLoS One, 2014. **9**(11): p. e112742.

111. Mazroui, R., et al., *Inhibition of ribosome recruitment induces stress granule formation independently of eukaryotic initiation factor 2alpha phosphorylation.* Mol Biol Cell, 2006. **17**(10): p. 4212-9.
112. Mokas, S., et al., *Uncoupling Stress Granule Assembly and Translation Initiation Inhibition.* Molecular Biology of the Cell, 2009. **20**(11): p. 2673-2683.
113. Kedersha, N., et al., *Stress granules and processing bodies are dynamically linked sites of mRNP remodeling.* The Journal of Cell Biology, 2005. **169**(6): p. 871-884.
114. Souquere, S., et al., *Unravelling the ultrastructure of stress granules and associated P-bodies in human cells.* J Cell Sci, 2009. **122**(Pt 20): p. 3619-26.
115. Nie, M., et al., *Genetic and proteomic evidence for roles of Drosophila SUMO in cell cycle control, Ras signaling, and early pattern formation.* PLoS One, 2009. **4**(6).
116. Miller, M.J., et al., *Proteomic analyses identify a diverse array of nuclear processes affected by small ubiquitin-like modifier conjugation in Arabidopsis.* Proc Natl Acad Sci U S A, 2010. **107**(38): p. 16512-7.
117. Hannich, J.T., et al., *Defining the SUMO-modified proteome by multiple approaches in Saccharomyces cerevisiae.* J Biol Chem, 2005. **280**(6): p. 4102-10.
118. Watts, F.Z., et al., *Weighing up the possibilities: Controlling translation by ubiquitylation and sumoylation.* Translation, 2014. **2**(1): p. e29211.
119. Negrini, S., V.G. Gorgoulis, and T.D. Halazonetis, *Genomic instability [mdash] an evolving hallmark of cancer.* Nat Rev Mol Cell Biol, 2010. **11**(3): p. 220-228.
120. Bienko, M., et al., *Ubiquitin-Binding Domains in Y-Family Polymerases Regulate Translesion Synthesis.* Science, 2005. **310**(5755): p. 1821-1824.
121. Christmann, M., M.T. Tomicic, and B. Kaina, *Phosphorylation of mismatch repair proteins MSH2 and MSH6 affecting MutS α mismatch-binding activity.* Nucleic Acids Research, 2002. **30**(9): p. 1959-1966.
122. Hu, J., et al., *Phosphorylation of human oxoguanine DNA glycosylase (α-OGG1) modulates its function.* Nucleic Acids Research, 2005. **33**(10): p. 3271-3282.
123. Bhakat, K.K., et al., *Role of acetylated human AP-endonuclease (APE1/Ref-1) in regulation of the parathyroid hormone gene.* The EMBO Journal, 2003. **22**(23): p. 6299-6309.
124. Sugasawa, K., et al., *UV-Induced Ubiquitylation of XPC Protein Mediated by UV-DDB-Ubiquitin Ligase Complex.* Cell, 2005. **121**(3): p. 387-400.
125. Pizzolato, J., et al., *FANCD2-associated nuclease 1, but not exonuclease 1 or flap endonuclease 1, is able to unhook DNA interstrand cross-links in vitro.* J Biol Chem, 2015. **290**(37): p. 22602-11.
126. Zahurancik, W.J., S.J. Klein, and Z. Suo, *Significant contribution of the $3' \rightarrow 5'$ exonuclease activity to the high fidelity of nucleotide incorporation catalyzed by human DNA polymerase ϵ.* Nucleic Acids Research, 2014. **42**(22): p. 13853-13860.
127. Palles, C., et al., *Germline mutations affecting the proofreading domains of POLE and POLD1 predispose to colorectal adenomas and carcinomas.* Nat Genet, 2013. **45**(2): p. 136-144.
128. Kunkel, T.A. and D.A. Erie, *Eukaryotic Mismatch Repair in Relation to DNA Replication.* Annu Rev Genet, 2015. **49**: p. 291-313.
129. Paquet, N., et al., *hSSB1 (NABP2/ OBFC2B) is required for the repair of 8-oxo-guanine by the hOGG1-mediated base excision repair pathway.* Nucleic Acids Research, 2015. **43**(18): p. 8817-8829.
130. Beard, W.A. and S.H. Wilson, *Structure and mechanism of DNA polymerase beta.* Biochemistry, 2014. **53**(17): p. 2768-80.
131. Fu, Y., et al., *DNA cytosine and methylcytosine deamination by APOBEC3B: enhancing methylcytosine deamination by engineering APOBEC3B.* Biochemical Journal, 2015. **471**(Pt 1): p. 25-35.

132. An, R., et al., *Non-Enzymatic Depurination of Nucleic Acids: Factors and Mechanisms.* PLoS ONE, 2014. **9**(12): p. e115950.
133. Li, M., et al., *APE1 Incision Activity at Abasic Sites in Tandem Repeat Sequences.* Journal of Molecular Biology, 2014. **426**(11): p. 2183-2198.
134. Busso, C.S., C.M. Wedgeworth, and T. Izumi, *Ubiquitination of human AP-endonuclease 1 (APE1) enhanced by T233E substitution and by CDK5.* Nucleic Acids Research, 2011. **39**(18): p. 8017-8028.
135. Marteijn, J.A., et al., *Understanding nucleotide excision repair and its roles in cancer and ageing.* Nat Rev Mol Cell Biol, 2014. **15**(7): p. 465-481.
136. Li, C.-L., et al., *Tripartite DNA Lesion Recognition and Verification by XPC, TFIIH, and XPA in Nucleotide Excision Repair.* Molecular Cell, 2015. **59**(6): p. 1025-1034.
137. Coin, F., et al., *Nucleotide excision repair driven by the dissociation of CAK from TFIIH.* Mol Cell, 2008. **31**(1): p. 9-20.
138. Moser, J., et al., *Sealing of chromosomal DNA nicks during nucleotide excision repair requires XRCC1 and DNA ligase III alpha in a cell-cycle-specific manner.* Mol Cell, 2007. **27**(2): p. 311-23.
139. Fousteri, M., et al., *Cockayne syndrome A and B proteins differentially regulate recruitment of chromatin remodeling and repair factors to stalled RNA polymerase II in vivo.* Mol Cell, 2006. **23**(4): p. 471-82.
140. Anindya, R., et al., *A Ubiquitin-Binding Domain in Cockayne Syndrome B Required for Transcription-Coupled Nucleotide Excision Repair.* Molecular Cell, 2010. **38**(5): p. 637-648.
141. Hegi, M.E., et al., *MGMT Gene Silencing and Benefit from Temozolomide in Glioblastoma.* New England Journal of Medicine, 2005. **352**(10): p. 997-1003.
142. Arai, H., et al., *Leukemia cells are sensitized to temozolomide, carmustine and melphalan by the inhibition of O(6)-methylguanine-DNA methyltransferase.* Oncology Letters, 2015. **10**(2): p. 845-849.
143. Eustermann, S., et al., *Structural Basis of Detection and Signaling of DNA Single-Strand Breaks by Human PARP-1.* Molecular Cell. **60**(5): p. 742-754.
144. Caldecott, K.W., *Mammalian single-strand break repair: Mechanisms and links with chromatin.* DNA Repair, 2007. **6**(4): p. 443-453.
145. Kim, J., et al., *TopBP1 deficiency impairs V(D)J recombination during lymphocyte development.* EMBO J, 2014. **33**(3): p. 217-28.
146. Burma, S., et al., *ATM phosphorylates histone H2AX in response to DNA double-strand breaks.* J Biol Chem, 2001. **276**(45): p. 42462-7.
147. You, Z., et al., *ATM Activation and Its Recruitment to Damaged DNA Require Binding to the C Terminus of Nbs1.* Molecular and Cellular Biology, 2005. **25**(13): p. 5363-5379.
148. Kijas, A.W., et al., *ATM-dependent phosphorylation of MRE11 controls extent of resection during homology directed repair by signalling through Exonuclease 1.* Nucleic Acids Res, 2015. **43**(17): p. 8352-67.
149. Deshpande, R.A., et al., *ATP‐driven Rad50 conformations regulate DNA tethering, end resection, and ATM checkpoint signaling.* The EMBO Journal, 2014. **33**(5): p. 482-500.
150. Kuo, L.J. and L.X. Yang, *Gamma-H2AX - a novel biomarker for DNA double-strand breaks.* In Vivo, 2008. **22**(3): p. 305-9.
151. Stucki, M., et al., *MDC1 directly binds phosphorylated histone H2AX to regulate cellular responses to DNA double-strand breaks.* Cell, 2005. **123**(7): p. 1213-26.
152. Chapman, J.R. and S.P. Jackson, *Phospho-dependent interactions between NBS1 and MDC1 mediate chromatin retention of the MRN complex at sites of DNA damage.* EMBO Rep, 2008. **9**(8): p. 795-801.
153. So, S., A.J. Davis, and D.J. Chen, *Autophosphorylation at serine 1981 stabilizes ATM at DNA damage sites.* J Cell Biol, 2009. **187**(7): p. 977-90.

154. Thorslund, T., et al., *Histone H1 couples initiation and amplification of ubiquitin signalling after DNA damage.* Nature, 2015. **527**(7578): p. 389-93.
155. Fradet-Turcotte, A., et al., *53BP1 is a reader of the DNA-damage-induced H2A Lys 15 ubiquitin mark.* Nature, 2013. **499**(7456): p. 50-4.
156. Shibata, A., et al., *DNA Double-Strand Break Repair Pathway Choice Is Directed by Distinct MRE11 Nuclease Activities.* Molecular Cell, 2014. **53**(1): p. 7-18.
157. Walker, J.R., R.A. Corpina, and J. Goldberg, *Structure of the Ku heterodimer bound to DNA and its implications for double-strand break repair.* Nature, 2001. **412**(6847): p. 607-14.
158. Gottlieb, T.M. and S.P. Jackson, *The DNA-dependent protein kinase: Requirement for DNA ends and association with Ku antigen.* Cell, 1993. **72**(1): p. 131-142.
159. Grundy, G.J., et al., *APLF promotes the assembly and activity of non-homologous end joining protein complexes.* The EMBO Journal, 2013. **32**(1): p. 112-125.
160. Riballo, E., et al., *A Pathway of Double-Strand Break Rejoining Dependent upon ATM, Artemis, and Proteins Locating to γ-H2AX Foci.* Molecular Cell, 2004. **16**(5): p. 715-724.
161. Jiang, W., et al., *Differential Phosphorylation of DNA-PKcs Regulates the Interplay between End-Processing and End-Ligation during Nonhomologous End-Joining.* Molecular Cell, 2015. **58**(1): p. 172-185.
162. Yamtich, J. and J.B. Sweasy, *DNA Polymerase Family X: Function, Structure, and Cellular Roles.* Biochimica et biophysica acta, 2010. **1804**(5): p. 1136-1150.
163. Wang, M., et al., *PARP-1 and Ku compete for repair of DNA double strand breaks by distinct NHEJ pathways.* Nucleic Acids Research, 2006. **34**(21): p. 6170-6182.
164. Truong, L.N., et al., *Microhomology-mediated End Joining and Homologous Recombination share the initial end resection step to repair DNA double-strand breaks in mammalian cells.* Proc Natl Acad Sci U S A, 2013. **110**(19): p. 7720-5.
165. Newman, Joseph A., et al., *Structure of the Helicase Domain of DNA Polymerase Theta Reveals a Possible Role in the Microhomology-Mediated End-Joining Pathway.* Structure, 2015. **23**(12): p. 2319-2330.
166. Kent, T., et al., *Mechanism of microhomology-mediated end-joining promoted by human DNA polymerase θ.* Nat Struct Mol Biol, 2015. **22**(3): p. 230-237.
167. Cho, N.W. and R.A. Greenberg, *DNA repair: Familiar ends with alternative endings.* Nature, 2015. **518**(7538): p. 174-176.
168. Eid, W., et al., *DNA end resection by CtIP and exonuclease 1 prevents genomic instability.* EMBO Rep, 2010. **11**(12): p. 962-8.
169. Chen, H., M. Lisby, and L.S. Symington, *RPA coordinates DNA end resection and prevents formation of DNA hairpins.* Mol Cell, 2013. **50**(4): p. 589-600.
170. Gaines, W.A., et al., *Promotion of presynaptic filament assembly by the ensemble of S. cerevisiae Rad51 paralogues with Rad52.* Nat Commun, 2015. **6**: p. 7834.
171. Ragunathan, K., C. Liu, and T. Ha, *RecA filament sliding on DNA facilitates homology search.* eLife, 2012. **1**.
172. Forget, A.L. and S.C. Kowalczykowski, *Single-molecule imaging of DNA pairing by RecA reveals a three-dimensional homology search.* Nature, 2012. **482**(7385): p. 423-427.
173. Wright, William D. and W.-D. Heyer, *Rad54 Functions as a Heteroduplex DNA Pump Modulated by Its DNA Substrates and Rad51 during D Loop Formation.* Molecular Cell, 2014. **53**(3): p. 420-432.
174. Sebesta, M., et al., *Role of PCNA and TLS polymerases in D-loop extension during homologous recombination in humans.* DNA Repair, 2013. **12**(9): p. 691-698.
175. Matos, J. and S.C. West, *Holliday junction resolution: Regulation in space and time.* DNA Repair, 2014. **19**: p. 176-181.

176. Castor, D., et al., *Cooperative Control of Holliday Junction Resolution and DNA Repair by the SLX1 and MUS81-EME1 Nucleases.* Molecular Cell, 2013. **52**(2): p. 221-233.
177. Xue, X., et al., *Role of Replication Protein A in Double Holliday Junction Dissolution Mediated by the BLM-Topo III α-RMI1-RMI2 Protein Complex.* Journal of Biological Chemistry, 2013. **288**(20): p. 14221-14227.
178. Wyatt, Haley D.M., et al., *Coordinated Actions of SLX1-SLX4 and MUS81-EME1 for Holliday Junction Resolution in Human Cells.* Molecular Cell, 2013. **52**(2): p. 234-247.
179. Paliwal, S., et al., *Human RECQ5 helicase promotes repair of DNA double-strand breaks by synthesis-dependent strand annealing.* Nucleic Acids Research, 2014. **42**(4): p. 2380-2390.
180. Boisvert, F.M., et al., *The GAR motif of 53BP1 is arginine methylated by PRMT1 and is necessary for 53BP1 DNA binding activity.* Cell Cycle, 2005. **4**(12): p. 1834-41.
181. Pei, H., et al., *MMSET regulates histone H4K20 methylation and 53BP1 accumulation at DNA damage sites.* Nature, 2011. **470**(7332): p. 124-8.
182. Tuzon, C.T., et al., *Concerted activities of distinct H4K20 methyltransferases at DNA double-strand breaks regulate 53BP1 nucleation and NHEJ-directed repair.* Cell Rep, 2014. **8**(2): p. 430-8.
183. Acs, K., et al., *The AAA-ATPase VCP/p97 promotes 53BP1 recruitment by removing L3MBTL1 from DNA double-strand breaks.* Nat Struct Mol Biol, 2011. **18**(12): p. 1345-50.
184. Butler, L.R., et al., *The proteasomal de-ubiquitinating enzyme POH1 promotes the double-strand DNA break response.* The EMBO Journal, 2012. **31**(19): p. 3918-3934.
185. Mallette, F.A., et al., *RNF8‐and RNF168‐dependent degradation of KDM4A/JMJD2A triggers 53BP1 recruitment to DNA damage sites.* The EMBO Journal, 2012. **31**(8): p. 1865-1878.
186. Zgheib, O., et al., *An Oligomerized 53BP1 Tudor Domain Suffices for Recognition of DNA Double-Strand Breaks.* Molecular and Cellular Biology, 2009. **29**(4): p. 1050-1058.
187. Mattiroli, F., et al., *RNF168 Ubiquitinates K13-15 on H2A/H2AX to Drive DNA Damage Signaling.* Cell, 2012. **150**(6): p. 1182-1195.
188. Doil, C., et al., *RNF168 Binds and Amplifies Ubiquitin Conjugates on Damaged Chromosomes to Allow Accumulation of Repair Proteins.* Cell, 2009. **136**(3): p. 435-446.
189. Jowsey, P., et al., *Characterisation of the sites of DNA damage-induced 53BP1 phosphorylation catalysed by ATM and ATR.* DNA Repair, 2007. **6**(10): p. 1536-1544.
190. Zimmermann, M., et al., *53BP1 regulates DSB repair using Rif1 to control 5' end resection.* Science, 2013. **339**(6120): p. 700-4.
191. Callen, E., et al., *53BP1 Mediates Productive and Mutagenic DNA Repair through Distinct Phosphoprotein Interactions.* Cell, 2013. **153**(6): p. 1266-1280.
192. Boos, D., M. Yekezare, and J.F. Diffley, *Identification of a heteromeric complex that promotes DNA replication origin firing in human cells.* Science, 2013. **340**(6135): p. 981-4.
193. Cescutti, R., et al., *TopBP1 functions with 53BP1 in the G1 DNA damage checkpoint*. Vol. 29. 2010. 3723-3732.
194. Derbyshire, D.J., et al., *Crystal structure of human 53BP1 BRCT domains bound to p53 tumour suppressor.* The EMBO Journal, 2002. **21**(14): p. 3863-3872.
195. Joo, W.S., et al., *Structure of the 53BP1 BRCT region bound to p53 and its comparison to the Brca1 BRCT structure.* Genes & Development, 2002. **16**(5): p. 583-593.
196. Lee, J.H., et al., *53BP1 promotes ATM activity through direct interactions with the MRN complex.* The EMBO Journal, 2009. **29**(3): p. 574-585.
197. Huen, M.S.Y., et al., *Regulation of chromatin architecture by the PWWP domain-containing DNA damage responsive factor EXPAND1.* Molecular cell, 2010. **37**(6): p. 854-864.

198. Kilkenny, M.L., et al., *Structural and functional analysis of the Crb2–BRCT2 domain reveals distinct roles in checkpoint signaling and DNA damage repair.* Genes & Development, 2008. **22**(15): p. 2034-2047.
199. Hammet, A., et al., *Rad9 BRCT domain interaction with phosphorylated H2AX regulates the G1 checkpoint in budding yeast.* EMBO Rep, 2007. **8**(9): p. 851-7.
200. Jowsey, P., et al., *Characterisation of the sites of DNA damage-induced 53BP1 phosphorylation catalysed by ATM and ATR.* DNA Repair (Amst), 2007. **6**(10): p. 1536-44.
201. Falck, J., et al., *The ATM-Chk2-Cdc25A checkpoint pathway guards against radioresistant DNA synthesis.* Nature, 2001. **410**(6830): p. 842-847.
202. Noon, A.T., et al., *53BP1-dependent robust localized KAP-1 phosphorylation is essential for heterochromatic DNA double-strand break repair.* Nat Cell Biol, 2010. **12**(2): p. 177-84.
203. Goodarzi, A.A., T. Kurka, and P.A. Jeggo, *KAP-1 phosphorylation regulates CHD3 nucleosome remodeling during the DNA double-strand break response.* Nat Struct Mol Biol, 2011. **18**(7): p. 831-839.
204. Dimitrova, N., et al., *53BP1 promotes non-homologous end joining of telomeres by increasing chromatin mobility.* Nature, 2008. **456**(7221): p. 524-8.
205. Bothmer, A., et al., *Regulation of DNA end joining, resection, and immunoglobulin class switch recombination by 53BP1.* Mol Cell, 2011. **42**(3): p. 319-29.
206. Difilippantonio, S., et al., *53BP1 facilitates long-range DNA end-joining during V(D)J recombination.* Nature, 2008. **456**(7221): p. 529-33.
207. Sartori, A.A., et al., *Human CtIP promotes DNA end resection.* Nature, 2007. **450**(7169): p. 509-514.
208. Chapman, J.R., et al., *BRCA1-associated exclusion of 53BP1 from DNA damage sites underlies temporal control of DNA repair.* J Cell Sci, 2012. **125**(Pt 15): p. 3529-34.
209. Zhang, H., et al., *A cell cycle-dependent BRCA1-UHRF1 cascade regulates DNA double-strand break repair pathway choice.* Nat Commun, 2016. **7**: p. 10201.
210. Kakarougkas, A., et al., *Co-operation of BRCA1 and POH1 relieves the barriers posed by 53BP1 and RAP80 to resection.* Nucleic Acids Res, 2013. **41**(22): p. 10298-311.
211. Alagoz, M., et al., *SETDB1, HP1 and SUV39 promote repositioning of 53BP1 to extend resection during homologous recombination in G2 cells.* Nucleic Acids Res, 2015. **43**(16): p. 7931-44.
212. Bunting, S.F., et al., *53BP1 inhibits homologous recombination in Brca1-deficient cells by blocking resection of DNA breaks.* Cell, 2010. **141**(2): p. 243-54.
213. Callen, E., et al., *53BP1 mediates productive and mutagenic DNA repair through distinct phosphoprotein interactions.* Cell, 2013. **153**(6): p. 1266-80.
214. Wang, J., et al., *PTIP associates with Artemis to dictate DNA repair pathway choice.* Genes & Development, 2014. **28**(24): p. 2693-2698.
215. Xu, G., et al., *REV7 counteracts DNA double-strand break resection and impacts PARP inhibition.* Nature, 2015. **521**(7553): p. 541-544.
216. Stiff, T., et al., *Replication independent ATR signalling leads to G2/M arrest requiring Nbs1, 53BP1 and MDC1.* Human Molecular Genetics, 2008. **17**(20): p. 3247-3253.
217. Goodarzi, A.A., et al., *ATM signaling facilitates repair of DNA double-strand breaks associated with heterochromatin.* Mol Cell, 2008. **31**(2): p. 167-77.
218. Garvin, A.J., et al., *The deSUMOylase SENP7 promotes chromatin relaxation for homologous recombination DNA repair.* EMBO Rep, 2013. **14**(11): p. 975-83.
219. Lottersberger, F., et al., *53BP1 and the LINC Complex Promote Microtubule-Dependent DSB Mobility and DNA Repair.* Cell, 2015. **163**(4): p. 880-893.

220. Rappas, M., A.W. Oliver, and L.H. Pearl, *Structure and function of the Rad9-binding region of the DNA-damage checkpoint adaptor TopBP1.* Nucleic Acids Research, 2011. **39**(1): p. 313-324.
221. Wardlaw, C.P., A.M. Carr, and A.W. Oliver, *TopBP1: A BRCT-scaffold protein functioning in multiple cellular pathways.* DNA Repair (Amst), 2014.
222. Zegerman, P. and J.F.X. Diffley, *Phosphorylation of Sld2 and Sld3 by cyclin-dependent kinases promotes DNA replication in budding yeast.* Nature, 2007. **445**(7125): p. 281-285.
223. Kumagai, A., et al., *Treslin Collaborates with TopBP1 in Triggering the Initiation of DNA Replication.* Cell, 2010. **140**(3): p. 349-359.
224. Wang, R.-H., et al., *SIRT1 Deacetylates TopBP1 and Modulates Intra-S-Phase Checkpoint and DNA Replication Origin Firing.* International Journal of Biological Sciences, 2014. **10**(10): p. 1193-1202.
225. Zhou, Z.W., et al., *An essential function for the ATR-activation-domain (AAD) of TopBP1 in mouse development and cellular senescence.* PLoS Genet, 2013. **9**(8): p. e1003702.
226. Bermudez, V.P., et al., *Loading of the human 9-1-1 checkpoint complex onto DNA by the checkpoint clamp loader hRad17-replication factor C complex in vitro.* Proceedings of the National Academy of Sciences, 2003. **100**(4): p. 1633-1638.
227. Takeishi, Y., et al., *Casein kinase 2-dependent phosphorylation of human Rad9 mediates the interaction between human Rad9-Hus1-Rad1 complex and TopBP1.* Genes to Cells, 2010. **15**(7): p. 761-771.
228. Lindsey-Boltz, L.A., et al., *RHINO forms a stoichiometric complex with the 9-1-1 checkpoint clamp and mediates ATR-Chk1 signaling.* Cell Cycle, 2015. **14**(1): p. 99-108.
229. Mordes, D.A., et al., *TopBP1 activates ATR through ATRIP and a PIKK regulatory domain.* Genes & Development, 2008. **22**(11): p. 1478-1489.
230. Feijoo, C., et al., *Activation of mammalian Chk1 during DNA replication arrest: a role for Chk1 in the intra-S phase checkpoint monitoring replication origin firing.* The Journal of Cell Biology, 2001. **154**(5): p. 913-924.
231. Wu, C.S., et al., *SUMOylation of ATRIP potentiates DNA damage signaling by boosting multiple protein interactions in the ATR pathway.* Genes Dev, 2014. **28**(13): p. 1472-84.
232. Duursma, Anja M., et al., *A Role for the MRN Complex in ATR Activation via TOPBP1 Recruitment.* Molecular Cell, 2013. **50**(1): p. 116-122.
233. Wang, Q., et al., *Rad17 recruits the MRE11‐RAD50‐NBS1 complex to regulate the cellular response to DNA double‐strand breaks.* The EMBO Journal, 2014. **33**(8): p. 862-877.
234. Liu, K., et al., *Akt Switches TopBP1 Function from Checkpoint Activation to Transcriptional Regulation through Phosphoserine Binding-Mediated Oligomerization.* Molecular and Cellular Biology, 2013. **33**(23): p. 4685-4700.
235. Liu, K., et al., *Regulation of p53 by TopBP1: a Potential Mechanism for p53 Inactivation in Cancer.* Molecular and Cellular Biology, 2009. **29**(10): p. 2673-2693.
236. Wang, J., J. Chen, and Z. Gong, *TopBP1 controls BLM protein level to maintain genome stability.* Mol Cell, 2013. **52**(5): p. 667-78.
237. Blackford, A.N., et al., *TopBP1 interacts with BLM to maintain genome stability but is dispensable for preventing BLM degradation.* Mol Cell, 2015. **57**(6): p. 1133-41.
238. Qu, M., et al., *Phosphorylation-dependent assembly and coordination of the DNA damage checkpoint apparatus by Rad4(TopBP(1)).* Mol Cell, 2013. **51**(6): p. 723-36.
239. Gamper, A.M., et al., *ATR kinase activation in G1 phase facilitates the repair of ionizing radiation-induced DNA damage.* Nucleic Acids Res, 2013. **41**(22): p. 10334-44.
240. Leung, C.C., et al., *Structural insights into recognition of MDC1 by TopBP1 in DNA replication checkpoint control.* Structure, 2013. **21**(8): p. 1450-9.

241. Rozen, F., et al., *Bidirectional RNA helicase activity of eucaryotic translation initiation factors 4A and 4F.* Mol Cell Biol, 1990. **10**(3): p. 1134-44.
242. Izaurralde, E., *A role for eIF4AII in microRNA-mediated mRNA silencing.* Nat Struct Mol Biol, 2013. **20**(5): p. 543-5.
243. Feoktistova, K., et al., *Human eIF4E promotes mRNA restructuring by stimulating eIF4A helicase activity.* Proc Natl Acad Sci U S A, 2013. **110**(33): p. 13339-44.
244. Oberer, M., A. Marintchev, and G. Wagner, *Structural basis for the enhancement of eIF4A helicase activity by eIF4G.* Genes Dev, 2005. **19**(18): p. 2212-23.
245. Chang, J.H., et al., *Crystal structure of the eIF4A-PDCD4 complex.* Proc Natl Acad Sci U S A, 2009. **106**(9): p. 3148-53.
246. Schutz, P., et al., *Comparative structural analysis of human DEAD-box RNA helicases.* PLoS One, 2010. **5**(9).
247. Sophie Mokas, J.R.M., Cristina Garreau, Marie-Jose´e Fournier, Francis Robert, Prabhat Arya, Randal J. Kaufman, Jerry Pelletier, and Rachid Mazroui, *Uncoupling Stress Granule Assembly and Translation Initiation Inhibition.* Molecular biology of the cell, 2009. **20**: p. 2673–2683.
248. Kedersha, N., et al., *Stress granules and processing bodies are dynamically linked sites of mRNP remodeling.* J Cell Biol, 2005. **169**(6): p. 871-84.
249. Kimball, S.R., et al., *Mammalian stress granules represent sites of accumulation of stalled translation initiation complexes.* American Journal of Physiology - Cell Physiology, 2003. **284**(2): p. C273-C284.
250. Kira Bettermann, M.B., Serge Weis, Johannes Haybaeck, *SUMOylation in carcinogenesis.* Cancer Letters, 2012. **316**: p. 113-125.
251. Vertegaal, A.C.O., et al., *A Proteomic Study of SUMO-2 Target Proteins.* Journal of Biological Chemistry, 2004. **279**(32): p. 33791-33798.
252. Girdwood, D., et al., *p300 Transcriptional Repression Is Mediated by SUMO Modification.* Molecular Cell, 2003. **11**(4): p. 1043-1054.
253. Tanaka, S., et al., *Efficient initiation of DNA replication in eukaryotes requires Dpb11/TopBP1-GINS interaction.* Mol Cell Biol, 2013. **33**(13): p. 2614-22.
254. Furuya, K., et al., *Chk1 activation requires Rad9 S/TQ-site phosphorylation to promote association with C-terminal BRCT domains of Rad4TOPBP1.* Genes Dev, 2004. **18**(10): p. 1154-64.
255. Ohashi, E., et al., *Interaction between Rad9-Hus1-Rad1 and TopBP1 activates ATR-ATRIP and promotes TopBP1 recruitment to sites of UV-damage.* DNA Repair (Amst), 2014. **21**: p. 1-11.
256. Kumagai, A., et al., *TopBP1 Activates the ATR-ATRIP Complex.* Cell, 2006. **124**(5): p. 943-955.
257. Noon, A.T. and A.A. Goodarzi, *53BP1-mediated DNA double strand break repair: insert bad pun here.* DNA Repair (Amst), 2011. **10**(10): p. 1071-6.
258. Joo, W.S., et al., *Structure of the 53BP1 BRCT region bound to p53 and its comparison to the Brca1 BRCT structure.* Genes Dev, 2002. **16**(5): p. 583-93.
259. Lee, J.H., et al., *53BP1 promotes ATM activity through direct interactions with the MRN complex.* EMBO J, 2010. **29**(3): p. 574-85.
260. Ward, I.M., et al., *Accumulation of checkpoint protein 53BP1 at DNA breaks involves its binding to phosphorylated histone H2AX.* J Biol Chem, 2003. **278**(22): p. 19579-82.
261. Kocylowski, M.K., et al., *Ubiquitin-H2AX fusions render 53BP1 recruitment to DNA damage sites independent of RNF8 or RNF168.* Cell Cycle, 2015: p. 0.
262. Rogakou, E.P., et al., *DNA double-stranded breaks induce histone H2AX phosphorylation on serine 139.* J Biol Chem, 1998. **273**(10): p. 5858-68.
263. Stucki, M., et al., *MDC1 Directly Binds Phosphorylated Histone H2AX to Regulate Cellular Responses to DNA Double-Strand Breaks.* Cell, 2005. **123**(7): p. 1213-1226.

264. Arndt-Jovin, D.J. and T.M. Jovin, *Fluorescence labeling and microscopy of DNA.* Methods Cell Biol, 1989. **30**: p. 417-48.
265. Guo, Z., et al., *Induction of H2AX phosphorylation in tumor cells by gossypol acetic acid is mediated by phosphatidylinositol 3-kinase (PI3K) family.* Cancer Cell International, 2014. **14**: p. 141.
266. Stiff, T., et al., *ATM and DNA-PK function redundantly to phosphorylate H2AX after exposure to ionizing radiation.* Cancer Res, 2004. **64**(7): p. 2390-6.
267. Woodbine, L., et al., *Endogenously induced DNA double strand breaks arise in heterochromatic DNA regions and require ataxia telangiectasia mutated and Artemis for their repair.* Nucleic Acids Res, 2011. **39**(16): p. 6986-97.
268. Adams, M.M., et al., *53BP1 oligomerization is independent of its methylation by PRMT1.* Cell Cycle, 2005. **4**(12): p. 1854-61.
269. Du, L.L., B.A. Moser, and P. Russell, *Homo-oligomerization is the essential function of the tandem BRCT domains in the checkpoint protein Crb2.* J Biol Chem, 2004. **279**(37): p. 38409-14.
270. de Jager, M., et al., *DNA-binding and strand-annealing activities of human Mre11: implications for its roles in DNA double-strand break repair pathways.* Nucleic Acids Res, 2001. **29**(6): p. 1317-25.
271. Bakkenist, C.J. and M.B. Kastan, *DNA damage activates ATM through intermolecular autophosphorylation and dimer dissociation.* Nature, 2003. **421**(6922): p. 499-506.
272. Pierce, A.J., et al., *XRCC3 promotes homology-directed repair of DNA damage in mammalian cells.* Genes & Development, 1999. **13**(20): p. 2633-2638.
273. Cheng, C.T., C.Y. Kuo, and D.K. Ann, *KAPtain in charge of multiple missions: Emerging roles of KAP1.* World J Biol Chem, 2014. **5**(3): p. 308-20.
274. Ubersax, J.A. and J.E. Ferrell Jr, *Mechanisms of specificity in protein phosphorylation.* Nat Rev Mol Cell Biol, 2007. **8**(7): p. 530-541.
275. Blackwell, L.J. and J.A. Borowiec, *Human replication protein A binds single-stranded DNA in two distinct complexes.* Molecular and Cellular Biology, 1994. **14**(6): p. 3993-4001.
276. Ramírez-Lugo, J.S., et al., *CtIP interacts with TopBP1 and Nbs1 in the response to double-stranded DNA breaks (DSBs) in Xenopus egg extracts.* Cell Cycle, 2011. **10**(3): p. 469-480.
277. Adams, K.E., et al., *Recruitment of ATR to sites of ionising radiation-induced DNA damage requires ATM and components of the MRN protein complex.* Oncogene, 2006. **25**(28): p. 3894-3904.
278. Harbour, J.W., et al., *Cdk Phosphorylation Triggers Sequential Intramolecular Interactions that Progressively Block Rb Functions as Cells Move through G1.* Cell, 1999. **98**(6): p. 859-869.
279. DeGregori, J., T. Kowalik, and J.R. Nevins, *Cellular targets for activation by the E2F1 transcription factor include DNA synthesis- and G1/S-regulatory genes.* Molecular and Cellular Biology, 1995. **15**(8): p. 4215-24.
280. Qin, X.Q., et al., *Deregulated transcription factor E2F-1 expression leads to S-phase entry and p53-mediated apoptosis.* Proceedings of the National Academy of Sciences, 1994. **91**(23): p. 10918-10922.
281. Liu, K., et al., *Regulation of E2F1 by BRCT Domain-Containing Protein TopBP1.* Molecular and Cellular Biology, 2003. **23**(9): p. 3287-3304.
282. Kleiner, R.E., et al., *Chemical proteomics reveals a [gamma]H2AX-53BP1 interaction in the DNA damage response.* Nat Chem Biol, 2015. **11**(10): p. 807-814.
283. Lou, Z., et al., *MDC1 maintains genomic stability by participating in the amplification of ATM-dependent DNA damage signals.* Mol Cell, 2006. **21**(2): p. 187-200.

284. Lukas, C., et al., *Mdc1 couples DNA double-strand break recognition by Nbs1 with its H2AX-dependent chromatin retention.* EMBO J, 2004. **23**(13): p. 2674-83.
285. Derbyshire, D.J., et al., *Crystal structure of human 53BP1 BRCT domains bound to p53 tumour suppressor.* EMBO J, 2002. **21**(14): p. 3863-72.
286. Hartlerode, A.J., et al., *Recruitment and activation of the ATM kinase in the absence of DNA-damage sensors.* Nat Struct Mol Biol, 2015. **22**(9): p. 736-743.
287. Taddei, A., et al., *Duplication and Maintenance of Heterochromatin Domains.* The Journal of Cell Biology, 1999. **147**(6): p. 1153-1166.
288. Ward, I.M. and J. Chen, *Histone H2AX is phosphorylated in an ATR-dependent manner in response to replicational stress.* J Biol Chem, 2001. **276**(51): p. 47759-62.
289. Shiotani, B. and L. Zou, *Single-Stranded DNA Orchestrates an ATM-to-ATR Switch at DNA Breaks.* Molecular Cell, 2009. **33**(5): p. 547-558.
290. Bakr, A., et al., *Involvement of ATM in homologous recombination after end resection and RAD51 nucleofilament formation.* Nucleic Acids Res, 2015. **43**(6): p. 3154-66.
291. Zou, L. and S.J. Elledge, *Sensing DNA Damage Through ATRIP Recognition of RPA-ssDNA Complexes.* Science, 2003. **300**(5625): p. 1542-1548.
292. Chiolo, I., et al., *Double-Strand Breaks in Heterochromatin Move Outside of a Dynamic HP1a Domain to Complete Recombinational Repair.* Cell, 2011. **144**(5): p. 732-744.
293. Peterson, S.E., et al., *Activation of DSB processing requires phosphorylation of CtIP by ATR.* Mol Cell, 2013. **49**(4): p. 657-67.

8. Publications

OPEN ACCESS Freely available online

PLOS ONE

The *S. pombe* Translation Initiation Factor eIF4G Is Sumoylated and Associates with the SUMO Protease Ulp2

Jirapas Jongjitwimol[1☯], Min Feng[1☯¤a], Lihong Zhou[1], Oliver Wilkinson[1¤b], Lauren Small[1], Robert Baldock[1], Deborah L. Taylor[1], Duncan Smith[2], Lucas D. Bowler[1¤c], Simon J. Morley[3], Felicity Z. Watts[1]*

1 Genome Damage and Stability Centre, School of Life Sciences, University of Sussex, Falmer, Brighton, United Kingdom, **2** Paterson Institute for Cancer Research, The University of Manchester, Manchester, United Kingdom, **3** Biochemistry and Biomedical Sciences, School of Life Sciences, University of Sussex, Falmer, Brighton, United Kingdom

Abstract

SUMO is a small post-translational modifier, that is attached to lysine residues in target proteins. It acts by altering protein-protein interactions, protein localisation and protein activity. SUMO chains can also act as substrates for ubiquitination, resulting in proteasome-mediated degradation of the target protein. SUMO is removed from target proteins by one of a number of specific proteases. The processes of sumoylation and desumoylation have well documented roles in DNA metabolism and in the maintenance of chromatin structure. To further analyse the role of this modification, we have purified protein complexes containing the *S. pombe* SUMO protease, Ulp2. These complexes contain proteins required for ribosome biogenesis, RNA stability and protein synthesis. Here we have focussed on two translation initiation factors that we identified as co-purifying with Ulp2, eIF4G and eIF3h. We demonstrate that eIF4G, but not eIF3h, is sumoylated. This modification is increased under conditions that produce cytoplasmic stress granules. Consistent with this we observe partial co-localisation of eIF4G and SUMO in stressed cells. Using HeLa cells, we demonstrate that human eIF4GI is also sumoylated; *in vitro* studies indicate that human eIF4GI is modified on K1368 and K1588, that are located in the C-terminal eIF4A- and Mnk-binding sites respectively.

Citation: Jongjitwimol J, Feng M, Zhou L, Wilkinson O, Small L, et al. (2014) The *S. pombe* Translation Initiation Factor eIF4G Is Sumoylated and Associates with the SUMO Protease Ulp2. PLoS ONE 9(5): e94182. doi:10.1371/journal.pone.0094182

Editor: Thomas Preiss, The John Curtin School of Medical Research, Australia

Received November 22, 2013; **Accepted** March 13, 2014; **Published** May 12, 2014

Copyright: © 2014 Jongjitwimol et al. This is an open-access article distributed under the terms of the Creative Commons Attribution License, which permits unrestricted use, distribution, and reproduction in any medium, provided the original author and source are credited.

Funding: MF, LZ and OW were funded by CRUK grant nos C1206/A5451, C1206/A1845 and C1206/A11978. DLT was funded by a BBSRC Special Studentship no (G/03524), LS and RB were funded by the University of Sussex, and JJ was funded by a Royal Thai Government scholarship. The funders had no role in study design, data collection and analysis, decision to publish, or preparation of the manuscript.

Competing Interests: The authors have declared that no competing interests exist.

* E-mail: f.z.watts@sussex.ac.uk

☯ These authors contributed equally to this work.

¤a Current address: Genome Institute of Singapore, Genome, #02-01, Singapore, Singapore
¤b Current address: School of Biochemistry, Clifton, Bristol, United Kingdom
¤c Current address: Centre for Biomedical and Health Science Research, School of Pharmacy and Biomolecular Sciences, University of Brighton, Brighton, United Kingdom

Introduction

Sumoylation is a post-translational protein modification that is required for numerous processes within cells, including transcription, chromosome segregation, DNA damage responses, cell signalling and meiosis (reviewed in [1–7]). At the molecular level it functions by altering the surface of target molecules to affect protein-protein interactions e.g. of PCNA (proliferating cell nuclear antigen) and Srs2 (a DNA helicase) [8,9], by altering the intracellular localisation of proteins e.g. of RanGAP [10], or by changing the conformation of target proteins (e.g. in the case of thymine DNA glycosylase [11]). SUMO chains attached to target proteins can also be ubiquitinated and thus result in proteolysis of the target.

SUMO is a small ubiquitin-like modifier that is attached to lysine residues in target proteins. The yeasts *Schizosaccharomyces pombe* and *Saccharomyces cerevisiae* both have a single gene for SUMO: *pmt3* and *SMT3*, respectively, while mammals have four, SUMO-1, -2, -3 and -4 (although the role of SUMO-4 is not well defined). SUMO-2 and -3 are 97% identical to each other and about 50% identical to SUMO-1 (reviewed in [1]). SUMO is produced as a precursor protein that needs to be cleaved into the mature form in order to act as a substrate in the sumoylation reaction. Processing of SUMO requires a specific SUMO-protease [12–14], and involves the removal of a small number of amino acids from the C-terminus of precursor SUMO to reveal a Gly-Gly motif. Mature SUMO is then activated by the formation of a thioester bond between the C-terminal glycine residue and a cysteine residue in one subunit of the SUMO activating enzyme (E1). From here SUMO is passed to the SUMO conjugating enzyme (E2), where it again forms a thioester bond with another cysteine residue. SUMO can then be attached to one or more lysine residues in the target protein. In some cases, one of a small

number of SUMO ligases (E3) is required for conjugation. In many cases the lysine is contained within the consensus motif ψKxE, where ψ is a hydrophobic amino acid, and x is any amino acid. SUMO can be added to target proteins as a monomer or as poly-SUMO in the form of chains. The removal of SUMO from target proteins or dismantling of SUMO chains occurs via the action of SUMO-specific proteases [14,15].

In *S. cerevisiae* there are two SUMO proteases, Ulp1 and Ulp2, both of which can deconjugate SUMO from target proteins, but which have different target specificities [12]. Only Ulp1 is capable of processing precursor SUMO to the mature form [12,15]. Ulp1 and Ulp2 are differently localised within the cell: Ulp1 is located at nuclear pores, while Ulp2 is located mainly within the nucleus [15]. Mammalian cells have six SUMO-specific proteases (SENPs). These are also differentially localised within cells and have different abilities to cleave precursor SUMO and to deconjugate SUMO from targets e.g. [16,17]. The *S. pombe* Ulp1 protease has been characterised and shown to process SUMO to the mature form, and like *S. cerevisiae* Ulp1, to be located at the nuclear periphery [13]. However, little is known about Ulp2 in this organism.

Translation initiation factors, which play key roles in cell survival and oncogenesis [18–22], can be modified by sumoylation [6,7,23–31]. Protein synthesis is carried out in three stages (initiation, elongation and termination), with the initiation stage of translation generally accepted as a major site of regulation of gene expression in mammalian cells [18–22]. This step in protein synthesis is regulated by a family of proteins, the initiation factors [18,21,22] which interact with each other and the mRNA. These proteins modulate the binding of mRNA to the ribosome, a process facilitated by the assembly of the cap binding protein (eIF4E), a helicase (eIF4A) and a scaffold protein (eIF4G), to form the eIF4F complex (eIF4E/eIF4A/eIF4G). The eIF4G scaffold protein possesses domains that interact with eIF4E, eIF4A, eIF3 and the poly(A) binding protein (PABP) [18,20–22]. The activity of the eIF4F complex is regulated by a family of proteins, the eIF4E binding proteins (4E-BPs). Using a conserved motif, 4E-BPs compete with eIF4G for a common surface on eIF4E and inhibit eIF4F assembly. In mammalian cells, activation of the mechanistic target of rapamycin (mTORC1) leads to the multi-site phosphorylation of 4E-BP1 [18,22,32] preventing 4E-BP1 from binding to eIF4E and thereby allowing formation of the eIF4F initiation complex and ribosomal recruitment of mRNA [18,21,22]. More recently, phosphorylated human eIF4E has been shown to be modified by sumoylation on five lysine residues [33]. Consistent with a role in modulating protein-protein interactions [34], sumoylation did not interfere with mRNA recognition but enhanced eIF4F complex level assembly on the mRNA cap, promoting the expression of ornithine decarboxylase, c-myc and Bcl-2, thereby driving the anti-apoptotic and oncogenic activity of eIF4E [33].

Since the majority of SUMO in cells is present in the nucleus, much of the work undertaken to understand the role of sumoylation has focussed on its role in regulating events associated with DNA metabolism, such as the maintenance of chromatin structure, recombination and DNA damage responses [3,5,8,9]. More recently it has been demonstrated that sumoylation is required in the nucleolus to regulate ribosome biogenesis e.g. [35]. In order to obtain a fuller understanding of the role of sumoylation we have begun to investigate the protein-protein interactions and localisation of the mostly uncharacterised *S. pombe* SUMO protease, Ulp2. Our results from gel filtration and immunofluorescence studies indicate that Ulp2 is present in at least two high Mr complexes, which are distinct from the nuclear pore complex that contains Ulp1. We demonstrate that it co-purifies with a number of proteins, many of which are involved in RNA metabolism or protein synthesis. We have investigated whether two of these proteins, eIF4G and eIF3h, are sumoylated, with the result that we observe SUMO modification of eIF4G but not eIF3h. Exposure of cells to conditions that lead to the formation of stress granules, results in increased sumoylation of eIF4G, and partial co-localisation of eIF4G and SUMO in the cytoplasm. Finally, we demonstrate that human eIF4G is sumoylated in HeLa cells, by both SUMO-1 and SUMO-2.

Materials and Methods

Strains and plasmids

The strains used in this work are described in Table 1. The strains containing myc-, HA or TAP-tagged *ulp1*, *ulp2*, *pli1*, *eIF4G* and *eIF3h* were created using the method of Bahler et al [36]. pREP41-His-SUMO was constructed by cloning the *pmt3* ORF into pREP41-His (created in this study). The *S. pombe* and human eIF4G and eIF4GI constructs, Sp C-term, N-FAG, M-FAG and C-FAG contain different fragments of the eIF4G/eIF4GI Orfs cloned into pET15b [37]. HeLa cell lines stably transfected with His-SUMO-1 and His-SUMO-2 were gifts from Prof R Hay (University of Dundee) [38,39].

Ulp2 expression and assay

The *ulp2* ORF was amplified from cDNA, by PCR and cloned into pFastBacHTa (GibcoBRL). Recombinant baculoviruses were generated according to GibcoBRL instructions. 50 ml infected cells were lysed in 50 mM Tris HCl pH 8, 5 mM β-mercaptoethanol, 1% nonidet, 1 mM PMSF. Ulp2 protein was purified using Talon resin. Ulp2 activity assays were conducted as described for Ulp1 [13].

Protein purification methods

His-tagged SUMO was recovered from *S. pombe* and human whole cell extracts under denaturing conditions with Ni^{2+} agarose beads. Cell extracts were prepared as follows: 10^8 cells (*S. pombe*) or $6–8\times10^6$ cells (Hela) were washed in ice cold water before being lysed by vortexing in 1.85 M NaOH, 7.5% v/v β-mercaptoethanol. The lysate was incubated on ice for 20 min after which TCA was added to a final concentration of 25%. Following a further 20 min incubation on ice, precipitated proteins were collected by centrifugation and resuspended and solubilised in 1 ml buffer A (6 M guanidinium HCl, 0.1 M NaH_2PO_4, 10 mM Tris-HCl, pH 8). Insoluble material was removed by centrifugation. The cell extract was then incubated with Ni^{2+} agarose (Novagen) in Buffer A in the presence of 0.05% Tween-20, 150 mM imidazole. Purification on Ni^{2+} agarose was carried out according to the manufacturer's instructions. Samples were analysed by SDS-PAGE and Western blotting. His-tagged *S. pombe* and human eIF4GI fragments for *in vitro* sumoylation assays were purified from *E. coli* using Ni^{2+} agarose according to the manufacturer's instructions.

For gel filtration, 200 ml logarithmically growing cells were harvested, washed and then broken in 1 ml ice cold lysis buffer (45 mM HEPES pH 7.8, 300 mM KCl, 5 mM $MgCl_2$, 5 mM EDTA, 5 mM EGTA, 12 mM NaF, 10% glycerol, 80 mM β-glycerophosphate, 0.1 mM sodium orthovanadate, 1 mM PMSF, 1 mM DTT, supplemented with Roche complete protease inhibitor). The extract was clarified by two rounds of centrifugation at 20,000 rpm for 10 min. 1.5 mg protein was loaded onto either a Superdex 200 or Superose 6 column pre-equilibrated in

Table 1. List of strains.

Strain	Genotype	Reference
Sp.011	*ade6-704, leu1-32, ura4-D18, h*$^-$	[72]
Sp.611	*ulp1-myc:kan, ade6-704, leu1-32, ura4-D18, h*$^-$	This study
Sp.614	*ulp2-myc:kan, ade6-704, leu1-32, ura4-D18, h*$^-$	This study
Sp.658	*ulp1::ura4, ade6-704, leu1-32, ura4-D18, h*$^-$	[13]
Sp.723	*pli1-myc:kan, ade6-704, leu1-32, ura4-D18, h*$^-$	This study
Sp.874	*pmt3-GG:ura4, ade6-704, leu1-32, ura4-D18, h*$^-$	This study
sp.851	*ulp1::ura4, pmt3-GG:ura4, ade6-704, leu1-32, ura4-D18, h*$^-$	This study
sp.855	*ulp2::ura4, pmt3-GG:ura4, ade6-704, leu1-32, ura4-D18, h*$^-$	This study
Sp.1470	*ulp2-TAP, ade6-704, leu1-32, ura4-D18, h*$^-$	This study
Sp.2047	*eIF3h-HA:Nat, ade6-704, leu1-32, ura4-D18, h*$^+$	This study
Sp.2048	*ulp2-myc:kan, eIF3h-HA:Nat, ade6-704, leu1-32, ura4-D18, h*$^-$	This study
Sp.2068	*ulp2-myc:kan, eIF4G-HA:Nat, ade6-704, leu1-32, ura4-D18, h*$^-$	This study
Sp.2085	*ulp2::kan, ade6-704, leu1-32, ura4-D18, h*$^-$	This study
Sp.2088	*eIF4G-HA:Nat, ade6-704, leu1-32, ura4-D18, h*$^+$	This study

doi:10.1371/journal.pone.0094182.t001

lysis buffer. 0.5 ml fractions were collected and 15 µl of each was analysed by SDS PAGE.

For TAP-purification, 60 l *ulp2-TAP* cells were grown to mid-log phase, harvested and frozen at −80°C until required. Ulp2-TAP was purified using a modification of the method described by Seraphin et al. [40]. Specifically, the cells were broken in a 6850 freezer mill in 20 mM Tris-HCl, pH 7.5, 10 mM NaCl, 1 mM DTT, 0.5 mM EDTA, 2 mM $MgCl_2$, 0.1 mM NaF, 0.1% Nonidet NP40, 1 mM PMSF, 5 mM sodium orthovanadate, 80 mM β-glycerophosphate, 10 mM N-ethylmaleimide, supplemented with Roche complete protease inhibitor. All subsequent procedures were carried out at 4°C. The cell extract was centrifuged twice for 1 h at 10,000 rpm. Samples were precleared by incubation with 200 µl Dynabeads for 30 min to remove proteins that bound non-specifically to the beads. The extracts were incubated with 300 µl IgG-coated Dynabeads for 2 h. The beads were collected and washed extensively before being resuspended in TEV buffer (50 mM Tris-HCl pH 8.0, 0.5 mM EDTA, 1 mM DTT) with 250 units AcTEV protease (Invitrogen) for 3 h. The IgG-coated Dynabeads were removed from the preparation and Ulp2-TAP containing complexes were snap frozen in liquid nitrogen.

In vitro sumoylation assay

Recombinant His-tagged *S. pombe* eIF4G and human eIF4GI fragments were purified from *E. coli* and tested for sumoylation in an *in vitro* sumoylation assay as described elsewhere [41]. SUMO-TRGG (Pmt3-L109R,GG: the mature form of *S. pombe* SUMO containing a trypsin cleavage site immediately upstream of the diglycine motif) was used in the assay to facilitate the identification of the sumoylation sites by mass spectrometry.

Immunological methods

Western analysis was carried out as described previously [13]. Production of anti-SUMO and anti-eIF4GI (against the KRERK epitope) antisera has been described elsewhere [41,42], anti-myc antibodies for immunofluorescence were purified from cell supernatant (cell line CRL1729, from ATCC) using protein G-sepharose or were from Santa Cruz (sc-40), anti-HA antisera were from Santa Cruz (sc-7392) and monoclonal anti-tubulin antibodies were from Sigma (T5168). Immunofluorescence was undertaken as described in Moreno et al. [43]. Cells were observed using an Applied Precision Deltavision Spectris microscope using deconvolution software.

Mass spectrometry

Complexes purified by purification of TAP-Ulp2 were analysed by SDS PAGE. Protein bands were visualised by staining with colloidal Coommassie, excised and subjected to trypsin in-gel digestion essentially as described by Schevchenko et al. [44]. The supernatant from the digested samples was removed and acidified to 0.1% TFA, dried down, and reconstituted in 0.1% TFA prior to LC MS/MS analysis. Each sample was loaded and desalted at a flow rate of 5 µl/min on a C18 trap column (200 µm ID x 1 cm, 5 µm PepMap 100, Dionex) in buffer A (acetonitrile (2% v/v): water (97.9% v/v): formic acid (0.1% v/v)). The tryptic peptides were fractionated on a C18 reverse phase column (75 µm ID x 25 cm, 3 µm PepMap 100, Dionex) using an Ultimate U3000 nano-LC system (Dionex) and a 2 hr linear gradient from 95% buffer A to 50% buffer B (acetonitrile (95% v/v): water (4.9% v/v): formic acid (0.1% v/v) at a flow rate of 300 nl/min. Eluted peptides were directly analysed by tandem mass spectrometry using a LTQ Orbitrap XL hybrid FTMS (ThermoScientific) operated in parallel acquisition IDA mode with nominal resolution of 60,000 (FWHM) at m/z 400 for MS1 and the top six most abundant multiply charged ions being selected for CID fragmentation in the linear ion trap followed by dynamic exclusion for 90 secs.

Derived MS/MS data were searched against the *S. pombe* subset of the UniProt Knowledgebase release 15.13 database using Sequest version SRF v. 5 as implemented in Bioworks v 3.3.1 (Thermo Fisher Scientific), assuming carboxyamidomethylation (Cys), deamidation (Asn and Gln) and oxidation (Met) as variable modifications and using a peptide tolerance of 10 ppm and a fragment ion tolerance of 0.8 Da. One missed cleavage was allowed and filtering criteria used for positive protein identifications were Xcorr values greater than 1.9 for +1 spectra, 2.2 for +2 spectra and 3.75 for +3 spectra and a delta correlation (DCn) cut-off of 0.1.

For the identification of sumoylation sites, reduction and alkylation were instead performed using TCEP and MMTS respectively as previously described [45] and bioinformatics analysis following conversion of LTQ-Orbitrap (.raw) raw data files to Mascot generic format (MGF) via Mascot Distiller (Matrix Science) performed essentially as described by Chicooree et al. [46] using the MASCOT search engine with the UniProt Knowledgebase release 15.13 database with the *S. pombe* subset as selected taxonomy. Precursor ion tolerances were again set at 10 ppm and MS/MS peptide ion tolerance to 0.8 Da, and the same variable modifications assumed. However, two missed trypsin cleavages were allowed.

Following trypsin digestion, cleavage of the SUMO moiety was expected to leave a Gly-Gly isotag on modified residues. The GG isotag (on lys) was accordingly also searched as a variable modification. Following MASCOT searches, putative sites of SUMOylation were noted and the relevant raw MS/MS spectra subsequently examined manually to confirm presence of the modification (the GG isotag).

Results

Biochemical characterisation of *S. pombe* Ulp2

A comparison of the *S. pombe* Ulp2 sequence was made with those of the two *S. cerevisiae* SUMO proteases, Ulp1 and Ulp2 [47]. Since *S. pombe* Ulp2 more closely resembles *S. cerevisiae* Ulp2 (required solely for deconjugating SUMO from high Mr SUMO-containing species) than it does Ulp1 (which is required for both processing and deconjugating), it is likely that the main activity of *S. pombe* Ulp2 is in deconjugating SUMO from sumoylated targets rather than in processing SUMO to the mature form. Before proceeding to analyse the localisation or protein-protein interactions of Ulp2, we first confirmed its proposed biochemical activity. His-tagged Ulp2 was purified from insect cells as described in Materials and Methods. Using assays we described previously [13], we demonstrate that Ulp2 is significantly less able than Ulp1 to process SUMO to the mature form (Figure 1A, lane 2 (Ulp1) and lane 3 (Ulp2)), but is capable of deconjugating SUMO from high Mr species in an N-ethylmaleimide- (NEM)-dependent manner (Figure 1B). These results confirm that like *S. cerevisiae* Ulp2, *S. pombe* Ulp2 is a cysteine protease whose main function is in deconjugating SUMO from target proteins.

Deletion of the *ulp2* gene results in a severe growth defect and sensitivity to a range of stresses

Deletion of *pmt3* (which encodes SUMO), *hus5* (the gene encoding the SUMO-conjugating enzyme, E2), *rad31* (which encodes one sub-unit of the SUMO activating enzyme, E1) or *ulp1* (another SUMO-specific protease gene) results in severe growth and morphological abnormalities [13,48–50]. We therefore wished to determine whether disrupting the *ulp2* gene has any effect on cell growth or viability. Disruption of the gene is not lethal. However, *ulp2-d* cells form very small colonies and show distinct morphological abnormalities resembling *hus5* and *rad31* mutants (data not shown). Comparison of SUMO-containing species in *ulp1-d* and *ulp2-d* cells (Figure 1C, lanes 3 and 4) supports the notion that the main function of Ulp2 is in the removal or dismantling of high Mr SUMO-containing species, rather than in processing precursor SUMO. Provision of the mature form of SUMO (Pmt3-GG) in *ulp1-d* cells (lane 5) results in the incorporation of SUMO into high Mr species (unlike the situation in *ulp1-d* cells, lane 3), while in *ulp2-d* cells (lane 6), the level of high Mr species is slightly increased.

To begin to identify cellular processes involving Ulp2, we tested whether *ulp2-d* cells are sensitive to the DNA synthesis inhibitor, hydroxyurea (HU) and other stresses (Figure 1D), and compared these responses to those of *ulp1-d,pmt3-GG* cells (where the mature form of SUMO is provided, so that cells are only defective in the deconjugating activity of Ulp1). Since *ulp2-d* and *ulp1-d,pmt3-GG* cultures contain a high proportion of dead cells, it was necessary to plate more cells for these strains compared to wild type (approximately 10 fold). These data indicate that *ulp2-d* cells are temperature sensitive, unlike the *ulp1-d,pmt3-GG* strain, but similar to the *S. cerevisiae ulp2Δ* strain [51], and sensitive to the DNA synthesis inhibitor, hydroxyurea (HU, 2 mM). They are also sensitive to the protein synthesis inhibitor, cycloheximide (CHX, 10 and 20 μg/ml) and KCl (1 M) indicating that Ulp2 likely has roles in numerous cellular processes.

Ulp2 is present in high molecular weight complexes

Throughout most of the cell cycle, Ulp1 is associated with the nuclear envelope [13], and specifically with the nuclear pore complex [52,53]. To determine whether Ulp2 is also part of a high Mr complex we undertook gel filtration analysis. Figure 2A indicates that, as expected, Ulp1 elutes in the void volume, consistent with it being present in a high Mr complex. Ulp2 also elutes in the void volume like Ulp1, but additionally, it is present in fractions corresponding to an approximate Mr of 670 kDa. This suggests that Ulp2 is likely to be present in at least two different complexes. In contrast to the results obtained for Ulp1 and Ulp2, Pli1, an E3 SUMO ligase [54], does not elute in these high Mr fractions, implying that it likely exists in cells as a monomer or possibly a dimer.

Ulp2 is located in both the nucleus and cytoplasm, but is predominantly nuclear

Since a proportion of Ulp2 co-elutes with Ulp1 in the void volume, we wished to determine whether some or all of the Ulp2 co-localises with Ulp1 in cells, i.e. is at the nuclear periphery. We therefore analysed the localisation of Ulp2. Figure 3 indicates that Ulp2 is present in foci that are predominantly nuclear, with a small proportion in the cytoplasm. Little if any Ulp2 is located at the nuclear periphery. Thus the location of Ulp2 is distinct from that of Ulp1 [13], indicating that it is unlikely to be part of nuclear pore complexes. In many cases, Ulp2 co-localises with SUMO. Ulp1 undergoes distinct changes in localisation during the cell cycle, its localisation changing from the nuclear periphery where it is for most of the cell cycle, to the region between the separating DNA masses during mitosis [13]. In contrast, the location of Ulp2 appears to be relatively unchanged in cells at different cell cycle stages. For example, during mitosis (Figure 3, TRITC panel, cells labelled 4), a time when Ulp1 relocalises, the distribution of intranuclear Ulp2 foci is very similar to that observed at other times in the cell cycle (cells labelled 1–3) and is unchanged.

Ulp2 co-purifies with proteins associated with RNA metabolism and protein synthesis

To begin to identify the nature of the complexes observed in Figure 2, we C-terminally-tagged Ulp2 with TAP in the genome (*ulp2-TAP*) and isolated the tagged protein and associated proteins as described in Materials and Methods. Protein complexes were analysed by SDS PAGE (Figure 4) and fractions excised from the gel for mass spectrometric analysis. As shown in Table S1 and Table 2, the majority of the proteins identified are associated with RNA metabolism, such as RNA processing, ribosome biogenesis or initiation of translation. To ensure that these proteins co-

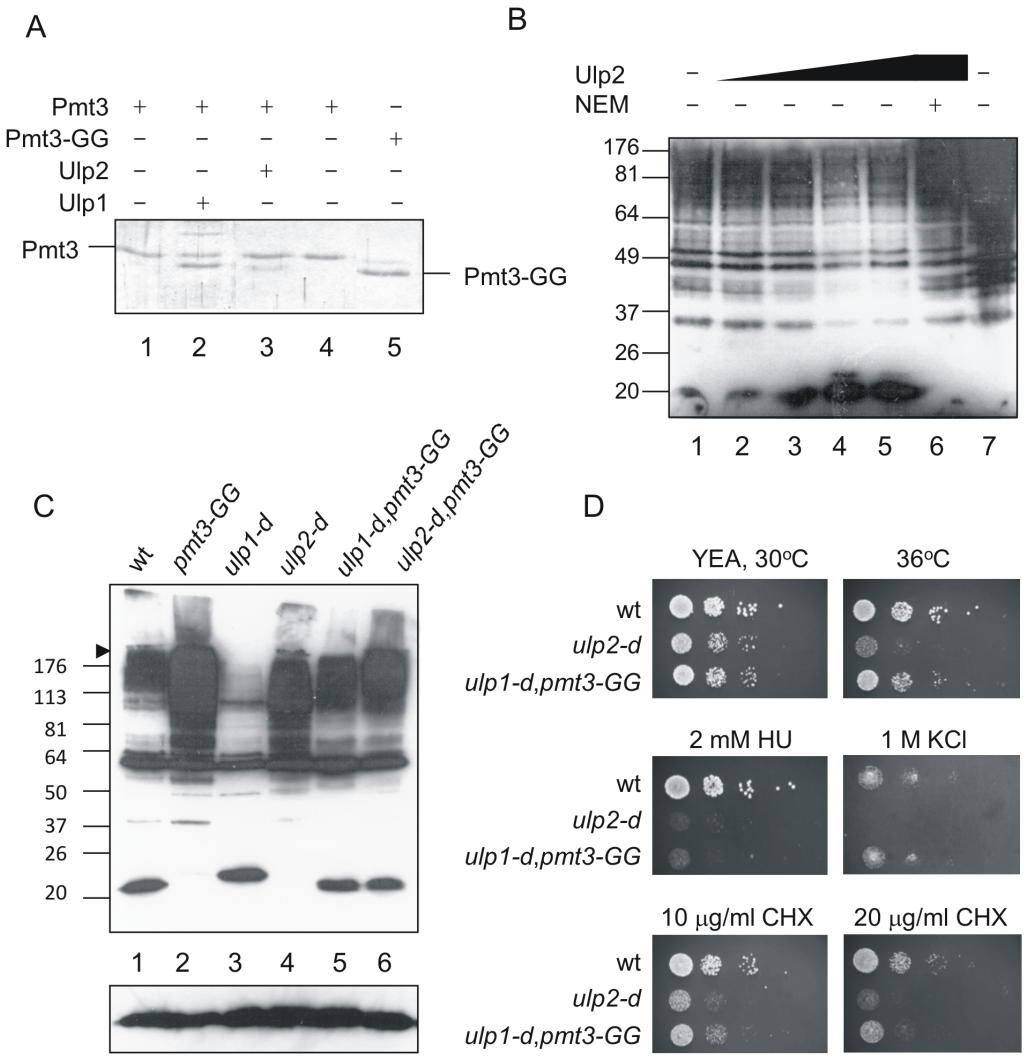

Figure 1. Analysis of Ulp2 function. A. Assay for SUMO-processing activity. Lanes 1–4 contain full length SUMO, lane 5 SUMO-GG. Lanes 1,5, unincubated controls, lanes 2–4 were incubated at 20°C for 2 h following addition of 0.72 μg Ulp1 (lane 2), 2.32 μg Ulp2 (lane 3) or 2 μl buffer (lane 4). Proteins were analysed by SDS PAGE followed by staining with Coommassie Brilliant Blue. B. Assay for de-conjugating activity. *S. pombe* cell extracts were prepared using standard native extraction procedures. Extracts were incubated at 20°C for 2 h (lanes 1–6), lane 1 5 μl of fraction from extract from *E. coli* cells transformed with empty vector, equivalent in volume to the Ulp2-containing fraction from *ulp2*-transformed cells, lane 2 0.6 μg Ulp2, lane 3 1.2 μg Ulp2, lane 4 2.4 μg (5 μl) Ulp2, lane 5 4.8 μg Ulp2, lane 6 1.2 μg Ulp2 pre-incubated with 5 mM NEM, lane 7 total cell extract without incubation at 20°C. Assays were analysed by Western blotting with anti-SUMO antisera. C. Western analysis of total cell extracts using anti-SUMO antisera. Both the separating and stacking gels (6% polyacrylamide in the stacking gel) were blotted. D. Ten microlitre of 10 fold serial dilutions of cells were plated onto YEP agar plates with or without additives as indicated. 10x amount of cells of *ulp2-d* and *ulp1-d,pmt3-GG* were used compared to wild type.
doi:10.1371/journal.pone.0094182.g001

purified specifically with Ulp2, a parallel purification was undertaken using Rad9-TAP, and from cells expressing the TAP tag alone (Figure S1). Rad9 is a member of the 9-1-1 complex required for the DNA integrity checkpoint [55], and would not be expected to interact with a the same proteins as those that interact with Ulp2. Very little protein co-purified with the TAP-tag alone, while purification of Rad9-TAP yielded a quite different set of bands. Most of the proteins co-purifying with Rad9 were associated with DNA metabolism as expected (data not shown) and only one protein, glyceraldehyde 3-phosphate dehydrogenase, was common to the Ulp2-TAP and Rad9-TAP preparations.

A number of proteins required for ribosome biogenesis, including some of those we identified by mass spectrometry, have recently been demonstrated to be sumoylated (Table 2) [6,7,23–27,56–58]. However, little is known about the effect of sumoylation on the function of translation factors. We therefore selected two translation initiation factors, eIF4G and eIF3h for further study. The analysis of some of the other factors will be described elsewhere. eIF4G has been well characterised in *S. cerevisiae* and mammalian cells [18,22] and to some extent in *S. pombe* [59]. eIF4G acts as a scaffold protein as part of the eIF4F complex to recruit mRNA to the ribosome for translation [21], while eIF3h is a non-core subunit of the eIF3 complex linking eIF4F/mRNA to the ribosome in mammalian cells [60]. Gel filtration analysis of whole cell extracts from cells containing Ulp2-myc and either eIF4G-HA or eIF3h-HA indicates that the majority of eIF4G co-elutes with Ulp2 (Figure 2B). In contrast, eIF3h elutes in multiple

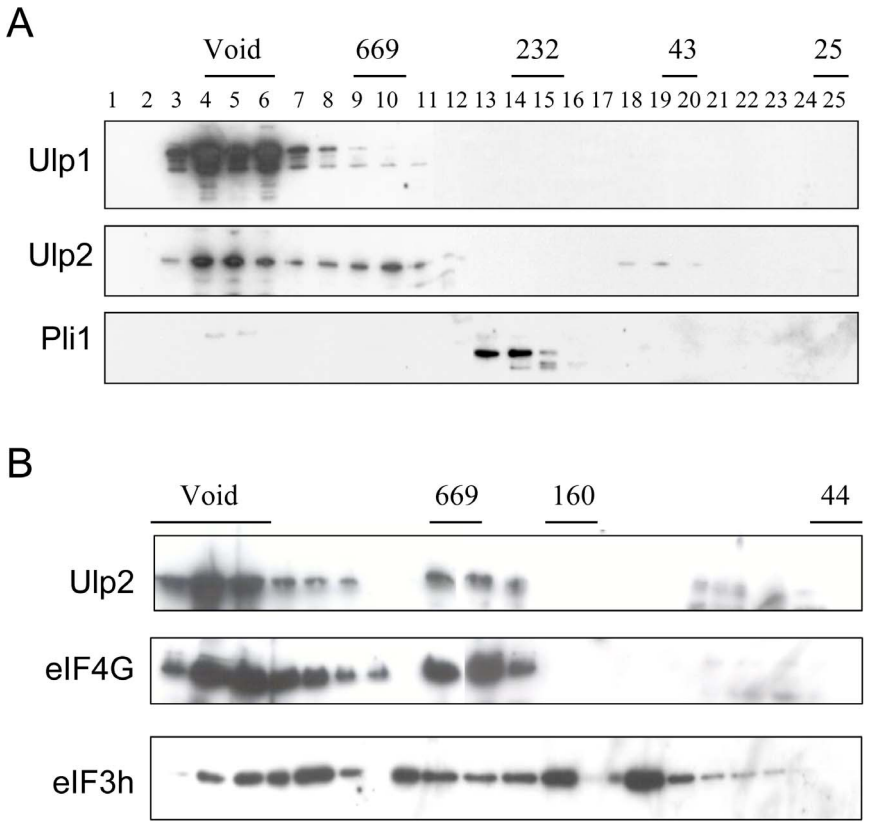

Figure 2. Ulp2 is present in high Mr complexes. Analysis of complexes by gel filtration. A. Total cell extracts from *ulp1-myc*, *ulp2-myc* or *pli1-myc* strains were analysed on a Sephadex 200 column, and fractions were western blotted with anti-myc antibodies. B. Total cell extracts from *ulp2-myc*,*eIF4G-HA* and *ulp2-myc*,*eIF3h-HA* strains were analysed on a Superose 6 column, fractions were western blotted with anti-myc and anti-HA antibodies.
doi:10.1371/journal.pone.0094182.g002

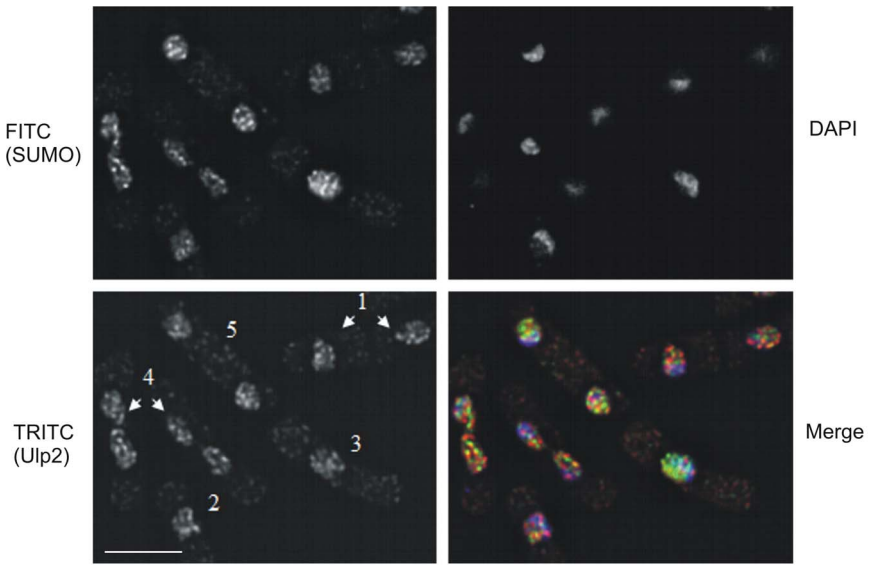

Figure 3. Ulp2 is localised predominantly within the nucleus. A. Cells containing myc-tagged *ulp2* as the sole copy of the *ulp2* gene were incubated with anti-myc antisera (mouse monoclonal) and anti-SUMO antisera (rabbit polyclonal) followed by TRITC-conjugated anti-mouse IgG antisera, FITC-conjugated anti-rabbit IgG antisera and DAPI. Merge = overlay of TRITC (red), FITC (green) and DAPI (blue) staining. 1: early G2 cells, 2,3: late G2 cells, 4: mitotic cells, 5: S phase cells. Bar = 5 μm.
doi:10.1371/journal.pone.0094182.g003

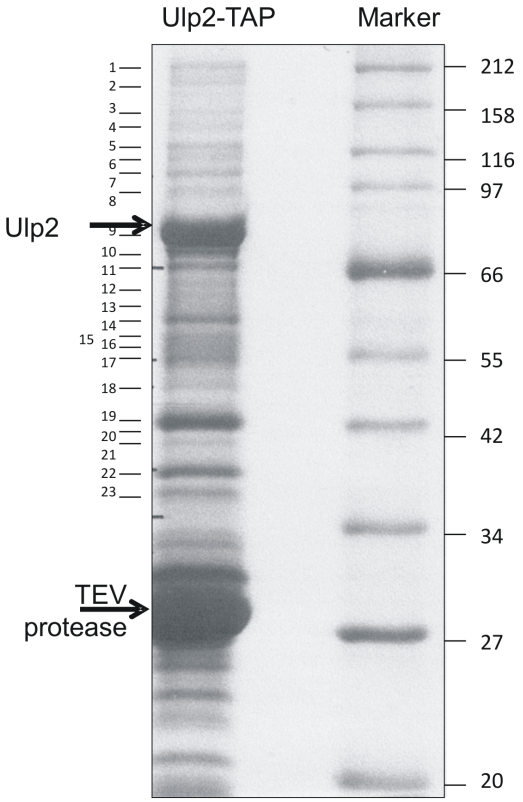

Figure 4. Purification of Ulp2-TAP. SDS-PAGE of Ulp2-Tap and associated proteins. TEV = TEV protease, used to cleave Ulp2 from TAP tag. Numbers refer to gel slices analysed by mass spectrometry.
doi:10.1371/journal.pone.0094182.g004

fractions, suggesting it is present in several different sized complexes.

eIF4G, but not eIF3h, is sumoylated in *S. pombe*

One possibility to explain the interaction of eIF4G and eIF3h with the SUMO protease Ulp2 is that they are themselves modified by SUMO. In order to determine whether this is the case, cells containing genomic copies of HA-tagged eIF4G or eIF3h were co-transformed with pREP41-His-SUMO. His-tagged SUMO was purified on Ni^{2+} agarose. Denaturing conditions (with 6 M guanidinium HCl in the binding buffer, followed by 6 M urea, 300 mM imidazole washes) were used to ensure that sumoylation of the individual proteins was being observed, rather than that of other components of the eIF4F or eIF3 complexes). Figure 5A, shows that eIF4G is specifically recovered in the presence of His-tagged SUMO (lane 1), but not in the absence of His-tagged SUMO (lane 2), indicating that it is sumoylated in *S. pombe*. In contrast, eIF3h is not recovered in either the absence or presence of His-tagged SUMO (Figure 5B), indicating that this translation factor is not sumoylated in fission yeast. Its co-purification with Ulp2 may thus be through the interaction of Ulp2 with other member(s) of the eIF3 complex.

Conditions that induce stress granules affect the localisation and sumoylation of eIF4G

Since one of the functions of sumoylation is to affect protein localisation, we next investigated whether eIF4G and SUMO co-localise. Figure 6 shows that in untreated cells, as has been shown previously [61], the majority of eIF4G is cytoplasmic as expected for a translation initiation factor. As has been observed in *S. cerevisiae* and human cells [62,63], a small amount of eIF4G is also present in the nucleus, where it is proposed to couple RNA processing events in the nucleus with translation in the cytoplasm. In contrast to the situation with eIF4G, the majority of the SUMO protein is present in the nucleus (Figures 3 and 6). We observe that a significant proportion of the nuclear eIF4G co-localises with SUMO, suggesting sumoylation of eIF4G may have a role in regulating RNA processing or localisation.

Protein synthesis can be inhibited by a variety of factors. For example, cycloheximide (CHX) interacts with ribosomes and inhibits the elongation step, while exposure of *S. pombe* cells to 1 M KCl inhibits protein synthesis by the sequestration of translation initiation factors and mRNA into cytoplasmic stress granules [64]. Following treatment with CHX, eIF4G staining is slightly more punctate than in untreated cells, while the pattern of SUMO staining is unchanged. In these cells, there is a low level of colocalisation of eIF4G and SUMO in the nucleus. Interestingly, exposure of cells to CHX results in distorted nuclei. The reason for this is not known, but it could be due to disruption of RNA processing and/or localisation by CHX.

In *S. pombe* and mammalian cells eIF4G and eIF4GI respectively, are among the translation factors present in stress granules [61,65,66]. To investigate stress granule formation in *S. pombe*, we exposed cells to 1 M KCl. In these cells, eIF4G is present in fewer, but quite bright, punctate cytoplasmic foci (Figure 6). This pattern of staining is similar to what has been observed for stress granules in *S. pombe*, and in particular, what has previously been observed for eIF4G in this organism [61,64]. In these cells, there was occasional co-localisation of the two proteins in the cytoplasm and this appeared to reflect the appearance of eIF4G and SUMO in the same granule.

Table 2. Summary of proteins identified by mass spectrometry that co-purified with TAP-Ulp2.

Function	Protein
Translation	eIF2α, eIF2β, eIF3a, eIF3b, eIF3c, eIF3γ, eIF3h, eIF4G, EF1α EF2B, eEF3B, EF2, Pabp
RNA synthesis	Rpa1, Rpa2,
RNA processing	Rrp5, SPAC694.02, Exo2, Dhp1, Upf1, SPBC19G7.10C, Nop2, Dbp2, Prp19, Sla1,
Ribosome biogenesis	aconitate hydrolase/mitochondrial ribosomal protein subunit L49, SPAC22G7.05, SPAC1142.04(Noc2 predicted), Hsc1/Sks2, Rpl301, Rpl302, Rml2
DNA metabolism	Tcg1, Rfc5,
Other	Pfk1, SPBC16h5.12C, glutamate 5-kinase (predicted), Gpd1, Gpd3

Data from [6,7,23–26,56–58].
doi:10.1371/journal.pone.0094182.t002

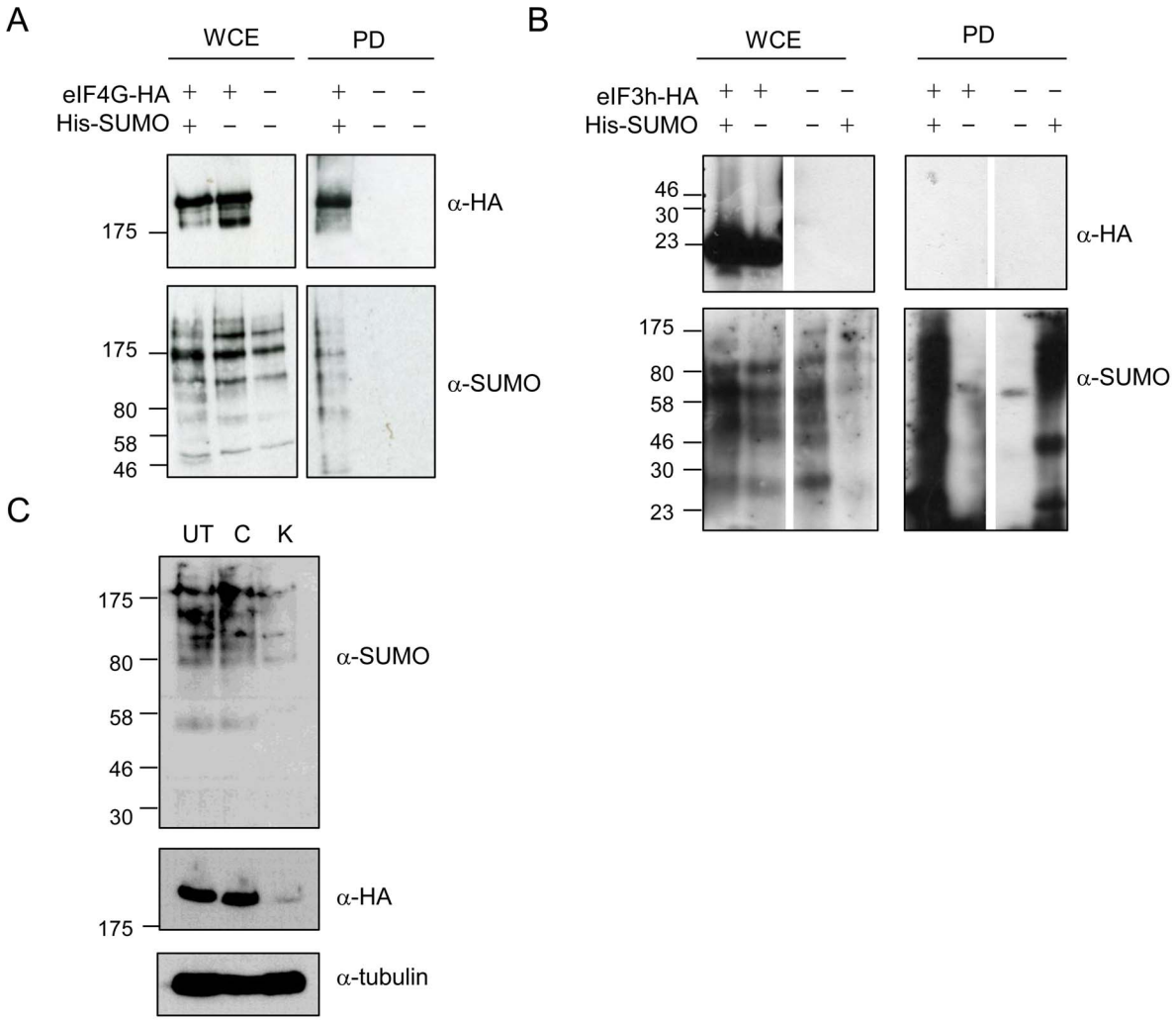

Figure 5. eIF4G, but not eIF3h, is sumoylated. His-tagged SUMO was expressed in cells containing genomically tagged (HA) copies of eIF4G (A) and eIF3h (B). WCE = whole cell extract, PD = Ni^{2+}-agarose pull down. Blots were probed with anti-HA or anti-SUMO antisera. C. Western blot of whole cell extracts from cells containing genomically tagged eIF4G-HA. UT = untreated, C, K = incubated for 30 min with 100 μg/ml CHX (C) or 1 M KCl (K).
doi:10.1371/journal.pone.0094182.g005

Another protein known to be present in stress granules is polyA-binding protein (PABP) [61]. We therefore compared the localisation of eIF4G and PABP in cells exposed to 1 M KCl. We observe PABP in large cytoplasmic granules, which are different to those we observe in cells only containing HA-tagged eIF4G-HA (Figure S2A and Figure 6). Curiously, in some of the cells that contain both eIF4G-HA and PABP-RFP, eIF4G is now also present in large granules where it co-localises with PABP. Further analysis of PABP-RFP containing cells indicated that a proportion of the SUMO is mislocalised to the cytoplasm (Figure S2B). This suggests that C-terminal RFP-tagging of PABP may affect its function and/or localisation.

Following exposure to 1 M KCl, we noticed that there was less staining of both eIF4G and SUMO compared to that in untreated cells. Western analysis of eIF4G and SUMO levels indicates that in response to 1 M KCl the levels of both proteins are significantly reduced (Figure 5C). The reason for this is unknown, but may be due to the fact that a proportion of the eIF4G and SUMO is insoluble and not recovered in the extract. Alternatively, and in our view the more likely explanation, we propose that in response to this stress, there is increased proteolysis of both proteins.

We next investigated whether sumoylation of eIF4G is affected by exposure of cells to either CHX (100 μg/ml) or KCl (1 M). Figure 7A indicates that there is an increase in sumoylation in response to KCl, with levels of sumoylation unaffected by exposure to CHX, when compared to levels in untreated cells (with relative levels being 1:1:1.5; wt, CHX-treated, KCl-treated, respectively). These data suggest that sumoylation of eIF4G may be associated with stress granule formation and/or proteolysis of the translation initiation factor.

Human eIF4GI is sumoylated

In order to analyse the role of sumoylation of *S. pombe* eIF4G we investigated the possibility of testing the protein for ability to be sumoylated in our *in vitro* sumoylation assay, as this could help us identify the sumoylated lysine residue(s). However, two factors make this identification difficult. Firstly, in order to purify protein for an *in vitro* sumoylation assay, we would need to clone the full length *S. pombe* eIF4G cDNA. We have previously observed that

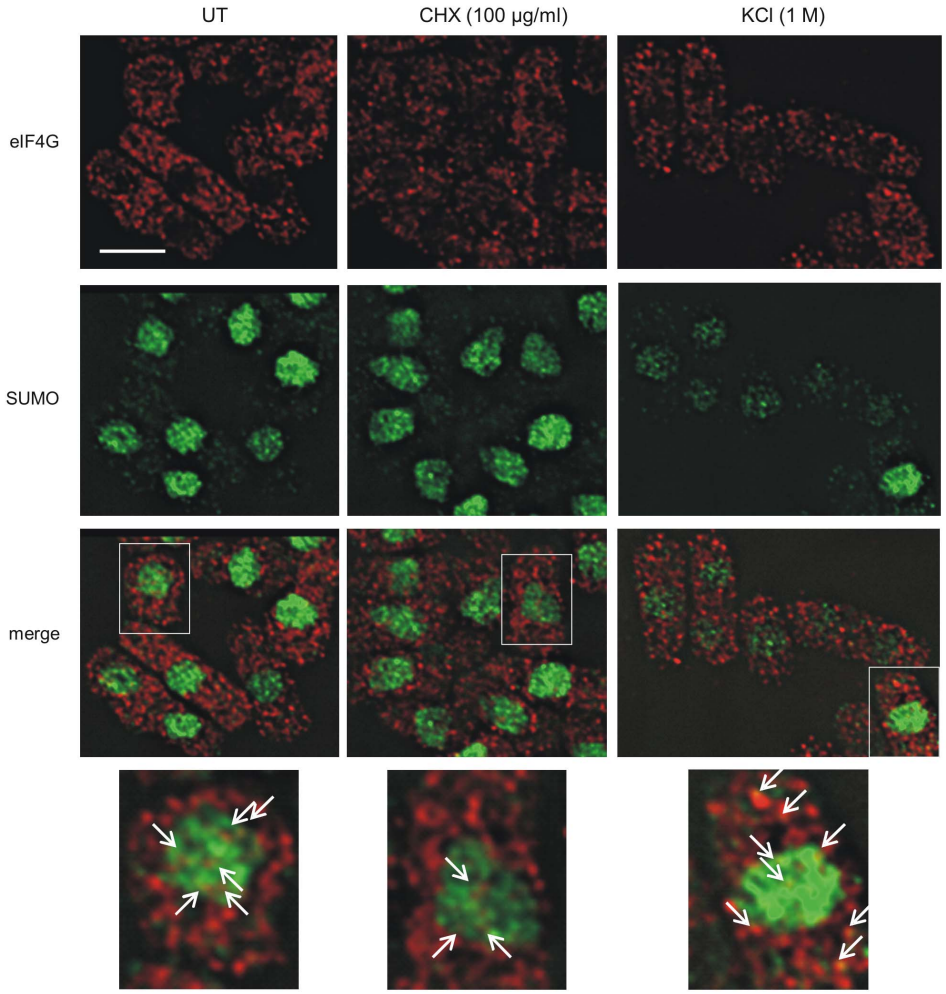

Figure 6. Effect of cycloheximide and KCl on localisation of eIF4G and SUMO. Cells containing eIF4G-HA, untreated (UT) or exposed to CHX (100 µg/ml) or KCl (1 M) as indicated, were incubated with anti-SUMO antisera (green) and anti-HA antisera (red). Bar = 5 µm. Bottom panel, regions indicated by boxes in panel above. Arrows indicate sites of colocalisation of SUMO and eIF4G.
doi:10.1371/journal.pone.0094182.g006

plasmids containing the N-terminus of the *S. pombe* eIF4G coding sequence cannot be tolerated in *E. coli* [59], so that full length eIF4G cannot be expressed in *E. coli*. The reason for this is unknown, but may be due to the presence of a highly repeated sequence within the eIF4G coding sequence. Secondly, this highly repeated sequence (present in the coding sequence in the *S. pombe*, but not in the *S. cerevisiae* or human proteins) contains 16 repeats of a perfect sumoylation site consensus motif (AKRE), which would likely make identification of the site(s) difficult, even if we were able to express the full length protein. We therefore expressed a C-terminal fragment (comprising aa 970–1403), which contains eIF4E, eIF4A and eIF3 binding sites (Figure 7B) and tested this in our *in vitro* sumoylation assay. We did not observe any sumoylation of this fragment, implying that sumoylation likely occurs in the N-terminus of the protein.

To further analyse the role of sumoylation we set out to determine whether human eIF4GI is sumoylated and if so, to identify the sumoylation site(s) in this protein. We used HeLa cell lines stably transfected with either His-SUMO-1 or His-SUMO-2 [38,39]. His-tagged SUMO was recovered from cell extracts prepared under denaturing conditions. Figure 7C indicates that eIF4GI is not recovered from extracts of cells that do not contain His-tagged SUMO (lane1), but is isolated from extracts of cells containing His-SUMO-1 (lane 2) and to a lesser extent from cells expressing His-SUMO-2 (lane 3). This confirms that, like *S. pombe* eIF4G, human eIF4GI is sumoylated.

We next sought to identify the sumoylation sites on human eIF4GI. In order to facilitate our analysis, we used three different human eIF4G fragments, N-FAG, M-FAG and C-FAG (Figure 7B, [37]). These protein fragments were purified from *E. coli* and tested in our *in vitro* sumoylation assay (data not shown). Slow migrating forms of eIF4G were excised from gels and analysed by mass spectrometry. Two sumoylation sites were identified: K1368 and K1588 (Figure 7D). These map to two domains of eIF4GI which interact with eIF4A and the protein kinase, Mnk1, respectively [18,21,22]. These results suggest that sumoylation may affect the interaction of eIF4GI with these two proteins.

Discussion

In order to analyse the role of *S. pombe* Ulp2, we purified Ulp2-TAP-containing complexes. We identified proteins involved in RNA synthesis or processing, ribosome biogenesis and translation. This is consistent with recent reports that a number of proteins required for ribosome biogenesis and RNA processing are sumoylated [6,67,68]. While this manuscript was in preparation,

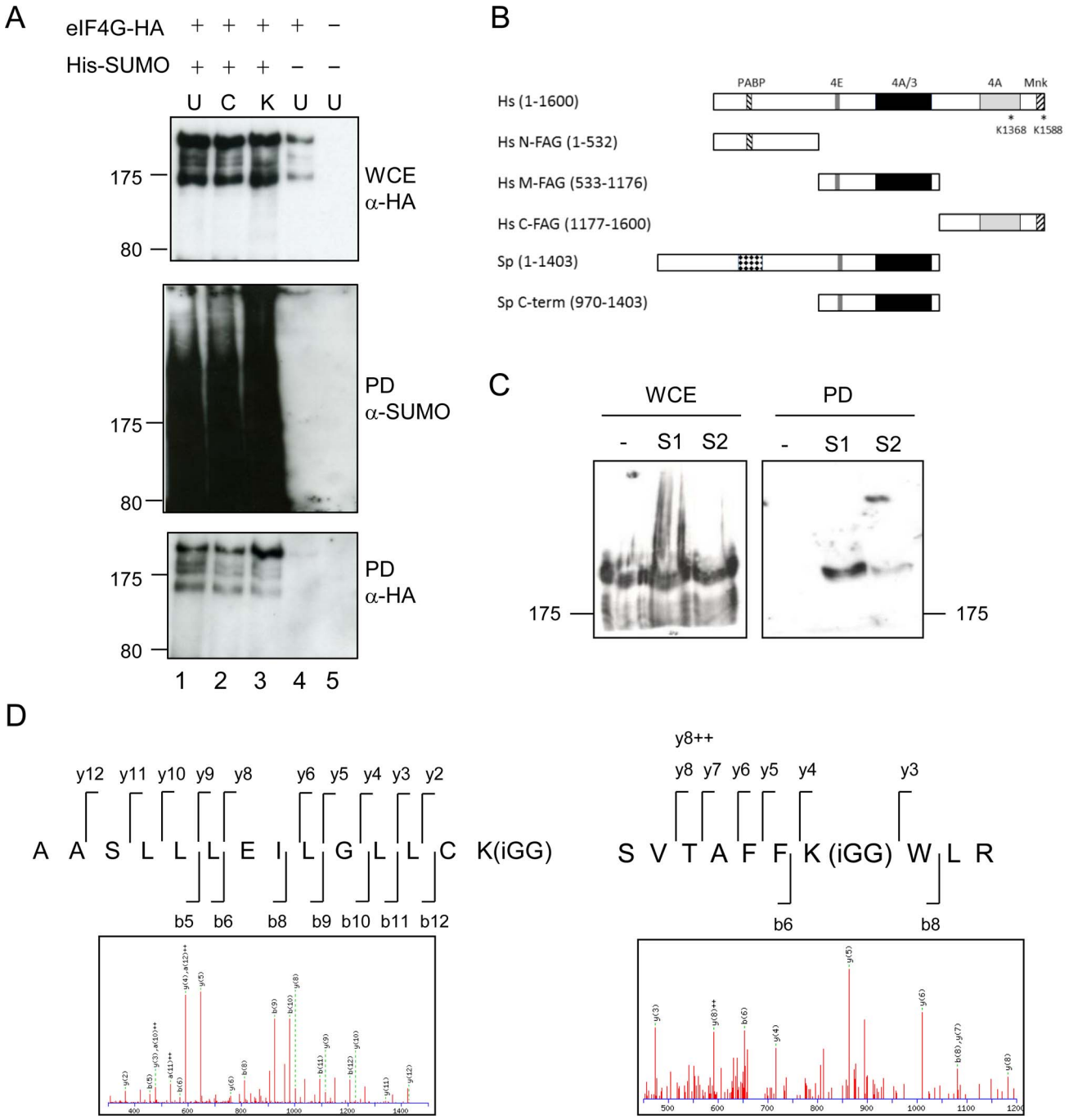

Figure 7. Human eIF4G is sumoylated. A. *S. pombe* cells containing His-tagged SUMO and HA-tagged eIF4G as indicated were treated with CHX (100 μg/ml) or KCl (1 M), and His-tagged SUMO pulled down, and analysed as in Figure 5. B. Comparison of human and eIF4G proteins, indicating protein binding domains: PABP = polyA binding protein, 4E = eIF4E, 4A = eIF4A, 3 = eIF3, Mnk = MAP kinase-interacting kinase 1. C. Whole cell extracts (WCE) and Ni^{2+} pull-down (PD) from extracts of HeLa cells stably transfected with His-tagged SUMO-1 (S1) or SUMO-2 (S2) or nothing (-). Western blots probed with anti-eIF4GI (KRERK epitope) antisera. D. Representative eIF4G ion mass spectra (MS/MS spectra) showing identification of the *in vitro* sites of sumoylation.
doi:10.1371/journal.pone.0094182.g007

a global analysis of the SUMO system interactome in *S. cerevisiae* identified a range of proteins including a number required for ribosome biogenesis and rRNA processing that interact with Ulp2 [69]. Additionally, the nucleolar SUMO-specific protease, SENP3, has been demonstrated to reverse the SUMO modification of nucleophosmin to be required for rRNA processing [70].

Although a number of translation factors, required for both the initiation and elongation steps of protein synthesis, have been identified in global screens as being sumoylated e.g. [23–28,30,31], little is known about the role of sumoylation of these proteins. This is in contrast to the situation with the role of sumoylation in ribosome biogenesis. We therefore focussed our attention on two *S. pombe* translation initiation factors in our list of Ulp2-interactors:

eIF4G and eIF3h. Both proteins are known to be present in high Mr complexes, with eIF4G being part of the eIF4F complex while eIF3h is part of the eIF3 complex [22]. We demonstrate here that eIF4G, but not eIF3h is sumoylated *in vivo*. These results are supported by the genome-wide analyses of sumoylated proteins that have been undertaken, that indicate that eIF4G is sumoylated [24,28] but which have not to date identified eIF3h as a sumoylation target.

As the most prominent role of translation initiation factors is in cytoplasmic protein synthesis, we began by investigating whether Ulp2 is associated with polysomes. However, we observed that while Ulp2 migrated at the same position in sucrose gradients as polysomes, it was still present in these fractions under conditions (2.5 mM EDTA) where polysomes were disrupted, indicating that the majority of Ulp2 is not associated with actively translating polysomes (data not shown). This result confirms our gel filtration analysis and localisation studies, and indicates that Ulp2 is present in very high molecular weight complexes, but discounts the possibility that Ulp2 is associated with actively translating polysomes.

The role of sumoylation of translation factors has not been well studied, apart from that of eIF4E [29,33]. eIF4E is an mRNA cap-binding protein, and one of the proteins that interacts with eIF4G to form the eIF4F complex [22]. eIF4E is regulated by phosphorylation and by interaction with eIF4E-binding proteins (4E-BPs). Sumoylation of eIF4E on five lysines is promoted by its phosphorylation at S209, and results in its dissociation from 4E-BP1. Sumoylation did not interfere with mRNA recognition but enhanced eIF4F complex assembly on the mRNA cap, promoting the expression of ornithine decarboxylase, c-myc and Bcl-2, driving the anti-apoptotic and oncogenic activity of eIF4E [33]. As phosphorylation of eIF4E has been shown to play a role in selective nuclear export of mRNA [71], it is likely that sumoylation of eIF4E occurs in the nucleus and/or as it emerges into the cytoplasm

We have shown that in response to osmotic stress (1 M KCl), conditions that induce stress granules in fission yeast, the overall levels of SUMO and eIF4G are reduced. We have also shown that under these conditions, there is increased sumoylation of eIF4G. The role of this modification is not known. Our results suggest two possible scenarios: the first being that sumoylation is targeting eIF4G for degradation, possibly via the action of a SUMO-targeted ubiquitin ligase (STUbL). The second possibility is that sumoylation may be targeting eIF4G to stress granules. Further work is needed to distinguish between these two possibilities.

The two sumoylation sites in human eIF4GI that we have identified are not conserved in fission yeast eIF4G, as this protein lacks the C-terminal domains present in human eIF4GI (Figure 7B). Their positions suggest that sumoylation of this protein may be affecting interactions of eIF4GI with eIF4A and Mnk1. eIF4A is a DEAD-box protein that participates in translation initiation and binds to eIF4GI [18,21,22]. Functioning as an ATP-dependent RNA helicase, eIF4A is believed to unwind secondary structure in the 5′-untranslated region of mRNAs to enable ribosome scanning. The RNA-stimulated ATPase and ATP-dependent helicase activities of eIF4A are enhanced by its interaction with two domains on eIF4GI, one in the C-terminus and one in the middle domain [18,22]. Interaction and subsequent recycling of eIF4A from the eIF4G/eIF4A complex stimulates the eIF4A helicase activity required for the mRNA scanning process. It is possible that sumoylation of eIF4GI either directly or indirectly affects the interaction with eIF4A, thereby regulating translation initiation. Mnk1 is a kinase which binds at the extreme C-terminus of eIF4GI and regulates the phosphorylation of eIF4E at Ser209 [18,21,22]. Phosphorylated eIF4E has been shown to be modified by sumoylation on five lysine residues [33] promoting eIF4F complex formation and specific protein synthesis [33]. Sumoylation of K1588 on eIF4GI could prevent the binding of Mnk1, reduce eIF4E phoshorylation and thereby abrogate sumoylation of eIF4E and specific mRNA translation. As phosphorylation of eIF4E is associated with tumour cell formation and increased resistance of tumour cells to apoptosis, sumoylation of eIF4GI at this site could provide a novel and undiscovered mechanism to regulate cell growth and proliferation in mammalian cells. Further work needs to be done to address this.

In conclusion, our results demonstrate that *S. pombe* and human eIF4GI are both sumoylated, and that in *S. pombe* this modification is increased under conditions that promote the formation of stress granules. We have also identified the target lysine residues that are used for sumoylation *in vitro* in human eIF4GI. It will be of interest to determine whether these sites are also used *in vivo*, and to identify the role of this sumoylation.

Supporting Information

Figure S1 Comparison of proteins co-purifying with Ulp2-Tap and Rad9-Tap. Extracts from cells expressing Ulp2-Tap, Rad9-Tap (Methods S1) or Tap alone were subjected to the same purification procedure and analysed by SDS-PAGE followed by staining with colloidal coommassie.
(TIF)

Figure S2 Colocalisation of eIF4G with PABP. A. Strain containing eIF4G-HA and PABP-RFP stained with anti-HA and anti-RFP antisera. Secondary antisera: anti-rabbit FITC conjugated, anti-mouse TRITC-conjugated. B. Strains containing either eIF4G-HA or Pabp-RFP (Methods S1) as indicated, stained with anti-SUMO antisera.
(TIF)

Table S1 Identity of proteins co-purifying with Ulp2-TAP. Proteins identified by LC MS/MS (Methods S1).
(DOCX)

Methods S1
(DOCX)

Author Contributions

Conceived and designed the experiments: FZW SJM DLT. Performed the experiments: JJ MF LZ OW LS RB DS LDB FZW DLT. Analyzed the data: MF DS LDB SJM FZW. Contributed reagents/materials/analysis tools: JJ MF LZ LS RB DS LDB SJM FZW. Wrote the paper: FZW SJM.

References

1. Hay RT (2005) SUMO: a history of modification. Mol Cell 18: 1–12.
2. Watts FZ, Hoffmann E (2011) SUMO meets meiosis: an encounter at the synaptonemal complex: SUMO chains and sumoylated proteins suggest that heterogeneous and complex interactions lie at the centre of the synaptonemal complex. BioEssays: news and reviews in molecular, cellular and developmental biology 33: 529–537.
3. Jackson SP, Durocher D (2013) Regulation of DNA damage responses by ubiquitin and SUMO. Molecular cell 49: 795–807.
4. Ouyang J, Valin A, Gill G (2009) Regulation of transcription factor activity by SUMO modification. Methods in molecular biology 497: 141–152.
5. Wan J, Subramonian D, Zhang XD (2012) SUMOylation in control of accurate chromosome segregation during mitosis. Current protein & peptide science 13: 467–481.

6. Westman BJ, Verheggen C, Hutten S, Lam YW, Bertrand E, et al. (2010) A proteomic screen for nucleolar SUMO targets shows SUMOylation modulates the function of Nop5/Nop58. Molecular cell 39: 618–631.
7. Hannich JT, Lewis A, Kroetz MB, Li SJ, Heide H, et al. (2005) Defining the SUMO-modified proteome by multiple approaches in Saccharomyces cerevisiae. J Biol Chem 280: 4102–4110.
8. Pfander B, Moldovan GL, Sacher M, Hoege C, Jentsch S (2005) SUMO-modified PCNA recruits Srs2 to prevent recombination during S phase. Nature 436: 428–433.
9. Papouli E, Chen S, Davies AA, Huttner D, Krejci L, et al. (2005) Crosstalk between SUMO and ubiquitin on PCNA is mediated by recruitment of the helicase Srs2p. Mol Cell 19: 123–133.
10. Joseph J, Tan SH, Karpova TS, McNally JG, Dasso M (2002) SUMO-1 targets RanGAP1 to kinetochores and mitotic spindles. J Cell Biol 156: 595–602.
11. Hardeland U, Steinacher R, Jiricny J, Schar P (2002) Modification of the human thymine-DNA glycosylase by ubiquitin-like proteins facilitates enzymatic turnover. Embo J 21: 1456–1464.
12. Li SJ, Hochstrasser M (2003) The Ulp1 SUMO isopeptidase: distinct domains required for viability, nuclear envelope localization, and substrate specificity. J Cell Biol 160: 1069–1081.
13. Taylor DL, Ho JC, Oliver A, Watts FZ (2002) Cell-cycle-dependent localisation of Ulp1, a Schizosaccharomyces pombe Pmt3 (SUMO)-specific protease. J Cell Sci 115: 1113–1122.
14. Hickey CM, Wilson NR, Hochstrasser M (2012) Function and regulation of SUMO proteases. Nature reviews Molecular cell biology 13: 755–766.
15. Li SJ, Hochstrasser M (2000) The yeast ULP2 (SMT4) gene encodes a novel protease specific for the ubiquitin-like Smt3 protein. Mol Cell Biol 20: 2367–2377.
16. Yeh ET (2009) SUMOylation and De-SUMOylation: wrestling with life's processes. J Biol Chem 284: 8223–8227.
17. Kolli N, Mikolajczyk J, Drag M, Mukhopadhyay D, Moffatt N, et al. (2010) Distribution and paralogue specificity of mammalian deSUMOylating enzymes. Biochem J 430: 335–344.
18. Sonenberg N, Hinnebusch AG (2009) Regulation of translation initiation in eukaryotes: mechanisms and biological targets. Cell 136: 731–745.
19. Guertin DA, Sabatini DM (2007) Defining the role of mTOR in cancer. Cancer Cell 12: 9–22.
20. Laplante M, Sabatini DM (2012) mTOR signaling in growth control and disease. Cell 149: 274–293.
21. Morley SJ, Coldwell MJ, Clemens MJ (2005) Initiation factor modifications in the preapoptotic phase. Cell death and differentiation 12: 571–584.
22. Jackson RJ, Hellen CU, Pestova TV (2010) The mechanism of eukaryotic translation initiation and principles of its regulation. Nature reviews Molecular cell biology 11: 113–127.
23. Blomster HA, Hietakangas V, Wu J, Kouvonen P, Hautaniemi S, et al. (2009) Novel proteomics strategy brings insight into the prevalence of SUMO-2 target sites. Mol Cell Proteomics 8: 1382–1390.
24. Matafora V, D'Amato A, Mori S, Blasi F, Bachi A (2009) Proteomics analysis of nucleolar SUMO-1 target proteins upon proteasome inhibition. Mol Cell Proteomics 8: 2243–2255.
25. Yang W, Thompson JW, Wang Z, Wang L, Sheng H, et al. (2012) Analysis of oxygen/glucose-deprivation-induced changes in SUMO3 conjugation using SILAC-based quantitative proteomics. J Proteome Res 11: 1108–1117.
26. Panse VG, Hardeland U, Werner T, Kuster B, Hurt E (2004) A proteome-wide approach identifies sumoylated substrate proteins in yeast. J Biol Chem 279: 41346–41351.
27. Miller MJ, Barrett-Wilt GA, Hua Z, Vierstra RD (2010) Proteomic analyses identify a diverse array of nuclear processes affected by small ubiquitin-like modifier conjugation in Arabidopsis. Proceedings of the National Academy of Sciences of the United States of America 107: 16512–16517.
28. Bruderer R, Tatham MH, Plechanovova A, Matic I, Garg AK, et al. (2011) Purification and identification of endogenous polySUMO conjugates. EMBO Rep 12: 142–148.
29. Xu X, Vatsyayan J, Gao C, Bakkenist CJ, Hu J (2010) HDAC2 promotes eIF4E sumoylation and activates mRNA translation gene specifically. J Biol Chem 285: 18139–18143.
30. Nie M, Xie Y, Loo JA, Courey AJ (2009) Genetic and proteomic evidence for roles of Drosophila SUMO in cell cycle control, Ras signaling, and early pattern formation. PloS one 4: e5905.
31. Becker J, Barysch SV, Karaca S, Dittner C, Hsiao HH, et al. (2013) Detecting endogenous SUMO targets in mammalian cells and tissues. Nature structural & molecular biology 20: 525–531.
32. Gingras AC, Gygi SP, Raught B, Polakiewicz RD, Abraham RT, et al. (1999) Regulation of 4E-BP1 phosphorylation: a novel two-step mechanism. Genes & development 13: 1422–1437.
33. Xu X, Vatsyayan J, Gao C, Bakkenist CJ, Hu J (2010) Sumoylation of eIF4E activates mRNA translation. EMBO Rep 11: 299–304.
34. Gareau JR, Lima CD (2010) The SUMO pathway: emerging mechanisms that shape specificity, conjugation and recognition. Nat Rev Mol Cell Biol 11: 861–871.
35. Finkbeiner E, Haindl M, Raman N, Muller S (2011) SUMO routes ribosome maturation. Nucleus 2: 527–532.
36. Bahler J, Wu JQ, Longtine MS, Shah NG, McKenzie A 3rd, et al. (1998) Heterologous modules for efficient and versatile PCR-based gene targeting in Schizosaccharomyces pombe. Yeast 14: 943–951.
37. Coldwell MJ, Hashemzadeh-Bonehi L, Hinton TM, Morley SJ, Pain VM (2004) Expression of fragments of translation initiation factor eIF4GI reveals a nuclear localisation signal within the N-terminal apoptotic cleavage fragment N-FAG. Journal of cell science 117: 2545–2555.
38. Girdwood D, Bumpass D, Vaughan OA, Thain A, Anderson LA, et al. (2003) P300 transcriptional repression is mediated by SUMO modification. Mol Cell 11: 1043–1054.
39. Vertegaal AC, Ogg SC, Jaffray E, Rodriguez MS, Hay RT, et al. (2004) A proteomic study of SUMO-2 target proteins. J Biol Chem 279: 33791–33798.
40. Seraphin B (2002) Identification of transiently interacting proteins and of stable protein complexes. Adv Protein Chem 61: 99–117.
41. Ho JC, Warr NJ, Shimizu H, Watts FZ (2001) SUMO modification of Rad22, the Schizosaccharomyces pombe homologue of the recombination protein Rad52. Nucleic Acids Res 29: 4179–4186.
42. Coldwell MJ, Sack U, Cowan JL, Barrett RM, Vlasak M, et al. (2012) Multiple isoforms of the translation initiation factor eIF4GII are generated via use of alternative promoters, splice sites and a non-canonical initiation codon. The Biochemical journal 448: 1–11.
43. Moreno S, Klar A, Nurse P (1991) Molecular genetic analysis of fission yeast Schizosaccharomyces pombe. Methods Enzymol 194: 795–823.
44. Shevchenko A, Tomas H, Havlis J, Olsen JV, Mann M (2006) In-gel digestion for mass spectrometric characterization of proteins and proteomes. Nature protocols 1: 2856–2860.
45. Ross PL, Huang YN, Marchese JN, Williamson B, Parker K, et al. (2004) Multiplexed protein quantitation in Saccharomyces cerevisiae using amine-reactive isobaric tagging reagents. Molecular & cellular proteomics: MCP 3: 1154–1169.
46. Chicooree N, Griffiths JR, Connolly Y, Tan CT, Malliri A, et al. (2013) A novel approach to the analysis of SUMOylation with the independent use of trypsin and elastase digestion followed by database searching utilising consecutive residue addition to lysine. Rapid communications in mass spectrometry: RCM 27: 127–134.
47. Watts FZ (2004) SUMO Proteases. In: Wilson VG, editor. Sumoylation Molecular Biology and Biochemistry. Wymondham: Horizon Bioscience. pp. 113–130.
48. Tanaka K, Nishide J, Okazaki K, Kato H, Niwa O, et al. (1999) Characterization of a fission yeast SUMO-1 homologue, pmt3p, required for multiple nuclear events, including the control of telomere length and chromosome segregation. Mol Cell Biol 19: 8660–8672.
49. al-Khodairy F, Enoch T, Hagan IM, Carr AM (1995) The Schizosaccharomyces pombe hus5 gene encodes a ubiquitin conjugating enzyme required for normal mitosis. J Cell Sci 108: 475–486.
50. Shayeghi M, Doe CL, Tavassoli M, Watts FZ (1997) Characterisation of Schizosaccharomyces pombe rad31, a UBA-related gene required for DNA damage tolerance. Nucleic Acids Res 25: 1162–1169.
51. Bylebyl GR, Belichenko I, Johnson ES (2003) The SUMO isopeptidase Ulp2 prevents accumulation of SUMO chains in yeast. J Biol Chem 278: 44113–44120.
52. Takahashi Y, Mizoi J, Toh EA, Kikuchi Y (2000) Yeast Ulp1, an Smt3-Specific Protease, Associates with Nucleoporins. J Biochem (Tokyo) 128: 723–725.
53. Panse VG, Kuster B, Gerstberger T, Hurt E (2003) Unconventional tethering of Ulp1 to the transport channel of the nuclear pore complex by karyopherins. Nat Cell Biol 5: 21–27.
54. Xhemalce B, Seeler JS, Thon G, Dejean A, Arcangioli B (2004) Role of the fission yeast SUMO E3 ligase Pli1p in centromere and telomere maintenance. Embo J 23: 3844–3853.
55. Parrilla-Castellar ER, Arlander SJ, Karnitz L (2004) Dial 9-1-1 for DNA damage: the Rad9-Hus1-Rad1 (9-1-1) clamp complex. DNA repair 3: 1009–1014.
56. Zhao Y, Kwon SW, Anselmo A, Kaur K, White MA (2004) Broad spectrum identification of cellular small ubiquitin-related modifier (SUMO) substrate proteins. J Biol Chem 279: 20999–21002.
57. Denison C, Rudner AD, Gerber SA, Bakalarski CE, Moazed D, et al. (2005) A proteomic strategy for gaining insights into protein sumoylation in yeast. Mol Cell Proteomics 4: 246–254.
58. Wohlschlegel JA, Johnson ES, Reed SI, Yates JR 3rd (2004) Global analysis of protein sumoylation in Saccharomyces cerevisiae. J Biol Chem 279: 45662–45668.
59. Hashemzadeh-Bonehi L, Curtis PS, Morley SJ, Thorpe JR, Pain VM (2003) Overproduction of a conserved domain of fission yeast and mammalian translation initiation factor eIF4G causes aberrant cell morphology and results in disruption of the localization of F-actin and the organization of microtubules. Genes to cells: devoted to molecular & cellular mechanisms 8: 163–178.
60. Masutani M, Sonenberg N, Yokoyama S, Imataka H (2007) Reconstitution reveals the functional core of mammalian eIF3. The EMBO journal 26: 3373–3383.
61. Nilsson D, Sunnerhagen P (2011) Cellular stress induces cytoplasmic RNA granules in fission yeast. RNA 17: 120–133.
62. Kafasla P, Barrass JD, Thompson E, Fromont-Racine M, Jacquier A, et al. (2009) Interaction of yeast eIF4G with spliceosome components: implications in pre-mRNA processing events. RNA biology 6: 563–574.

63. McKendrick L, Thompson E, Ferreira J, Morley SJ, Lewis JD (2001) Interaction of eukaryotic translation initiation factor 4G with the nuclear cap-binding complex provides a link between nuclear and cytoplasmic functions of the m(7) guanosine cap. Molecular and cellular biology 21: 3632–3641.
64. Wang CY, Wen WL, Nilsson D, Sunnerhagen P, Chang TH, et al. (2012) Analysis of stress granule assembly in Schizosaccharomyces pombe. RNA 18: 694–703.
65. Kedersha N, Anderson P (2007) Mammalian stress granules and processing bodies. Methods in enzymology 431: 61–81.
66. Brengues M, Parker R (2007) Accumulation of polyadenylated mRNA, Pab1p, eIF4E, and eIF4G with P-bodies in Saccharomyces cerevisiae. Molecular biology of the cell 18: 2592–2602.
67. Finkbeiner E, Haindl M, Muller S (2011) The SUMO system controls nucleolar partitioning of a novel mammalian ribosome biogenesis complex. EMBO J 30: 1067–1078.
68. Panse VG, Kressler D, Pauli A, Petfalski E, Gnadig M, et al. (2006) Formation and nuclear export of preribosomes are functionally linked to the small-ubiquitin-related modifier pathway. Traffic 7: 1311–1321.
69. Srikumar T, Lewicki MC, Raught B (2013) A global S. cerevisiae small ubiquitin-related modifier (SUMO) system interactome. Molecular systems biology 9: 668.
70. Haindl M, Harasim T, Eick D, Muller S (2008) The nucleolar SUMO-specific protease SENP3 reverses SUMO modification of nucleophosmin and is required for rRNA processing. EMBO Rep 9: 273–279.
71. Topisirovic I, Ruiz-Gutierrez M, Borden KL (2004) Phosphorylation of the eukaryotic translation initiation factor eIF4E contributes to its transformation and mRNA transport activities. Cancer research 64: 8639–8642.
72. Murray JM, Carr AM, Lehmann AR, Watts FZ (1991) Cloning and characterisation of the rad9 DNA repair gene from Schizosaccharomyces pombe. Nucleic Acids Res 19: 3525–3531.

Translation

ISSN: (Print) 2169-0731 (Online) Journal homepage: http://www.tandfonline.com/loi/ktrs20

Weighing up the possibilities: Controlling translation by ubiquitylation and sumoylation

Felicity Z Watts, Robert Baldock, Jirapas Jongjitwimol & Simon J Morley

To cite this article: Felicity Z Watts, Robert Baldock, Jirapas Jongjitwimol & Simon J Morley (2014) Weighing up the possibilities: Controlling translation by ubiquitylation and sumoylation, Translation, 2:2, e959366, DOI: 10.4161/2169074X.2014.959366

To link to this article: http://dx.doi.org/10.4161/2169074X.2014.959366

Published online: 30 Oct 2014.

Submit your article to this journal

Article views: 36

View related articles

View Crossmark data

Full Terms & Conditions of access and use can be found at
http://www.tandfonline.com/action/journalInformation?journalCode=ktrs20

Download by: [2.101.165.190] **Date:** 17 January 2016, At: 09:47

Translation 2:2, e959366; September 1, 2014; © 2014 Taylor & Francis Group, LLC

Weighing up the possibilities: Controlling translation by ubiquitylation and sumoylation

Felicity Z Watts[1,*], Robert Baldock[1], Jirapas Jongjitwimol[1], and Simon J Morley[2,*]

[1]Genome Damage and Stability Center; School of Life Sciences; University of Sussex; Falmer, Brighton, UK; [2]Department of Biochemistry and Biomedical Science; School of Life Sciences; University of Sussex; Brighton, UK

Keywords:

Abbreviations: eIF, eukaryotic initiation factor; PABP, poly(A) binding protein; 4E-BP, eIF4E-binding protein; mTORC, mechanistic target of rapamycin; Ubl, ubiquitin-like protein; HDAC, histone deacetylase

Regulation of protein synthesis is of fundamental importance to cells. It has a critical role in the control of gene expression, and consequently cell growth and proliferation. The importance of this control is supported by the fact that protein synthesis is frequently upregulated in tumor cells. The major point at which regulation occurs is the initiation stage. Initiation of translation involves the interaction of several proteins to form the eIF4F complex, the recognition of the mRNA by this complex, and the subsequent recruitment of the 40S ribosomal subunit to the mRNA. This results in the formation of the 48S complex that then scans the mRNA for the start codon, engages the methionyl-tRNA and eventually forms the mature 80S ribosome which is elongation-competent. Formation of the 48S complex is regulated by the availability of individual initiation factors and through specific protein-protein interactions. Both of these events can be regulated by post-translational modification by ubiquitin or Ubls (ubiquitin-like modifiers) such as SUMO or ISG15. We provide here a summary of translation initiation factors that are modified by ubiquitin or Ubls and, where they have been studied in detail, describe the role of these modifications and their effects on regulating protein synthesis.

Downloaded by [2.101.165.190] at 09:47 17 January 2016

Introduction

Initiation of protein synthesis

Protein synthesis is of fundamental importance in cells and its regulation is crucial for the continued viability of organisms. The process comprises 3 stages: initiation, elongation and termination. Of these, initiation is generally considered to be one of the major regulatory steps of gene expression in mammalian cells. Initiation requires the function of a number of translation initiation factors (**Fig. 1**), several of which have key roles in cell survival and oncogenesis. These proteins modulate the binding of mRNA to the ribosome, a process facilitated by the assembly of the cap binding protein (eIF4E), a helicase (eIF4A) and a scaffold protein (eIF4G), to form the eIF4F complex (eIF4E/eIF4A/eIF4G).[1-3] The eIF4G scaffold protein possesses domains that interact with eIF4E, eIF4A, eIF3 and the poly(A) binding protein, PABP.[1-4] PABP itself is regulated by interaction with other proteins; binding of Paip1 to PABP stimulates protein synthesis while interaction with Paip2 is inhibitory to translation.[5,6] The activity of the eIF4F complex is regulated by a family of proteins, the eIF4E binding proteins (4E-BPs). Using a conserved motif, 4E-BPs compete with eIF4G for a common surface on eIF4E and inhibit eIF4F assembly. In mammalian cells, activation of the mechanistic target of rapamycin (mTORC1) leads to phosphorylation of 4E-BP1 in a hierarchical manner. This promotes protein synthesis by releasing eIF4E and enabling eIF4F complex assembly on the m^7GTP cap of mRNA, mediating 40S ribosomal subunit binding by a bridging interaction between eIF4G and eIF3.[1-3]

In most organisms there is more than one isoform of most of these translation initiation factors. For example, there are 3 isoforms of eIF4A, eIF4G and PABP.[7-9] In some cases the functions of the isoforms are indistinguishable, in others there are indications that the different isoforms display mRNA-specific regulation.[7-9] Further work will be required to uncover the full range of functions and specificities of these isoforms.

Ubiquitin like proteins

Ubiquitin-like proteins (Ubls) comprise a family of structurally related proteins. The different members of the family share sequence similarities, and in particular the proteins contain a conserved β-grasp fold consisting of 5 β sheets and one α helix.[10] Ubiquitin is a 76 amino acid protein and is the most highly conserved member of the Ubl family, with 96% identity between yeast and human ubiquitin. SUMO (small ubiquitin-like modifier) is less conserved between species and contains a longer, more variable N-terminal extension than ubiquitin being around 100–110 amino acids in total length.[11] ISG15, between 155–165 amino acids in length, contains 2 ubiquitin-like domains.[12] It was the first member of the family to be identified and, unlike ubiquitin and SUMO, is present only in vertebrates. The gene was so named because it was observed to be an interferon stimulated gene encoding a 15 kDa protein.[13] Most members of the Ubl family are synthesized as precursor proteins that need to be processed to a mature form to reveal a di-glycine motif at the

*Correspondence to: Felicity Z Watts; Email: f.z.watts@sussex.ac.uk; Simon J Morley; Email: s.j.morley@sussex.ac.uk

Submitted: 03/24/2014; Revised: 05/01/2014; Accepted: 05/12/2014
http://dx.doi.org/10.4161/2169074X.2014.959366

Downloaded by [2.101.165.190] at 09:47 17 January 2016

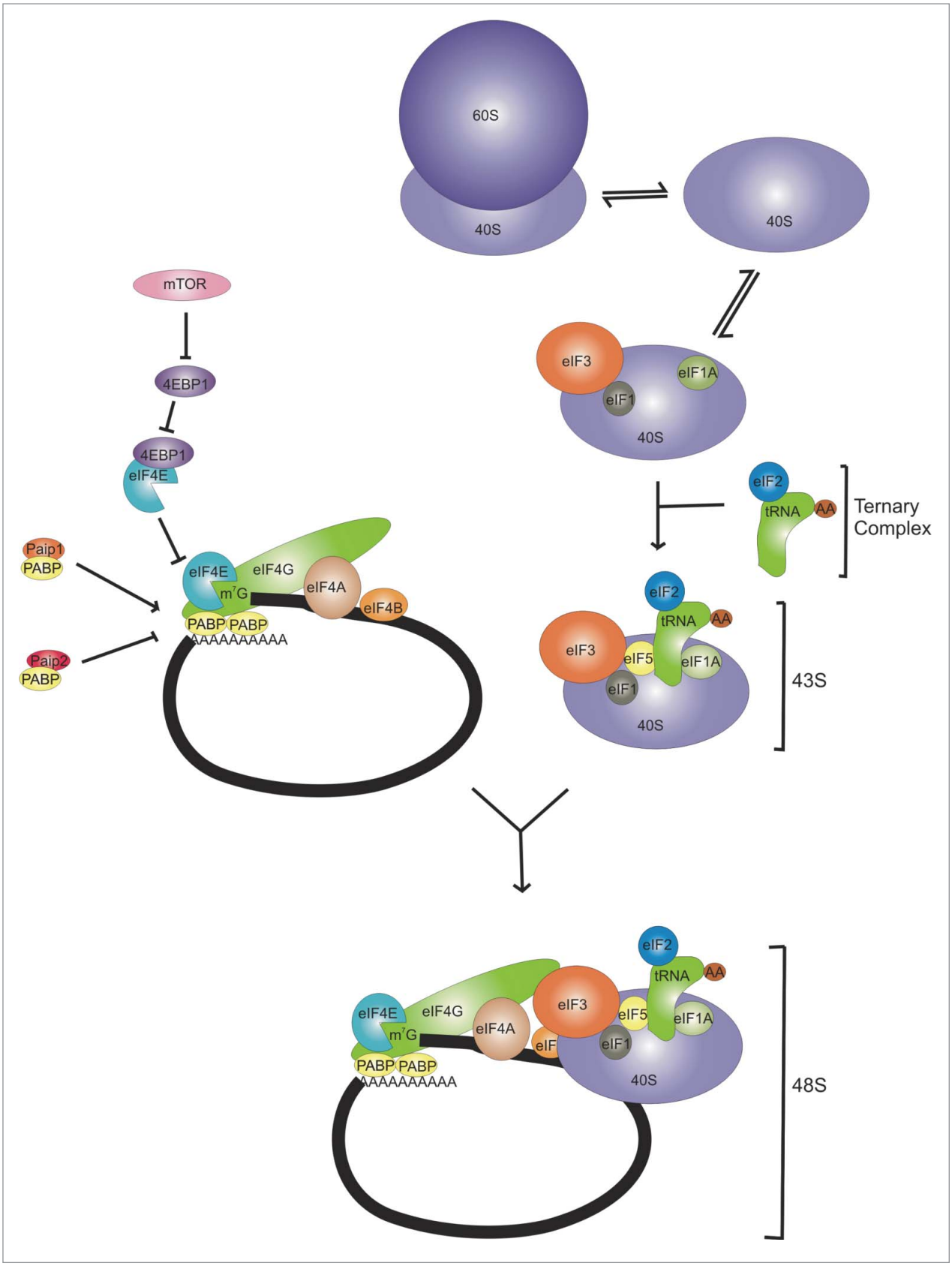

Figure 1. For figure legend, see page e959366-3.

C-terminus that is required for activation and subsequent conjugation of the Ubl to target proteins. The exception to this is ISG15 in fish and bovine species where the protein is synthesized in the mature form.[14] Ubls are attached to one or more lysine residues in target proteins. There are no known consensus sequences for conjugation sites for ubiquitin and ISG15. However SUMO is frequently, although not always, attached to lysine residues present within the consensus sequence ψKxE, where ψ = a hydrophobic amino acid and x is any amino acid.[11]

Ubiquitylation

Ubiquitin can be covalently attached to lysine residues in target proteins as a monomer or in the form of chains. This occurs via the activity of a number of proteins, the E1 (ubiquitin activating enzyme), E2 (ubiquitin conjugating enzyme) and E3 (ubiquitin ligase) proteins (**Fig. 2**). In most organisms there is a single E1, around 40 E2s and hundreds of E3s (reviewed in[15,16]). Ubiquitin is produced as a precursor protein that is processed to the mature form by one of a small number of specific ubiquitin proteases, to reveal a diglycine motif at the C-terminus. Ubiquitin is then activated in an ATP-dependent manner, by the formation of a thioester bond between the C-terminal glycine residue and a cysteine residue on the E1 activating enzyme. From here it is passed to an E2 ubiquitin conjugating enzyme, again, via the formation of a thioester bond between the C-terminal glycine residue and a cysteine residue. Attachment of ubiquitin requires one of a large number of E3 ubiquitin ligases, which in many cases interact directly with target proteins, but which in some instances interact with targets via an adaptor protein. In the main, the E3s provide the specificity for the modification. Ubiquitin chain formation occurs via lysine residues within ubiquitin itself, and also requires the activities of the E1, E2 and E3 enzymes. The most common linkages are via K11, K48 and K63.[17,18] Ubiquitin can be removed from targets by the actions of deubiquitinating enzymes (DUBs). Ubiquitylation has 2 main roles: targeting of proteins for proteolysis and modification of protein function. The best studied role of ubiquitylation is its targeting of proteins for proteasome-mediated degradation. This involves the recognition of K11- and K48-linked ubiquitin chains by the 26S proteasome.[19] However, there is a rapidly expanding literature on other roles for ubiquitylation. For example ubiquitylation of PCNA is required for the recruitment of an error-prone polymerase to undertake translesion DNA synthesis e.g,[20] while ubiquitylation of membrane proteins is required for endocytosis and ubiquitylation of PIN2 is required for vacuolar sorting (reviewed in[21]). In these cases the modification involves a single ubiquitin or K63-linked chains.

Sumoylation

The process of sumoylation is very similar to that of ubiquitylation, involving SUMO-specific E1 (SUMO activating enzyme), E2 (SUMO conjugating enzyme) and E3 (SUMO ligase) proteins.[11] There is a single E1 (a heterodimer), a single E2 (Ubc9) and to date around 12 E3s have been identified. Unlike ubiquitylation, an E3 is not always required for modification, as the E2 is in some cases sufficient, and can provide a degree of target specificity.[22] Like ubiquitin, SUMO can be attached to proteins either as a monomer or in the form of poly-SUMO chains.[11] Sumoylation affects protein-protein interactions,[23,24] protein activity[25] and protein localization.[26] In addition, SUMO chains interact with STUbLs (SUMO-targeted ubiquitin ligases) that bring about ubiquitylation of the target protein and associated SUMO chains, resulting in proteasome–mediated proteolysis.[27]

ISGylation

ISG15 is conjugated to target proteins in a manner similar to that of ubiquitin and SUMO.[28] ISG15 expression and modification (ISGylation) are activated by Type I interferon (IFN), which is one of a number of critical cytokines in the innate immune response. As is the case for ubiquitin and SUMO, there are proteases that are specific for processing ISG15 and deconjugating it from target proteins (e.g., USP43,[29]) and a specific E1 enzyme for ISG15.[29] However, some of the E2s (e.g., UbcH8) and E3s (e.g., Efp—the partner of UbcH8, and HHARI—the human homolog of *Drosophila* ariadne) involved in ISGylation also appear to be involved in ubiquitylation.[30,31]

Identification of Ubl Attachment Sites and the Roles of Modification

Early methods for the identification of modified sites involved site-directed mutagenesis of individual lysine residues in target proteins, followed by analysis in vitro or in vivo to determine whether modification still occurred. While this has been successful in some cases (e.g.,[32]) in many cases it has been problematic since other lysine residues are frequently used instead of the normal sites in the mutant proteins. More recently, mass spectrometry has been used successfully for site identification (e.g.,[33]). This involves the cleavage of modified proteins by trypsin or other suitable protease to release peptides from the target. This method is facilitated by having a protease cleavage site close to the C-terminal diglycine motif attached to the target, so that only a few extra amino acids remain attached to the modified site. Modification sites are thus detected by the identification of peptides that are increased in Mr by an amount dependent on the position of the cleavage site within the Ubl.

Figure 1. (See previous page). Formation of the 48S preinitiation complex. eIF1, 1A and 3 interact with the 40S ribosomal subunit. This then interacts with eIF5 and the ternary complex (eIF2-GTP-Met-tRNA) to form the 43S complex. In parallel, eIF4E and eIF4A are recruited by eIF4G to form the eIF4F complex. The availability of eIF4E is controlled by 4E-BP1, which in turn is regulated by phosphorylation by mTOR. The eIF4F complex binds to the cap on mRNA along with Poly(A)-binding protein (PABP) and eIF4B. PABP is regulated via interactions with 2 PABP proteins, PAIP1 and PAIP2. The 43S complex then binds close to the cap from where it can scan the mRNA for the start codon.

Downloaded by [2.101.165.190] at 09:47 17 January 2016

Downloaded by [2.101.165.190] at 09:47 17 January 2016

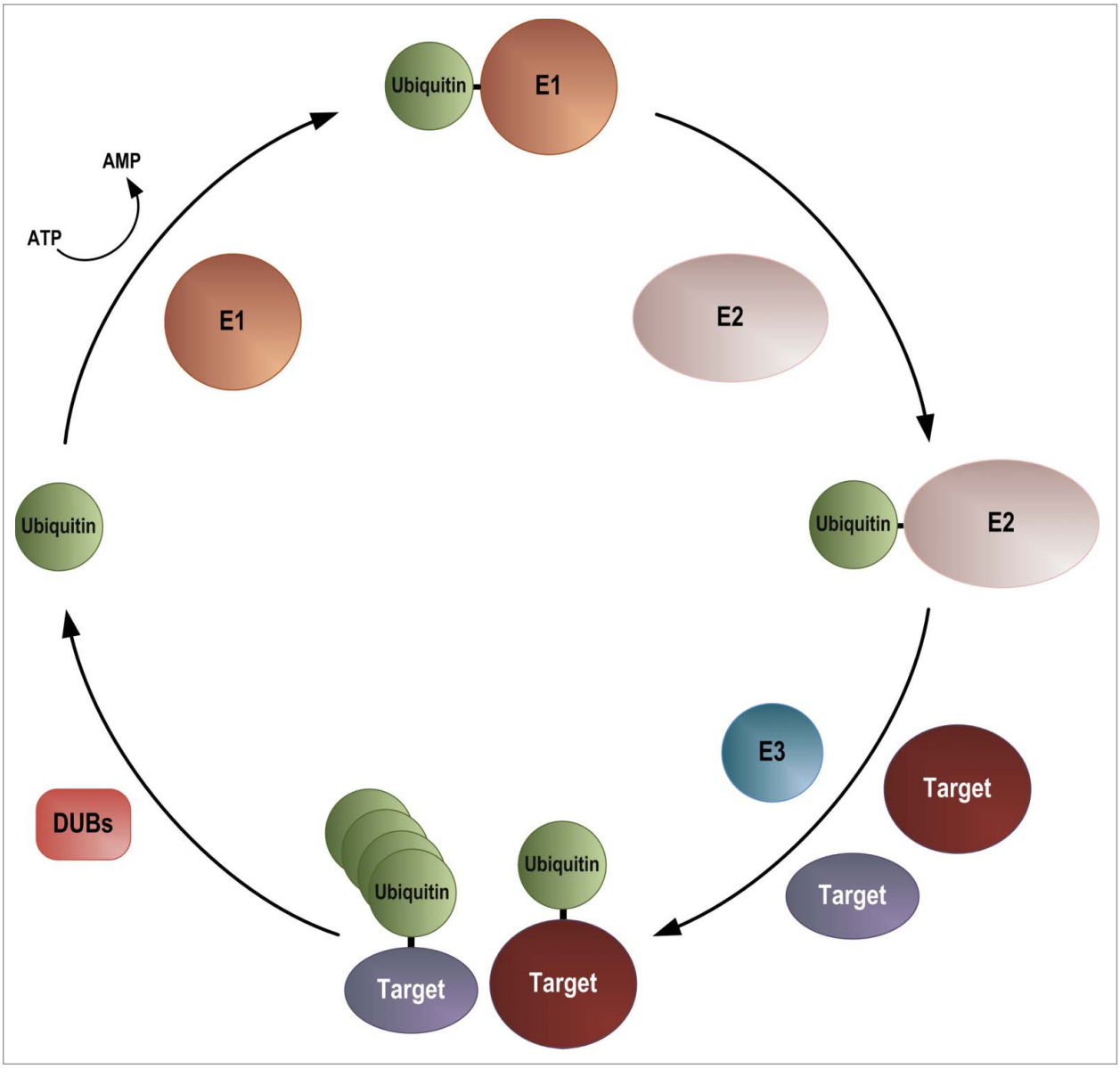

Figure 2. Ubiquitylation pathway. E1 = Ubiquitin activating enzyme, E2 = ubiquitin conjugating enzyme, E3 = ubiquitin ligase, DUB = deubiquitylating enzyme. Ubiquitin is activated by the formation of a ubiquitin-adenylate before forming a thioester bond with a cysteine residue in the E1 ubiquitin activating enzyme. Ubiquitin is passed to an E2 ubiquitin conjugating enzyme, again forming a thioester bond. Target proteins are recognized by E3 ubiquitin ligases, either directly or via an adaptor, and ubiquitin is attached via the formation of an ε-amino bond. Ubiquitin can be attached to target proteins either as a monomer, or in the form of ubiquitin chains. Ubiquitin can be removed from target proteins by the action of one of a number of DUBs.

Analysis of the role of the modifications is hampered by the fact that frequently, only low levels of modified forms are observed in cells. The reason for this could be that the modifications are transient, are labile, or as in the case of poly-ubiquitylation and poly-sumoylation, are targeting the protein for proteasome-mediated destruction. It is also possible that modification may be confined to target molecules in a particular cellular location. Additionally, it is proposed that this form of post-translational modification is not like modifications such as phosphorylation—i.e., an on/off switch. For example, in the case of SUMO, it is proposed that in some cases modification results in a change in conformation of the target protein that is maintained even after desumoylation occurs. Thus analysis of the roles of these modifications has lagged behind analysis of the function of other types of modifications.

Identification of the roles of the modifications has been undertaken, in the main using in vitro assays to look at relative binding abilities of wild type and unsumoylatable mutant proteins for their binding partners e.g.,[32] or by introduction of mutant coding sequences into cells to determine the effect of inability to modify a particular protein. This is relatively straightforward in yeast where a mutant copy can be integrated in the genome as

the sole copy of the coding sequence e.g.,[34] In mammalian cells, the mutant sequence can be introduced by transfection, but is dependent on having cells where the gene has been knocked out or where siRNA depletion is efficient. Depletion of the any of the enzymes in the conjugation pathway would be likely to affect multiple targets and would not be appropriate.

Role of Modification by Ubiquitin or Ubls in Translation Initiation Factors

A series of recent proteomic screens have identified numerous translation initiation factors that are modified by either ubiquitin or SUMO, or in many cases, by both (**Table 1**). Additionally, some of the screens have identified the lysine residues required for the modification. Early studies involved the overexpression of the modifier, but recently more refined methods using diGly capture techniques have been used to identify sites when the modifier is expressed at endogenous levels e.g.[35,36] These studies use mass spectrometry to identify diGly-modified peptides obtained by trypsin digestion of cellular proteins. A list of modified sites can be found at PhosphoSitePlus[37] (http://www.phosphosite.org/home). In many cases, individual lysine residues are identified as a single 'hit', making them less likely target sites than lysine residues that are highly represented, as for example is observed in eIF4A and eIF4G proteins.

More detailed studies on the role of modification of a number of the individual proteins by ubiquitin, SUMO and in one case, ISG15 have also been reported. We summarize here what is known about the roles of these post-translational modifications and how they might affect translation rates in mammalian cells.

eIF4E

Regulation of eIF4E levels is important for normal cell growth, as disruption of its expression or its over-production leads to aberrant cell growth or oncogenesis.[38] Additionally,

Downloaded by [2.101.165.190] at 09:47 17 January 2016

Table 1. Proteins identified in proteomic screens as being modified by ubiquitin or SUMO

Initiation factor	Ubiquitin	SUMO	Reference
eIF1A	Hs Ubiquitin*Mm Ubiquitin	Rn SUMO-3	35,36,58,59
eIF2A	Hs Ubiquitin*Mm Ubiquitin	Hs SUMO-2*At SUMO	35,55,59,80
eIF2α	Hs Ubiquitin*Mm Ubiquitin	Dm SUMO	36,56,59
eIF2B-β	Hs Ubiquitin*Mm Ubiquitin	Hs SUMO-1/2	36,59,81
eIF2β	Hs Ubiquitin*Mm Ubiquitin	At SUMO*Sc SUMO-1	36,59,80,82
eIF2 subunit 1	Hs Ubiquitin*Mm Ubiquitin	Rn SUMO-3	35,58,59
eIF2γ	Hs Ubiquitin*Mm Ubiquitin	Dm SUMO*Hs SUMO-1*Hs SUMO-2/3*Sc SUMO	35,36,56,57,59,82,83, *
eIF5B*	Hs Ubiquitin*Mm Ubiquitin	Hs SUMO-2*Hs SUMO-1*	55,59,61(A)
eIF3A	Hs Ubiquitin*Mm Ubiquitin*Rn Ubiquitin	Hs SUMO-2*Hs SUMO-1	36,55,59,61(B)*
eIF3B	Hs Ubiquitin*Mm Ubiquitin	Hs SUMO-2	35,55,59
eIF3C	Hs Ubiquitin*Mm Ubiquitin	Hs SUMO 1/2	35,59,81
eIF3D	Hs Ubiquitin*Mm Ubiquitin	Rn SUMO-3	35,58,59
eIF3E	Hs Ubiquitin*Mm Ubiquitin	Hs SUMO-1/2	35,59,81
eIF3F	Hs Ubiquitin*Mm Ubiquitin		59,74(C)
eIF3G	Hs Ubiquitin*Mm Ubiquitin		35,36,59
eIF3H	Hs Ubiquitin*Mm Ubiquitin*Rn Ubiquitin		35,36,59(D)*
eIF3I	Hs Ubiquitin	Sc SUMO*Hs SUMO-1/2	35,36,59,60,82–84
eIF3J	Hs Ubiquitin*Mm Ubiquitin		36,59
eIF3K	Hs Ubiquitin*Mm Ubiquitin		35,36*
eIF3L	Hs Ubiquitin*Mm Ubiquitin		35,59
eIF3M	Hs Ubiquitin*Mm Ubiquitin	Hs SUMO-1	35,59,83
eIF3X		Hs SUMO-2	55
eIF4A1	Hs Ubiquitin*Mm Ubiquitin*Rn Ubiquitin	Dm SUMO*Rn SUMO-3*Hs SUMO-1/2*At SUMO	35,36,55–62(D)
eIF4A2	Hs Ubiquitin*Mm Ubiquitin	Hs SUMO-1	35,59,61
eIF4E	Hs Ubiquitin*Mm Ubiquitin	Hs SUMO-1	36,46,59
eIF4GI	Hs Ubiquitin*Mm Ubiquitin	Hs SUMO-1/2	36,57,59,61
eIF4GII	Hs Ubiquitin		35
eIF4GIII	Hs Ubiquitin*Mm Ubiquitin		35,36
eIF5A	Hs Ubiquitin*Mm Ubiquitin*Rn Ubiquitin	Hs SUMO-1/2	35,59,83(D)
PABP1	Hs Ubiquitin*Mm Ubiquitin	Hs SUMO-2*Sc SUMO	35,55,57,59,85
PABP4	Hs Ubiquitin*Mm Ubiquitin	Hs SUMO-2	35,55,59

Hs: human, Rn: rat, Mm: mouse, Sc: *S. cerevisiae*, At: *Arabidospsis*. (A) (2010) CST Curation Set: 9913; Year: 2010; SILAC: N; Biosample/Treatment: AMO-1(cell line)/Velcade; Disease: -; Specificity of Antibody Used to Purify Peptides prior to MS2: anti-UbK Antibody Used to Purify Peptides prior to MS2: Ubiquitin (D4A7A10) XP(R) Rabbit mAb Cat#: 3925, PTMScan(R) Ubiquitin Branch Motif (K-e-GG) Immunoaffinity Beads Cat#: 1990. (B) (2008) CST Curation Set: 3970; Year: 2008; SILAC: N; Biosample/Treatment: brain(tissue)/untreated; Disease: -; Specificity of Antibody Used to Purify Peptides prior to MS2: anti-UbK. (C) (2009) CST Curation Set: 8668; Year: 2009; SILAC: N; Biosample/Treatment: RPMI-8266(cell line)/Velcade; Disease: -; Specificity of Antibody Used to Purify Peptides prior to MS2: anti-UbK Antibody Used to Purify Peptides prior to MS2: Ubiquitin (D4A7A10) XP(R) Rabbit mAb Cat#: 3925, PTMScan(R) Ubiquitin Branch Motif (K-e-GG) Immunoaffinity Beads Cat#: 1990. (D) (2007) CST Curation Set: 3578; Year: 2007; SILAC: N; Biosample/Treatment: brain(tissue)/ischemia and Reperfusion; Disease: -; Specificity of Antibody Used to Purify Peptides prior to MS2: anti-UbK.

eIF4E protein levels increase during differentiation e.g.,[39] eIF4E is both mono- and poly-ubiquitylated[40,41] and this has been demonstrated to occur mainly on K159.[40] This modification is enhanced by the E3 ubiquitin ligase, Chip (carboxy terminus of Hsp-70 interacting protein) which is known to have a role in regulating protein quality control.[42] A mutant form of eIF4E that is unable to interact with eIF4G or 4E-BP1 is more highly ubiquitylated than wild type eIF4E. This results in increased degradation by the proteasome of the mutant form, consistent with a role for ubiquitylation of eIF4E in a quality control process, removing inactive forms of the protein from the cell.[40] A role for ubiquitylation in quality control is supported by a number of observations. First, that binding of eIF4E to 4E-BP1 (eIF4E binding protein that is also regulated by ubiquitylation—see below) suppresses ubiquitylation and degradation and that only non-ubiquitylated eIF4E binds eIF4G. Second, overexpression of 4E-BP1 prevents ubiquitin-mediated degradation of eIF4E. Third, heat shock (45°C 10 min, conditions that would result in a degree of protein misfolding) also induces ubiquitylation of eIF4E, as does exposure to another form of stress, cadmium chloride.[41]

While poly-ubiquitylation clearly has a role in targeted destruction of eIF4E, little work has been performed to determine whether there is a different role for mono-ubiquitylation in regulating levels or subcellular localization of eIF4E. In contrast, the biological significance of eIF4E phosphorylation and its effect on translation have been studied over many years; however, the role of phosphorylation in modulating the activity of the protein is still not completely understood, although enhanced levels of eIF4E phosphorylation are associated with a number of human tumors.[43,44] Biophysical studies have suggested that phosphorylation of eIF4E decreases its affinity for the mRNA cap of mRNA, possibly allowing rapid recycling of eIF4E between competing mRNAs.[45] However, it has also been suggested that phosphorylation of S209 causes a retractable salt bridge to form with K159 (the ubiquitylation site) which leads to increased binding of capped mRNA.[40] Mutation of K159 to alanine but not arginine, reduces association with cap analogs, indicating that a positive charge is required at this position. Despite the fact that the K159R mutant cannot be ubiquitylated, it has been proposed that mono-ubiquitylation may stabilize the distance between S209 and K159, or that ubiquitin itself may form part of the bridge between S209 and K159.[40]

eIF4E is also modified by SUMO,[32,46] in a process that is promoted by HDAC2 (histone deacetylase 2).[46] Sumoylation occurs on several lysine residues, namely K36, 49, 162, 206 and 212. Interestingly, unlike what has been observed with a number of other proteins, such as IκBα and PCNA,[34,47] sumoylation and ubiquitylation of eIF4E do not occur on the same lysine residues. Sumoylation of eIF4E is dependent on phosphorylation, but the reverse is not true: inability to sumoylate eIF4E does not affect its ability to be phosphorylated.[32] Sumoylation results in the induction of translation of a subset of mRNAs required for cell proliferation and apoptosis. A mutant form of eIF4E that cannot be sumoylated is still able to bind m^7GTP, indicating that cap-binding is unaffected. However, compared with wild type protein, the mutant form binds significantly better to 4E-BP1 than it does to eIF4G, and is unable to form stable eIF4F complexes. It has been suggested that sumoylation induces a conformational change in eIF4E producing a change in interaction surfaces resulting in release from 4E-BP1 and promoting interaction with eIF4G. The inability of the mutant protein to be sumoylated results in an increase in the amount of eIF4E interacting with 4E-BP1.[32] While overexpression of wild type eIF4E in NIH-3T3 cells results in increased expression of eIF4E-regulated genes, this is not observed when unsumoylatable eIF4E is overexpressed.[32] At this time is unclear whether sumoylation of eIF4E has any effect of global rates of translation or rates of export of specific mRNAs from the nucleus.

4EHP

4EHP, also known as eIF4E2, binds to the m^7GTP cap in a manner similar to that of eIF4E. However, unlike eIF4E, it does not bind eIF4G and therefore does not allow ribosome recruitment. It thus competes with eIF4E for the mRNA and prevents translation.[48] It is targeted for ubiquitylation[49] and interestingly, also for modification with another Ubl, ISG15.[50] Curiously, the E3 ligase HHARI, which has recently been shown to be a marker of cellular proliferation,[51] stimulates both ubiquitylation and ISGylation of 4EHP.[49,50] Proteomic studies have identified K239 as a ubiquitylation site, but this has not been verified in a detailed study. In contrast, ISGylation, which occurs on K134 and K222, has been analyzed in some detail.[50] Binding studies indicate that ISGylated 4EHP has a higher affinity for m^7GTP than the unmodified form. It has been proposed that this modification is used by cells to inhibit translation of specific mRNAs in innate immune responses. Interestingly, despite its similarity to 4EHP, eIF4E is not ISGylated.

4E-BP Family

The eIF4E binding proteins (4E-BPs) are key regulators of protein synthesis.[1-3] As their name suggests, they function by interacting with eIF4E. This inhibits eIF4E function by preventing it from interacting with eIF4G to form the mature eIF4F complex. The 4E-BP proteins are phosphorylated following activation of mTORC1, in response to changes in growth conditions, and interaction of eIF4E with 4E-BP1 and -2 occurs with the hypophosphorylated form.[1-5] A key factor in the regulation of translation initiation is that the relative levels of eIF4E and 4E-BP1 and -2 are highly controlled.[52] The hypophosphorylated form, but not the hyperphosphorylated form, of 4E-BP1 is unstable if not bound to eIF4E. Under these conditions, 4E-BP1 is ubiquitylated and targeted for proteasome-mediated proteolysis.[52,53] The role of ubiquitylation was identified following some rather unexpected results obtained when knockdown of eIF4E using shRNA was demonstrated to have no effect on protein synthesis.[52] This was subsequently shown to be due to concomitant degradation of 4E-BP1, which resulted in the release of eIF4E molecules to compensate for the loss brought about by the reduced expression. K57, a lysine residue conserved between all 3 4E-BPs, was identified by the Sonenberg lab as the ubiquitylation site in 4E-BP1,[52] and a screen of an siRNA library identified the

Downloaded by [2.101.165.190] at 09:47 17 January 2016

KLHL25-CUL3 as the E3 ubiquitin ligase responsible for 4E-BP1 degradation. Knockdown of KLHL25 resulted in a decrease in translation, consistent with it having a role in controlling levels of 4E-BP1.[52]

Proteasome activity (presumed to be a result of poly-ubiquitylation) has also been demonstrated to be required for the formation of a truncated form of 4E-BP1 (tr4E-BP) in murine erythroleukemia (MEL) cells containing activated p53.[54] This truncated form is 3 kDa smaller than full-length protein, is unphosphorylated and relatively stable. It also binds to eIF4E in preference to the full-length protein. It has been proposed that the production of this p53-induced form may be contributing to the ability of p53 to regulate apoptosis and malignancy.

eIF4A

Two isoforms of eIF4A have been identified in proteomic screens as being modified by ubiquitin and SUMO.[35,36,55-62] In contrast to what is observed with some of the other initiation factors, modified peptides from both eIF4A1 and eIF4A2 are highly abundant in the proteomic screens designed to identify ubiquitylation sites, implying that modification is likely to have a key role (s) in the regulation of the function of these 2 proteins. In the ubiquitin screens, most of the modified sites identified in the human eIF4A proteins were also observed in the mouse proteins, suggesting that they are likely to be true 'hits' and not false positives. Interestingly, eIF4A2 (but not eIF4A1) and translational repression have both been shown to be essential for miRNA-mediated gene regulation.[63] However, the post-translational modification of these proteins by ubiquitin or Ubls has not been analyzed in detail and to date there are no reports on whether it affects the activity of the eIF4A protein or miRNA-mediated translational control.

In a role unrelated to its function in translation, ubiquitylation of *Drosophila* eIF4A has been shown to be linked with Decapentaplegic (Dpp) signaling.[64] Additionally, rice DRM2 (required for RNA-directed DNA methylation) interacts with eIF4A via its ubiquitin associated (UBA) domain, (although whether this occurs with a ubiquitylated form has not been analyzed).[65]

eIF4G

There are 3 isoforms of the scaffold protein, eIF4G, eIF4GI-III. As observed with eIF4A, diGly-modified peptides from these proteins are abundant in proteomic screens designed to identify ubiquitylation sites,[35,36,57,59,61] and again most are observed in both the human and mouse proteins. In eIF4GI these sites (6 in total, 4 common to both human and mouse) map to lysine residues occurring between amino acids 593–925 which map close to, or in the region of, the eIF4E and eIF4A/3 binding sites. The abundance of these modified tryptic fragments and their position in the protein suggests that this post-translational modification is likely to be important for regulating the functions of these proteins, possibly by affecting the interaction of eIF4G with other members of the eIF4F complex. Again, these modifications have not been analyzed in detail and to date there are no reports on whether they affect the activity of eIF4GI. In addition to this modification by ubiquitin, eIF4GI has been shown to be sumoylated in both fission yeast and human cells.[66] Sumoylation of *S. pombe* eIF4G is increased following exposure of cells to 1 M KCl or arsenite, conditions which result in the formation of stress granules. In vitro sumoylation studies have identified 2 sumoylation sites in mammalian eIF4GI, K1368 and K1588, residing in the eIF3/4A binding site and the Mnk-binding domain, respectively. (Mnks (MAP kinase-interacting kinases) are kinases which bind to the C-terminus of eIF4G and phosphorylate eIF4E which is bound to the N-terminus of eIF4G.[67]) These data suggest that sumoylation may be affecting interactions of eIF4GI with associated proteins, e.g., eIF4E, and possibly the assembly of eIF4G into stress granules.

Paip2

Poly(A)-binding protein (PABP) is regulated through the interaction with 2 proteins, Paip1 and Paip2.[5,6] Paip1, which also interacts with eIF3g, is eIF4G-like and is stimulatory for translation, while Paip2 represses PABP function by decreasing the affinity of PABP for polyadenylated mRNA, thus inhibiting translation. Paip1 and Paip2 both have 2 domains, PAM1 and PAM2 which interact with PABP. This interaction occurs through RRM-1 and PABC domains, respectively.[68] Additionally, PAM2 is capable of interacting with EDD (a member of the HECT domain family of E3 ubiquitin ligases) which also contains a PABC domain.[69] In cells where levels of PABP are depleted, Paip2A is ubiquitylated in an EDD-dependent manner prior to proteasome-mediated degradation.[70] Interestingly, the affinity of the PAM2 domain of Paip2 for the PABC domain of PABP is greater than that of the affinity for the PABC of EDD. Thus, it is proposed that interaction of PABP with Paip2 competes with EDD for interaction with PAM2 on Paip2, and that this normally prevents ubiquitylation of Paip2.[70] However, in apparently contradictory work, it has been demonstrated that during human cytomegalovirus infection PABP levels rise concomitantly with the levels of both Paip2 and EDD1. The reason for this is not known, but it has been proposed that it may provide cells with a process to allow rapid changes in protein levels if necessary.[71] Paip2B is also polyubiquitylated, although at a somewhat lower level that Paip2, and is hence more stable.[72]

eIF3

Proteomic studies have identified many of the eIF3 subunits as targets for ubiquitylation and/or sumoylation. However, independent of these studies, eIF3f is the only eIF3 subunit where the function of these modifications has been studied in any detail. eIF3f is a non-core subunit of the eIF3 complex. It can act both as a repressor and as an enhancer of translation (reviewed in[73]). Its role as a translational enhancer came to light in a study on muscle atrophy.[74] Here, eIF3f is ubiquitylated by the MAFbnx/Atrogin1 protein which is a muscle-specific F-box protein ubiquitin E3 ligase.[75] This E3 is upregulated and essential for accelerated muscle protein loss in a number of disorders.[76] Ubiquitylation of eIF3f occurs on multiple (6) lysines in the C-terminus[74] and results in its ubiquitin-mediated proteolysis in myotubes undergoing atrophy. Under these conditions both

Downloaded by [2.101.165.190] at 09:47 17 January 2016

MAFbnx and eIF3f are detected in the nucleus.[75] It has been proposed that this ubiquitylation may be associated with the rapid downregulation of certain proteins during muscle atrophy. eIF3f also interacts with the ubiquitin E3 ligase TRC8 to inhibit protein synthesis. The mechanism by which this occurs is unknown, but it has been proposed that TRC8 targets an eIF3 subunit for ubiquitylation.[77] Unrelated to its role in translation, eIF3f can act as a deubiquitylating enzyme (DUB). In this capacity it is capable of deubiquitylating, and thus contributing to the activation of, the Notch signaling receptor in *Drosophila*.[78]

Interestingly, recent work has shown that eIF3e is involved in eIF4E phosphorylation; Mnk1 binding to eIF4F is dependent on eIF3e, and eIF3e is sufficient to promote Mnk1-binding to eIF4G.[79] As eIF3e is modified by both ubiquitylation and sumoylation, it would be interesting to know if these modifications of eIF3e also have a role in controlling eIF4E phosphorylation.

Summary

In conclusion, despite the fact that numerous translation initiation factors have been shown to be ubiquitylated and/or sumoylated in proteomic screens, relatively little is known about the effects of the modifications on the functions of individual proteins. In part this is due to the transient nature of these modifications, e.g., in many cases of sumoylation, less than 5% of a particular protein is modified at any one time, and the sumoylated species appear to be very labile in certain organisms due to highly active SUMO-specific proteases. Additionally, since ubiquitylation targets proteins for destruction, analysis of ubiquitylated proteins, other than in the presence of a proteasome inhibitor, is difficult.

The recent use of proteomic screens to identify modified proteins and the modified site(s) suggests that there are many more cases where post-translational modification by ubiquitin or Ubls is likely to affect translation initiation factors. For example, sumoylation of eIF4A1/2 might have a role in regulating both the unwinding of mRNA secondary structure and the ability of eIF4A2 to mediate miRNA-dependent gene expression in mammalian cells. Further work on these modifications is required to fully elucidate their effect on individual proteins and on translational control of gene expression as a whole.

Disclosure of Potential Conflicts of Interest

No potential conflicts of interest were disclosed.

References

1. Sonenberg N, Hinnebusch AG. Regulation of translation initiation in eukaryotes: mechanisms and biological targets. Cell 2009; 136:731-45; PMID:19239892; http://dx.doi.org/10.1016/j.cell.2009.01.042
2. Morley SJ, Coldwell MJ, Clemens MJ. Initiation factor modifications in the preapoptotic phase. Cell Death Differ 2005; 12:571-84; PMID:15900314; http://dx.doi.org/10.1038/sj.cdd.4401591
3. Jackson RJ, Hellen CU, Pestova TV. The mechanism of eukaryotic translation initiation and principles of its regulation. Nat Rev Mol Cell Biol 2010; 11:113-27; PMID:20094052; http://dx.doi.org/10.1038/nrm2838
4. Laplante M, Sabatini DM. mTOR signaling in growth control and disease. Cell 2012; 149:274-93; PMID:22500797; http://dx.doi.org/10.1016/j.cell.2012.03.017
5. Craig AW, Haghighat A, Yu AT, Sonenberg N. Interaction of polyadenylate-binding protein with the eIF4G homologue PAIP enhances translation. Nature 1998; 392:520-3; PMID:9548260; http://dx.doi.org/10.1038/33198
6. Khaleghpour K, Svitkin YV, Craig AW, DeMaria CT, Deo RC, Burley SK, Sonenberg N. Translational repression by a novel partner of human poly(A) binding protein, Paip2. Mol Cell 2001; 7:205-16; PMID:11172725; http://dx.doi.org/10.1016/S1097-2765(01)00168-X
7. Li Q, Imataka H, Morino S, Rogers GW Jr., Richter-Cook NJ, Merrick WC, Sonenberg N. Eukaryotic translation initiation factor 4AIII (eIF4AIII) is functionally distinct from eIF4AI and eIF4AII. Mol Cell Biol 1999; 19:7336-46; PMID:10523622
8. Gorgoni B, Richardson WA, Burgess HM, Anderson RC, Wilkie GS, Gautier P, Martins JP, Brook M, Sheets MD, Gray NK. Poly(A)-binding proteins are functionally distinct and have essential roles during vertebrate development. Proc Natl Acad Sci U S A 2011; 108:7844-9; PMID:21518916; http://dx.doi.org/10.1073/pnas.1017664108
9. Sun F, Palmer K, Handel MA. Mutation of Eif4g3, encoding a eukaryotic translation initiation factor, causes male infertility and meiotic arrest of mouse spermatocytes. Development 2010; 137:1699-707; PMID:20430745; http://dx.doi.org/10.1242/dev.043125
10. Burroughs AM, Iyer LM, Aravind L. Structure and evolution of ubiquitin and ubiquitin-related domains. Methods Mol Biol 2012; 832:15-63; PMID:22350875; http://dx.doi.org/10.1007/978-1-61779-474-2_2
11. Ulrich HD. The SUMO system: an overview. Methods Mol Biol 2009; 497:3-16; PMID:19107407; http://dx.doi.org/10.1007/978-1-59745-566-4_1
12. Bogunovic D, Boisson-Dupuis S, Casanova JL. ISG15: leading a double life as a secreted molecule. Exp Mol Med 2013; 45:e18; PMID:23579383; http://dx.doi.org/10.1038/emm.2013.36
13. Reich N, Evans B, Levy D, Fahey D, Knight E Jr, Darnell JE Jr. Interferon-induced transcription of a gene encoding a 15-kDa protein depends on an upstream enhancer element. Proc Natl Acad Sci U S A 1987; 84:6394-8; PMID:3476954; http://dx.doi.org/10.1073/pnas.84.18.6394
14. Liu M, Reimschuessel R, Hassel BA. Molecular cloning of the fish interferon stimulated gene, 15 kDa (ISG15) orthologue: a ubiquitin-like gene induced by nephrotoxic damage. Gene 2002; 298:129-39; PMID:12426101; http://dx.doi.org/10.1016/S0378-1119(02)00932-0
15. Hershko A, Ciechanover A. The ubiquitin system. Annu Rev Biochem 1998; 67:425-79; PMID:9759494; http://dx.doi.org/10.1146/annurev.biochem.67.1.425
16. Lorenz S, Cantor AJ, Rape M, Kuriyan J. Macromolecular juggling by ubiquitylation enzymes. BMC Biol 2013; 11:65; PMID:23800009; http://dx.doi.org/10.1186/1741-7007-11-65
17. Pickart CM, Fushman D. Polyubiquitin chains: polymeric protein signals. Curr Opin Chem Biol 2004; 8:610-6; PMID:15556404; http://dx.doi.org/10.1016/j.cbpa.2004.09.009
18. Wickliffe KE, Williamson A, Meyer HJ, Kelly A, Rape M. K11-linked ubiquitin chains as novel regulators of cell division. Trends Cell Biol 2011; 21:656-63; PMID:21978762; http://dx.doi.org/10.1016/j.tcb.2011.08.008
19. Ciechanover A, Stanhill A. The complexity of recognition of ubiquitinated substrates by the 26S proteasome. Biochim Biophys Acta 2014; 1843:86-96; PMID:23872423; http://dx.doi.org/10.1016/j.bbamcr.2013.07.007
20. Ulrich HD. How to activate a damage-tolerant polymerase: consequences of PCNA modifications by ubiquitin and SUMO. Cell Cycle 2004; 3:15-8; PMID:14657656; http://dx.doi.org/10.4161/cc.3.1.623
21. Tomanov K, Luschnig C, Bachmair A. Ubiquitin Lys 63 chains - second-most abundant, but poorly understood in plants. Front Plant Sci 2014; 5:15; PMID:24550925; http://dx.doi.org/10.3389/fpls.2014.00015
22. Knipscheer P, Flotho A, Klug H, Olsen JV, van Dijk WJ, Fish A, Johnson ES, Mann M, Sixma TK, Pichler A. Ubc9 sumoylation regulates SUMO target discrimination. Mol Cell 2008; 31:371-82; PMID:18691969; http://dx.doi.org/10.1016/j.molcel.2008.05.022
23. Pfander B, Moldovan GL, Sacher M, Hoege C, Jentsch S. SUMO-modified PCNA recruits Srs2 to prevent recombination during S phase. Nature 2005; 436:428-33; PMID:15931174
24. Papouli E, Chen S, Davies AA, Huttner D, Krejci L, Sung P, Ulrich HD. Crosstalk between SUMO and ubiquitin on PCNA is mediated by recruitment of the helicase Srs2p. Mol Cell 2005; 19:123-33; PMID:15989970; http://dx.doi.org/10.1016/j.molcel.2005.06.001
25. Hardeland U, Steinacher R, Jiricny J, Schär P. Modification of the human thymine-DNA glycosylase by ubiquitin-like proteins facilitates enzymatic turnover. EMBO J 2002; 21:1456-64; PMID:11889051; http://dx.doi.org/10.1093/emboj/21.6.1456
26. Joseph J, Tan SH, Karpova TS, McNally JG, Dasso M. SUMO-1 targets RanGAP1 to kinetochores and mitotic spindles. J Cell Biol 2002; 156:595-602; PMID:11854305; http://dx.doi.org/10.1083/jcb.200110109
27. Sriramachandran AM, Dohmen RJ. SUMO-targeted ubiquitin ligases. Biochim Biophys Acta 2014; 1843:75-85; PMID:24018209; http://dx.doi.org/10.1016/j.bbamcr.2013.08.022

Downloaded by [2.101.165.190] at 09:47 17 January 2016

Downloaded by [2.101.165.190] at 09:47 17 January 2016

28. van der Veen AG, Ploegh HL. Ubiquitin-like proteins. Annu Rev Biochem 2012; 81:323-57; PMID:22404627; http://dx.doi.org/10.1146/annurev-biochem-093010-153308
29. Jeon YJ, Yoo HM, Chung CH. ISG15 and immune diseases. Biochim Biophys Acta 2010; 1802:485-96; PMID:20153823; http://dx.doi.org/10.1016/j.bbadis.2010.02.006
30. Zou W, Zhang DE. The interferon-inducible ubiquitin-protein isopeptide ligase (E3) EFP also functions as an ISG15 E3 ligase. J Biol Chem 2006; 281:3989-94; PMID:16352599; http://dx.doi.org/10.1074/jbc.M510787200
31. Dao CT, Zhang DE. ISG15: a ubiquitin-like enigma. Front Biosci: J Virtual Libr 2005; 10:2701-22; PMID:15970528
32. Xu X, Vatsyayan J, Gao C, Bakkenist CJ, Hu J. Sumoylation of eIF4E activates mRNA translation. EMBO Rep 2010; 11:299-304; PMID:20224576; http://dx.doi.org/10.1038/embor.2010.18
33. Plant LD, Dementieva IS, Kollewe A, Olikara S, Marks JD, Goldstein SA. One SUMO is sufficient to silence the dimeric potassium channel K2P1. Proc Natl Acad Sci U S A 2010; 107:10743-8; PMID:20498050; http://dx.doi.org/10.1073/pnas.1004712107
34. Stelter P, Ulrich HD. Control of spontaneous and damage-induced mutagenesis by SUMO and ubiquitin conjugation. Nature 2003; 425:188-91; PMID:12968183; http://dx.doi.org/10.1038/nature01965
35. Kim W, Bennett EJ, Huttlin EL, Guo A, Li J, Possemato A, Sowa ME, Rad R, Rush J, Comb MJ, et al. Systematic and quantitative assessment of the ubiquitin-modified proteome. Mol Cell 2011; 44:325-40; PMID:21906983; http://dx.doi.org/10.1016/j.molcel.2011.08.025
36. Wagner SA, Beli P, Weinert BT, Nielsen ML, Cox J, Mann M, Choudhary C. A proteome-wide, quantitative survey of in vivo ubiquitylation sites reveals widespread regulatory roles. Mol Cell Proteomics: MCP 2011; 10(10):M111 013284; PMID:21890473; http://dx.doi.org/10.1074/mcp.M111.013284
37. Hornbeck PV, Kornhauser JM, Tkachev S, Zhang B, Skrzypek E, Murray B, Latham V, Sullivan M. PhosphoSitePlus: a comprehensive resource for investigating the structure and function of experimentally determined post-translational modifications in man and mouse. Nucleic Acids Res 2012; 40:D261-70; PMID:22135298; http://dx.doi.org/10.1093/nar/gkr1122
38. Mamane Y, Petroulakis E, LeBacquer O, Sonenberg N. mTOR, translation initiation and cancer. Oncogene 2006; 25:6416-22; PMID:17041626; http://dx.doi.org/10.1038/sj.onc.1209888
39. Walsh D, Meleady P, Power B, Morley SJ, Clynes M. Increased levels of the translation initiation factor eIF4E in differentiating epithelial lung tumor cell lines. Differentiation; Res Biol Diversity 2003; 71(2):126-34; PMID:12641566
40. Murata T, Shimotohno K. Ubiquitination and proteasome-dependent degradation of human eukaryotic translation initiation factor 4E. J Biol Chem 2006; 281:20788-800; PMID:16720573; http://dx.doi.org/10.1074/jbc.M600563200
41. Othumpangat S, Kashon M, Joseph P. Sodium arsenite-induced inhibition of eukaryotic translation initiation factor 4E (eIF4E) results in cytotoxicity and cell death. Mol Cell Biochem 2005; 279:123-31; PMID:16283521; http://dx.doi.org/10.1007/s11010-005-8284-2
42. Qian SB, McDonough H, Boellmann F, Cyr DM, Patterson C. CHIP-mediated stress recovery by sequential ubiquitination of substrates and Hsp70. Nature 2006; 440:551-5; PMID:16554822; http://dx.doi.org/10.1038/nature04600
43. Lee T, Pelletier J. Eukaryotic initiation factor 4F: a vulnerability of tumor cells. Future Med Chem 2012; 4:19-31; PMID:22168162; http://dx.doi.org/10.4155/fmc.11.150
44. McKendrick L, Morley SJ, Pain VM, Jagus R, Joshi B. Phosphorylation of eukaryotic initiation factor 4E (eIF4E) at Ser209 is not required for protein synthesis in vitro and in vivo. Eur J Biochem 2001; 268:5375-85; PMID:11606200; http://dx.doi.org/10.1046/j.0014-2956.2001.02478.x
45. Scheper GC, van Kollenburg B, Hu J, Luo Y, Goss DJ, Proud CG. Phosphorylation of eukaryotic initiation factor 4E markedly reduces its affinity for capped mRNA. J Biol Chem 2002; 277:3303-9; PMID:11723111; http://dx.doi.org/10.1074/jbc.M103607200
46. Xu X, Vatsyayan J, Gao C, Bakkenist CJ, Hu J. HDAC2 promotes eIF4E sumoylation and activates mRNA translation gene specifically. J Biol Chem 2010; 285:18139-43; PMID:20421305; http://dx.doi.org/10.1074/jbc.C110.131599
47. Desterro JM, Rodriguez MS, Hay RT. SUMO-1 modification of IkappaBalpha inhibits NF-kappaB activation. Mol Cell 1998; 2:233-9; PMID:9734360; http://dx.doi.org/10.1016/S1097-2765(00)80133-1
48. Rom E, Kim HC, Gingras AC, Marcotrigiano J, Favre D, Olsen H, Burley SK, Sonenberg N. Cloning and characterization of 4EHP, a novel mammalian eIF4E-related cap-binding protein. J Biol Chem 1998; 273:13104-9; PMID:9582349; http://dx.doi.org/10.1074/jbc.273.21.13104
49. Tan NG, Ardley HC, Scott GB, Rose SA, Markham AF, Robinson PA. Human homologue of ariadne promotes the ubiquitylation of translation initiation factor 4E homologous protein, 4EHP. FEBS Lett 2003; 554:501-4; PMID:14623119; http://dx.doi.org/10.1016/S0014-5793(03)01235-3
50. Okumura F, Zou W, Zhang DE. ISG15 modification of the eIF4E cognate 4EHP enhances cap structure-binding activity of 4EHP. Genes Dev 2007; 21:255-60; PMID:17289916; http://dx.doi.org/10.1101/gad.1521607
51. Elmehdawi F, Wheway G, Szymanska K, Adams M, High AS, Johnson CA, Robinson PA. Human Homolog of Drosophila Ariadne (HHARI) is a marker of cellular proliferation associated with nuclear bodies. Exp Cell Res 2013; 319:161-72; PMID:23059369; http://dx.doi.org/10.1016/j.yexcr.2012.10.002
52. Yanagiya A, Suyama E, Adachi H, Svitkin YV, Aza-Blanc P, Imataka H, Mikami S, Martineau Y, Ronai ZA, Sonenberg N. Translational homeostasis via the mRNA cap-binding protein, eIF4E. Mol Cell 2012; 46:847-58; PMID:22578813; http://dx.doi.org/10.1016/j.molcel.2012.04.004
53. Elia A, Constantinou C, Clemens MJ. Effects of protein phosphorylation on ubiquitination and stability of the translational inhibitor protein 4E-BP1. Oncogene 2008; 27:811-22; PMID:17653084; http://dx.doi.org/10.1038/sj.onc.1210678
54. Constantinou C, Elia A, Clemens MJ. Activation of p53 stimulates proteasome-dependent truncation of eIF4E-binding protein 1 (4E-BP1). Biol Cell / Under Auspices Eur Cell Biol Organ, 2008; 100(5):279-89; PMID:18021075
55. Blomster HA, Hietakangas V, Wu J, Kouvonen P, Hautaniemi S, Sistonen L. Novel proteomics strategy brings insight into the prevalence of SUMO-2 target sites. Mol Cell Proteomics 2009; 8:1382-90; PMID:19240082; http://dx.doi.org/10.1074/mcp.M800551-MCP200
56. Nie M, Xie Y, Loo JA, Courey AJ. Genetic and proteomic evidence for roles of Drosophila SUMO in cell cycle control, Ras signaling, and early pattern formation. PLoS One 2009; 4:e5905; PMID:19529778; http://dx.doi.org/10.1371/journal.pone.0005905
57. Bruderer R, Tatham MH, Plechanovova A, Matic I, Garg AK, Hay RT. Purification and identification of endogenous polySUMO conjugates. EMBO Rep 2011; 12:142-8; PMID:21252943; http://dx.doi.org/10.1038/embor.2010.206
58. Yang W, Thompson JW, Wang Z, Wang L, Sheng H, Foster MW, Moseley MA, Paschen W. Analysis of oxygen/glucose-deprivation-induced changes in SUMO3 conjugation using SILAC-based quantitative proteomics. J Proteome Res 2012; 11:1108-17; PMID:22082260; http://dx.doi.org/10.1021/pr200834f
59. Wagner SA, Beli P, Weinert BT, Schölz C, Kelstrup CD, Young C, Nielsen ML, Olsen JV, Brakebusch C, Choudhary C. Proteomic analyses reveal divergent ubiquitylation site patterns in murine tissues. Mol Cell Proteomics 2012; 11:1578-85; PMID:22790023; http://dx.doi.org/10.1074/mcp.M112.017905
60. Shi Y, Chan DW, Jung SY, Malovannaya A, Wang Y, Qin J. A data set of human endogenous protein ubiquitination sites. Mol Cell Proteomics: MCP 2011; 10(5):M110 002089; PMID:20972266; http://dx.doi.org/10.1074/mcp.M110.002089
61. Matafora V, D'Amato A, Mori S, Blasi F, Bachi A. Proteomics analysis of nucleolar SUMO-1 target proteins upon proteasome inhibition. Mol Cell Proteomics 2009; 8:2243-55; PMID:19596686; http://dx.doi.org/10.1074/mcp.M900079-MCP200
62. Mazur MJ, van den Burg HA. Global SUMO Proteome Responses Guide Gene Regulation, mRNA Biogenesis, and Plant Stress Responses. Front Plant Sci 2012; 3:215; PMID:23060889; http://dx.doi.org/10.3389/fpls.2012.00215
63. Meijer HA, Kong YW, Lu WT, Wilczynska A, Spriggs RV, Robinson SW, Godfrey JD, Willis AE, Bushell M. Translational repression and eIF4A2 activity are critical for microRNA-mediated gene regulation. Science 2013; 340:82-5; PMID:23559250; http://dx.doi.org/10.1126/science.1231197
64. Li J, Li WX. A novel function of Drosophila eIF4A as a negative regulator of Dpp/BMP signalling that mediates SMAD degradation. Nat Cell Biol 2006; 8:1407-14; PMID:17115029; http://dx.doi.org/10.1038/ncb1506
65. Dangwal M, Malik G, Kapoor S, Kapoor M. De novo methyltransferase, OsDRM2, interacts with the ATP-dependent RNA helicase, OseIF4A, in rice. J Mol Biol 2013; 425:2853-66; PMID:23732981; http://dx.doi.org/10.1016/j.jmb.2013.05.021
66. Jongjitwimol. The S. pombe translation initiation factor eIF4G is sumoylated and assocaites with the SUMO protease Ulp2. PLoS ONE 2014; 40.
67. Buxade M, Parra-Palau JL, Proud CG. The Mnks: MAP kinase-interacting kinases (MAP kinase signal-integrating kinases). Front Biosci 2008; 13:5359-73; PMID:18508592; http://dx.doi.org/10.2741/3086
68. Khaleghpour K, Kahvejian A, De Crescenzo G, Roy G, Svitkin YV, Imataka H, O'Connor-McCourt M, Sonenberg N. Dual interactions of the translational repressor Paip2 with poly(A) binding protein. Mol Cell Biol 2001; 21:5200-13; PMID:11438674; http://dx.doi.org/10.1128/MCB.21.15.5200-5213.2001
69. Deo RC, Sonenberg N, Burley SK. X-ray structure of the human hyperplastic discs protein: an ortholog of the C-terminal domain of poly(A)-binding protein. Proc Natl Acad Sci U S A 2001; 98:4414-9; PMID:11287654; http://dx.doi.org/10.1073/pnas.071552198
70. Yoshida M, Yoshida K, Kozlov G, Lim NS, De Crescenzo G, Pang Z, Berlanga JJ, Kahvejian A, Gehring K, Wing SS, et al. Poly(A) binding protein (PABP) homeostasis is mediated by the stability of its inhibitor, Paip2. EMBO J 2006; 25:1934-44; PMID:16601676; http://dx.doi.org/10.1038/sj.emboj.7601079
71. McKinney C, Yu D, Mohr I. A new role for the cellular PABP repressor Paip2 as an innate restriction factor capable of limiting productive cytomegalovirus replication. Genes Dev 2013; 27:1809-20; PMID:23964095; http://dx.doi.org/10.1101/gad.221341.113
72. Berlanga JJ, Baass A, Sonenberg N. Regulation of poly (A) binding protein function in translation: characterization of the Paip2 homolog, Paip2B. RNA 2006; 12:1556-68; PMID:16804161; http://dx.doi.org/10.1261/rna.106506
73. Marchione R, Leibovitch SA, Lenormand JL. The translational factor eIF3f: the ambivalent eIF3

subunit. Cell Mol Life Sci 2013; 70:3603-16; PMID:23354061; http://dx.doi.org/10.1007/s00018-013-1263-y
74. Csibi A, Leibovitch MP, Cornille K, Tintignac LA, Leibovitch SA. MAFbx/Atrogin-1 controls the activity of the initiation factor eIF3-f in skeletal muscle atrophy by targeting multiple C-terminal lysines. J Biol Chem 2009; 284:4413-21; PMID:19073596; http://dx.doi.org/10.1074/jbc.M807641200
75. Lagirand-Cantaloube J, Offner N, Csibi A, Leibovitch MP, Batonnet-Pichon S, Tintignac LA, Segura CT, Leibovitch SA. The initiation factor eIF3-f is a major target for atrogin1/MAFbx function in skeletal muscle atrophy. EMBO J 2008; 27:1266-76; PMID:18354498; http://dx.doi.org/10.1038/emboj.2008.52
76. Sacheck, JM, Hyatt JP, Raffaello A, Jagoe RT, Roy RR, Edgerton VR, Lecker SH, Goldberg AL. Rapid disuse and denervation atrophy involve transcriptional changes similar to those of muscle wasting during systemic diseases. FASEB J: Off Publ Fed Am Soc Exp Biol 2007; 21(1):140-55; PMID:17116744
77. Lee JP, Brauweiler A, Rudolph M, Hooper JE, Drabkin HA, Gemmill RM. The TRC8 ubiquitin ligase is sterol regulated and interacts with lipid and protein biosynthetic pathways. Mol Cancer Res 2010; 8:93-106; PMID:20068067; http://dx.doi.org/10.1158/1541-7786.MCR-08-0491
78. Moretti J, Chastagner P, Gastaldello S, Heuss SF, Dirac AM, Bernards R, Masucci MG, Israël A, Brou C. The translation initiation factor 3f (eIF3f) exhibits a deubiquitinase activity regulating Notch activation. PLoS Biol 2010; 8:e1000545; PMID:21124883; http://dx.doi.org/10.1371/journal.pbio.1000545
79. Walsh D, Mohr I. Coupling 40S ribosome recruitment to modification of a cap-binding initiation factor by eIF3 subunit e. Genes Dev 2014; 28:835-40; PMID:24736843; http://dx.doi.org/10.1101/gad.236752.113
80. Miller MJ, Barrett-Wilt GA, Hua Z, Vierstra RD. Proteomic analyses identify a diverse array of nuclear processes affected by small ubiquitin-like modifier conjugation in Arabidopsis. Proc Natl Acad Sci U S A 2010; 107:16512-7; PMID:20813957; http://dx.doi.org/10.1073/pnas.1004181107
81. Westman BJ, Verheggen C, Hutten S, Lam YW, Bertrand E, Lamond AI. A proteomic screen for nucleolar SUMO targets shows SUMOylation modulates the function of Nop5/Nop58. Mol Cell 2010; 39:618-31; PMID:20797632; http://dx.doi.org/10.1016/j.molcel.2010.07.025
82. Panse VG, Hardeland U, Werner T, Kuster B, Hurt E. A proteome-wide approach identifies sumoylated substrate proteins in yeast. J Biol Chem 2004; 279:41346-51; PMID:15292183; http://dx.doi.org/10.1074/jbc.M407950200
83. Becker J, Barysch SV, Karaca S, Dittner C, Hsiao HH, Berriel Diaz M, Herzig S, Urlaub H, Melchior F. Detecting endogenous SUMO targets in mammalian cells and tissues. Nat Struct Mol Biol 2013; 20:525-31; PMID:23503365; http://dx.doi.org/10.1038/nsmb.2526
84. Danielsen JM, Sylvestersen KB, Bekker-Jensen S, Szklarczyk D, Poulsen JW, Horn H, Jensen LJ, Mailand N, Nielsen ML, Mass spectrometric analysis of lysine ubiquitylation reveals promiscuity at site level. Mol Cell Proteomics: MCP 2011; 10(3):M110 003590; PMID:21139048; http://dx.doi.org/10.1074/mcp.M110.003590
85. Hannich JT, Lewis A, Kroetz MB, Li SJ, Heide H, Emili A, Hochstrasser M. Defining the SUMO-modified proteome by multiple approaches in Saccharomyces cerevisiae. J Biol Chem 2005; 280:4102-10; PMID:15590687; http://dx.doi.org/10.1074/jbc.M413209200

Downloaded by [2.101.165.190] at 09:47 17 January 2016

Cell Reports

Report

ATM Localization and Heterochromatin Repair Depend on Direct Interaction of the 53BP1-BRCT$_2$ Domain with γH2AX

Graphical Abstract

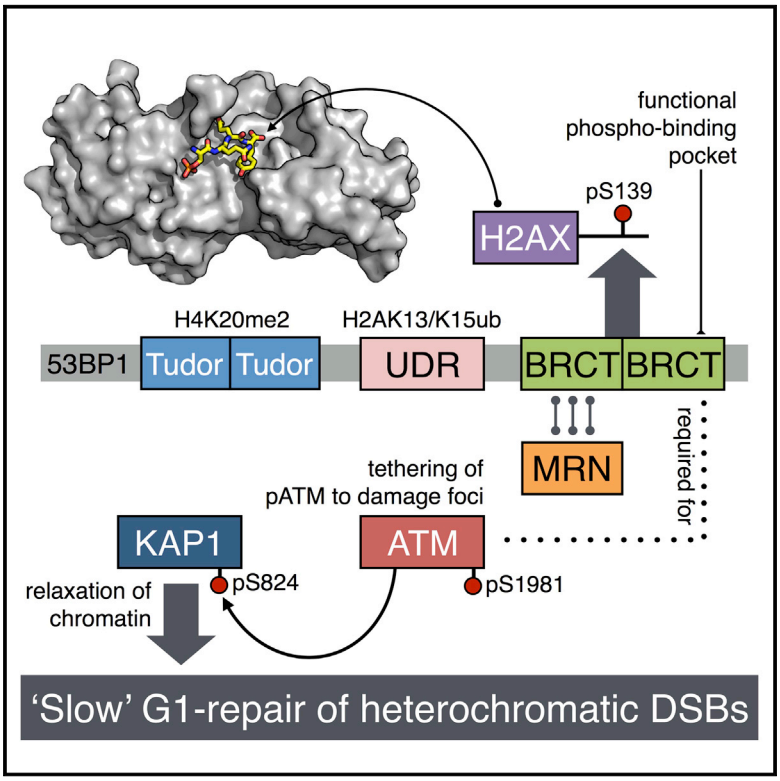

Authors

Robert A. Baldock, Matthew Day, Oliver J. Wilkinson, ..., Antony W. Oliver, Felicity Z. Watts, Laurence H. Pearl

Correspondence

f.z.watts@sussex.ac.uk (F.Z.W.), laurence.pearl@sussex.ac.uk (L.H.P.)

In Brief

Baldock et al. find that the BRCT$_2$ domain of 53BP1 specifically recognizes γH2AX, the primary chromatin mark at DNA double-strand breaks. Mutational disruption of this recognition in cells affects pATM recruitment into foci in G1 and results in a defect in repair of DNA damage in heterochromatin.

Highlights

- The BRCT$_2$ domain of 53BP1 binds the DNA damage chromatin mark γH2AX
- Crystal structure of γH2AX bound to 53BP1-BRCT$_2$ reveals the basis of specificity
- 53BP1-BRCT$_2$ responds to γH2AX formation by DNA damage in cells
- Disruption of γH2AX binding disrupts pATM foci and DSB repair in heterochromatin

Accession Numbers

5ECG

Baldock et al., 2015, Cell Reports *13*, 1–9
December 15, 2015 ©2015 The Authors
http://dx.doi.org/10.1016/j.celrep.2015.10.074

CellPress

Please cite this article in press as: Baldock et al., ATM Localization and Heterochromatin Repair Depend on Direct Interaction of the 53BP1-BRCT$_2$ Domain with γH2AX, Cell Reports (2015), http://dx.doi.org/10.1016/j.celrep.2015.10.074

Cell Reports
Report

OPEN ACCESS
CellPress

ATM Localization and Heterochromatin Repair Depend on Direct Interaction of the 53BP1-BRCT$_2$ Domain with γH2AX

Robert A. Baldock,[1,4] Matthew Day,[2,4] Oliver J. Wilkinson,[1,3] Ross Cloney,[1] Penelope A. Jeggo,[1] Antony W. Oliver,[2] Felicity Z. Watts,[1,*] and Laurence H. Pearl[2,*]
[1]Genome Damage and Stability Centre, School of Life Sciences, University of Sussex, Falmer, Brighton BN1 9RQ, UK
[2]Cancer Research UK DNA Repair Enzymes Group, Genome Damage and Stability Centre, School of Life Sciences, University of Sussex, Falmer, Brighton BN1 9RQ, UK
[3]Present address: School of Biochemistry, Medical Sciences Building, University Walk, Bristol BS8 1TD, UK
[4]Co-first author
*Correspondence: f.z.watts@sussex.ac.uk (F.Z.W.), laurence.pearl@sussex.ac.uk (L.H.P.)
http://dx.doi.org/10.1016/j.celrep.2015.10.074
This is an open access article under the CC BY-NC-ND license (http://creativecommons.org/licenses/by-nc-nd/4.0/).

SUMMARY

53BP1 plays multiple roles in mammalian DNA damage repair, mediating pathway choice and facilitating DNA double-strand break repair in heterochromatin. Although it possesses a C-terminal BRCT$_2$ domain, commonly involved in phospho-peptide binding in other proteins, initial recruitment of 53BP1 to sites of DNA damage depends on interaction with histone post-translational modifications—H4K20me2 and H2AK13/K15ub—downstream of the early γH2AX phosphorylation mark of DNA damage. We now show that, contrary to current models, the 53BP1-BRCT$_2$ domain binds γH2AX directly, providing a third post-translational mark regulating 53BP1 function. We find that the interaction of 53BP1 with γH2AX is required for sustaining the 53BP1-dependent focal concentration of activated ATM that facilitates repair of DNA double-strand breaks in heterochromatin in G1.

INTRODUCTION

TP53 binding protein 1 (53BP1) is a large multi-domain protein with multiple roles in the DNA damage response (Panier and Boulton, 2014; Zimmermann and de Lange, 2014). Following DNA damage and activation of the DNA-damage-responsive protein kinase ATM, 53BP1 is recruited rapidly to nuclear foci (Schultz et al., 2000) containing the primary mark of DNA damage—phosphorylation of Ser139 close to the C terminus of the histone H2A variant—H2AX (Rogakou et al., 1998), generally known as γH2AX. Although 53BP1 has a C-terminal tandem BRCT domain (BRCT$_2$), which in its orthologs, *Saccharomyces cerevisiae* Rad9p and *Schizosaccharomyces pombe* Crb2, mediates binding to the equivalents of γH2AX (Hammet et al., 2007; Kilkenny et al., 2008), the role of the 53BP1-BRCT$_2$ domain remains controversial. Although some studies indicated an interaction with γH2AX (Stewart et al., 2003; Ward et al., 2003), others have contradicted this (Stucki et al., 2005; Ward et al., 2006), and a significant role for this domain in the DNA damage response has been largely discounted (Bothmer et al., 2011; Callen et al., 2013).

Current models suggest that 53BP1 recruitment to ionizing radiation induced nuclear foci (IRIF) depends only indirectly on γH2AX and is instead mediated by two other post-translational modifications: (1) H2AK13/15-anchored ubiquitin chains (Fradet-Turcotte et al., 2013) generated by the E3 ubiquitin ligases RNF8 and RNF168, which are themselves recruited by MDC1, whose BRCT$_2$ domain interaction with γH2AX is required for its own recruitment (Bekker-Jensen and Mailand, 2010; Pinder et al., 2013); and (2) direct interaction of the tandem Tudor domains of 53BP1 with dimethylated H4K20 (Botuyan et al., 2006) exposed by release of JMJD2A and L3MBTL1 following their ubiquitylation by RNF8 and RNF168 (Acs et al., 2011; Mallette et al., 2012).

We have re-examined the role of the 53BP1-BRCT$_2$ domain and show unambiguously that it is a competent binding module for phosphorylated peptides with a clear specificity for the DNA-damage marker γH2AX, and in isolation from other parts of 53BP1 is sufficient for localization to sites of DNA damage in cells associated with γH2AX.

Structure-based mutational disruption of γH2AX binding by 53BP1 interferes with the 53BP1-dependent localization of pATM required for repair of DNA damage in regions of heterochromatin and results in a defect in the slow phase of DNA break repair in G1. These data add a third histone post-translational mark to the ligand repertoire of 53BP1, and a clear functional role for phosphopeptide binding by its BRCT$_2$ domain.

RESULTS AND DISCUSSION

53BP1-BRCT$_2$ Binds γH2AX In Vitro

Comparison of the tandem BRCT domains of 53BP1 with those of MDC1 (Rodriguez et al., 2003; Stucki et al., 2005) and Crb2 (Kilkenny et al., 2008) shows strong conservation of residues

Please cite this article in press as: Baldock et al., ATM Localization and Heterochromatin Repair Depend on Direct Interaction of the 53BP1-BRCT$_2$ Domain with γH2AX, Cell Reports (2015), http://dx.doi.org/10.1016/j.celrep.2015.10.074

OPEN ACCESS
CellPress

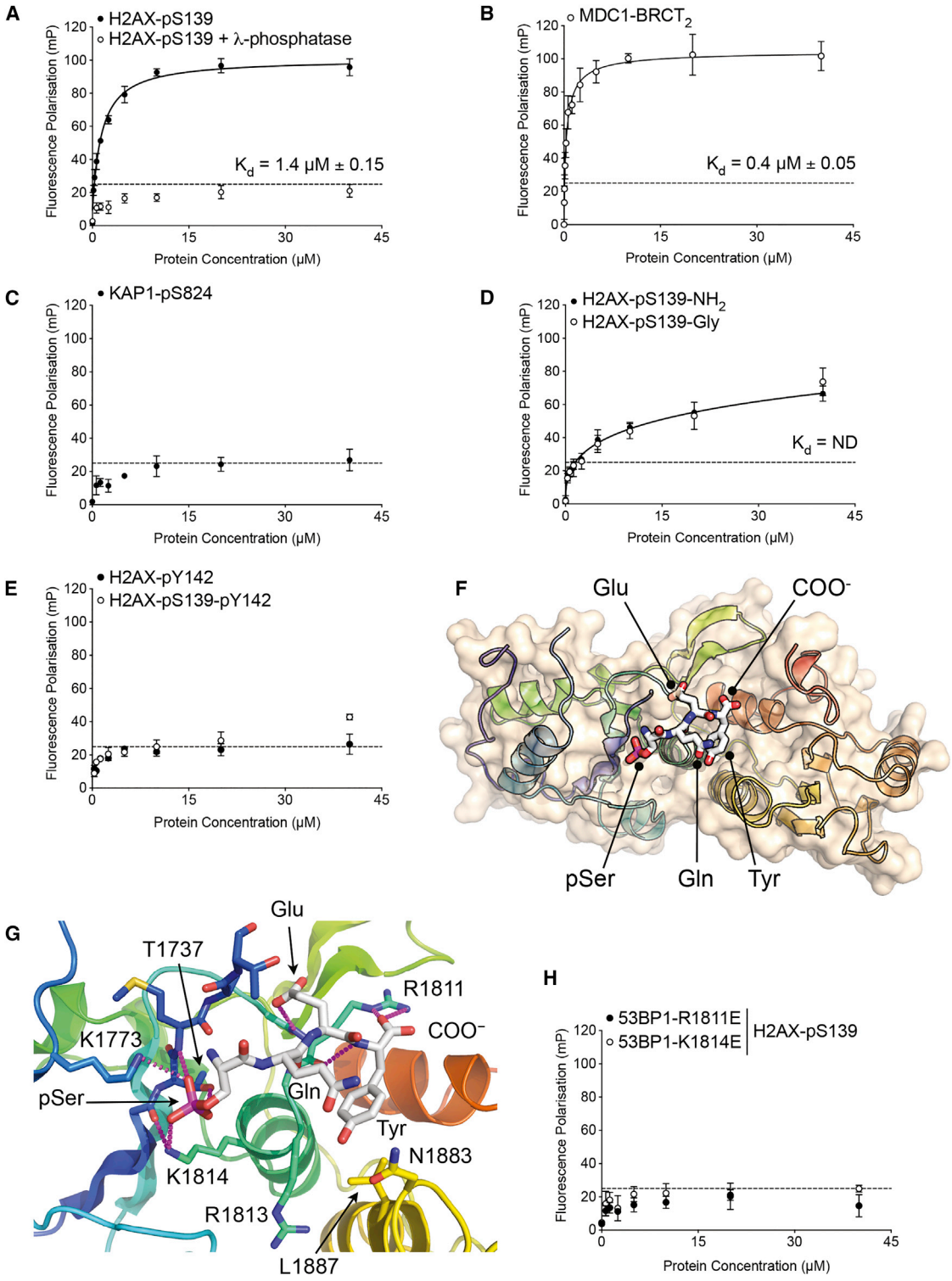

Figure 1. 53BP1 BRCT$_2$ Domain Binds γH2AX

(A) Fluorescence polarization assay (closed circle) showing binding of His$_6$-SUMO-53BP1-BRCT$_2$ to a fluorescein-tagged phosphopeptide (Flu-SGGKKATQApSQEY) corresponding to the last 13 residues of γH2AX. Data are means of four replicates with error bars showing 1 SD, and the K_D (1.4 μM ± 0.15) was calculated by least-squares fitting of a one-site binding model. Removal of the phosphate group on Ser139 by addition of λ-phosphatase (open circle) abrogates the interaction. The dashed line indicates a signal level consistent with non-specific interaction.

(B) As (A) but for His$_6$-SUMO-MDC1-BRCT$_2$ binding to the fluorescein-tagged γH2AX phosphopeptide.

(legend continued on next page)

implicated in specific binding of phosphorylated histone H2A tails. To determine whether 53BP1 shared this property, we measured the binding of the isolated 53BP1-BRCT$_2$ segment to a fluorescently labeled phosphopeptide (fluorescein-SGGKKATQApSQEY) corresponding to the last 13 residues of human γH2AX, by fluorescence polarization (see Experimental Procedures). 53BP1-BRCT$_2$ bound the phosphopeptide with a K_D of ~1.4 μM (Figure 1A), an affinity ~3.5-fold lower than MDC1-BRCT$_2$ (K_D = ~0.4 μM) when measured under the same experimental conditions (Figure 1B), but well within the range that is highly likely to be physiologically functional. The dephosphorylated H2AX peptide showed no significant binding (Figure 1A), nor did a comparable phosphopeptide from another protein (KAP1-pS824: fluorescein-*GYG*-SLPGAGLSpSQELSGG), showing the interaction is both phospho-dependent and sequence specific (Figure 1C).

Given that γH2AX is not the only phosphorylated ligand bound specifically by other BRCT$_2$ domains, we further defined the parameters of phosphopeptide recognition by 53BP1-BRCT$_2$. A γH2AX peptide with an amidated C terminus (H2AX-pS139-NH_2 or with an additional glycine (H2AX-pS139-Gly) bound 53BP1-BRCT$_2$ far less tightly than the peptide with the free charged α-carboxyl (Figure 1D). (Although the phosphorylated serine in human H2AX is encoded by codon 140 of the *H2AFX* gene, the initiator methionine is removed, and therefore not generally counted in the prevalent literature. For consistency, we here refer to this residue as Ser139.) We also explored the effect on binding to 53BP1-BRCT$_2$ of phosphorylation of H2AX-Tyr142, believed to mediate a switch between DNA repair and apoptosis (Cook et al., 2009). An H2AX peptide phosphorylated on Tyr142 bound far less tightly than the γH2AX peptide, as did a peptide *bis*-phosphorylated on both Ser139 and Tyr142 (Figure 1E). These data reinforce the conclusion that the canonical DNA-damage-responsive mark γH2AX is a specific ligand of 53BP1-BRCT$_2$.

To further characterize the interaction, we determined the crystal structure of 53BP1-BRCT$_2$ in complex with the core DNA-binding domain of P53 and a short "pSQEY" peptide corresponding to the last four residues of γH2AX (Figure 1F; Table S1). The phosphopeptide bound in a similar conformation to its interaction with the BRCT$_2$ domain of MDC1, with the phosphate group on γH2AX-Ser139 bound by the side chain of 53BP1-Thr1737, the peptide backbone of Met1738, and the side chains of Lys1773 and Lys1814 (Figure 1G). The side-chain carboxyl of γH2AX-Glu141 interacts with the peptide backbone of 53BP1-Arg1811, while the α-carboxyl of γH2AX-Tyr142 forms ionic and hydrogen bonding interactions with the side chain of 53BP1-Arg1811, explaining the strong preference for an unblocked C terminus in our binding assays (Figure 1D). The side chain of Tyr142 protrudes into a hydrophobic pocket lined by the side chains of Leu1887, Asn1883, and the main chain of Arg1813, an interaction that would be precluded by its phosphorylation. Consistent with the structure, charge reversal mutation of Lys1814, which interacts with the phosphate on H2AX-pSer139, or Arg1811, which binds the α-carboxyl of H2AX-Tyr142, abrogated interaction of 53BP1-BRCT$_2$ with the γH2AX phosphopeptide (Figure 1H). As the BRCT$_2$ domain of 53BP1 is a dimer in solution, like that of its yeast homolog Crb2 (Kilkenny et al., 2008), we confirmed that dimerization was not affected by the phospho-binding mutations (Figure S1).

53BP1-BRCT$_2$ Binds γH2AX in Cells

To determine whether the in vitro interaction that we observed for 53BP1-BRCT$_2$ is reflected in its behavior in cells, we transfected HeLa cells with an eYFP$_{NLS}$-53BP1-BRCT$_2$ construct. Laser micro-irradiation of the nuclei of live transfected cells caused a distinct time-dependent accumulation of fluorescence along the laser track, consistent with recruitment of the tagged 53BP1-BRCT$_2$ construct to sites of DNA damage; a construct lacking the BRCT$_2$ segment or with mutations that abolish γH2AX binding in vitro did not (Figures 2A and 2B; Movies S1 and S2). Although it was not possible to directly image γH2AX formation in live HeLa cells, recruitment of MDC1-BRCT$_2$ to the laser tracks confirms the presence of γH2AX (Movies S3), and clear γH2AX foci could be readily visualized in fixed cells following irradiation. The lower intensity of the recruited 53BP1-BRCT$_2$ compared to MDC1-BRCT$_2$ is consistent with the lower affinity of 53BP1-BRCT$_2$ for γH2AX we measured in vitro. Pre-treatment of the cells with KU55933, a specific inhibitor of ATM, substantially diminished γH2AX focus formation on irradiation, and this was further decreased by a DNA-PK inhibitor NU7441 (Figure 2C). When HeLa cells expressing the eYFP$_{NLS}$-53BP1-BRCT$_2$ construct were similarly pre-treated, recruitment of fluorescence to the laser stripe was greatly diminished, and with addition of NU7441, effectively abolished (Figure 2D). Consistent with this, the eYFP$_{NLS}$-53BP1-BRCT$_2$ construct did not localize to sites of DNA damage in mouse embryonic

(C) As (A) but with a fluorescein-tagged phosphopeptide derived from the major ATM phosphorylation site on the heterochromatin protein KAP-1 (Noon et al., 2010). No binding was observed.

(D) As (A) but for γH2AX peptides in which the C-terminal α-carboxyl group of Tyr142 is modified by either amidation (closed circle) or addition of a further glycine residue (open circle). Both modifications substantially reduce the affinity, and no K_D could be determined.

(E) As (A) but for H2AX peptides in which the side chain of Tyr142 is phosphorylated, either alone (closed circle) or in the presence of the γH2AX Ser139 phosphorylation (open circle). In both cases, phosphorylation of Tyr142 substantially diminished binding to His$_6$-SUMO-53BP1-BRCT$_2$.

(F) Overview of crystal structure of a phosphopeptide corresponding to the last four residues of γH2AX bound to the BRCT$_2$ domain of 53BP1. The core DNA-binding domain of P53, which is required for crystallogenesis, makes no interaction with the γH2AX peptide and is omitted for clarity.

(G) Detail of interactions made by the tail of γH2AX with the 53BP1-BRCT$_2$ domain. Carbon atoms in γH2AX are white; those of 53BP1 are rainbow colored to reflect their relative position within the protein sequence. The basic side chains of 53BP1 residues Lys1814 and Arg1811 provide neutralizing hydrogen bonding interactions with the acidic phosphate of γH2AX-pSer139 and the α-carboxyl of Tyr142, which are both required for binding of γH2AX to 53BP1-BRCT$_2$; see (A) and (C).

(H) As (A) but showing binding of the fluorescent γH2AX peptide to His$_6$-SUMO-53BP1-BRCT$_2$ with either an R1811E mutation (closed circle) or a K1814E mutation (open circle).

Please cite this article in press as: Baldock et al., ATM Localization and Heterochromatin Repair Depend on Direct Interaction of the 53BP1-BRCT$_2$ Domain with γH2AX, Cell Reports (2015), http://dx.doi.org/10.1016/j.celrep.2015.10.074

OPEN ACCESS
CellPress

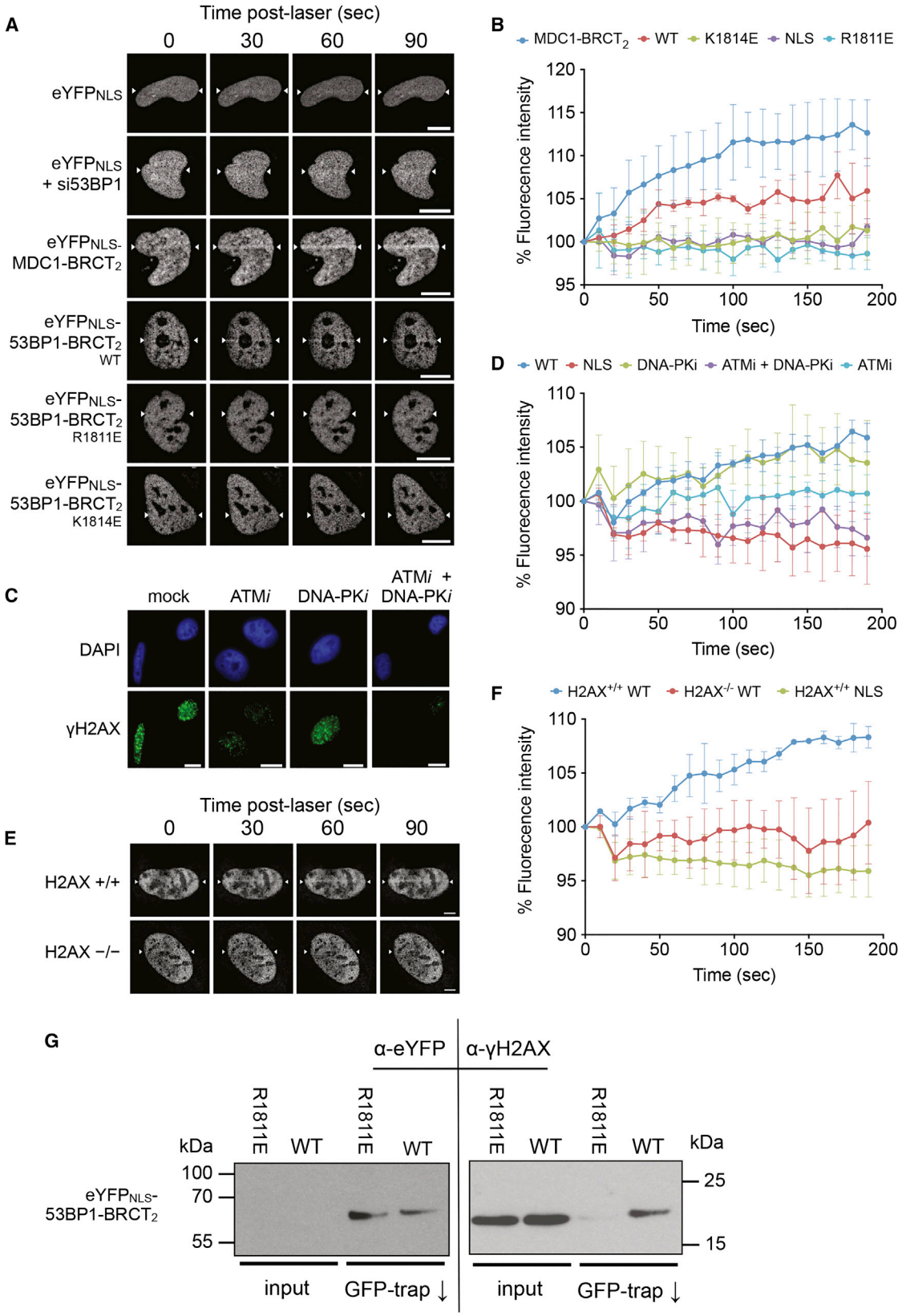

(legend on next page)

fibroblasts lacking H2AX (Figures 2E, 2F, and S2). Finally, we immunoprecipitated the wild-type eYFP$_{NLS}$-53BP1-BRCT$_2$ construct from HeLa cell extracts and were able to detect a co-precipitating γH2AX signal in western blots that was greatly diminished in immunoprecipitates of eYFP$_{NLS}$-53BP1-BRCT$_2$ with the R1811E mutation that abrogates γH2AX binding in vitro (Figure 2G).

Taken together, these structural, biochemical, and cellular observations provide compelling evidence that the BRCT$_2$ segment of 53BP1 has an inherent ability to localize to sites of DNA damage independently of other regions of the protein, and that this recruitment, which depends on phosphorylation of H2AX by DNA-damage-responsive PIKK kinases, is mediated by the clearly demonstrated ability of 53BP1-BRCT$_2$ to bind γH2AX both specifically and directly.

Phospho-Binding by 53BP1-BRCT$_2$ Regulates pATM Focal Localization

Having demonstrated the ability of 53BP1 to bind γH2AX directly, we sought to determine whether this ability contributed to any of the known roles of 53BP1 in the DNA damage response.

53BP1 is required for the focal localization of activated ATM, autophosphorylated on Ser1981 (Bakkenist and Kastan, 2003), and MRE11-RAD50-NBS1 (MRN) complexes at sites of DNA damage, and in the consequent activation of ATM checkpoint signaling (DiTullio et al., 2002; Mochan et al., 2004; Lee et al., 2010; Panier and Boulton, 2014). Consistent with this, small interfering RNA (siRNA) knockdown of 53BP1 in HeLa cells substantially diminished recruitment of activated pATM and MRN (visualized by NBS1), to nuclear ionizing radiation-induced foci (IRIF), with both of these proteins displaying a diffuse pan-nuclear distribution following irradiation (Figures 3 and S3).

Wild-type siRNA-resistant HA-tagged 53BP1 expressed in these knockdown cells, formed distinct foci itself following irradiation, and restored NBS1 and pATM foci that co-localized with those of 53BP1. However, a 53BP1 construct completely lacking the BRCT$_2$ domain still formed foci of its own but failed to restore NBS1 and pATM foci. By contrast 53BP1 constructs in which the BRCT$_2$ domain was present but contained mutations that disrupt binding to γH2AX (R1811E, K1814E) were able to recruit NBS1 into co-incident foci but had no effect on pATM, which retained the diffuse staining evident in the 53BP1 knockdown cells. A defect in pATM focus formation was evident with the K1814E mutant as early as 30 min post-irradiation (Figure S3B). A 53BP1 construct with a Tudor domain mutation (Y1502L) that abolishes recruitment to DNA damage (Huyen et al., 2004; Botuyan et al., 2006) eliminated 53BP1 foci and did not restore focal concentration of either NBS1 or pATM.

These data confirm previous observations that 53BP1 facilitates focal concentration of NBS1 (and thereby MRN) and pATM at DNA breaks in G1 but show that in both cases this is dependent on the BRCT$_2$ domain, and that focal recruitment of pATM is specifically dependent on the ability of that domain to interact with γH2AX. These data also indicate a function for the 53BP1-BRCT$_2$ in mediating an additional link between MRN complexes and chromatin modification, via its phosphorylation-independent interaction with RAD50 (Paull, 2015) and its phosphorylation-dependent interaction with γH2AX.

Phospho-Binding by 53BP1-BRCT$_2$ Contributes to Heterochromatin Repair

Double-strand break (DSB) repair in heterochromatin occurs more slowly than in euchromatin and requires 53BP1-dependent retention of pATM and consequent phosphorylation of the silencing factor KAP1/TRIM28 (Noon et al., 2010), which promotes its release with consequent relaxation of the heterochromatin. HeLa cells contact-inhibited in G0/G1, and transfected with 53BP1 siRNA, displayed significantly higher numbers of γH2AX foci 16–24 hr after irradiation than mock-transfected cells, or knockdown cells expressing a wild-type 53BP1 construct (Figure 4A). Consistent with their inability to localize pATM (Figure 3B), 53BP1 constructs lacking the BRCT$_2$ domain or with γH2AX-binding defective mutations failed to rescue the knockdown phenotype and resulted in significantly increased levels of γH2AX foci at later time points (Figures 4B and S4). Simultaneous knockdown of KAP1, whose phosphorylation depends on pATM localization, reduced the number of persistent γH2AX foci seen with these mutants

Figure 2. 53BP1 BRCT$_2$ Domain Localizes to DNA Damage through Phospho-Specific Interactions

(A) HeLa cells were reverse transfected with 53BP1 siRNA. 48 hr later, cells were transfected with eYFP-SV40$_{NLS}$ or eYFP-SV40$_{NLS}$-53BP1-BRCT$_2$ constructs containing either wild-type or mutant BRCT domains, or eYFP-SV40$_{NLS}$-MDC1-BRCT$_2$. 16 hr after this cells were damaged using laser micro-irradiation along a line indicated by the white arrowheads, and images were recorded over 3 min. Scale bar, 10 μm.

(B) eYFP fluorescence was tracked over 3 min to observe localization. Profiles of fluorescence intensity along the laser track in (A) were generated using Slidebook6 software (n = 30 from three experimental repeats). Error bars, 1 SD.

(C) Cells were treated with either KU55933 (ATMi), NU7441 (DNA-PKi), or both for 1 hr prior to irradiation with 3 Gy of IR. Cells were incubated for a further 30 min before fixing and staining for γH2AX. Scale bar, 10 μm.

(D) Cells were processed as before with the addition of either DNA-PKi, ATMi, or both for 1 hr prior to laser micro-irradiation. eYFP-fluorescence was tracked over 3 min to observe localization. Fluorescence intensity profiles were generated using Slidebook6 software (n = 30 from three experimental repeats). Error bars, 1 SD.

(E) H2AX$^{+/+}$ and H2AX$^{-/-}$ mouse embryonic fibroblasts were reverse transfected with 53BP1 siRNA. 24 hr later, cells were transfected with either the eYFP-SV40$_{NLS}$-53BP1-BRCT$_2$ construct or the eYFP-SV40$_{NLS}$ control. 16 hr after this, cells were damaged using laser micro-irradiation. eYFP fluorescence was tracked over 3 min to observe localization. Scale bar, 10 μm.

(F) Fluorescence intensity profiles from (E) were generated using Slidebook6 software (n = 30 from three experimental repeats). Error bars, 1 SD.

(G) eYFP-SV40$_{NLS}$-53BP1-BRCT$_2$ was immunoprecipitated using GFP-trap beads (ChromoTek), from benzonase-treated, γ-irradiated HeLa cell lysates, and eYFP-SV40$_{NLS}$-53BP1-BRCT$_2$ or γH2AX detected by western blot. Inputs represent 1/1,000 of the total sample used in the immunoprecipitation.

OPEN ACCESS
CellPress

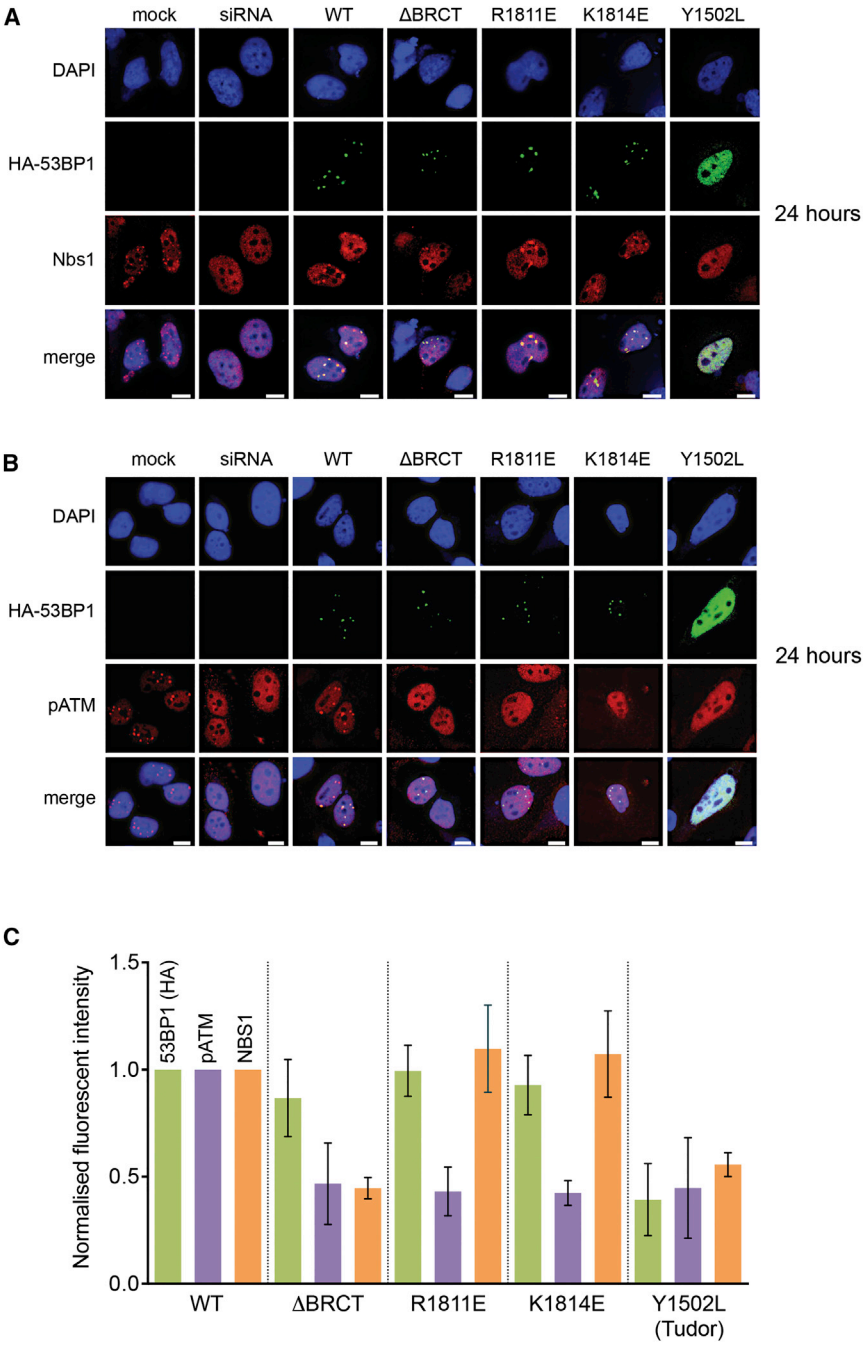

Figure 3. Co-localization of pATM Is Disrupted in 53BP1-BRCT$_2$ Phospho-Binding Mutants

(A) HeLa cells were reverse transfected with 53BP1 siRNA. 48 hr later, cells were transfected with an siRNA-resistant construct containing wild-type HA-53BP1, one of the BRCT mutants, or a Tudor domain mutant (Y1502L). 16 hr after this, cells were exposed to either 8 Gy for mock and wild-type (WT) or 3 Gy of ionizing radiation for the mutants and allowed to recover for 24 hr before staining for HA and NBS1. Scale bar, 5 μm.

(B) As (A) but stained for pATM.

(C) Cells processed in (A) and (B) were analyzed by measuring foci intensity of HA, pATM, and NBS1 (n = 30). Foci intensities were normalized to the average wild-type foci intensity for their respective channel. Normalized HA foci intensities from cells transfected with either WT or BRCT mutants indicates comparable expression of the plasmid constructs. Graph shows average of three experiments with 1 SD.

back down to wild-type levels (Figure 4C), confirming that these persistent foci were due to damage sites in heterochromatin (Goodarzi et al., 2008).

Biological Roles of 53BP1 Binding to γH2AX

To date, BRCT$_2$ domains of three mammalian proteins—MCPH1, PTIP, and MDC1—have been found to specifically recognize the primary mark of DNA damage, γH2AX (Yan et al., 2011; Stucki et al., 2005; Singh et al., 2012). Our data show unambiguously that this is a property shared by the BRCT$_2$ domain of 53BP1, and that this interaction plays a role in the biological functions of 53BP1—a very similar conclusion was reached by Kleiner et al. (2015). This observation further strengthens the idea that 53BP1 is the functional ortholog of the fission yeast and budding yeast proteins Crb2 and Rad9p (Hammet et al., 2007; Kilkenny et al., 2008).

Although the ability of the BRCT$_2$ domain of 53BP1 to bind γH2AX contributes to efficient repair of DNA damage, it is not required for initial recruitment of 53BP1 to IRIF in the immediate response to DNA damage in G1. 53BP1 recruitment is downstream of recognition of γH2AX by MDC1, whose BRCT$_2$ domain has a higher affinity for γH2AX. Nonetheless, once recruited to damaged chromatin 53BP1's interaction with γH2AX would be favored by its interaction with the other post-translational modifications it recognizes, and the γH2AX interaction might only become functionally significant at a later stage of the IRIF-centered repair processes or in specific situations such as the repair of damage in heterochromatin, as we show here.

Recruitment and retention of 53BP1 at sites of DNA damage facilitates co-localization and retention of other factors required for signaling and repair (Panier and Boulton, 2014). In the case of MRN, this is mediated by a phospho-independent interaction between RAD50 and the 53BP1-BRCT$_2$ (Lee et al., 2010). Regions within the MRN complex have, in turn, been implicated in recruiting and activating ATM at sites of DNA damage (Paull, 2015), but it is not clear what role these play in retaining pATM

OPEN ACCESS
CellPress

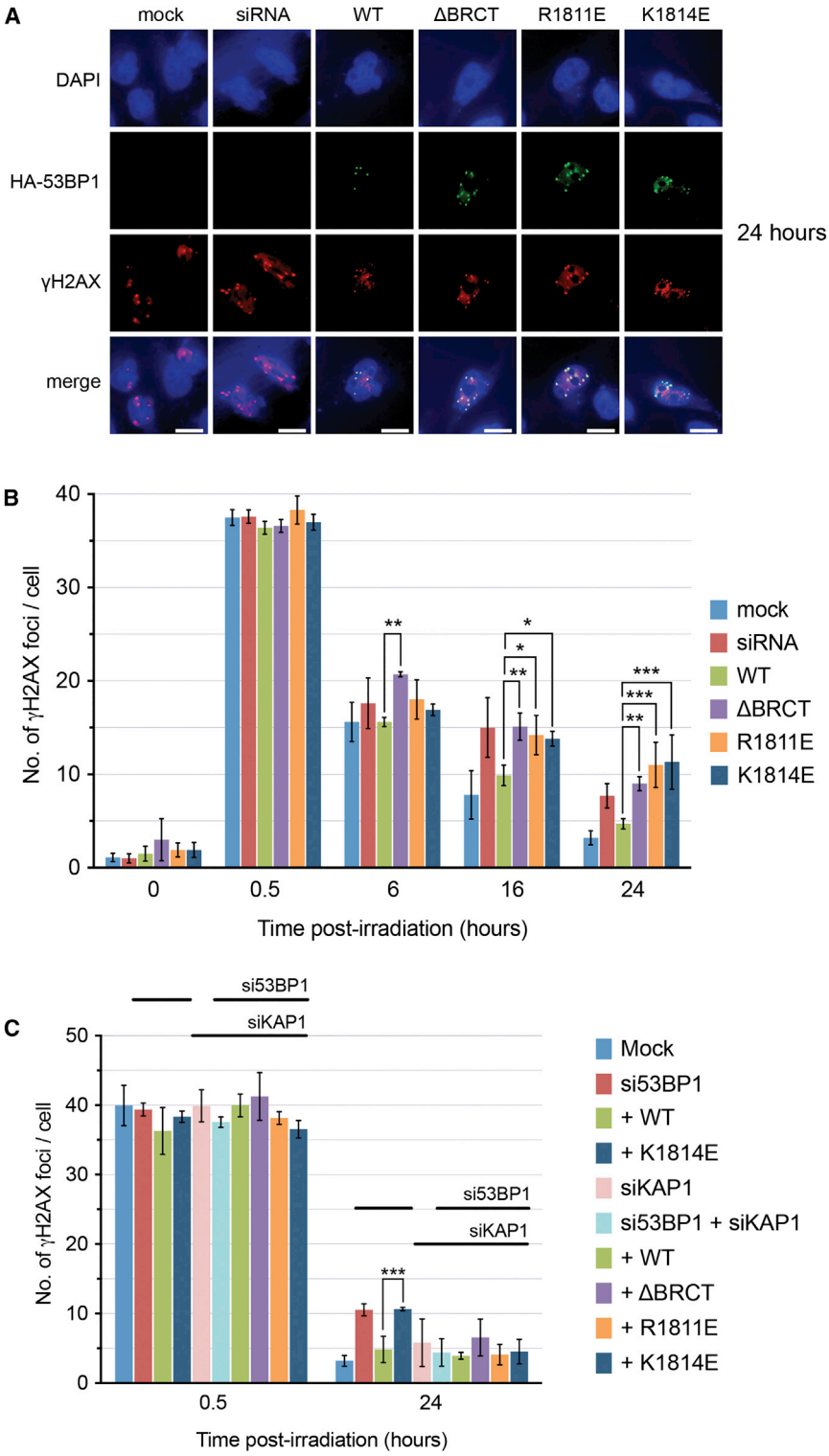

Figure 4. Slow Repair of Damage in Heterochromatin Is Defective in 53BP1-BRCT$_2$ Phospho-Binding Mutants

(A) HeLa cells were reverse transfected with 53BP1 siRNA. 48 hr later, cells were transfected with an siRNA-resistant construct containing wild-type HA-tagged 53BP1 or one of the BRCT mutants. 16 hr later, cells were exposed to 3 Gy of ionizing radiation and allowed to recover for the indicated time before staining for HA-53BP1 and γH2AX. Higher numbers of γH2AX foci were evident 24 hr after irradiation in siRNA-treated cells and siRNA-treated cells transfected with 53BP1 mutant constructs.

(B) Quantitation of γH2AX focus persistence. Graphs show the mean of three experiments; error bars, 1 SD. 53BP1 constructs lacking the BRCT domain or with point mutations that abrogate γH2AX binding in vitro show significantly higher levels of persistent γH2AX foci than wild-type (one-way ANOVA).

(C) As (A) but with 53BP1 and/or KAP-1 siRNA. Persistence of significantly higher levels of γH2AX foci in the presence of 53BP1 mutants is suppressed when KAP-1 is also knocked down, indicating that persistence is due to a defect in KAP-1 phosphorylation by ATM as a result of the failure of the 53BP1 mutants to localize pATM to heterochromatinized sites of damage.

in damage foci downstream of initial activation. Our data indicate that focal concentration and retention of pATM at slowly repaired sites of DNA damage in G1 (Noon et al., 2010) is independent of MRN recruitment but dependent on 53BP1 recruitment and, significantly, the histone modifications it engages with. Thus, while removal of the ability of 53BP1 to bind γH2AX does not affect focal co-localization of MRN and 53BP1, it substantially reduces pATM localization, which, in turn, results in a defect in DSB repair in heterochromatin. These data highlight a role for the 53BP1-BRCT$_2$ domain in reinforcing links between MRN complexes and chromatin modification, via its phosphorylation-independent interaction with RAD50 (Noon et al., 2010) and its phosphorylation-dependent interaction with γH2AX.

The means by which 53BP1 facilitates pATM concentration and retention in IRIFs remains unclear. There is little indication in the literature of a direct interaction of ATM with 53BP1, although both proteins have well-documented interactions with other proteins in common. The dependence we demonstrate here on 53BP1's ability to bind γH2AX suggests that this is likely to involve complex features of local chromatin conformation and histone modifications and further work will be required to define this. It is highly likely that other of the myriad functions of 53BP1 will also involve this hitherto disregarded property of 53BP1, and work is ongoing to uncover and characterize these.

Please cite this article in press as: Baldock et al., ATM Localization and Heterochromatin Repair Depend on Direct Interaction of the 53BP1-BRCT$_2$ Domain with γH2AX, Cell Reports (2015), http://dx.doi.org/10.1016/j.celrep.2015.10.074

EXPERIMENTAL PROCEDURES

See the Supplemental Experimental Procedures for full details.

Protein Expression and Purification

Proteins for biochemical and structural analysis were expressed in *E. coli* and purified by affinity and conventional chromatography.

Fluorescence Polarization Experiments

Binding to BRCT$_2$ domains was determined using fluorescein-labeled peptides and His$_6$-SUMO-BRCT$_2$ fusion proteins. Dissociation constants (K_D) were determined by non-linear regression to a one site-specific binding model.

Crystallization, X-Ray Diffraction Data Collection, Phasing, Model Building, and Refinement

Crystals of P53^{Core}/53BP1-BRCT$_2$ were grown by vapor diffusion and soaked with the γH2AX-pS139 peptide (pSQEY) for 60 min prior to plunge-freezing in liquid nitrogen. Diffraction data were collected at the Diamond Synchrotron Lightsource, and the structure was determined by molecular replacement.

Tissue Culture, Cell Lines, and Reagents

HeLa, H2AX$^{+/+}$, and H2AX$^{-/-}$ mouse embryonic fibroblast (MEF) cells were cultured in DMEM supplemented with 10% (v/v) fetal calf serum (FCS), penicillin, streptomycin, and L-glutamine. Caffeine (Sigma-Aldrich) was used at a final concentration of 10 mM. ATMi (KU55933, Abcam), DNA-PKi (NU7441, Santa Cruz Biotechnology), and ATRi (ATR-kinase inhibitor II, Merck Millipore) were all used at a concentration of 10 μM, except for the CHK1 inhibitor UCN-01 (Sigma-Aldrich) that was used at a concentration of 200 nM. Cells were irradiated using a Caesium^{137} gamma source.

siRNA Depletion of 53BP1/KAP-1 and siRNA-Resistant Expression of 53BP1

HeLa cells were seeded at high confluence onto 35-mm plates and reverse transfected with either 53BP1-siRNA or negative control oligonucleotides diluted into serum free media Cells were cultured for a further 48 hr for efficient depletion. Subsequently cells were transfected with 53BP1 constructs rendered siRNA-resistant by three silent point mutations in the 53BP1 cDNA clone in pCMH6K (A231G, A234G, and A237C) (Noon et al., 2010) and incubated for a further 16 hr before irradiation.

Antibodies

All antibodies used were from standard commercial sources (see the Supplemental Experimental Procedures for full details).

Immunofluorescence

Cells were fixed on coverslips and washed three times before incubation at room temperature with the primary antibodies. Cells were washed a further three times before incubation with the secondary, fluorophore-coupled, antibodies, and washed a final three times before mounting on glass slides with DAPI mounting media.

Live-Cell Imaging and UV-Laser Microirradiation

Cells were seeded at low confluence before 53BP1 depletion by siRNA, and eYFP-SV40$_{NLS}$-53BP1-BRCT$_2$ plasmid constructs were transfected into cells. Cells were incubated for 20 min with 100 μg/ml Hoechst 34580 prior to excitation with a 405-nm laser. Protein localization was tracked over 3 min using a 488-nm laser.

GFP-Trap

Stable cell lines were generated for HeLa cells transfected with wild-type or R1811E mutant forms of the eYFP-SV40$_{NLS}$-53BP1-BRCT$_2$ expression construct. Cellular lysates were generated by re-suspension of frozen pellets, and incubated with GFP-Trap A resin. Retained protein was detected by chemiluminescent western blot.

ACCESSION NUMBERS

The accession number for the crystallographic data reported here is PDB: 5ECG.

SUPPLEMENTAL INFORMATION

Supplemental Information includes Supplemental Experimental Procedures, four figures, one table, and three movies and can be found with this article online at http://dx.doi.org/10.1016/j.celrep.2015.10.074.

AUTHOR CONTRIBUTIONS

Conceptualization: A.W.O., F.Z.W., and L.H.P.; Methodology: P.A.J., A.W.O., F.Z.W., and L.H.P.; Investigation: R.A.B., M.D., O.J.W., R.C., and A.W.O.; Writing–Original Draft: L.H.P.; Writing–Review & Editing: R.A.B., M.D., P.A.J., A.W.O., F.Z.W., and L.H.P.; Visualization R.A.B., A.W.O., and L.H.P.; Supervision: A.W.O., F.Z.W., and L.H.P.; Funding Acquisition: F.Z.W. and L.H.P.

ACKNOWLEDGMENTS

We thank Mark Roe for assistance with X-ray data collection, Stuart Rulten for expertise with UVA laser microirradiation experiments, Lihong Zhou for assistance with cell culture, and Tony Carr and Jessica Downs for useful discussion. We thank Diamond Light Source, Didcot, for access to synchrotron radiation and the Wellcome Trust for support for X-ray diffraction facilities at the University of Sussex. This work was supported by Cancer Research UK Project Grant C1206/A11978 (F.Z.W. and L.H.P.) and Cancer Research UK Programme Grant C302/A14532 (L.H.P. and A.W.O.).

Received: June 16, 2015
Revised: September 28, 2015
Accepted: October 26, 2015
Published: November 25, 2015

REFERENCES

Acs, K., Luijsterburg, M.S., Ackermann, L., Salomons, F.A., Hoppe, T., and Dantuma, N.P. (2011). The AAA-ATPase VCP/p97 promotes 53BP1 recruitment by removing L3MBTL1 from DNA double-strand breaks. Nat. Struct. Mol. Biol. *18*, 1345–1350.

Bakkenist, C.J., and Kastan, M.B. (2003). DNA damage activates ATM through intermolecular autophosphorylation and dimer dissociation. Nature *421*, 499–506.

Bekker-Jensen, S., and Mailand, N. (2010). Assembly and function of DNA double-strand break repair foci in mammalian cells. DNA Repair (Amst.) *9*, 1219–1228.

Bothmer, A., Robbiani, D.F., Di Virgilio, M., Bunting, S.F., Klein, I.A., Feldhahn, N., Barlow, J., Chen, H.T., Bosque, D., Callen, E., et al. (2011). Regulation of DNA end joining, resection, and immunoglobulin class switch recombination by 53BP1. Mol. Cell *42*, 319–329.

Botuyan, M.V., Lee, J., Ward, I.M., Kim, J.E., Thompson, J.R., Chen, J., and Mer, G. (2006). Structural basis for the methylation state-specific recognition of histone H4-K20 by 53BP1 and Crb2 in DNA repair. Cell *127*, 1361–1373.

Callen, E., Di Virgilio, M., Kruhlak, M.J., Nieto-Soler, M., Wong, N., Chen, H.T., Faryabi, R.B., Polato, F., Santos, M., Starnes, L.M., et al. (2013). 53BP1 mediates productive and mutagenic DNA repair through distinct phosphoprotein interactions. Cell *153*, 1266–1280.

Cook, P.J., Ju, B.G., Telese, F., Wang, X., Glass, C.K., and Rosenfeld, M.G. (2009). Tyrosine dephosphorylation of H2AX modulates apoptosis and survival decisions. Nature *458*, 591–596.

DiTullio, R.A., Jr., Mochan, T.A., Venere, M., Bartkova, J., Sehested, M., Bartek, J., and Halazonetis, T.D. (2002). 53BP1 functions in an ATM-dependent checkpoint pathway that is constitutively activated in human cancer. Nat. Cell Biol. *4*, 998–1002.

Fradet-Turcotte, A., Canny, M.D., Escribano-Díaz, C., Orthwein, A., Leung, C.C., Huang, H., Landry, M.C., Kitevski-LeBlanc, J., Noordermeer, S.M., Sicheri, F., and Durocher, D. (2013). 53BP1 is a reader of the DNA-damage-induced H2A Lys 15 ubiquitin mark. Nature *499*, 50–54.

Goodarzi, A.A., Noon, A.T., Deckbar, D., Ziv, Y., Shiloh, Y., Löbrich, M., and Jeggo, P.A. (2008). ATM signaling facilitates repair of DNA double-strand breaks associated with heterochromatin. Mol. Cell *31*, 167–177.

Hammet, A., Magill, C., Heierhorst, J., and Jackson, S.P. (2007). Rad9 BRCT domain interaction with phosphorylated H2AX regulates the G1 checkpoint in budding yeast. EMBO Rep. *8*, 851–857.

Huyen, Y., Zgheib, O., Ditullio, R.A., Jr., Gorgoulis, V.G., Zacharatos, P., Petty, T.J., Sheston, E.A., Mellert, H.S., Stavridi, E.S., and Halazonetis, T.D. (2004). Methylated lysine 79 of histone H3 targets 53BP1 to DNA double-strand breaks. Nature *432*, 406–411.

Kilkenny, M.L., Doré, A.S., Roe, S.M., Nestoras, K., Ho, J.C., Watts, F.Z., and Pearl, L.H. (2008). Structural and functional analysis of the Crb2-BRCT2 domain reveals distinct roles in checkpoint signaling and DNA damage repair. Genes Dev. *22*, 2034–2047.

Kleiner, R.E., Verma, P., Molloy, K.R., Chait, B.T., and Kapoor, T.M. (2015). Chemical proteomics reveals a γH2AX-53BP1 interaction in the DNA damage response. Nat. Chem. Biol. *11*, 807–814.

Lee, J.H., Goodarzi, A.A., Jeggo, P.A., and Paull, T.T. (2010). 53BP1 promotes ATM activity through direct interactions with the MRN complex. EMBO J. *29*, 574–585.

Mallette, F.A., Mattiroli, F., Cui, G., Young, L.C., Hendzel, M.J., Mer, G., Sixma, T.K., and Richard, S. (2012). RNF8- and RNF168-dependent degradation of KDM4A/JMJD2A triggers 53BP1 recruitment to DNA damage sites. EMBO J. *31*, 1865–1878.

Mochan, T.A., Venere, M., DiTullio, R.A., Jr., and Halazonetis, T.D. (2004). 53BP1, an activator of ATM in response to DNA damage. DNA Repair (Amst.) *3*, 945–952.

Noon, A.T., Shibata, A., Rief, N., Löbrich, M., Stewart, G.S., Jeggo, P.A., and Goodarzi, A.A. (2010). 53BP1-dependent robust localized KAP-1 phosphorylation is essential for heterochromatic DNA double-strand break repair. Nat. Cell Biol. *12*, 177–184.

Panier, S., and Boulton, S.J. (2014). Double-strand break repair: 53BP1 comes into focus. Nat. Rev. Mol. Cell Biol. *15*, 7–18.

Paull, T.T. (2015). Mechanisms of ATM Activation. Annu. Rev. Biochem. *84*, 711–738.

Pinder, J.B., Attwood, K.M., and Dellaire, G. (2013). Reading, writing, and repair: the role of ubiquitin and the ubiquitin-like proteins in DNA damage signaling and repair. Front. Genet. *4*, 45.

Rodriguez, M., Yu, X., Chen, J., and Songyang, Z. (2003). Phosphopeptide binding specificities of BRCA1 COOH-terminal (BRCT) domains. J. Biol. Chem. *278*, 52914–52918.

Rogakou, E.P., Pilch, D.R., Orr, A.H., Ivanova, V.S., and Bonner, W.M. (1998). DNA double-stranded breaks induce histone H2AX phosphorylation on serine 139. J. Biol. Chem. *273*, 5858–5868.

Schultz, L.B., Chehab, N.H., Malikzay, A., and Halazonetis, T.D. (2000). p53 binding protein 1 (53BP1) is an early participant in the cellular response to DNA double-strand breaks. J. Cell Biol. *151*, 1381–1390.

Singh, N., Basnet, H., Wiltshire, T.D., Mohammad, D.H., Thompson, J.R., Héroux, A., Botuyan, M.V., Yaffe, M.B., Couch, F.J., Rosenfeld, M.G., and Mer, G. (2012). Dual recognition of phosphoserine and phosphotyrosine in histone variant H2A.X by DNA damage response protein MCPH1. Proc. Natl. Acad. Sci. USA *109*, 14381–14386.

Stewart, G.S., Wang, B., Bignell, C.R., Taylor, A.M., and Elledge, S.J. (2003). MDC1 is a mediator of the mammalian DNA damage checkpoint. Nature *421*, 961–966.

Stucki, M., Clapperton, J.A., Mohammad, D., Yaffe, M.B., Smerdon, S.J., and Jackson, S.P. (2005). MDC1 directly binds phosphorylated histone H2AX to regulate cellular responses to DNA double-strand breaks. Cell *123*, 1213–1226.

Ward, I.M., Minn, K., Jorda, K.G., and Chen, J. (2003). Accumulation of checkpoint protein 53BP1 at DNA breaks involves its binding to phosphorylated histone H2AX. J. Biol. Chem. *278*, 19579–19582.

Ward, I., Kim, J.E., Minn, K., Chini, C.C., Mer, G., and Chen, J. (2006). The tandem BRCT domain of 53BP1 is not required for its repair function. J. Biol. Chem. *281*, 38472–38477.

Yan, W., Shao, Z., Li, F., Niu, L., Shi, Y., Teng, M., and Li, X. (2011). Structural basis of γH2AX recognition by human PTIP BRCT5-BRCT6 domains in the DNA damage response pathway. FEBS Lett. *585*, 3874–3879.

Zimmermann, M., and de Lange, T. (2014). 53BP1: pro choice in DNA repair. Trends Cell Biol. *24*, 108–117.